



Delft University of Technology

Nonconventional regeneration methods for oxygenases

van Schie, Morten

DOI

[10.4233/uuid:8172a3b3-7730-4176-a94e-3276dce13716](https://doi.org/10.4233/uuid:8172a3b3-7730-4176-a94e-3276dce13716)

Publication date

2019

Document Version

Final published version

Citation (APA)

van Schie, M. (2019). *Nonconventional regeneration methods for oxygenases*. [Dissertation (TU Delft), Delft University of Technology]. <https://doi.org/10.4233/uuid:8172a3b3-7730-4176-a94e-3276dce13716>

Important note

To cite this publication, please use the final published version (if applicable).
Please check the document version above.

Copyright

Other than for strictly personal use, it is not permitted to download, forward or distribute the text or part of it, without the consent of the author(s) and/or copyright holder(s), unless the work is under an open content license such as Creative Commons.

Takedown policy

Please contact us and provide details if you believe this document breaches copyrights.
We will remove access to the work immediately and investigate your claim.

Nonconventional regeneration methods for oxygenases

Proefschrift

ter verkrijging van de graad van doctor
aan de Technische Universiteit Delft,
op gezag van de Rector Magnificus Prof.dr.ir. T.H.J.J. van der Hagen
voorzitter van het College voor Promoties,
in het openbaar te verdedigen op
vrijdag, 20 december, 2019 om 12:30 uur

Door

Morten Martinus Cornelis Harald VAN SCHIE

Master of Science in Life Science and Technology, Technische Universiteit Delft,
Nederland
geboren te Veghel, Nederland

Dit proefschrift is goedgekeurd door de promotoren:

Samenstelling promotiecommissie bestaat uit:

Rector magnificus	Voorzitter
Prof. dr. F. Hollmann	TU Delft, promotor
Prof. dr. I.W.C.E. Arends	Universiteit Utrecht, promotor
Dr. C.E. Paul	TU Delft, copromotor

Onafhankelijke leden:

Prof. dr. J.H. van Esch	TU Delft
Prof. dr. W.J.H. van Berkel	Wageningen University, Nederland
Prof. dr. R. Kourist	TU Graz, Oostenrijk
Dr. S. Kara	Aarhus University, Denemarken

Reservelid:

Prof. dr. U. Hanefeld	TU Delft
-----------------------	----------

This research was supported by The Netherlands Organization for Scientific Research through a VICI grant (No.724.014.003).

ISBN/EAN: 978-94-6366-225-3
Cover by: Douwe van Schie, douwevanschie.com
Printed by: Gildeprint, Enschede

Table of Contents

Samenvatting	5
Summary	9
Chapter 1: General introduction	15
Chapter 2: Photocatalysis to promote cell-free biocatalytic reactions	37
Chapter 3: Photoenzymatic epoxidation of styrenes	71
Chapter 4: Deazaflavins as photocatalyst for the direct reductive regeneration of flavoenzymes	99
Chapter 5: Selective oxyfunctionalisation reactions driven by sulfite oxidase-catalysed in situ generation of H ₂ O ₂	123
Chapter 6: H ₂ O ₂ Production at low over-potentials for biocatalytic halogenation reactions	141
Chapter 7: Cascading g-C ₃ N ₄ and peroxygenases for selective oxyfunctionalization reactions	157
Chapter 8: Biocatalytic synthesis of Green Note <i>trans</i> -2-hexenal using aryl alcohol oxidase from <i>Pleurotus eryngii</i> : overcoming solubility limitations	187
Chapter 9: Discussion	211
Curriculum Vitae	229
List of publications	230
Acknowledgements	232

Samenvatting

In biokatalyse gebruiken we enzymen om chemische reacties te versnellen. De voordelen van enzymen ten opzichte van andere chemische katalysatoren zijn hun uitzonderlijke prestatie op het gebied van reactiviteit, regio-selectiviteit en enantiomeer-selectiviteit. De relatief milde omstandigheden waar ze optimaal onder kunnen presteren maakt ze zeer bruikbaar als duurzame alternatieven voor bestaande chemische processen. De hoeveelheid verschillende beschikbare enzymen blijft groeien, evenals de variatie aan reacties die we met ze kunnen uitvoeren.

Enzymen zijn verdeeld over zeven verschillende klassen, afhankelijk van de reacties die ze katalyseren. Klasse 1, waar deze thesis zich op richt, is die van de oxidoreductases. Deze enzymen katalyseren redox reacties, ofwel de specifieke overdracht van elektronen van of naar een reactant. Om de redox-balans vervolgens sluitend te maken zijn deze enzymen afhankelijk van zogenoemde co-enzymen, organische structuren die in stoichiometrische hoeveelheden nodig zijn. De stoichiometrische additie van deze stoffen is echter een obstakel voor de reactie, zowel vanuit een economisch als ecologisch oogpunt. Ter compensatie wordt er doorgaans een tweede enzymreactie geïntroduceerd om deze co-enzymen te regenereren. Hoewel dit een gangbare methode is, maakt het de reacties gecompliceerder en veroorzaakt het een extra afval stroom. In deze thesis richten wij ons daarom op alternatieven voor deze regeneratie systemen.

Binnen de klasse van oxidoreductases richt deze thesis zich specifiek op de subklassen van oxidases en oxygenases, welke afhankelijk zijn van zuurstof in de reactiemechanismen. Deze enzymen kunnen onder andere regio- en enantio-selectief een hetero-atoom inbrengen in moleculaire structuren, zelfs in verbindingen die niet geactiveerd zijn. Dit zijn reacties die zeer lastig, dan wel onmogelijk, uit te voeren zijn met behulp van “klassieke” chemische methoden.

Om te beginnen richten we ons op fotochemie als alternatief voor co-enzym regeneratie. In **hoofdstuk 2** geven we een overzicht van de huidige situatie in het samengestelde veld van de fotobiokatalyse. In **hoofdstuk 3** dragen wij hier aan bij door een fotochemische regeneratie methode te presenteren voor een co-enzym en tevens fotomediator: FADH_2 . Deze flavine kan vervolgens worden gebruikt door een styreen mono-oxygenase. Wij bewijzen dat dit systeem mogelijk is en geven de knelpunten weer. Dit zijn voornamelijk de verscheidene zij-reacties die mogelijk worden na foto-excitatie van de flavine.

Eén van de obstakels is het zogenoemde “zuurstof dilemma”. Zuurstof is nodig voor de mono-oxygenase reactie, maar kan ook direct reageren met de gereduceerde flavine buiten het enzym om. Hierdoor neemt zuurstof de geïnvesteerde elektronen weg van de reactie en vormt het daarbij waterstof peroxide. Dit is een bekend fenomeen voor nagenoeg alle mono-oxygenase reacties. We richten ons vervolgens dan ook op verschillende manieren om dit dilemma op te lossen. De eerste optie, in **hoofdstuk 4**, is het gebruik van deazaflavine als de fotomediator in plaats van natuurlijke flavine. Deazaflavines leken veelbelovend na eerder bewijs dat deze gereduceerde stoffen resistent waren voor zuurstof. Helaas vinden wij dat ze deze stabiliteit verliezen na foto-excitatie.

Wij verleggen daarom onze aandacht vervolgens naar andere manieren om het zuurstof dilemma te omzeilen. Bijvoorbeeld door het gebruik van enzymen die de ontkoppeling van elektronen juist kunnen omdraaien voor de regeneratie van het actieve centrum. Dit is het geval voor de heem proteïnen die bekend staan als de peroxygenasen. In het reactiemechanisme van deze eiwitten valt H_2O_2 direct de heem groep aan, waarna de actieve “compound I” wordt gevormd. Op deze manier worden zowel de elektronen als het zuurstofatoom geleverd aan het enzym. Echter, stoichiometrische additie van H_2O_2 aan het begin van de reactie zal het enzym oxidatief deactiveren. Deze reacties zijn daardoor enkel mogelijk als de H_2O_2 op een gecontroleerde manier wordt toegevoegd. We richten ons daarom op verschillende methoden om de H_2O_2 *in situ* te genereren, ideaal gezien via de reductie van zuurstof ten kostte van kleine elektron donoren. We stellen verschillende methodes voor gebaseerd op biokatalytische, elektrochemische en fotochemische technieken.

In **hoofdstuk 5** gebruiken we de oxidatie van sulfiet naar sulfaat met behulp van een sulfiet oxidase om de H_2O_2 te genereren. Hier blijkt vooral de reactiviteit van sulfiet zelf een centrale rol te spelen. Door te wisselen tussen sulfiet zouten die in meer of mindere mate oplosbaar zijn in water weten we de prestatie van de reactie te beïnvloeden.

In **hoofdstuk 6** kijken we naar elektrochemie om de H_2O_2 te genereren. Op papier is elektrochemie de meest efficiënte manier voor H_2O_2 generatie aangezien de elektronen hier direct kunnen worden gebruikt om zuurstof te reduceren. Over het algemeen is er echter een over-potentiaal nodig om deze reactie mogelijk te maken, wat resulteert in extra energieverspilling. Om dit op te lossen maken we gebruik van elektroden die bedekt zijn met geoxideerde koolstof nanobuisjes, die erom bekend staan deze potentiaal te verlagen. De gevormde H_2O_2 gebruiken we vervolgens om een reactie met een vanadium chloroperoxidase te katalyseren.

In **hoofdstuk 7** gebruiken we heterogene fotokatalysatoren om H_2O_2 te genereren. We concluderen dat graphitic carbonnitrides zeer efficiënt zuurstof kunnen reduceren ten koste van formiaat. Tijdens deze reacties worden er echter ook reactieve zuurstofcomponenten en radicalen gegenereerd, die vervolgens de enzymen deactiveren. Om dit te voorkomen stellen wij voor om de foto-katalytische en biokatalytische reacties fysiek te scheiden.

In hoofdstukken 5, 6 en 7 richten we onze aandacht op reducerende processen waar H_2O_2 in wordt geconsumeerd. In **hoofdstuk 8** laten we zien hoe een alcohol oxidase in een oxiderend proces juist H_2O_2 genereert. Deze enzymen gebruiken de ontkoppeling van elektronen naar zuurstof na een omzetting van een substraat om zo de elektronen balans sluitend te maken. Dit geeft de oxidases een groot voordeel ten opzichte van alcohol dehydrogenases die gewoonlijk voor zulke reacties worden gebruikt. Als voorbeeld gebruiken we hier een aryl alcohol oxidase voor de productie van een industrieel relevante geurstof. Deze reactie verloopt zo goed dat niet de kinetiek van het enzym maar de fysische transportverschijnselen de limiterende factor worden. Vandaar dat wij on voornamelijk moeten richten op het reactor ontwerp, in plaats van het reactie ontwerp. We gebruiken micro-flow reactoren om zuurstof transport limitatie op te heffen en introduceren een tweede organische laag om substraat transport te verhogen.

Tot slot geven we in **hoofdstuk 9** een overzicht van de gepresenteerde resultaten en plaatsen we ze in perspectief ten opzichte van de wetenschappelijke literatuur. We geven aan dat de combinatie tussen biokatalyse en fotochemie, hoe intrigerend ook, zich nog in een te vroeg stadium bevindt om aantrekkelijk te zijn voor daadwerkelijke applicatie op productie schaal. Het gebruik van andere enzymen voor regeneratie is nog steeds de meest gangbare manier. Wij geloven echter dat de elektrochemische regeneratie van co-enzymen een veelbelovend alternatief is voor de toekomst.

Al met al presenteren wij in deze thesis een scala aan mogelijkheden voor de toepassing van oxidoreductases die afhankelijk zijn van zuurstof. Vanwege de unieke reactiviteit van zuurstof kan men uitdagingen tegenkomen die lastig op te lossen zijn via gebruikelijke methoden. We hopen hier te laten zien hoe het “lenen” van technieken uit andere wetenschappelijke velden zeer profijtelijk kan zijn voor het toepasbaar maken van deze veelbelovende katalysatoren.

Summary

In biocatalysis we use enzymes to accelerate chemical reactions. The advantage of enzymes over other chemical catalysts is their excellent performance in respect to reactivity, regioselectivity and enantioselectivity. The gentle environment at which they can optimally function further enhances their applicability to provide more sustainable alternatives for our chemical processes. The amount of different enzymes available to us is increasing, as is the variety of reactions we can catalyse with them.

Enzymes are divided in 7 classes, depending on the reactions they catalyse. The first class of enzymes, the one this thesis is focussing on, is the oxidoreductase family. As the name implies, these enzymes catalyse redox reactions, the specific transfer of electrons from or to a certain reactant. To close this redox-balance, these enzymes naturally rely on coenzymes, organic structures which are needed in a stoichiometric amount. As stoichiometric addition of these compounds would greatly strain the aspired reactions, both economically as ecologically, these coenzymes are conventionally regenerated using a second enzyme system and co-substrate. Though this practice is established, it does further complicate the reaction schemes and adds waste streams to the reaction. We therefore aim at replacing these systems with new alternatives.

Within the enzyme class of oxidoreductases, this thesis focuses on the subclass of oxidases and oxygenases, which all rely on oxygen in their reaction mechanisms. These enzymes are i.a. able to catalyse the regio- and enantioselective insertion of heteroatoms into molecular structures, even on inactivated bonds. These are reactions which are challenging, if not impossible, to perform using “classical” chemical methods.

We first use photochemistry to approach the challenge of coenzyme regeneration. In **chapter 2** we show an overview of the current state of the combinational field of biocatalysis and photochemistry. In **chapter 3**, we aim at contributing to this field by presenting a photochemical regeneration method for the co-enzyme, and photo mediator, FADH₂. This flavin will then drive a styrene monooxygenase. A proof of principle is established and the main bottlenecks are identified; mainly several side reactions that occur at the excited flavin. One issue found is the uncoupling of the electrons at the reduced flavin to oxygen. In other words, the oxygen, required for the enzyme catalysed reaction, can also directly take up the electrons from the mediator and form peroxide. This phenomenon is also called the oxygen dilemma and is seen for all monooxygenases. We therefore focussed on several ways to solve this challenge. The first option, as shown in **chapter 4**, is to replace regular flavins by deazaflavins as the photomediator.

Deazaflavins are promising as their reduced state has been reported to be stable against molecular oxygen. Unfortunately they appear to lose this stability upon illumination.

We therefore direct our attention to enzymes able to reverse the oxygen dilemma. This requires the use of the uncoupling mechanism to regenerate the active site, as done by the heme-containing proteins known as the peroxygenases. In their reaction mechanism, H_2O_2 directly attacks the heme group, forming the active compound I which supplies both the electrons as the oxygen atom. However, stoichiometric addition of H_2O_2 at the beginning of a reaction will oxidatively deactivate these proteins. These reactions are thus only viable when the H_2O_2 is supplied in a controlled manner. We therefore seek out to generate this H_2O_2 *in situ* in the reaction mixtures, ideally *via* reduction of oxygen at the expense of small sacrificial electron donors. We suggest a biocatalytic, an electrochemical and a photochemical method.

In **chapter 5**, we use the oxidation of sulfite to sulfate by a sulfite oxidase to provide the H_2O_2 . Here, the reactivity of sulfite itself appears to be pivotal. By switching between well- and poorly-soluble sulfite salts, the reaction performance can be significantly altered.

In **chapter 6**, we apply electrochemistry to generate the peroxide. In a way, electrochemistry is the most elegant way of atom efficient H_2O_2 generation as the electrons are directly used to reduce the oxygen. However, an over potential is needed to drive these reactions, increasing the amount of energy needed for the reaction. We therefore set out to use electrodes coated with oxidized carbon nanotubes, previously reported to lower this required over potential, to drive a vanadium dependant chloroperoxidase.

In **chapter 7**, we set out to generate the H_2O_2 using heterogeneous photo catalysts. Here we find graphitic carbon nitrides to be efficient at reducing oxygen at the expense of formate. One challenge in these reactions is the enzyme deactivation by reactive oxygen species and radicals concurrently generated by the photo excitable semiconductors. One solution to this problem that we suggest is the spatial separation of the photocatalyst and the biocatalyst within the reactor.

In chapter 5, 6 and 7 we focussed on reductive processes utilizing H_2O_2 . In **chapter 8** we show an alcohol oxidase to do the reversed in an oxidative manner. These enzymes use the uncoupling of the electrons to oxygen to release peroxide after a substrate conversion. This gives them a great advantage over the established alcohol dehydrogenases conventionally used for these reactions. As an example, we show the application of an aryl alcohol oxidase for the production of an industrially relevant fragrance. This reaction performs so well that not enzyme kinetics, but phase transfer

phenomena become rate-limiting. We tackle this challenge via reactor design, focussing on flow chemistry to alleviate oxygen transfer limitations and a two liquid phase approach to overcome substrate transfer limitations.

Finally, in **chapter 9**, we present an overview of the main results presented in this thesis and put them into perspective. We believe that the combination of biocatalysis and photochemistry, though intriguing, is still at an early stage in development and therefore not yet attractive for practical application. The biocatalytic regeneration of cofactors is the most conventional of those presented. We do believe though, that the electrochemical methods presented might prove to be an interesting alternative in the future.

Altogether, we have presented an array of different methods to apply oxidoreductases that rely on oxygen for their function. Because of the unique reactivity of oxygen, one can encounter challenges not easily solved with the classical ways. We really hope to convey the profitability of “borrowing” techniques from the other fields of science to approach these challenges.

Chapter 1



General introduction

Chapter 1

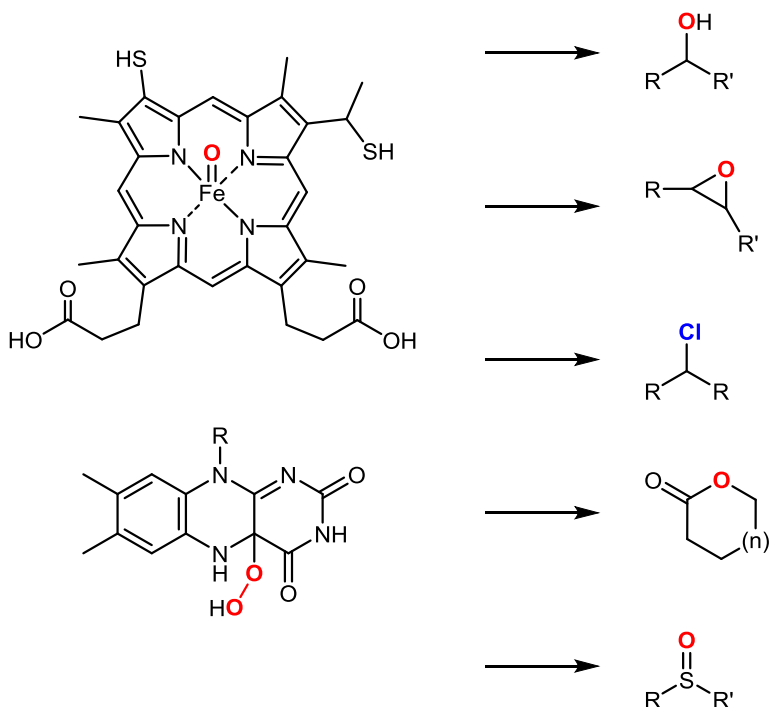
Biocatalysis

In 1897, Eduard Buchner found the formation of alcohols from sugar to occur upon addition of cell-free yeast extract. With this, he was the first to observe the proteins from the extract, the enzymes, to act as a catalyst for chemical reactions which later earned him the noble prize in chemistry [1]. Now, over a century later, we are able to modify, produce and use these biocatalysts to accelerate a large range of chemical reactions [2-4]. The application of enzymes for chemical synthesis comes with several perks. First of all, as is general for catalysts, enzymes can lower the amount of free energy needed for a certain reaction to occur. This results in a significant increase in reaction rates and, in some cases, obsoletes the need for stoichiometric amounts of reactant. Furthermore, enzymes generally excel at reaction specificity as compared to other chemical catalysts. Due to the specific architecture of the enzyme, these biocatalysts can very specifically alter the molecular structure of the compounds accepted, minimizing the amount of side products, and thus waste, produced. The mesotrophic conditions at which these enzymes can work further makes them the ideal candidates for performing “green chemistry” [5]. In other words, the use of enzymes for production of reagents used in our daily life, could significantly make our way of living more sustainable.

Enzymes are categorized into seven distinct classes. Amongst those, enzymes in the class of oxidoreductases (EC 1) are able to selectively transfer electrons from or to a substrate under environmentally benign conditions. This makes them very promising catalysts for the synthesis of chemicals needed for our daily life [6-8]. Within the class of oxidoreductases, there are several examples of enzymes able to activate oxygen. For example, oxygenases are able to activate molecular oxygen and to insert an oxygen atom into a chemical structure [9], whereas oxidases use molecular oxygen as an electron acceptor to close a redox-balance of a preceding reduction reaction [10]. These reactions can be very difficult, if not impossible, to perform using classical chemical methods. Here, especially on regio- and enantioselectivity, enzymes greatly excel over their chemical counterparts.

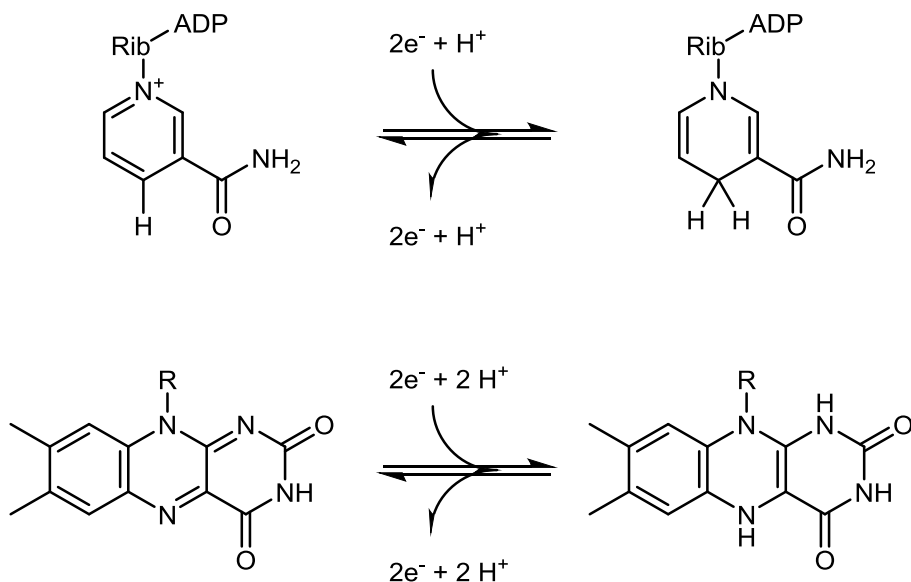
The chemistry happening at the enzyme active site is often enabled by cofactors. Common (metallo-) organic cofactors, and most relevant for this thesis, are the flavin [11, 12] and heme prosthetic groups (scheme 1) [13]. Furthermore, active sites of oxidoreductases can also contain inorganic cofactors such as copper [14], vanadium [15], (non-heme) iron [16], molybdopterin [17], tungstenpterin [18] or zinc groups [19]. These cofactors can be versatile in the type of reaction they catalyse. Flavoproteins can, for example, enable hydroxylation, epoxidation, halogenation, Baeyer-Villiger oxidation and sulfoxidation reactions [9]. The large scaffold of the enzyme, in turn, shapes the architecture of the

active site, thereby providing the high enantio- and regio-selectivity for the product converted.



Scheme 1: the versatility of flavin and heme prosthetic groups in oxygenation reactions.

Oxidoreductases owe these extraordinary properties to millions of years of evolution aimed at smoothly guiding all the redox-processes occurring in a living cell. To guarantee a controlled transfer of electrons from the solution to the active site and *vice versa*, most oxidoreductases rely on coenzymes as carriers. These coenzymes mainly encompass nicotinamide and flavin structures, as depicted in scheme 2. In other cases, complete proteins, like ferredoxins, can act as electron carrier.



Scheme 2: The oxidized (left) and reduced (right) state of nicotinamide (top) and flavin (bottom) coenzymes. For flavins, also a semiquinone radical intermediate state is possible in the case of single electron transfers.

Their preference for these electron carriers, however, becomes an issue when one tries to take the enzyme outside the cell and use it in a reactor. This, as a stoichiometric amount of the coenzyme is needed, which would significantly increase the cost and environmental impact of the reaction [20].

Coenzyme regeneration

The classical solution to this challenge is to have these compounds present in a catalytic amount and to introduce a regeneration system, either *in vivo* or *in vitro*. The *in vivo* solution would be to express the biocatalytic reaction in a host, which will then consume an energy-rich substrate to obtain the reducing equivalents [21]. For the other option, the *in vitro* approach, a second enzyme regenerating the coenzyme at the expense of a cosubstrate is introduced to the reaction [22].

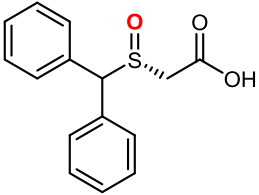
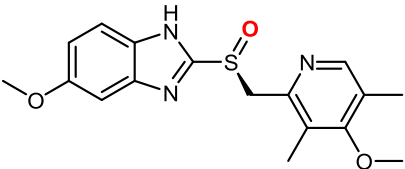
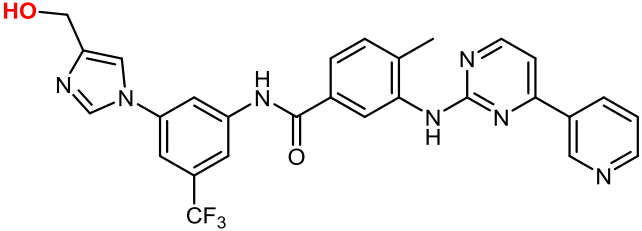
Neither of these systems are ideal. The implementation of the desired redox reaction into a microorganism is relatively cost-effective, but requires consideration of all the side reactions occurring in a living cell. Both substrate and product could participate in other

metabolic processes, stirring the carbon flux away from the desired product. In addition, the high concentrations of substrate and product required to make the system economical, 100 to 250 mM in the case of small compounds [23], could affect the well-being of the host.

For the biocatalytic regeneration of coenzymes, the biocatalyst of choice is often an alcohol dehydrogenase (ADH) or a ketoreductase (KRED). The second enzyme oxidizes an alcohol to a ketone to provide the reducing equivalents of a coenzyme while the reverse reaction is applied to drive oxidative reactions. The introduction of a second enzyme to the reaction can often turn out unfavourable. First, the two biocatalytic reactions need to be compatible in temperature, pH and substrate in order to function in the same solution. Often, compromises need be made to make both work. Second, stoichiometric amounts of cosubstrate are required, which decreases the atom efficiency. Furthermore stoichiometric amounts of coproduct are formed, which complicates downstream processing [24]. Despite these hurdles, multiple examples of oxygenases producing industrially relevant compounds are reported [25]. Notable examples are shown in table 1.

Chapter 1

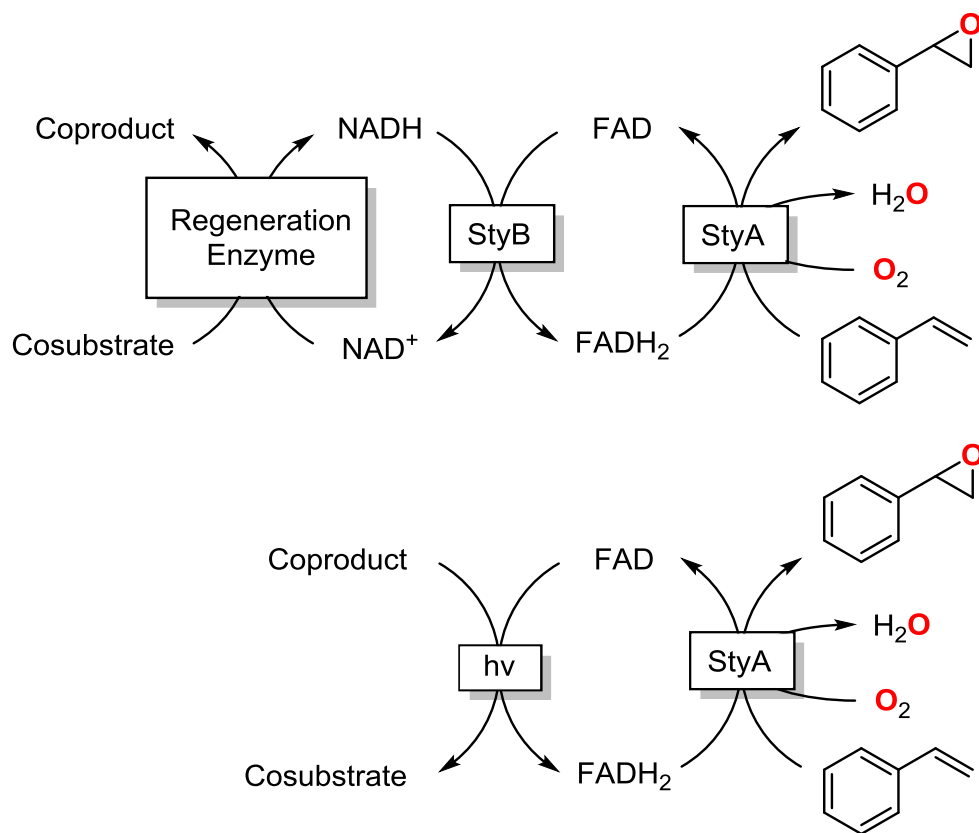
Table 1: Examples from industry of pharmaceuticals where oxidoreductases were involved for the production of pharmaceuticals. CHMO: Cyclohexanone monooxygenase. CYP450: Cytochrome P450. KRED: Ketoreductase. PrOH: isopropanol. PEG: Polyethyleneglycol. DMSO: Dimethylsulfoxide. All shown examples were designed by Codexis.

Enzyme	Product	Specifications
CHMO	 <p>Armodafinil</p>	<p>NADPH, FADH₂, KRED Water/PrOH/ PEG 35 °C, 48 h 15 g isolated yield</p>
CHMO	 <p>Esomeprazole</p>	<p>NADPH, KRED Buffer pH 9.0/PrOH 25 °C, 48 h 87% yield 26 g isolated yield</p>
CYP450	 <p>Nilotinib</p>	<p>Water/DMSO, 30 °C 34% conversion 10 mg isolated yield</p>

In summary, the regeneration methods available at the moment mainly rely on second enzyme systems for coenzyme regeneration, which leads to elaborate reaction schemes. Despite this, the selectivity of these oxygenases can still make them the catalyst of choice in cases of highly valuable end products. Still, considerable gain can be achieved by finding ways around these regeneration methods, both in terms of cost and simplicity. Consequently, an increasing amount of research is performed on finding alternative ways to regenerate oxidoreductase systems.

Alternative regeneration methods for oxygenases

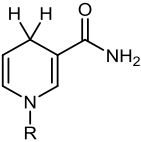
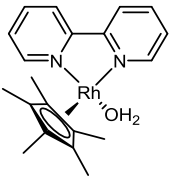
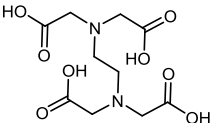
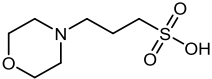
Several reviews already discuss methods for indirect regeneration of oxidoreductases: to keep the interaction between the coenzyme and enzyme intact, but to regenerate the coenzyme in a non-biocatalytic manner (scheme 3). Research has mainly focussed on regenerating flavin coenzymes, rather than nicotinamide coenzymes. This could be explained by the more versatile chemistry of the flavin, like the possibilities of accepting photons or single electrons, which creates more options for creative solutions in balancing redox reactions [12, 26]. Furthermore, in the case of chemical regeneration of NADH, the regeneration can be complicated by the formation of reduced isomers or dimers of the nicotinamide ring [27]. This formation of biologically inactive variants is circumvented with biocatalytic regeneration methods.



Scheme 3: Example of an alternative regeneration method in order to simplify electron transfer schemes, as elaborated in **chapter 3**. Instead of three enzymes, only a monooxygenase and a light source are required.

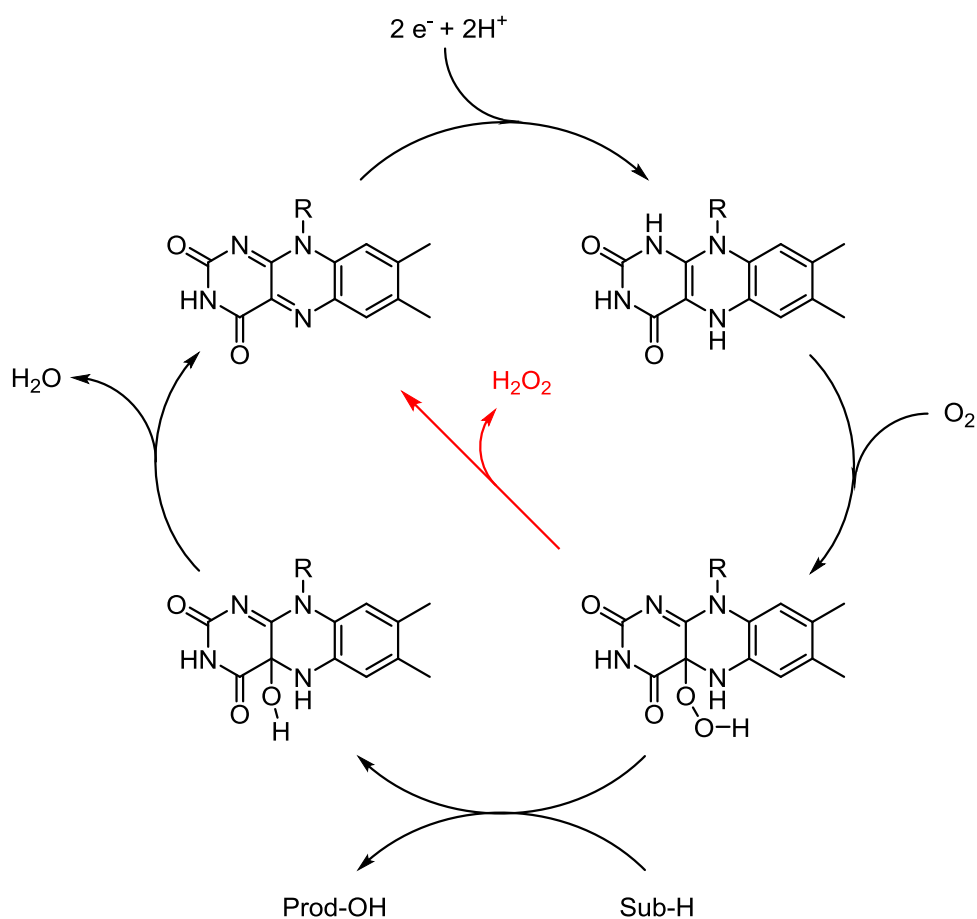
For flavins and flavoenzymes, the reported regeneration methods are numerous. Amongst others, flavins have been reduced using homogenous catalysis, heterogeneous catalysis, electrochemistry and photochemistry. Some examples are summarized in table 2.

Table 2: Assortment of alternative regeneration methods of flavoenzymes. StyA: Styrene monooxygenase. CYP450: Cytochrome P450. RebH: Halogenase from *Lechevalieria aerocolonigenes*. OYE: Old yellow enzyme. PAMO: Phenylacetone monooxygenase.

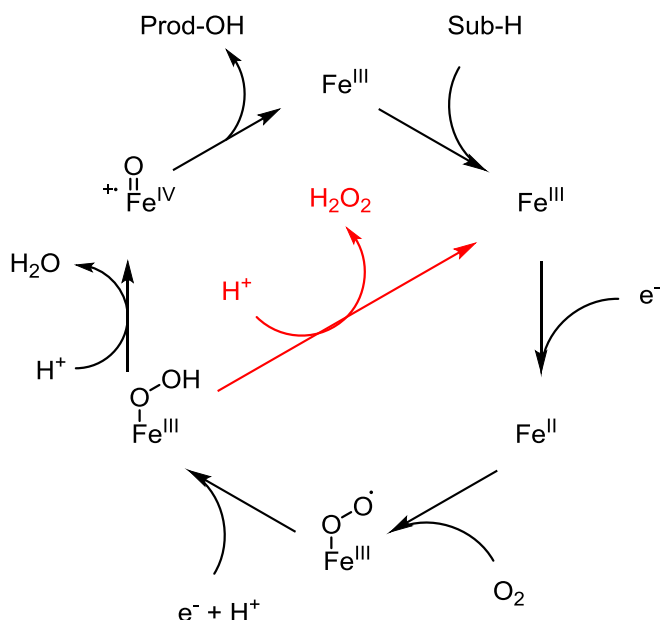
Method	Co-catalyst	Electron donor	Enzyme	Reaction	Ref
Nicotinamide mimics	-		StyA	Epoxidation	[28]
			CYP450	Hydroxylation	[29]
			RebH	Halogenation	[30]
			OYE	Ene reduction	[31]
Rhodium catalyst		HCOOH	StyA	Epoxidation	[32]
		Cathode	OYE	Ene reduction	[33]
Electro-chemistry	-	Cathode	StyA	Epoxidation	[34, 35]
			CYP450	Hydroxylation	[36]
Photo-chemistry	FMN		OYE	Ene reduction	[37]
			PAMO	Bayer-Villiger oxidation	[38]
	TiO ₂		OYE	Ene reduction	[39]

The oxygen dilemma

If oxygenase-catalysed reactions are considered, one challenge is the so-called oxygen dilemma [40]. When molecular oxygen is bound to the reduced flavin or heme group in the enzyme active site, the reaction sequence does not necessarily follow the enzymatic oxygenation reaction of a substrate. Instead, the oxygen can also be eliminated, forming hydrogen peroxide in the process, which results in a loss of electrons. This phenomenon is called uncoupling of the electron flow.



Scheme 4: Redox cycle and oxygen activation for flavins, with the uncoupling of electrons in red.



Scheme 5: Redox cycle and oxygen activation of the iron in heme groups. The uncoupling of electrons is shown in red.

The extent of uncoupling is influenced by factors like substrate and product concentration and the active site architecture. It occurs in as much as 30% of reaction cycles for so-called “cautious” monooxygenases (oxygenases that rely on the substrate to be readily available to avoid uncoupling) [41, 42]. As a consequence, up to one third of all electrons invested into the system are lost. The peroxide formed can also induce oxidative damage to the reaction components, but this harm can easily be averted by adding catalase to the reaction mixture. Furthermore, uncoupling not only occurs at the flavin and heme groups in enzyme active sites, but also affects free flavins and other mediators in solution or with electron transfer proteins. In the least favourable conditions, for instance when the reaction requires free diffusible flavins, the formation of H_2O_2 occurs for up to three quarters of the reduced flavins [32].

The oxygen dilemma can thus pose a large strain on the efficiency of monooxygenase-catalysed reactions. This is why several methods have been developed to work around, or minimize the effects of the side reaction. Efforts can be made on the enzyme engineering side, to make sure the C4a-peroxide flavin intermediate (scheme 1) is stabilized [43, 44]. On the other hand, reaction engineering can increase the efficiency: *In situ* product removal can decrease the uncoupling constants within the enzyme active site [45], while

Chapter 1

shortening of electron transfer chains can reduce electron loss towards the enzyme [46]. Furthermore, mediators less sensitive to uncoupling, like deazaflavins, can be applied [47, 48]. In general, mediators which participate in hydride transfers are less likely to react with oxygen than those able to be reduced *via* single electron transfers [49].

Peroxygenases

Oxygenases are able to catalyse some compelling reactions but can suffer from the oxygen dilemma. There are, however, alternative enzymes which can actually exploit the uncoupling reaction. This tactic can be approached with two distinct enzyme classes, the oxidases and the peroxygenases. Oxidases are mostly flavin containing enzymes, though examples of molybdenum [50] and copper [51] containing proteins also exist. As the name implies, these enzymes are able to perform oxidation reactions on an array of compounds. To close the electron balance, the electrons are subsequently uncoupled by oxygen, forming H_2O_2 , the unwanted reaction in the case of oxygenases.

For peroxygenases, the reversed path for H_2O_2 is used, *i.e.* peroxide directly attacks the oxidized coenzyme in order to form the active oxygenating species. Through this pathway, both the oxygen atom as the reducing equivalents are delivered. Though examples exist for flavoproteins [52] and vanadium containing halogenases [53], most reactions come from the heme-containing class of peroxygenases [54-56]. In these enzymes, the peroxide shunt pathway (red arrow in scheme 5) is reversed to form the active compound I species. This enables access to similar reactions as catalysed by other heme-oxygenases, but at the expense of peroxides instead of NAD(P)H and oxygen. In other words, both the need for an electron transport chain as the risk of electron loss *via* uncoupling are negated. The reactions catalysed are similar to those of their counterpart, the P450s. On the other hand, the availability of these peroxygenases is not yet as elaborate. Momentarily considerable work is invested in peroxygenase protein engineering and expanding the substrate scope for this class of enzymes.

Though the use of these peroxygenases results in much less complicated reaction schemes, they come with one main challenge. This is the sensitivity of the peroxygenases for the peroxide. As H_2O_2 is also a strong oxidant, a significant amount in solution could initiate the oxidation of labile amino acids on the peroxygenase surface [57]. Furthermore, heme-bleaching of the peroxygenase might occur, which is presumably due to the reaction between the compound III state of the heme coenzyme and H_2O_2 [58-60]. The exchange of oxidative prone-amino acids on the enzyme surface to more stable ones *via* protein engineering has been proven to be a viable solution [61], as is the tactic of enzyme

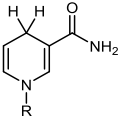
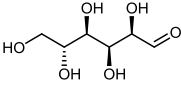
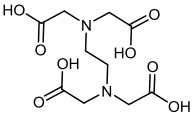
immobilization [62]. Furthermore, the addition of organoperoxides instead of hydrogen peroxide reduces the oxidative conditions in the reaction [63]. The most practical and universally applicable technique though, is the *in situ* generation of H_2O_2 *via* the reduction of molecular oxygen [54].

The most prominent example of *in situ* H_2O_2 generation is that of glucose oxidase [64]. In this system, glucose is added as a cosubstrate and oxidized to gluconolactone. The reduced flavin at the oxidase is subsequently uncoupled with oxygen to form the H_2O_2 . Though this method excels in simplicity, it will not support the progress of peroxygenases to larger applications. A large excess of glucose will greatly increase the viscosity of the solution and the product of the reaction in turn will acidify the solution. From green chemistry point of view the use of a 180 g/mol substrate to generate a 34 g/mol product cannot be considered benign.

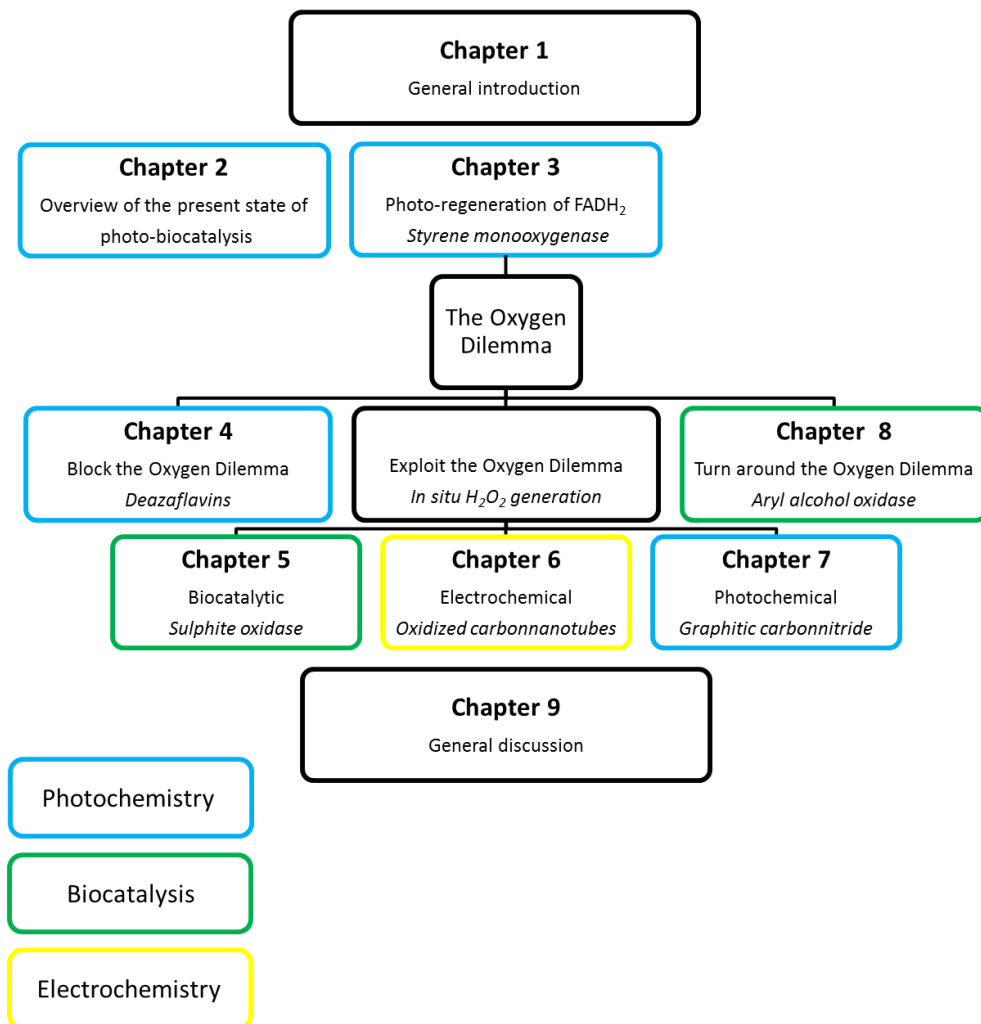
An array of alternatives have been reported in literature. Methods which generate the peroxide range from chemical, to biocatalytic, electrochemical and photochemical. For the generation method to work, it would need to reduce a steady amount of oxygen, while minimizing its effect on the peroxygenase. Some examples are shown in table 3.

Chapter 1

Table 3: Assortment of *in situ* H₂O₂ generation methods for peroxygenases. GOx: Glucose oxidase. AAOx: Aryl alcohol oxidase. FDM: Formate dismutase. FDH: Formate dehydrogenase. 3HB6H: 3-Hydroxybenzoate-6-hydroxylase. FOx: Formate oxidase. SWNT: Single walled nanotubes. MB: Methylene blue. PS: Phenosafranine. Au-TiO₂: Gold-doped titanium dioxide.

Method	Co-catalyst	Electron donor	Ref.
Chemical	Pd(0)	H ₂	[65]
	FMN		[66]
Biocatalytic	GOx		[67]
	AAOx / FDM / FDH / 3HB6H / NAD ⁺	MeOH	[68]
	FOx	HCOOH	[69]
Electro-chemical	-	Cathode	[70]
	Flavin-SWNT	Cathode	[71]
Photo-chemical	FMN		[72]
	FMN / MB / PS / FDH / NAD ⁺	HCOOH	[73]
	Au-TiO ₂	HCOOH	[74]
		H ₂ O	[75]
Nuclear	-	H ₂ O	[76]

Outline of the thesis



Scheme 6: Overview of the thesis outline. The catalysts used for the chapters are written in cursive.

Chapter 1

This thesis aims to elaborate a multitude of alternative ways for applying oxidoreductases in chemical synthesis reactions without relying on classical regeneration systems to provide the redox-equivalents. Specifically, we focus on biocatalysts able to use oxygen for their reactions.

After the general introduction in **chapter 1**, the first three chapters focus on photochemistry. In **chapter 2**, we give an overview of the present state of the use of photochemistry in biocatalysis.

In **chapter 3** we attempt to contribute to this field by presenting a photochemical regeneration method for FADH₂, at the expense of EDTA, to enable the enantioselective epoxidation of styrene by a styrene monooxygenase. A proof of concept is provided and the limitations of the suggested system are indicated.

One prominent challenge in these reactions appears to be the oxygen dilemma; the paradox of molecular oxygen which is needed as a substrate for these reactions but is also responsible for the uncoupling of electrons and loss of reducing equivalents. The rest of the thesis therefore aims at how to deal with this phenomenon with different approaches

We aim to block the oxygen dilemma in **chapter 4**, by investigation of the use of deazaflavins as photo excitable mediators for biocatalytic reactions. Unlike their natural counterparts, reduced deazaflavins are reported to be stable in presence of molecular oxygen and should therefore be able to counter the uncoupling. In this chapter, an example of coupling the photo-reduction of deazaflavins to an ene-reductase is shown.

We aim to exploit the oxygen dilemma in **chapter 5, 6 and 7**. Our approach here is to use peroxygenases, which are able to regenerate their active site with H₂O₂ to invert the uncoupling pathway usually observed in heme-proteins. The challenge here is to find efficient ways to generate the H₂O₂ *in situ*.

In **chapter 5** sulphite oxidases are tested as candidates for the biocatalytic generation of H₂O₂. In this case, sulphite is the sacrificial electron donor for the reaction, but the ions can also participate in chemo-enzymatic follow-up reactions. This reaction is then coupled to unspecific peroxygenases.

In **chapter 6** we focus on the electrochemical generation of H₂O₂. Specifically, we focus on the use of oxidized carbon nanotubes at the cathodic reaction side in order to decrease the required over-potential needed for oxygen reduction. The H₂O₂, in turn, used to drive a vanadium-dependant chloroperoxygenase.

In **chapter 7** the photochemical generation of H_2O_2 is evaluated. Here we expand the variety of heterogeneous catalysts for this purpose. Furthermore, we point out and solve some challenges and limitations of such chemo-enzymatic systems in combination with unspecific peroxygenases.

In **chapter 8** we aim at turning around the oxygen dilemma. Specifically, we focussed on the application of an aryl alcohol oxidase which performs oxidation reactions and actually uses the uncoupling with oxygen to close the redox balance. This works so well that not the enzyme, but the availability of substrates *via* phase transfers become reaction limiting. We improved the reaction design in order to overcome these transfer limitations.

Finally, in **chapter 9**, we place the obtained results into perspective with the state of the art literature available. Furthermore, we evaluate the opportunities and limitations of the investigated reactions.

References:

1. Buchner, E. and R. Rapp, *Alkoholische gährung ohne hefezellen*. Berichte der Deutschen Chemischen Gesellschaft, 1897. **30**(3): p. 2668-2678.
2. Bornscheuer, U., et al., *Engineering the third wave of biocatalysis*. Nature, 2012. **485**(7397): p. 185.
3. Cirino, P.C. and F.H. Arnold, *Protein engineering of oxygenases for biocatalysis*. Current Opinion in Chemical Biology, 2002. **6**(2): p. 130-135.
4. Roelfes, G., *LmrR: A privileged scaffold for artificial metalloenzymes*. Accounts of Chemical Research, 2019. **52**(3): p. 545-556.
5. Sheldon, R.A., *Metrics of green chemistry and sustainability: Past, present, and future*. ACS Sustainable Chemistry & Engineering, 2018. **6**(1): p. 32-48.
6. Hollmann, F., et al., *Enzyme-mediated oxidations for the chemist*. Green Chemistry, 2011. **13**(2): p. 226-265.
7. Hollmann, F., I.W.C.E. Arends, and D. Holtmann, *Enzymatic reductions for the chemist*. Green Chemistry, 2011. **13**(9): p. 2285-2313.
8. Dong, J.J., et al., *Biocatalytic oxidation reactions: A chemist's perspective*. Angewandte Chemie-International Edition, 2018. **57**(30): p. 9238-9261.
9. Huijbers, M.M., et al., *Flavin dependent monooxygenases*. Arch Biochem Biophys, 2014. **544**: p. 2-17.
10. Ewing, T., M. Fraaije, and W. van Berkel, *Oxidations using alcohol oxidases*, in *Science of Synthesis. Biocatalysis in Organic Synthesis 3*. 2014, Thieme. p. 157-185.
11. Fraaije, M.W. and A. Mattevi, *Flavoenzymes: diverse catalysts with recurrent features*. Trends in Biochemical Sciences, 2000. **25**(3): p. 126-132.
12. Romero, E., et al., *Same substrate, many reactions: Oxygen activation in flavoenzymes*. Chemical Reviews, 2018. **118**(4): p. 1742-1769.
13. Dubey, K.D. and S. Shaik, *Cytochrome P450-The wonderful nanomachine revealed through dynamic simulations of the catalytic cycle*. Accounts of Chemical Research, 2019. **52**(2): p. 389-399.
14. Guan, Z.B., et al., *Bacterial laccases: promising biological green tools for industrial applications*. Cellular and Molecular Life Sciences, 2018. **75**(19): p. 3569-3592.
15. Dong, J.J., et al., *Halofunctionalization of alkenes by vanadium chloroperoxidase from *Curvularia inaequalis**. Chemical Communications, 2017. **53**(46): p. 6207-6210.
16. de Visser, S.P., *Mechanistic insight on the activity and substrate selectivity of nonheme iron dioxygenases*. Chemical Record, 2018. **18**(10): p. 1501-1516.
17. Belaidi, A.A., et al., *Oxygen reactivity of mammalian sulfite oxidase provides a concept for the treatment of sulfite oxidase deficiency*. Biochemical Journal, 2015. **469**(2): p. 211-221.
18. Bevers, L.E., et al., *WOR5, a novel tungsten-containing aldehyde oxidoreductase from *Pyrococcus furiosus* with a broad substrate specificity*. Journal of Bacteriology, 2005. **187**(20): p. 7056-7061.
19. Plapp, B.V., et al., *Horse liver alcohol dehydrogenase: Zinc coordination and catalysis*. Biochemistry, 2017. **56**(28): p. 3632-3646.
20. Zhang, W. and F. Hollmann, *Nonconventional regeneration of redox enzymes - a practical approach for organic synthesis?* Chemical Communications, 2018. **54**(53): p. 7281-7289.
21. Rudroff, F., *Whole-cell based synthetic enzyme cascades-light and shadow of a promising technology*. Current Opinion in Chemical Biology, 2019. **49**: p. 84-90.
22. Kragl, U., et al., *Enzyme engineering aspects of biocatalysis: cofactor regeneration as example*. Biotechnology and Bioengineering, 1996. **52**(2): p. 309-319.

23. Huisman, G.W. and S.J. Collier, *On the development of new biocatalytic processes for practical pharmaceutical synthesis*. Current Opinion in Chemical Biology, 2013. **17**(2): p. 284-292.
24. Zambianchi, F., et al., *Use of isolated cyclohexanone monooxygenase from recombinant Escherichia coli as a biocatalyst for Baeyer–Villiger and sulfide oxidations*. Biotechnology and Bioengineering, 2002. **78**(5): p. 489-496.
25. Hughes, D.L., *Biocatalysis in drug development—Highlights of the recent patent literature*. Organic Process Research & Development, 2018. **22**(9): p. 1063-1080.
26. Chaiyen, P., M.W. Fraaije, and A. Mattevi, *The enigmatic reaction of flavins with oxygen*. Trends in Biochemical Sciences, 2012. **37**(9): p. 373-380.
27. Hofler, G.T., et al., *A Photoenzymatic NADH Regeneration System*. Chembiochem, 2018. **19**(22): p. 2344-2347.
28. Paul, C.E., et al., *Nonenzymatic regeneration of styrene monooxygenase for catalysis*. ACS Catalysis, 2015. **5**(5): p. 2961-2965.
29. Ryan, J.D., R.H. Fish, and D.S. Clark, *Engineering cytochrome P450 enzymes for improved activity towards biomimetic 1, 4-NADH cofactors*. ChemBioChem, 2008. **9**(16): p. 2579-2582.
30. Ismail, M., et al., *Straightforward regeneration of reduced flavin adenine dinucleotide required for enzymatic tryptophan halogenation*. ACS Catalysis, 2019. **9**(2): p. 1389-1395.
31. Paul, C.E., et al., *Mimicking nature: synthetic nicotinamide cofactors for C=C bioreduction using enoate reductases*. Organic Letters, 2013. **15**(1): p. 180-183.
32. Hollmann, F., et al., *Stereospecific biocatalytic epoxidation: The first example of direct regeneration of a FAD-dependent monooxygenase for catalysis*. Journal of the American Chemical Society, 2003. **125**(27): p. 8209-8217.
33. Tosstorff, A., et al., *Towards electroenzymatic processes involving old yellow enzymes and mediated cofactor regeneration*. Engineering in Life Sciences, 2017. **17**(1): p. 71-76.
34. Hollmann, F., et al., *Direct electrochemical regeneration of monooxygenase subunits for biocatalytic asymmetric epoxidation*. Journal of the American Chemical Society, 2005. **127**(18): p. 6540-6541.
35. Ruinatscha, R., et al., *Productive asymmetric styrene epoxidation based on a next generation electroenzymatic methodology*. Advanced Synthesis & Catalysis, 2009. **351**(14-15): p. 2505-2515.
36. Holtmann, D., K.-M. Mangold, and J. Schrader, *Entrapment of cytochrome P450 BM-3 in polypyrrole for electrochemically-driven biocatalysis*. Biotechnology Letters, 2009. **31**(5): p. 765-770.
37. Grau, M.M., et al., *Photoenzymatic reduction of C=C double bonds*. Advanced Synthesis & Catalysis, 2009. **351**(18): p. 3279-3286.
38. Taglieber, A., et al., *Light-driven biocatalytic oxidation and reduction reactions: scope and limitations*. ChemBioChem, 2008. **9**(4): p. 565-572.
39. Mifsud, M., et al., *Photobiocatalytic chemistry of oxidoreductases using water as the electron donor*. Nature Communications, 2014. **5**.
40. Holtmann, D. and F. Hollmann, *The oxygen dilemma: A severe challenge for the application of monooxygenases?* Chembiochem, 2016. **17**(15): p. 1391-1398.
41. Palfey, B.A. and C.A. McDonald, *Control of catalysis in flavin-dependent monooxygenases*. Arch Biochem Biophys, 2010. **493**(1): p. 26-36.
42. Suske, W.A., et al., *Purification and characterization of 2-hydroxybiphenyl 3-monooxygenase, a novel NADH-dependent, FAD-containing aromatic hydroxylase from Pseudomonas azelaica HBP1*. Journal of Biological Chemistry, 1997. **272**(39): p. 24257-24265.

43. Alfieri, A., et al., *Revealing the moonlighting role of NADP in the structure of a flavin-containing monooxygenase*. Proceedings of the National Academy of Sciences, 2008. **105**(18): p. 6572-6577.
44. Leferink, N.G.H., et al., *Identification of a gatekeeper residue that prevents dehydrogenases from acting as oxidases*. Journal of Biological Chemistry, 2009. **284**(7): p. 4392-4397.
45. Hilker, I., et al., *Preparative scale Baeyer–Villiger biooxidation at high concentration using recombinant Escherichia coli and in situ substrate feeding and product removal process*. Nature Protocols, 2008. **3**: p. 546.
46. Torres Pazmiño, D.E., et al., *Self-sufficient Baeyer–Villiger monooxygenases: Effective coenzyme regeneration for biooxygenation by fusion engineering*. Angewandte Chemie International Edition, 2008. **47**(12): p. 2275-2278.
47. Zilly, F.E., et al., *Deazaflavins as mediators in light-driven cytochrome P450 catalyzed hydroxylations*. Chemical Communications, 2009(46): p. 7152-7154.
48. Bliese, M., et al., *Photo-reduction of deazaflavin - spectroscopic investigations*. Australian Journal of Chemistry, 1983. **36**(9): p. 1873-1883.
49. Hemmerich, P., V. Massey, and H. Fenner, *Flavin and 5-deazaflavin - chemical evaluation of modified flavoproteins with respect to mechanisms of redox biocatalysis*. Febs Letters, 1977. **84**(1): p. 5-21.
50. Schwarz, G., R.R. Mendel, and M.W. Ribbe, *Molybdenum cofactors, enzymes and pathways*. Nature, 2009. **460**: p. 839.
51. Mayer, A.M., *Polyphenol oxidases in plants and fungi: Going places? A review*. Phytochemistry, 2006. **67**(21): p. 2318-2331.
52. de Gonzalo, G., et al., *Turning a riboflavin-binding protein into a self-sufficient monooxygenase by cofactor redesign*. Chemical Communications, 2011. **47**(39): p. 11050-11052.
53. Hemrika, W., et al., *Heterologous expression of the vanadium-containing chloroperoxidase from Curvularia inaequalis in Saccharomyces cerevisiae and site-directed mutagenesis of the active site residues His496, Lys353, Arg360, and Arg490*. Journal of Biological Chemistry, 1999. **274**(34): p. 23820-23827.
54. Burek, B.O., et al., *Hydrogen peroxide driven biocatalysis*. Green Chemistry, 2019.
55. van Rantwijk, F. and R.A. Sheldon, *Selective oxygen transfer catalysed by heme peroxidases: synthetic and mechanistic aspects*. Current Opinion in Biotechnology, 2000. **11**(6): p. 554-564.
56. Bormann, S., et al., *Specific oxyfunctionalisations catalysed by peroxygenases: opportunities, challenges and solutions*. Catalysis Science & Technology, 2015. **5**(4): p. 2038-2052.
57. Stadtman, E. and R. Levine, *Free radical-mediated oxidation of free amino acids and amino acid residues in proteins*. Amino acids, 2003. **25**(3-4): p. 207-218.
58. Valderrama, B., M. Ayala, and R. Vazquez-Duhalt, *Suicide inactivation of peroxidases and the challenge of engineering more robust enzymes*. Chemistry & Biology, 2002. **9**(5): p. 555-565.
59. Hernandez, K., et al., *Hydrogen peroxide in biocatalysis. A dangerous liaison*. Current Organic Chemistry, 2012. **16**(22): p. 2652-2672.
60. Karich, A., et al., *Exploring the catalase activity of unspecific peroxygenases and the mechanism of peroxide-dependent heme destruction*. Journal of Molecular Catalysis B: Enzymatic, 2016. **134**: p. 238-246.
61. Kim, S.J., et al., *Development of the radical-stable Coprinus cinereus peroxidase (CiP) by blocking the radical attack*. Journal of biotechnology, 2014. **189**: p. 78-85.

62. Vasudevan, P. and R. Weiland, *Deactivation of catalase by hydrogen peroxide*. Biotechnology and Bioengineering, 1990. **36**(8): p. 783-789.
63. Fernández-Fueyo, E., et al., *Towards preparative peroxygenase-catalyzed oxyfunctionalization reactions in organic media*. Journal of Molecular Catalysis B: Enzymatic, 2016. **134**: p. 347-352.
64. Pereira, P.C., I. Arends, and R.A. Sheldon, *Optimizing the chloroperoxidase-glucose oxidase system: The effect of glucose oxidase on activity and enantioselectivity*. Process Biochemistry, 2015. **50**(5): p. 746-751.
65. Karmee, S.K., et al., *Chemo-enzymatic cascade oxidation in supercritical carbon dioxide/water biphasic media*. Green Chemistry, 2009. **11**(7): p. 1052-1055.
66. Paul, C.E., et al., *In situ formation of H₂O₂ for P450 peroxygenases*. Bioorganic & Medicinal Chemistry, 2014. **22**(20): p. 5692-5696.
67. van Deurzen, M.P.J., F. van Rantwijk, and R.A. Sheldon, *Selective oxidations catalyzed by peroxidases*. Tetrahedron, 1997. **53**(39): p. 13183-13220.
68. Ni, Y., et al., *Peroxygenase-catalyzed oxyfunctionalization reactions promoted by the complete oxidation of methanol*. Angewandte Chemie International Edition, 2016. **55**(2): p. 798-801.
69. Tieves, F., et al., *Formate oxidase (FOx) from Aspergillus oryzae: One catalyst enables diverse H₂O₂-dependent biocatalytic oxidation reactions*. Angewandte Chemie International Edition, 2019. **58**(23): p. 7873-7877.
70. Horst, A.E.W., et al., *Electro-enzymatic hydroxylation of ethylbenzene by the evolved unspecific peroxygenase of Agrocybe aegerita*. Journal of Molecular Catalysis B: Enzymatic, 2016. **133**: p. S137-S142.
71. Choi, D.S., et al., *Photoelectroenzymatic oxyfunctionalization on flavin-hybridized carbon nanotube electrode platform*. Acs Catalysis, 2017. **7**(3): p. 1563-1567.
72. Churakova, E., et al., *Specific photobiocatalytic oxyfunctionalization reactions*. Angewandte Chemie International Edition, 2011. **50**(45): p. 10716-10719.
73. Willot, S.J.P., et al., *Expanding the spectrum of light-driven peroxygenase reactions*. ACS Catalysis, 2019. **9**(2): p. 890-894.
74. Zhang, W., et al., *Selective activation of C-H bonds in a cascade process combining photochemistry and biocatalysis*. Angewandte Chemie International Edition, 2017. **56**(48): p. 15451-15455.
75. Zhang, W., et al., *Selective aerobic oxidation reactions using a combination of photocatalytic water oxidation and enzymatic oxyfunctionalizations*. Nature Catalysis, 2018. **1**(1): p. 55-62.
76. Zhang, W., et al., *Radiolysis-induced water splitting to drive H₂O₂-dependent oxyfunctionalisation reactions*. Manuscript in preparation.

Chapter 2



Photocatalysis to promote cell-free biocatalytic reactions

Georg T. Höfler, Frank Hollmann, Caroline E. Paul, Marine C.R. Rauch, Morten M.C.H. van Schie, Sébastien J.-P. Willot

Based on:

Höfler G.T., Hollmann F., Paul C.E., Rauch M.C.R., Van Schie M.M.C.H., Willot S.J.-P., The autotrophic biorefinery: Organisms and enabling technologies. 2020: De Gruyter

Summary

In photocatalysis, light is used as a weightless and traceless reactant to excite catalysts and enable reactions otherwise not possible in dark. This principle can be elegantly applied for biocatalytic redox reactions as an alternative method to regenerate redox couples. The combination of these two fields is now slowly getting more attention and more examples are published on it every year. In this chapter, we give an overview of this field, compare the different methods and show some limitations.

Introduction

Organic synthesis using enzymes is usually called biocatalysis. During the past decades, biocatalysis has been enjoying an ever increasing popularity amongst synthetic organic chemists. Especially, the mild reaction conditions and the usually high selectivity of enzyme-catalysed reactions are valued on lab and industrial scale [1-4].

While industrial biocatalysis mostly relies on one-step transformations the trend in academic research more and more shifts towards multi-step syntheses transforming simple starting materials into significantly more complex (and value-added) products [5,6]. Such cascade reactions are particularly attractive if intermediate product isolation and – purification can be omitted leading to significant savings in solvent use and reduced environmental footprints [7]. Cascades comprising several enzymatic steps or combining transition metal catalysis, organo catalysis or heterogeneous catalysis are frequently reported nowadays [5,6]. Following them, photoenzymatic reactions (combining photocatalytic reactions with biocatalytic ones) are catching up [8-11].

Photobiocatalysis using isolated enzymes can be divided into (1) photocatalytic regeneration cascades, (2) ‘true’ photoenzymatic cascades and (3) photoenzymatic reactions. In photoenzymatic cascades, redox enzymes are supplied with redox equivalents needed for their catalytic cycles, i.e. photocatalytic regeneration of redox enzymes. ‘True’ photoenzymatic cascades combine a biocatalytic transformation with a photocatalytic generation of the enzyme’s starting material or a follow-up step of the enzymatic product. ‘Photoenzymes’ need light to perform their catalytic reaction.

In this contribution we critically review the current state-of-the-art of all types of photoenzymatic cascades.

Photocatalysis to regenerate redox enzymes

Reductive regeneration

A broad range of biocatalytic redox reactions require reductive regeneration, i.e. provision of the production enzyme with reducing equivalents. First, reduction reactions catalysed by reductases obviously require reducing equivalents. However, a wide variety of oxidation reactions involve reduction of the production enzymes (monooxygenases). This seeming contradiction can be explained by the catalytic mechanism of monooxygenases: molecular oxygen is reductively activated at the enzymes’ active sites to be incorporated into the substrates.

Principally, reductive regeneration of redox enzymes can be achieved either directly, i.e. by direct reduction of the enzymes' active sites or indirectly, i.e. involving the nicotinamide cofactors. Both approaches will be outlined in the following sections.

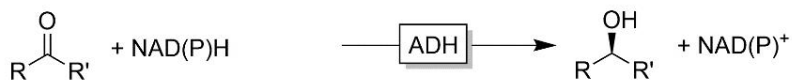
Via regeneration of reduced nicotinamide cofactors

The reduced nicotinamide cofactors NADH and NADPH play a pivotal role as electron donors in many biocatalytic redox reactions (scheme 1)

Chapter 2

Reduction reactions

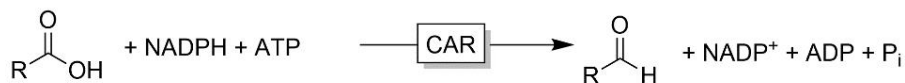
Reduction of aldehydes and ketones



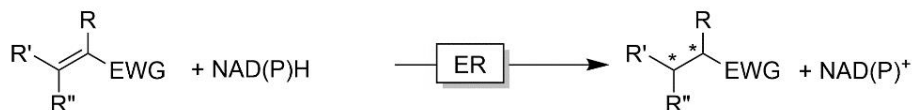
Reductive amination of aldehydes and ketones



Reduction of carboxylic acids



Reduction of conjugated C=C-double bonds

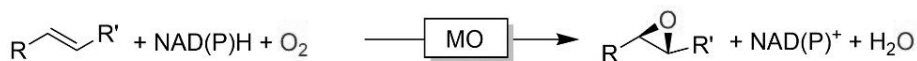


Oxidation reactions

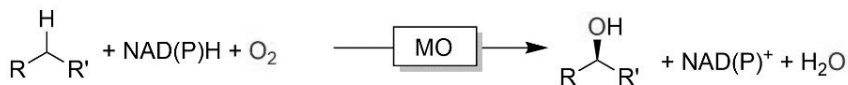
Baeyer-Villiger oxidation reactions



Epoxidation of C=C-double bonds



Hydroxylation of C-H-bonds



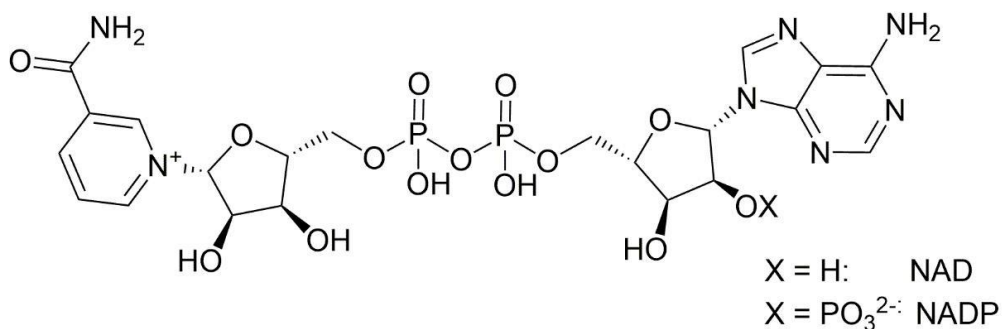
Heteroatom oxidations



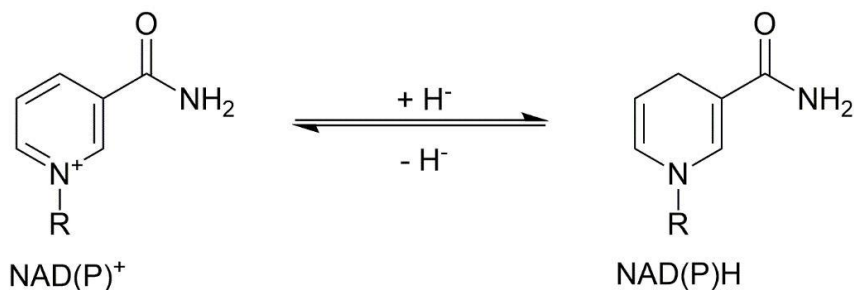
Scheme 1. Selection of preparatively relevant NAD(P)H-dependent redox reactions. ADH: alcohol dehydrogenase, IRED: imine reductase, CAR: carboxylic acid reductase, ER: ene reductase, BVMO: Baeyer-Villiger monooxygenase; MO: monooxygenase (general).

The basic electrochemical features of the nicotinamide cofactors are shown in scheme 2. In essence, NAD(P)H serves as biological hydride donor while its oxidised pendants (NAD(P)⁺) serve as hydride acceptors.

chemical structure of NAD and NADP



basic redox chemistry of NAD(P)

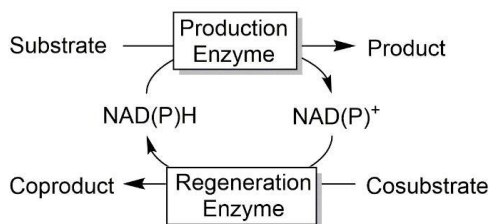


Scheme 2. Structure and basic electrochemistry of the nicotinamide cofactors.

The central role of NAD(P) as electron donor and –acceptor in biocatalytic redox reactions has motivated researchers to develop in situ regeneration systems to allow for the use of these costly cofactors in catalytic amounts and thereby reduce their cost contribution to the desired product [12].

Today, enzymatic regeneration systems prevail in preparative application, mostly due to their inherent compatibility with the enzymatic production systems but also due to the ease of application. The most common systems are shown in scheme 3.

Chapter 2



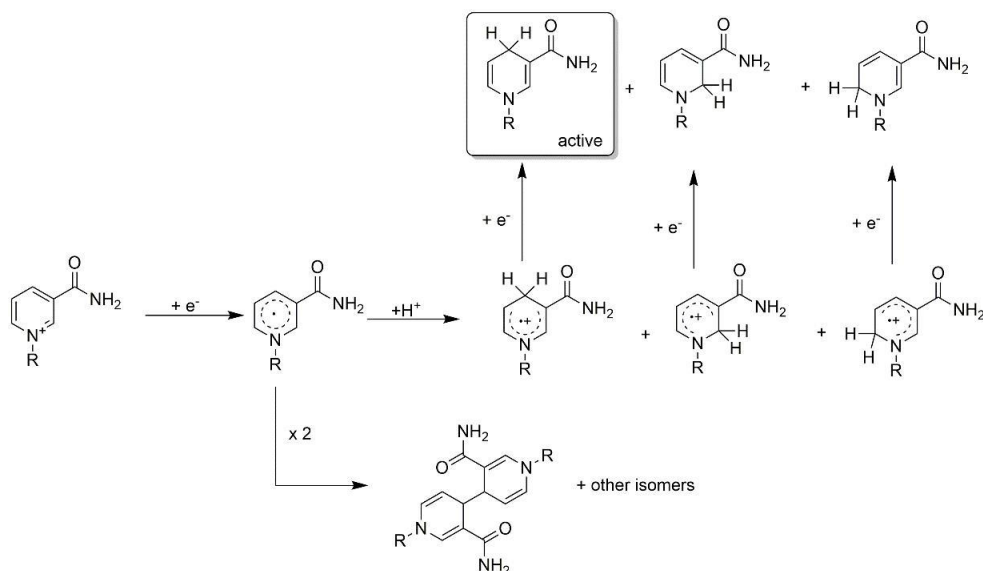
Regeneration Enzyme	Cosubstrate	Coproduct
Formate dehydrogenase (FDH)	HCO_2H	CO_2
Alcohol dehydrogenase (ADH)	$\text{R}-\text{CH}(\text{OH})-\text{R}'$	$\text{R}-\text{C}(=\text{O})-\text{R}'$
Glucose dehydrogenase (GDH)		
Phosphite dehydrogenase (PDH)	H_3PO_3	H_3PO_4
Hydrogenase (HAse)	H_2	-

Scheme 3. Selection of common enzymatic NAD(P)H regeneration systems.

Another reason for the dominance of enzymatic regeneration systems lies in their intrinsic regioselectivity. The reduction of NAD(P)^+ to NAD(P)H can principally lead to three different regioisomers of NAD(P)H while only the 1,4-NAD(P)H can be used by the production enzyme. Hence, a successful NAD(P)H regeneration system must be highly selective otherwise, losses in the costly nicotinamide cofactor due to formation of inactive regioisomers will make the approach economically unattractive [13].

Unfortunately, the majority of photocatalysts follow a so-called ECE (electron transfer – chemical – electron transfer) mechanism resulting in two major issues for the selective formation of 1,4-NAD(P)H. First, the intermediate NAD-radical can dimerise (comprising yet another pathway to inactivate the nicotinamide cofactor). Second, the chemical protonation step seldom is regioselective leading to the formation of the undesired NAD(P)H isomers (scheme 4) [14]

To circumvent (or at least alleviate) the loss of enzyme-active 1,4-NAD(P)H due to direct single electron reduction by the reduced photocatalyst, generally a relay system is applied to convert the ECE-steps into a regioselective hydride transfer step. The organometallic complex $[\text{Cp}^*\text{Rh}(\text{bpy})(\text{H}_2\text{O})]^{2+}$ proposed by Steckhan [15-20] or NAD(P)H:Flavin oxidoreductases [21-25] are the most frequently used for this purpose.



Scheme 4. ECE mechanism of NAD(P)⁺ reduction and its consequences for the formation of NAD(P)-dimers and NAD(P)H isomers.

A selection of photochemical NAD(P)H regeneration systems used to promote biocatalytic reduction reactions is summarised in table 1. Although various photocatalysts and relay systems have been reported in the past ten years, the overall NAD(P) turnover numbers and the product concentrations achieved so far are disillusioning. Compared to the multiple thousands (even millions) reported for enzymatic regeneration systems the current performance falls back by orders of magnitude.

Significant improvements will be necessary in the nearer future to make photochemical NAD(P)H regeneration systems a viable alternative (rather than a lab curiosity) to existing enzymatic systems.

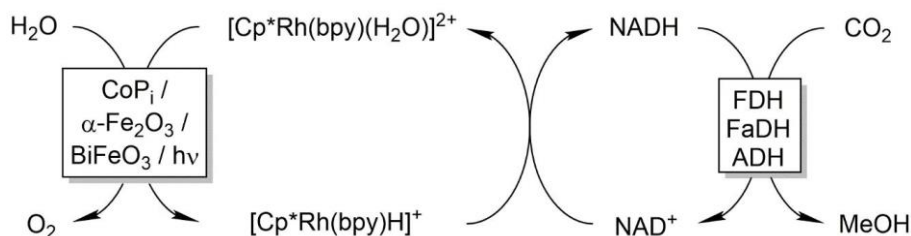
Chapter 2

Table 1. Selection of indirect photochemical NAD(P)H regeneration systems.

Cosubstrate	Photocatalyst	Enzyme / Product [mM]	TN (NAD(P) ⁺)	TN (Catalysts)	Ref
[Cp [*] Rh(bpy)(H ₂ O)] ²⁺ as relay system [26]					
TEOA	CNR	GluDH / Glutamate (10)	10	Rh: 20 / CNR: n.d. GluDH: n.d.	[27]
TEOA	mCNS	LacDH / Lactate (5)	5	Rh: 20 / mCNS: n.d. / LacDH: n.d.	[28]
TEOA	Eosin Y	GluDH / Glutamate (10)	200	Rh: 40 / Eosin Y: 500 / GluDH: n.d.	[29,30]
TEOA	[Ru(bpy) ₃] ²⁺	GluDH / Glutamate (5)	5		[31]
H ₂ O	[Co ₄ (H ₂ O) ₂ (PW ₉ O ₃₄) ₂] ¹⁰⁻	GluDH / Glutamate (5)	1.5		[31]
TEOA	Chemically converted graphene	LbADH / Various alcohols (<10 mM)	15	Rh: 30	[32,33]
TEOA	Chemically converted graphene	FDH / HCO ₂ H	116	Rh: 232	[34-36]
	Hydrogen-Terminated Silicon Nanowires	GluDH / Glutamate (5)	4	Rh: 20	[37]
NAD(P)H:Flavin oxidoreductases as relay system					
Asc. acid	Quantum dots	TbADH / Isobutanol	8	FNR: 3167	[23]
EDTA	DRf	ADH-A / Chiral alc. (<5 mM)	21	PDR: 870 / DRf: 72 / MV: 17	[21]

TEOA: triethanolamine; CNR: graphitic carbonitride nanorods; mCNS: mesoporous carbonitride spheres; LacDH: lactate dehydrogenase; GluDH: glutamate dehydrogenase; FDH: formate dehydrogenase; DRf: 5-deazariboflavin; MV: methyl viologen.

An interesting cascade for the complete reduction of CO₂ to methanol using solar-powered regeneration of NADH to promote dehydrogenase-catalysis was reported by Park and coworkers (scheme 5) [38]. The methanol yields and efficiency of the complex cascade still leave room for improvement, but nevertheless a convincing proof-of-concept was provided.



Scheme 5. Coupling photochemical water oxidation to enzymatic CO₂ reduction. The photocatalytic cascade comprises BiFeO₃ as photoactive catalyst transferring electrons to [Cp*Rh(bpy)(H₂O)]²⁺. The electrons are obtained from water by co-catalysis of cobalt phosphate (CoPi) and α-Fe₂O₃. The reduced Rh-complex specifically transfers NAD⁺ into NADH, which drives the reduction of CO₂ to MeOH through a cascade of formate dehydrogenase (FDH), formaldehyde dehydrogenase (FaDH) and alcohol dehydrogenase (ADH).

Conspicuously, most reduction reactions have been reported so far with few exceptions on monooxygenases [39,40]. A plausible explanation for this is the so-called Oxygen Dilemma [41]. Since most photochemical redox reactions follow single electron transfer mechanisms, radicals are involved in the NAD(P)H regeneration step. Radicals, however, react very fast (diffusion-controlled) with molecular oxygen thereby diverging the electron flow away from NAD(P)⁺ (or the relay catalysts) to O₂ [42].

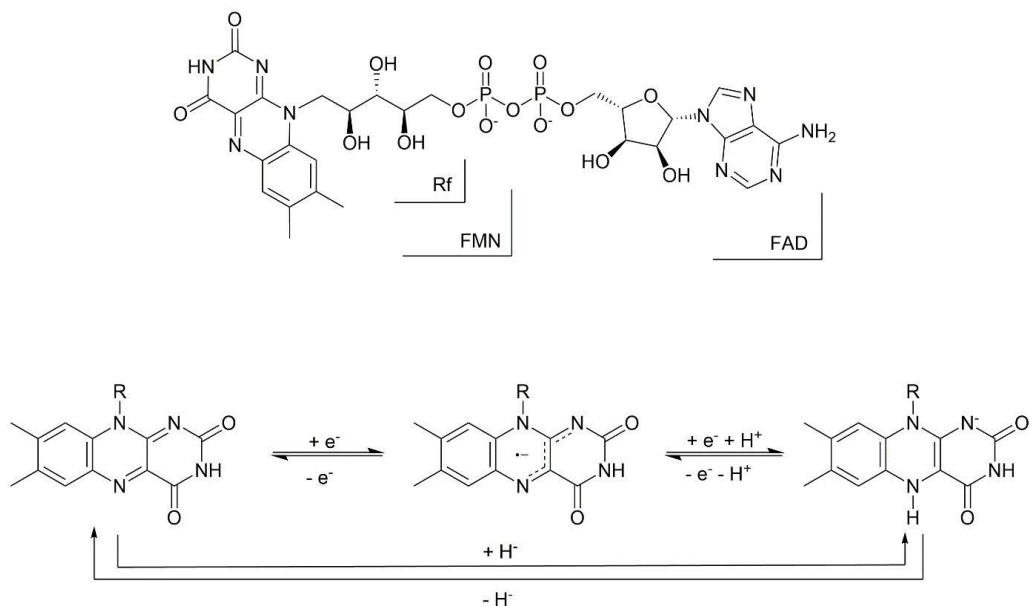
Via direct regeneration (NAD(P)H-independent approaches)

Although NAD(P)H serves as a universal reductant in biocatalytic systems, it is not necessarily involved in the enzymes' catalytic mechanisms. In these cases, other reductants can take over from NAD(P)H thereby significantly simplifying the overall regeneration scheme.

Flavin-dependent reductases

Chapter 2

Flavin-dependent old yellow enzyme (OYEs), for example, have been in focus of direct photochemical regeneration for some time now. Flavins (scheme 6) exhibit a more flexible redox chemistry especially if compared to the aforementioned nicotinamide cofactors. Therefore, flavoenzymes appear more suitable for direct (not including NAD(P)H) regeneration e.g. by reduced photosensitisers.



Scheme 6. Structural features and basic redox chemistry of flavins.

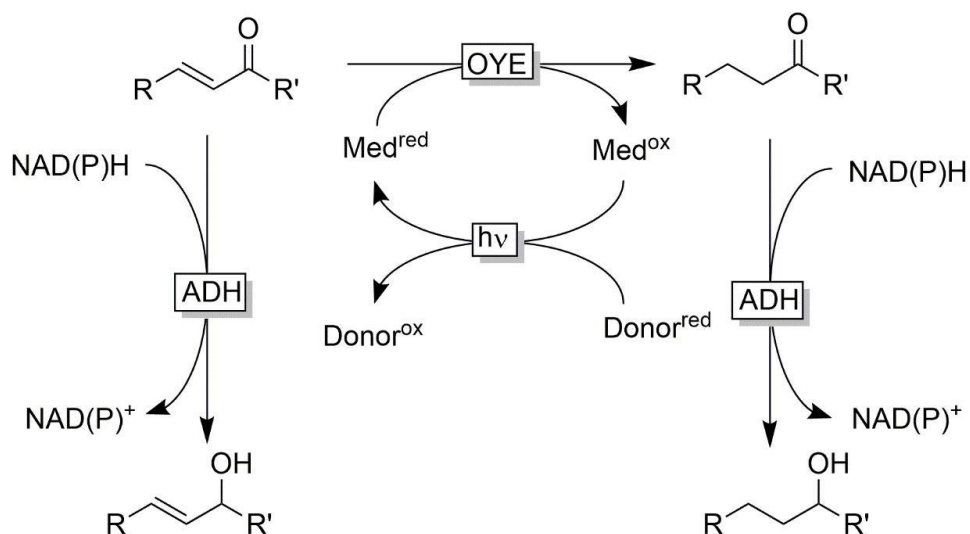
A selection of recent examples comprising photochemical regeneration of OYEs is listed (table 2).

Table 2. Selected examples of C=C-bond reductions using photochemically regenerated OYEs.

Product	Cosubstrate	OYE	Photocatalyst	Mediator	TN (OYE / Photocat. / Mediator)	ref
	EDTA	YqjM	FMN	FMN	10900 / 1000	[43, 44]
	TEOA	YqjM	CdSe	MV2 ⁺	n.d.	[45]
	MOPS/ H ₂ O	YqjM	Au-TiO ₂	FMN	650 / n.d. / 50	[46]
	Cathode	TsOYE	Flavin-modified CNT-cathode	-	230 / 2	[47]
		TsOYE	Rose bengal	-	250 / 40	[48]
	EDTA	DrER & RmER	FMN	-	2080 / 16	[49]
	H ₂ O	Flavocytochrome c (fcc3)	TiO ₂ -modified FTO anode for water oxidation	-	n.d.	[50]

YqjM: OYE from *Bacillus subtilis*; TsOYE: OYE from *Thermus scotoductus*; FTO: fluorine-doped tin oxide; MV: methyl viologen; FMN: flavin mononucleotide.

One advantage of the NAD(P)H-independent, direct regeneration of OYE is that the costly and instable nicotinamide cofactor (together with an enzymatic regeneration system) can be omitted from the reaction scheme. Furthermore, photochemical OYE-regeneration systems do not regenerate the nicotinamide cofactor. Thus, NAD(P)H-dependent enzymes are not regenerated and possible side-reactions such as ketoreduction are avoided. To achieve this chemoselectivity with traditional regeneration schemes, highly purified enzyme preparations (devoid of any ADHs) are required. Hence, photochemical, direct regeneration of OYE not only offers the opportunity of saving costs by omitting the nicotinamide cofactor (and its regeneration system) but also for products of higher purity due to the high chemoselectivity of the reaction (scheme 7)



Scheme 7. Increased chemoselectivity of OYE-catalysed reduction of conjugated C=C-double bonds via direct, NAD(P)H-independent regeneration of the flavin-prosthetic group. 'Contaminating' alcohol dehydrogenases (ADHs) catalysing the carbonyl reduction of both, the starting material and the products are not regenerated and therefore remain inactive.

Non-flavin-dependent reductases

In addition to the above-mentioned flavo-enzymes also metal-dependent oxidoreductases can be regenerated via direct (NAD(P)H-independent) electron transfer. Especially, the Armstrong group contributed a range of photocatalytic systems such as the

direct reductive regeneration of Ni-dependent CO-dehydrogenases to reduce CO₂ into CO, which could be used e.g. in Fischer-Tropsch-like syntheses of alkanes [51-54].

Formate dehydrogenase (FDH) is also widely studied especially by the Reisner lab for the reduction of CO₂ into formate. For example, dye-sensitised semiconductors combined with a formate dehydrogenase enable accumulation of millimolar concentrations of formate at the expense of triethanolamine (TEOA) as sacrificial electron donor [55]. More elegantly, water would serve as electron donor, which was demonstrated by the same group by combining the FDH-catalysed reduction reaction in a divided cell to the photosystem-catalysed oxidation of water [56].

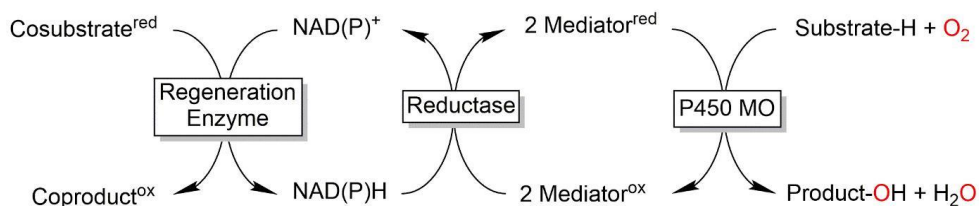
Photobiocatalytic H₂ production utilising hydrogenases have also been investigated intensively by these groups [57-62]. The turnover numbers observed with hydrogenases tend to be excellent ranging in the millions range. Finally, selective dehalogenations are worth mentioning here [63].

Direct reductive regeneration of monooxygenases

Monooxygenases catalyse a broad range of synthetically useful oxidation/oxygenation reactions for which classical chemical synthesis has not yet developed efficient catalysts. (Stereo)selective hydroxylation of non-activated sp³-C-H-bonds for example is a reaction where especially the so-called P450 monooxygenases excel [64-67].

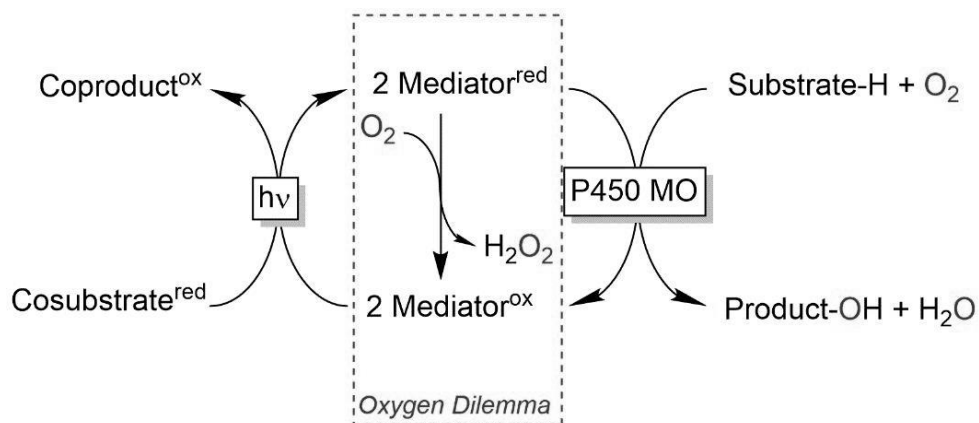
The catalytic mechanism of monooxygenases comprises reduction of the prosthetic group in the first step followed by reductive activation of molecular oxygen yielding a highly reactive oxyferryl species (in case of P450 monooxygenases) or an organic hydroperoxide (in case of flavin-dependent monooxygenases), which mediates the desired oxygenation reaction. The reducing equivalents needed in this mechanism are usually derived from reduced nicotinamide cofactors via more or less complex electron transport chains. Especially P450 monooxygenases, due to their O₂-activation mechanism comprising a sequence of single electron transfer, O₂-binding and –reduction followed by a second single electron transfer step and water elimination, require a relay system to transform the hydride donation step from NAD(P)H into the required single electron transfer steps. As a result, especially in case of P450 monooxygenases, the electron transfer chain tends to be rather complex (scheme 8).

Chapter 2



Scheme 8. Generalised molecular architecture of the electron transport chains of P450 monooxygenases.

Therefore, it is not very astonishing that especially P450 monooxygenases have also been investigated envisaging direct electron transfer from various electron donors. The aforementioned radical character of most reduced photosensitisers now appears beneficial in view of direct regeneration of P450 monooxygenases yielding simplified regeneration schemes (scheme 9) [68].



Scheme 9. Direct, photochemical regeneration of P450 monooxygenases. The photoreduced mediators can either reduce the P450 monooxygenase (desired reaction) or they can react with dissolved O_2 (undesired uncoupling reaction, *Oxygen Dilemma*).

Various photosensitisers/mediators have been evaluated in the past decade. Amongst them porphyrins [69-71] and further organic dyes such as eosin Y [72,73] or (deaza)flavins; [74,75] most popular, however, are photoactive Ru-complexes [76-82]. Wiring P450 monooxygenases to the natural photosystem for light-driven, water-utilising reactions

have also been reported [83,84]. Direct, photocatalytic regeneration of some flavin-dependent [85-87] and Cu-dependent monooxygenases [88] has also been tried.

Despite the promise of simplified and therefore more efficient regeneration of monooxygenases, preparative scale examples have yet to be delivered. Although a broad range of interesting oxyfunctionalisation reactions has been reported, the product titres tend to be in the lower millimolar, sometimes micromolar range. Obviously, this severely limits the preparative usefulness of direct (photochemical) regeneration approaches of P450 monooxygenases.

The major limitation of these approaches lies with their radical character. In contrast to hydride-reducing agents (such as NAD(P)H), single electron donors (radicals) readily react with (triplet) O_2 . Hence, under aerobic conditions, reduced photocatalysts can either deliver their reducing equivalents to the monooxygenases (desired electron transfer pathway) or can directly react with dissolved O_2 (thereby uncoupling the electron supply from the monooxygenase reaction) (scheme 9) [41].

So far, no satisfactory solution to the *oxygen dilemma* has been proposed, leaving this an open question in photochemically-driven monooxygenase reactions.

Oxidative regeneration

In oxidative regeneration of redox enzymes, again, principally NAD(P)-dependent and NAD(P)-independent approaches can be distinguished.

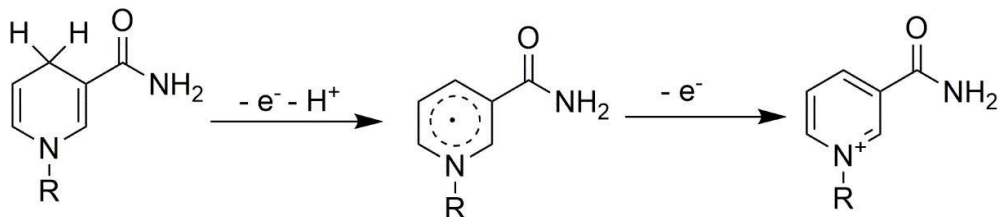
Photochemical NAD(P)⁺ regeneration to drive ADH-catalysed oxidation reactions

Compared to reductive use of ADHs, their application in the oxidative direction is far less common. One reason is that the oxidation of secondary alcohols usually destroys chiral information, whereas the reverse reaction, i.e. the reduction of ketones, leads to the formation of chiral (ideally enantiomerically pure) secondary alcohols. This also explains why the number of reported enzymatic NAD(P)⁺ regeneration systems falls back significantly behind the NAD(P)H regeneration systems. In essence, NADH-oxidases [89-92] and ADH-catalysed NAD(P)H oxidation [93-96] prevail.

Nevertheless, a range of photochemical NAD(P)⁺ regeneration systems have been reported. In contrast to the reverse reaction (photochemical reduction of NAD(P)⁺),

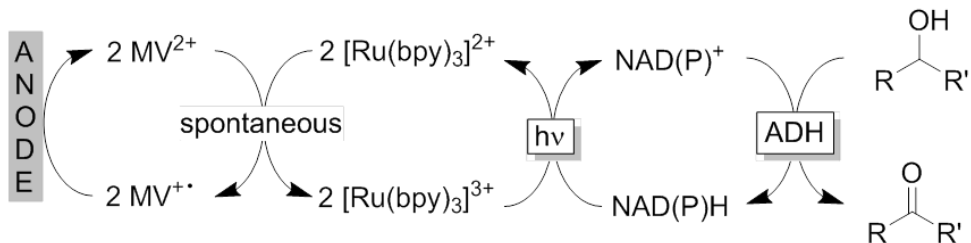
Chapter 2

selectivity issues play no role in the reaction mixtures are the desired product (NAD(P)^+) is aromatic and thereby thermodynamically stable without product isomers (scheme 10).



Scheme 10. ECE mechanism of NAD(P)H oxidation.

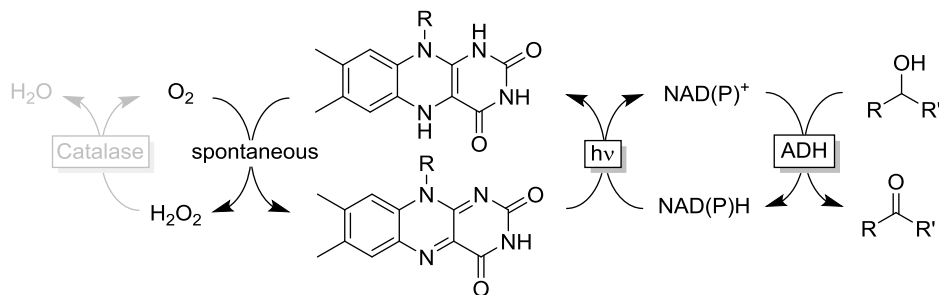
In an early contribution, Steckhan and coworkers reported a photoelectrochemical NAD(P)H oxidation system based on photoexcited $[\text{Ru}(\text{bpy})_3]^{3+}$ complexes (scheme 11)) [97]. The reducing equivalents transferred to the photoexcited Ru complexes were then, in a spontaneous cascade, transferred to an anode. Unfortunately, this system proved to be rather complex and not efficient enough to be of preparative use.



Scheme 11. The photoelectrochemical NAD(P)^+ regeneration system proposed by Steckhan and coworkers to promote ADH-catalysed oxidation reactions.

Later, we reported that photoexcited flavins are very efficient catalysts to oxidise NAD(P)H to NAD(P)^+ [98,99]. The spontaneous hydride transfer from NAD(P)H to oxidised flavins is actually known since decades [100-103]. The sluggish reaction rate, however, demanded large molar surpluses of the flavin 'catalyst' to achieve acceptable overall reaction rates. Simple illumination of the reaction system with blue light ($\lambda=450$ nm, i.e. the absorption

maximum of oxidised flavins) increased the reaction rate by orders of magnitude thereby enabling truly catalytic use of the flavin photocatalyst (scheme 12).



Scheme 12. Photochemical NAD(P)^+ regeneration system using photoexcited flavins. Please note, the mechanism shown here is highly simplified. Most likely, flavin-semiquinone radicals formed by SET from NAD(P)H to the photoexcited flavin are formed reacting with O_2 in a sequence of SETs.

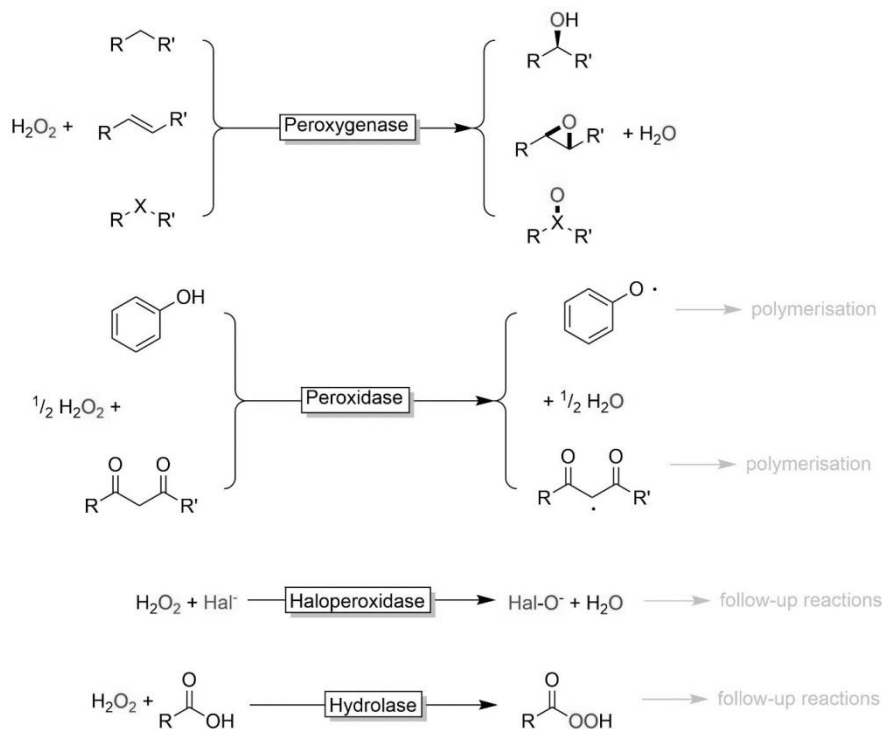
This approach is also applicable to various other photoactive redox dyes such as methylene blue, rose Bengal or Meldola's blue [104].

Photochemical regeneration of H_2O_2 -dependent enzymes

As mentioned above, photochemical systems in the presence of molecular oxygen tend to uncouple. In other words, the reduced photocatalysts/mediators (mostly being radicals) react swiftly with molecular oxygen directly. In the case of photochemical NAD(P)^+ regeneration systems this is the desired reaction. In cases where the reducing equivalents should be delivered to a biocatalyst (i.e. to a monooxygenase), this represents an undesired side reactions. In some cases, this side reaction dominates over the desired electron flow leading to a waste of up to 95% of the reducing equivalents (*oxygen dilemma*) [41]. The final product of this uncoupling reaction is H_2O_2 .

A range of enzymes (so-called peroxizymes), however, can use H_2O_2 productively in their catalytic mechanisms [105]. Hence, the *oxygen dilemma* can be used productively to promote peroxizyme-catalysed oxidation reactions!

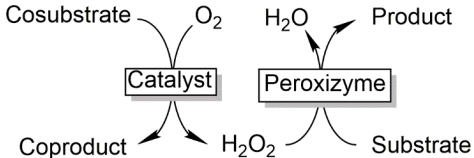
Chapter 2



Scheme 13: Peroxizymes utilise H_2O_2 to catalyse or initiate catalytic oxidation reactions.

Peroxygenases (UPO for unspecific peroxygenases) are the most prominent peroxizymes. UPOs catalyse a very broad range of synthetically useful oxyfunctionalisation reactions such as regio- and stereospecific hydroxylations and epoxidations as well as stereospecific heteroatom oxygenations (scheme 3). As heme-dependent enzymes, however, they are also prone to rapid oxidative inactivation in the presence of H_2O_2 [106]. Therefore, a range of *in situ* H_2O_2 generation approaches have been developed in the past to balance the H_2O_2 concentration to the UPO activity and thereby minimise oxidative inactivation.¹⁰⁵ Most prominent at present, are enzymatic systems based on oxidases (*i.e.* enzymes that couple the oxidation of their substrate to the reduction of O_2 to H_2O_2). In the past decade, we and others have developed a range of photocatalytic systems to drive peroxygenase- and peroxidase-reactions. As summary is given in table 3. Obviously, using water as cosubstrate would be the most attractive application of photocatalysis with peroxizymes. However the current state-of-the-art is hampered by the rather sluggish water oxidation rates making the resulting reaction systems rather slow. Next generation water oxidation catalysts are highly desired!

Table 3. Selection of peroxizyme reactions driven by photocatalytic H₂O₂ generation.

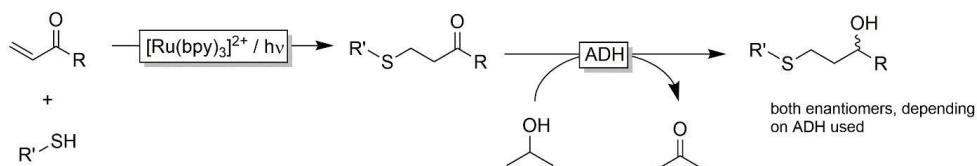
							
Catalyst	Cosub.	Coprod.	Peroxi- zyme	Product	TTN (Enz.)	Remarks	ref
Flavin	EDTA	EDTriA / H ₂ CO / CO ₂	<i>CfCPO</i>	thioanisole sulfoxide	22000	[a]	[107, 108]
Flavin	EDTA	EDTriA / H ₂ CO / CO ₂	<i>AaeUPO</i>	various	<40000		[109]
Flavin	EDTA	EDTriA / H ₂ CO / CO ₂	<i>OleT</i>	1-alkenes		[b]	[110, 111]
Flavin-mod. cathode	H ₂ O	O ₂	<i>AaeUPO</i>	1-phenyl ethanol	123000		[112]
Au-TiO ₂	MeOH	CO ₂	<i>AaeUPO</i>	various	>60000		[113]
Au-TiO ₂	H ₂ O	O ₂	<i>AaeUPO</i>	various	>30000		[114]
Various dyes / FDH	HCO ₂ H	CO ₂	<i>AaeUPO</i>	1-phenyl ethanol	>40000	[c]	[115]
Flavin	EDTA	EDTriA / H ₂ CO / CO ₂	CYT450 peroxy- genases	Hydroxy- myristic acid	200	[d]	[116]
Flavin	MES	n.d.	<i>AmVHCPO</i>	Various halogenated	2000	[e]	[117]

EDTA: ethylenediamine tetraacetate; EDTriA: ethylenediamine triacetate; MES: 2-(N-Morpholino)ethansulfonic acid; *AmVHCPO*: V-dependent haloperoxidase from *Acaryochloris marina*. [a]: Using a 2LPS approach significantly improved product formation. [b]: Photo-electrochemical approach. [c]: Combining color-complementary redox dyes allows for better usage of the visible light range. [d]: Low, due to poor solubility of the reagents. [e]: phenols and anilines

Photobiocatalytic cascades combining chemical and biocatalytic transformations

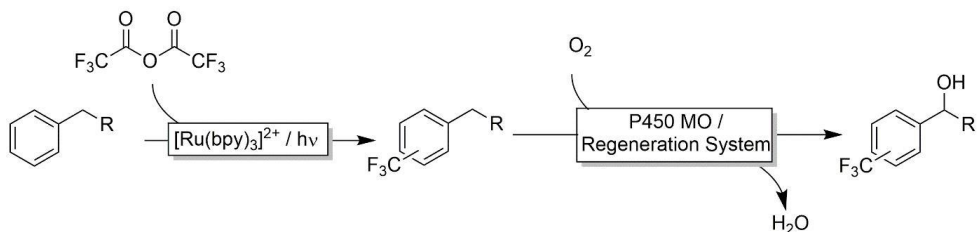
Next to the various examples using photocatalysis to provide redox enzymes with redox equivalents for catalysis, there is also a growing interest in combining photochemical with biocatalytic transformations.

Castagnolo and coworkers for example reported that a photo-catalysed thio-Michael addition yielding saturated ketones can be completed by an ADH-catalysed, stereoselective reduction of the carbonyl group yielding enantiomerically pure 1,3-mercaptoalkanols in a one-pot setup (scheme 14) [118].



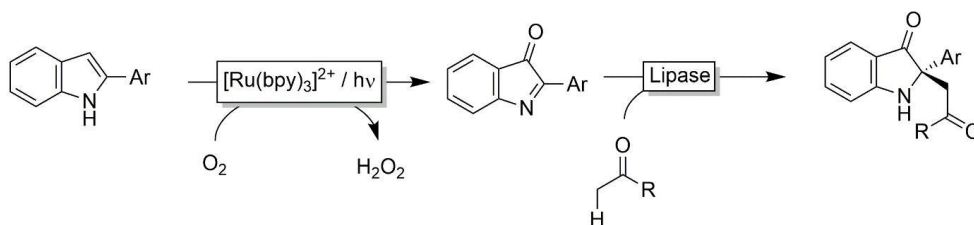
Scheme 14. Photoenzymatic cascade combining photoaccelerated thio-Michael addition and stereoselective, ADH-catalysed ketoreduction.

The group around Cheruzel investigated the photocatalytic trifluoromethylation of alkylarenes followed by P450 monooxygenase-catalysed hydroxylation of the intermediate product (scheme 15) [77].



Scheme 15. Cascade of photocatalytic trifluoromethylation of arenes followed by P450 monooxygenase-catalysed hydroxylation.

Another example of photocatalytic C-C-bond formation coupled to a selective biocatalytic reaction step was reported recently by He and coworkers (scheme 16) [119]. Here the authors combined the photocatalytic oxidation of 2-arylindoles to 2-arylindol-3-ones combined with an enantioselective, lipase-catalysed addition of enolisable ketones yielding enantioenriched 2,2-disubstituted indol-3-ones.

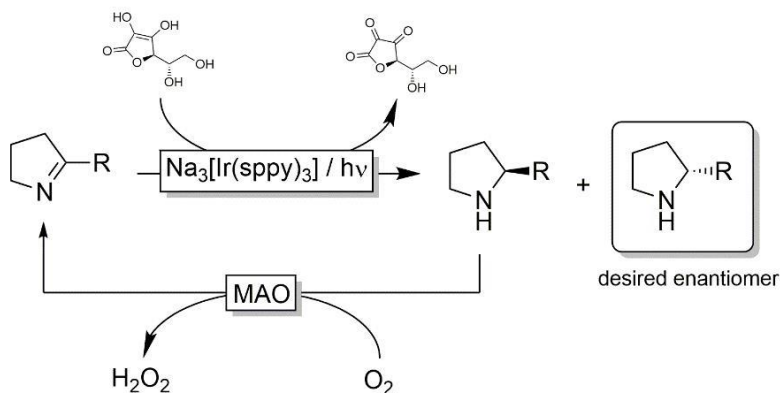


Scheme 16. Photocatalytic oxidation of 2-arylindoles to 2-arylindol-3-ones coupled to a lipase-catalysed C-C-bond formation.

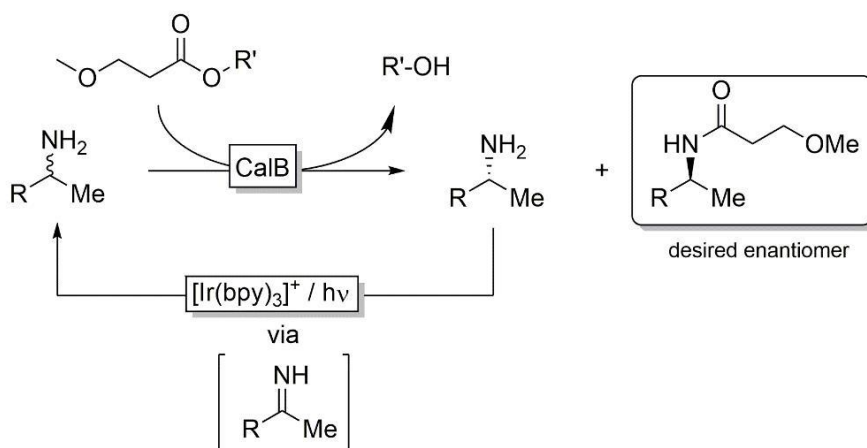
Photochemical reactions are generally not stereoselective, a fact that can be exploited in the deracemisation of chiral alcohols and amines if combined with a stereoselective enzymatic step. Interestingly, photoactivatable Ir-complexes have been reported for this purpose. In the first example, a photoexcited Ir-complex mediated the (ascorbate-driven), non-stereoselective reduction of (cyclic) imines. In combination with the well-known monoamine oxidase (MAO) catalysing the stereoselective oxidation of the resulting amine, a deracemisation was achieved (scheme 17a) [120,121]. In another example, an Ir-complex was used to racemise amines via a photoaccelerated H-borrowing reaction (i.e. catalysing the H-atom abstraction and non-selective re-donation from an amine). Through combination with an enantioselective, lipase-catalysed acylation step, complete transformation of racemic amines into enantiomerically pure amides was achieved (scheme 17b) [122].

Chapter 2

a) non-stereoselective reduction combined to stereoselective oxidation

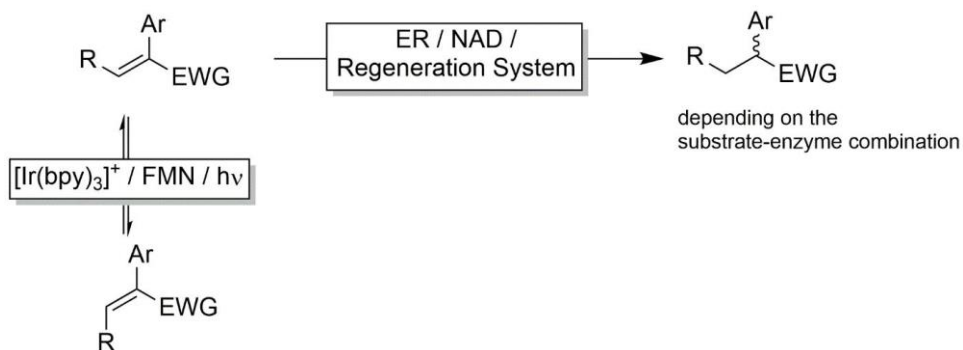


b) stereoselective acylation combined to photocatalytic re-racemisation



Scheme 17. Examples for photobiocatalytic deracemisation reactions combining non-selective photocatalytic redox reactions with enantioselective, biocatalytic kinetic resolutions.

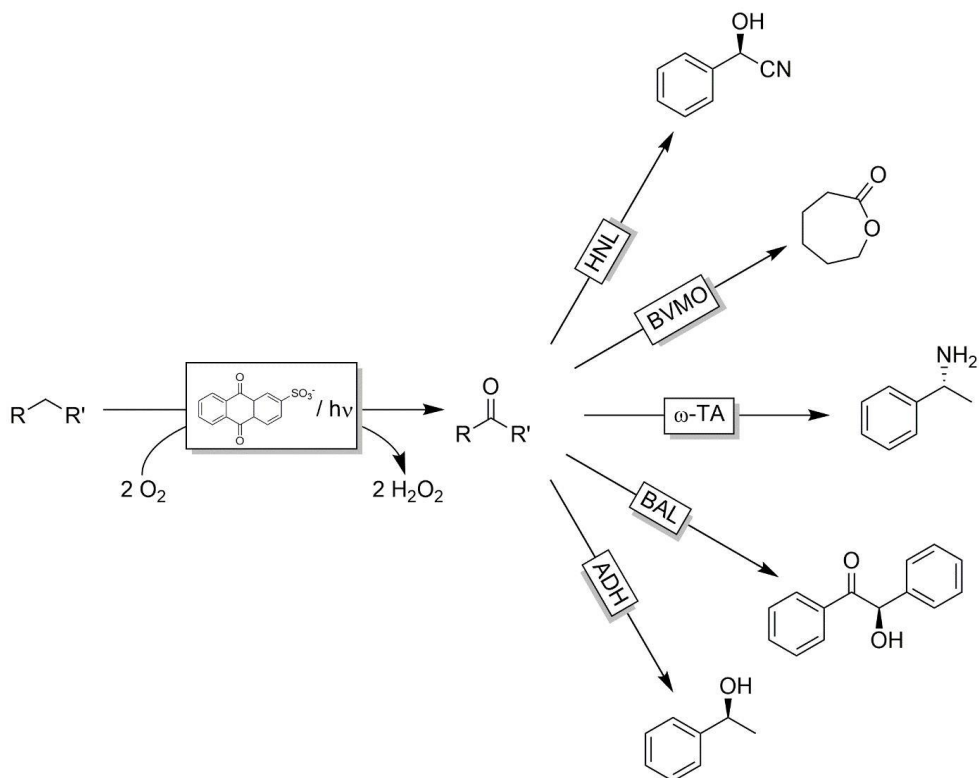
Another elegant combination of photocatalysts with biocatalysis was reported by Hartwig and coworkers combining photocatalytic E/Z-isomerisation of conjugated carbonyl groups with stereoselective reduction of the E-configured C=C-double bond by ene reductases (scheme 18) [123].



Scheme 18. Photocatalytic E/Z isomerisation for the complete conversion of trisubstituted alkenes by ene-reductases.

Finally, we have developed a range of photocatalytic oxidation reactions yielding prochiral ketones and aldehydes, which then in a subsequent biocatalytic step were converted into optically pure cyanohydrins, alcohols, amines, lactones, benzoin and others (scheme 19) [124-126]. The reactions generally gave better results (conversion) if the cascades were performed sequentially, i.e. performing the photocatalytic oxidation reaction followed by the biocatalytic reaction step. Reasons for this were manifold ranging from compatibility issues of the photo- and biocatalysts to cross-reactivities.

Similar compatibility issues were also observed by Kourist and coworkers combining OleT-catalysed decarboxylation of ω -fatty acids with Ru-catalysed metathesis of the resulting terminal alkene [111].



Scheme 19. Sequential photobiocatalytic cascades to transform non-functionalised alkanes into various (optically pure), functionalised products.

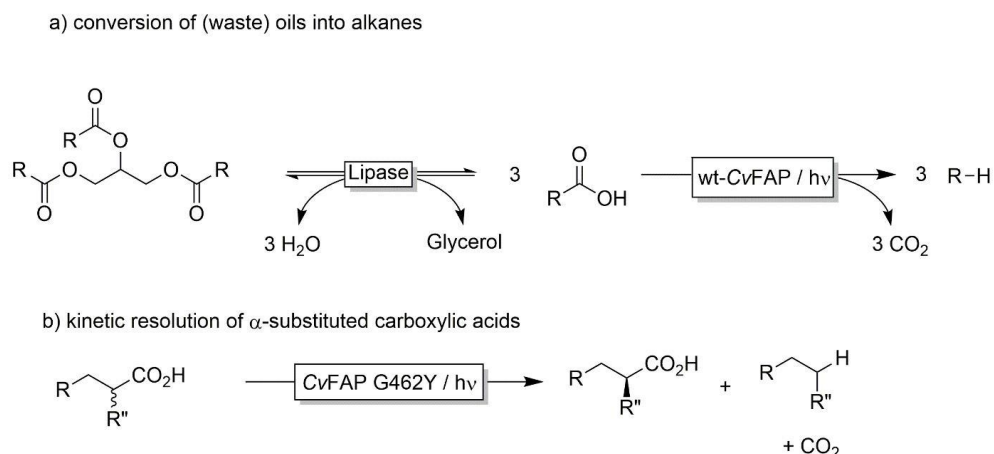
Photoactivated enzymes

Today, only a handful of enzymes necessitating light activation are known. The most important enzymes obviously are photosystem I and photosystem II, playing a fundamental role in life as we know it [127,128]. In addition, photolyases involved in DNA repair [129,130] and protochlorophyllide-reductases [131] involved in chlorophyll synthesis are known. Despite their fundamental importance for life, these enzymes have so far not found widespread interest and application in preparative biocatalysis [9,10].

In contrast, the recently discovered class of photodecarboxylases [132,133] has also found considerable interest as catalysts for the selective decarboxylation of (fatty)acids under very mild reaction conditions. The photodecarboxylase from *Chlorella variabilis* NC64A (CvFAP) efficiently cleaves carboxylic acids into the corresponding, C1-shortened alkanes, other functional groups remaining intact (scheme 20a) [134]. When combined with a

lipase, this enzyme may play a role in the synthesis of a next generation of biofuels from waste oils.

CvFAP has a somewhat limited substrate scope favouring long-chain fatty acids. This limitation can be overcome either by reaction engineering [135] or by protein engineering [136]. In the first case, CvFAP activity towards short chain carboxylic acids was increased considerably by filling up the rest of the substrate access channel with hydrophobic alkane decoy molecules. Wu and coworkers engineered the wild-type enzyme to broaden the substrate scope. The engineered variants also proved to be efficient catalysis for the kinetic resolution of α -substituted carboxylic acids (scheme 20b).



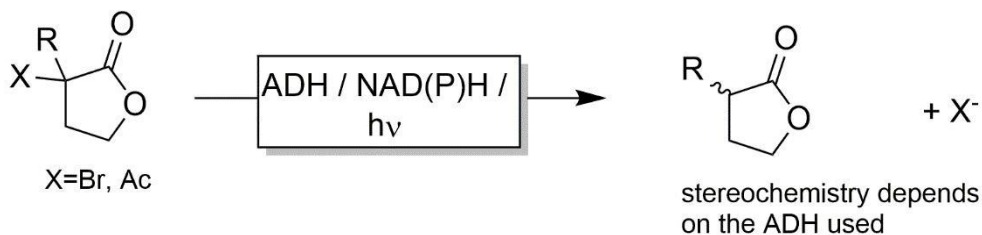
Scheme 20. Synthetic applications of CvFAP.

The photoactivity of CvFAP is conferred by the flavin prosthetic group, which under irradiation with blue light turns into a high-redox, photoexcited state capable of single electron abstraction from the bound carboxylate group thereby initiating the decarboxylation cascade [132].

Very recently Hyster and coworkers realised the potential of photoexcited cofactors to introduce 'non-natural' reactivities to cofactor dependent enzymes. In a first study, they utilised photoexcited reduced nicotinamide cofactors to catalyse the enantioselective dehalogenation or deacetylation of α -substituted lactones (**Error! Reference source not found.**) [137,138]. Later, the same group expanded this concept to flavin-dependent

Chapter 2

enzymes [139] also demonstrating that the application of photocatalysis can turn an ene-reductase into a ketoreductase [140].



Scheme 21. Turning an ADH into a dehalogenase using photochemistry.

Conclusions

Photobiocatalysis is a dynamically evolving field of research opening up new synthetic possibilities for the organic chemist.

To fully unfold this potential, compatibility will be the most pressing issue to be addressed. The high reactivity of photoexcited species frequently leads to inactivation of the biocatalyst and photocatalysts themselves. As a consequence, turnover numbers of the catalysts still tend to be rather low thereby limiting the preparative value of the systems.

Next to protein engineering approaches also reaction engineering approaches i.e. through physical separation of photo- and biocatalyst right now appear to be the most promising solution to the compatibility issue.

References

1. Torrelo G., et al., *Biocatalysis*. Catalysis Letters, 2015. **145**: p. 309-345.
2. Faber K. *Biotransformations in Organic Chemistry*. 6th ed. Berlin: Springer; 2011.
3. Drauz K., et al., *Enzyme Catalysis in Organic Synthesis*. Weinheim: Wiley-VCH; 2012.
4. Liese A., et al., *Industrial Biotransformations*. Weinheim: Wiley-VCH; 2006.
5. Schrittwieser J.H., et al., *Artificial Biocatalytic Linear Cascades for Preparation of Organic Molecules*. Chemical Reviews, 2017. **118**: p. 270-348.
6. Rudroff F., et al., *Opportunities and challenges for combining chemo- and biocatalysis*. Nature Catalysis, 2018. **1**: p. 12-22.
7. Ni Y., et al., *How green is biocatalysis? To calculate is to know*. ChemCatChem, 2014. **6**: p. 930-43.
8. Lee S.H., et al., *Coupling Photocatalysis and Redox Biocatalysis Toward Biocatalyzed Artificial Photosynthesis*. Chemistry – A European Journal, 2013. **19**: p. 4392–406.
9. Schmermund L., et al., *Photo-Biocatalysis: Biotransformations in the Presence of Light*. ACS Catalysis, 2019. **9**(5): p. 4115-4144.
10. Gulder T., Seel C.J., *Biocatalysis Fueled by Light: On the Versatile Combination of Photocatalysis and Enzymes*. ChemBioChem, 2019. **0**.
11. Maciá-Agulló J.A., et al., *Photobiocatalysis: The Power of Combining Photocatalysis and Enzymes*, Chemistry – A European Journal, 2015. **21**: p. 10940–10959.
12. Chenault H., Whitesides G. *Regeneration of nicotinamide cofactors for use in organic synthesis*, Applied Biochemistry and Biotechnology, 1987. **14**: p. 147-97.
13. Steckhan E., *Electroenzymatic synthesis*, Electrochemistry V. Berlin 33: Springer-Verlag Berlin; 1994. p. 83-111.
14. Hollmann F., Schmid A., *Electrochemical regeneration of oxidoreductases for cell-free biocatalytic redox reactions*. Biocatalysis and Biotransformation, 2004. **22**: p. 63-88.
15. Steckhan E., et al., *Continuous Generation of NADH from NAD⁺ and Formate Using a Homogeneous Catalyst with Enhanced Molecular-Weight in a Membrane Reactor*. Angewandte Chemie International Edition, 1990. **29**: p. 388-390.
16. Ruppert R., et al., *Very Efficient Reduction of NAD(P)⁺ with Formate Catalyzed by Cationic Rhodium Complexes*. Journal of the Chemical Society, Chemical Communications, 1988. p. 1150-1151.
17. Grammenudi S., et al., *The Rhodium Complex of a Tris(Bipyridine) Ligand - Its Electrochemical-Behavior and Function as Mediator for the Regeneration of NADH from NAD⁺*. Journal of Inclusion Phenomena, 1987. **5**: p. 695-707.
18. Wienkamp R., Steckhan E., *Selective Generation of NADH by Visible-Light*. Angewandte Chemie International Edition, 1983. **22**: p. 497-.
19. Wienkamp R., Steckhan E., *Indirect Electrochemical Processes.13. Indirect Electrochemical Regeneration of NADH by a Bipyridinerhodium(II) Complex as Electron-Transfer Agent*. Angewandte Chemie International Edition, 1982. **21**: p. 782-783.
20. Hollmann F., Witholt B., Schmid A., *[Cp*Rh(bpy)(H₂O)]²⁺: a versatile tool for efficient and non-enzymatic regeneration of nicotinamide and flavin coenzymes*. J Journal of Molecular Catalysis B: Enzymatic, 2002. **19-20**: p. 167-176.
21. Höfler G.T., et al., *A Photoenzymatic NADH Regeneration System*. ChemBioChem, 2018. **19**: p. 2344-2347.
22. Wan L., et al., *A hydrogen fuel cell for rapid, enzyme-catalysed organic synthesis with continuous monitoring*. Chemical Communications, 2018. **54**: p. 972-975.
23. Brown K.A., et al., *Photocatalytic Regeneration of Nicotinamide Cofactors by Quantum Dot–Enzyme Biohybrid Complexes*. ACS Catalysis, 2016. **6**: p. 2201-2204.

Chapter 2

24. Asada H., et al., *Glutamate synthesis via photoreduction of NADP⁽⁺⁾ by photostable chlorophyllide coupled with polyethylene-glycol*. Biotechnology and Bioengineering, 2001. **76**: p. 86-90.
25. Pueyo J.J., Gomezmoreno C., *Photochemical regeneration of NADPH using the enzyme ferredoxing-NADP⁺ reductase*. Enzyme and Microbial Technology, 1992. **14**: p. 8-12.
26. Lee S.H., et al., *Artificial Electron Carriers for Photoenzymatic Synthesis under Visible Light*. Chemistry – A European Journal, 2012. **18**: p. 5490-5495.
27. Liu J., et al., *Uniform Graphitic Carbon Nitride Nanorod for Efficient Photocatalytic Hydrogen Evolution and Sustained Photoenzymatic Catalysis*. ACS Applied Materials & Interfaces, 2014. **6**: p. 8434-8440.
28. Huang J.H., Antonietti M., Liu J., *Bio-inspired carbon nitride mesoporous spheres for artificial photosynthesis: photocatalytic cofactor regeneration for sustainable enzymatic synthesis*. Journal of Materials Chemistry A, 2014. **2**: p. 7686-7693.
29. Lee S.H., Nam D.H., Park C.B., *Screening Xanthene Dyes for Visible Light-Driven Nicotinamide Adenine Dinucleotide Regeneration and Photoenzymatic Synthesis*. Advanced Synthesis & Catalysis, 2009. **351**: p. 2589-2594.
30. Lee S.H., et al., *Eosin Y-Sensitized Artificial Photosynthesis by Highly Efficient Visible-Light-Driven Regeneration of Nicotinamide Cofactor*. ChemBioChem, 2009. **10**: p. 1621-1624.
31. Ryu J., et al., *Biocatalytic Photosynthesis with Water as an Electron Donor*. Chemistry – A European Journal, 2014. **20**: p. 12020–12025.
32. Choudhury S., et al., *A solar light-driven, eco-friendly protocol for highly enantioselective synthesis of chiral alcohols via photocatalytic/biocatalytic cascades*. Green Chemistry, 2014. **16**: p. 4389-4400
33. Choudhury S., et al., *A Photocatalyst/Enzyme Couple That Uses Solar Energy in the Asymmetric Reduction of Acetophenones*. Angewandte Chemie International Edition, 2012. **51**: p. 11624-11628.
34. Yadav R.K., et al., *Graphene-BODIPY as a photocatalyst in the photocatalytic-biocatalytic coupled system for solar fuel production from CO₂*. Journal of Materials Chemistry A, 2014. **2**: p. 5068-5076.
35. Yadav R.K., et al., *Highly Selective Solar-Driven Methanol from CO₂ by a Photocatalyst/Biocatalyst Integrated System*. Journal of the American Chemical Society, 2014. **136**: p.16728-16731.
36. Yadav R.K., et al., *A Photocatalyst-Enzyme Coupled Artificial Photosynthesis System for Solar Energy in Production of Formic Acid from CO₂*. Journal of the American Chemical Society, 2012. **134**: p. 11455-11461.
37. Lee H.Y., et al., *Biocatalyzed Artificial Photosynthesis by Hydrogen-Terminated Silicon Nanowires*. ChemSusChem, 2012. **5**: p. 2129-2132.
38. Kuk S.K., et al., *Photoelectrochemical Reduction of Carbon Dioxide to Methanol through a Highly Efficient Enzyme Cascade*. Angewandte Chemie International Edition, 2017. **129**: p. 3885–3890.
39. Lee S.H., et al., *Cytochrome P450-catalyzed O-dealkylation coupled with photochemical NADPH regeneration*. Biotechnology and Bioengineering, 2013. **110**: p. 383-390.
40. Lee J.H., et al., *Solar-to-chemical conversion platform by Robust Cytochrome P450-P(3HB) complex*. Journal of Industrial and Engineering Chemistry, 2016. **33**: p. 28-32.
41. Holtmann D., Hollmann F., *The Oxygen Dilemma: A Severe Challenge for the Application of Monoxygenases?* ChemBioChem, 2016. **17**: p. 1391-1398.
42. Chapter 4
43. Taglieber A., et al., *Light-Driven Biocatalytic Oxidation and Reduction Reactions: Scope and Limitations*. ChemBioChem 2008. **9**: p. 565-72.

44. Mifsud M., et al., *Photoenzymatic Reduction of C=C Double Bonds*. Advanced Synthesis & Catalysis, 2009. **351**: p. 3279-3286.
45. Burai T.N., et al., *Light-Driven, Quantum Dot-Mediated Regeneration of FMN To Drive Reduction of Ketoisophorone by Old Yellow Enzyme*. ACS Catalysis, 2012. **2**:p. 667-670.
46. Mifsud M., et al., *Photobiocatalytic chemistry of oxidoreductases using water as the electron donor*. Nature Communications, 2014. **5**.
47. Son E.J., et al., *Carbon Nanotube–Graphitic Carbon Nitride Hybrid Films for Flavoenzyme-Catalyzed Photoelectrochemical Cells*. Advanced Functional Materials, 2018. **28**: p. 1705232.
48. Lee S.H., et al., *Cofactor-Free, Direct Photoactivation of Enoate Reductases for Asymmetric Reduction of C=C Bonds*. Angewandte Chemie International Edition, 2017. **56**: p. 8681–8685.
49. Litthauer S., et al., *Heterologous expression and characterization of the Ene-reductases from Deinococcus radiodurans and Ralstonia metallidurans*. Journal of Molecular Catalysis B: Enzymatic, 2014. **99**: p. 89–95.
50. Bachmeier A., et al., *Heme Flavoenzyme as a Solar Conversion Catalyst*. Journal of the American Chemical Society, 2014. **136**: p. 12876–12879.
51. Woolerton T.W., et al., *Efficient and Clean Photoreduction of CO₂ to CO by Enzyme-Modified TiO₂ Nanoparticles Using Visible Light*. Journal of the American Chemical Society, 2010. **132**: p. 2132-2133.
52. Chaudhary Y.S., et al., *Visible light-driven CO₂ reduction by enzyme coupled CdS nanocrystals*. Chemical Communications, 2011. **48**: p. 58-60.
53. Zhang L., et al., *Fast and Selective Photoreduction of CO₂ to CO Catalyzed by a Complex of Carbon Monoxide Dehydrogenase, TiO₂, and Ag Nanoclusters*. ACS Catalysis 2018. **8**: p. 2789-2795.
54. Woolerton T.W., et al., *CO₂ photoreduction at enzyme-modified metal oxide nanoparticles*. Energy & Environmental Science, 2011. **4**: 2393-2399.
55. Miller M., et al., *Interfacing Formate Dehydrogenase with Metal Oxides for the Reversible Electrocatalysis and Solar-Driven Reduction of Carbon Dioxide*. Angewandte Chemie International Edition, 2019. **58**: p. 4601-4605.
56. Sokol K.P., et al., *Photoreduction of CO₂ with a Formate Dehydrogenase Driven by Photosystem II Using a Semi-artificial Z-Scheme Architecture*. Journal of the American Chemical Society, 2018. **140**: 16418-16422.
57. Reisner E., et al., *Visible Light-Driven H₂ Production by Hydrogenases Attached to Dye-Sensitized TiO₂ Nanoparticles*. Journal of the American Chemical Society, 2009. **131**: p. 18457-18466.
58. Reisner E., et al., *Catalytic electrochemistry of a [NiFeSe]-hydrogenase on TiO₂ and demonstration of its suitability for visible-light driven H₂ production*. Chemical Communications, 2009. P. 550-552.
59. Hutton G.A.M., et al., *Carbon dots as versatile photosensitizers for solar-driven catalysis with redox enzymes*. Journal of the American Chemical Society, 2016. **138**: p. 16722-16730.
60. Lee C.Y., et al., *Photoelectrochemical H₂ Evolution with a Hydrogenase Immobilized on a TiO₂-Protected Silicon Electrode*. Angewandte Chemie International Edition, 2016. **55**: p.5971-5974.
61. Mersch D., et al., *Wiring of Photosystem II to Hydrogenase for Photoelectrochemical Water Splitting*. Journal of the American Chemical Society, 2015. **137**: p. 8541-8549.
62. Caputo C.A., et al., *Photocatalytic Hydrogen Production using Polymeric Carbon Nitride with a Hydrogenase and a Bioinspired Synthetic Ni Catalyst*. Angewandte Chemie International Edition, 2014. **53**: p. 11538-11542.

63. Siritanaratkul B., et al., *Selective, light-driven enzymatic dehalogenations of organic compounds*. RSC Advances, 2016. **6**: p. 84882-84886.
64. Urlacher V.B., Girhard M., *Cytochrome P450 Monooxygenases in Biotechnology and Synthetic Biology*. Trends in Biotechnology, 2019.
65. Schulz S., et al., *Biocatalysis: Key to Selective Oxidations*. ChemCatChem, 2012. **4**: p. 1889-1895.
66. Fasan R., *Tuning P450 Enzymes as Oxidation Catalysts*. ACS Catalysis, 2012. **2**: p. 647-666
67. Dong J., et al., *Biocatalytic oxidation reactions - a Chemist's perspective*. Angewandte Chemie International Edition, 2018. **57**: p. 9238-9261.
68. Lee S.H., et al., *Photobiocatalysis: Activating Redox Enzymes by Direct or Indirect Transfer of Photoinduced Electrons*. Angewandte Chemie International Edition, 2018. **57**: p. 7958-7985.
69. Jiang L., et al., *Enhanced Metabolic Activity of Cytochrome P450 via Carbon Nanocage-Based Photochemical Bionanoreactor*. ACS Appl Mater Interfaces, 2018. **10**: p. 41956-41961.
70. Lu J., et al., *Enhanced light-driven catalytic performance of cytochrome P450 confined in macroporous silica*. Chemical Communications, 2016. **52**:7703-7706.
71. Fukuzumi S., Nam W., *Thermal and photoinduced electron-transfer catalysis of high-valent metal-oxo porphyrins in oxidation of substrates*. Journal of Porphyrins and Phthalocyanines, 2016. **20**: p. 35-44.
72. Fang X., et al., *Photochemical Bionanoreactor for Efficient Visible-Light-Driven in Vitro Drug Metabolism*. Analytical Chemistry 2017. **89**: p. 7365-7372.
73. Park J.H., et al., *Cofactor-Free Light-Driven Whole-Cell Cytochrome P450 Catalysis*. Angewandte Chemie International Edition, 2014. **54**: p. 969-973.
74. Le T.K., et al., *Solar-driven biocatalytic C-hydroxylation through direct transfer of photoinduced electrons*. Green Chemistry, 2019.
75. Zilly F.E., et al., *Deazaflavins as mediators in light-driven cytochrome P450 catalyzed hydroxylations*. Chemical Communications, 2009. P. 7152-7154.
76. Bains R.K., et al., *Light-Activated Electron Transfer and Turnover in Ru-Modified Aldehyde Deformylating Oxygenases*. Inorganic Chemistry, 2018. **57**: p. 8211-8217.
77. Sosa V., et al., *Selective Light-Driven Chemoenzymatic Trifluoromethylation/Hydroxylation of Substituted Arenes*. ACS Catalysis 2018. **8**: p. 2225-2229.
78. Shalan H., et al., *Correlating the para-Substituent Effects on Ru(II)-Polypyridine Photophysical Properties and on the Corresponding Hybrid P450 BM3 Enzymes Photocatalytic Activity*. Inorganic Chemistry, 2017. **56**: p. 6558-6564.
79. Kato M., et al. *Selective C-H bond functionalization with light-driven P450 biocatalysts*. Comptes Rendus Chimie, 2017. **20**: p. 237-242.
80. Tran N.H., et al., *An Efficient Light-Driven P450 BM3 Biocatalyst*. Journal of the American Chemical Society 2013. **135**: p. 14484-1447.
81. Lam Q., Kato M., Cheruzel L., *Ru(II)-diimine functionalized metalloproteins: From electron transfer studies to light-driven biocatalysis*. Biochimica et Biophysica Acta (BBA) – Bioenergetics, 2016. **1857**: p. 589-597.
82. Kato M., et al., *Regio- and stereoselective hydroxylation of 10-undecenoic acid with a light-driven P450 BM3 biocatalyst yielding a valuable synthon for natural product synthesis*. Bioorganic & Medicinal Chemistry, 2014. **22**: p. 5687-5691.
83. Jensen K., et al., *Light-Driven Cytochrome P450 Hydroxylations*. ACS Chemical Biology, 2011. **6**: p. 533-539.
84. Mellor S.B., et al., *Fusion of Ferredoxin and Cytochrome P450 Enables Direct Light-Driven Biosynthesis*. ACS Chemical Biology, 2016. **11**: p.1862-1869.

85. Hollmann F., et al., *A Light-Driven Stereoselective Biocatalytic Oxidation*. Angewandte Chemie International Edition, 2007. **46**: p. 2903-2906.
86. **Chapter 3**
87. Schroeder L., et al., *Photochemically Driven Biocatalysis of Halogenases for the Green Production of Chlorinated Compounds*. ChemCatChem, 2018. **10**: p. 3336-3341.
88. Bissaro B., et al., *Fueling biomass-degrading oxidative enzymes by light-driven water oxidation*. Green Chemistry, 2016. **18**: p. 5357-5366.
89. Park J.T., et al., *NAD(P)H oxidase V from Lactobacillus plantarum (NoxV) displays enhanced operational stability even in absence of reducing agents*. Journal of Molecular Catalysis B: Enzymatic: Enzyme, 2011. **71**: p. 159-165.
90. Jiang R., Bommaris A.S., *Hydrogen peroxide-producing NADH oxidase (nox-1) from Lactococcus lactis*. Tetrahedron Asymmetry, 2004. **15**: p. 2939-2944.
91. Riebel B., et al., *Cofactor Regeneration of both NAD⁺ from NADH and NADP⁺ from NADPH:NADH Oxidase from Lactobacillus sanfranciscensis*. Advanced Synthesis & Catalysis, 2003. **345**: p. 707-712.
92. Riebel B.R., et al., *Cofactor Regeneration of NAD⁺ from NADH: Novel Water-Forming NADH Oxidases*. Advanced Synthesis & Catalysis, 2002. **344**: p. 1156-1168.
93. Paul C.E., et al., *Escherichia coli/ADH-A: An All-Inclusive Catalyst for the Selective Biooxidation and Deracemisation of Secondary Alcohols*. ChemCatChem, 2013. **5**: p. 3875–3881.
94. Orbeagozo T., et al., *Biocatalytic oxidation of benzyl alcohol to benzaldehyde via hydrogen transfer*. Tetrahedron, 2009. **65**: p. 6805-6809.
95. Lavandera I., et al., *One-Way Biohydrogen Transfer for Oxidation of sec-Alcohols*. Organic Letters, 2008. **10**: p. 2155-2158.
96. Kroutil W., et al., *Biocatalytic Oxidation of Primary and Secondary Alcohols*. Advanced Synthesis & Catalysis, 2004. **346**: p. 125-142.
97. Ruppert R., Steckhan E. *Efficient Photoelectrochemical Insitu Regeneration of Nad(P)⁺ Coupled to Enzymatic Oxidation of Alcohols*. Journal of the Chemical Society, Perkin Transactions 2, 1989. P. 811-814.
98. Gargiulo S., Arends IWCE, Hollmann F. *A Photoenzymatic System for Alcohol Oxidation*. ChemCatChem. 2011. **3**: p. 338-342.
99. Rauch M., et al., *Photobiocatalytic alcohol oxidation using LED light sources*. Green Chemistry, 2017. **19**: p. 376-379.
100. Jones J.B., Taylor K.E., *Nicotinamide coenzyme regeneration – Flavin mononucleotide (riboflavin phosphate) as an efficient, economical, and enzyme-compatible recycling agent*. Canadian Journal of Chemistry, 1976. **54**: p. 2969-2973.
101. Boratyński F., et al., *Chemo-Enzymatic Synthesis of Optically Active γ - and δ -Decalactones and Their Effect on Aphid Probing, Feeding and Settling Behavior*. PLoS One, 2016. **11**: e0146160.
102. Boratynski F., Smuga M., Wawrzenczyk C., *Lactones 42. Stereoselective enzymatic/microbial synthesis of optically active isomers of whisky lactone*. Food Chemistry, 2013. **141**: p. 419-427.
103. Boratynski F., Kielbowicz G., Wawrzenczyk C., *Lactones 34. Application of alcohol dehydrogenase from horse liver (HLADH) in enantioselective synthesis of $[\delta]$ - and $[\text{var epsilon}]$ -lactones*. Journal of Molecular Catalysis B: Enzymatic, 2010. **65**: p. 30-36.
104. Kochius S, et al., *Light-Accelerated Biocatalytic Oxidation Reactions*. ChemPlusChem, 2014. **79**: p. 1554-1557.
105. Burek B.O.O., et al., *Hydrogen peroxide driven biocatalysis*. Green Chemistry, 2019.
106. Valderrama B., Ayala M., Vazquez-Duhalt R., *Suicide Inactivation of Peroxidases and the Challenge of Engineering More Robust Enzymes*. Chemistry & Biology, 2002. **9**: p. 555-565.

107. Perez D.I., et al., *Visible light-driven and chloroperoxidase-catalyzed oxygenation reactions*. Chemical Communications, 2009. **44**: p. 6848 - 6850.
108. Churakova E., Arends I.W.C.E., Hollmann F., *Increasing the Productivity of Peroxidase-Catalyzed Oxyfunctionalization: A Case Study on the Potential of Two-Liquid-Phase Systems*. ChemCatChem, 2013. **5**: p. 565-568.
109. Churakova E., et al., *Specific photobiocatalytic oxyfunctionalization reactions*. Angewandte Chemie International Edition, 2011. **50**: p. 10716-10719.
110. Zachos I., et al., *Photobiocatalytic decarboxylation for olefin synthesis*. Chemical Communications, 2015. **51**: p. 1918-1921.
111. Bojarra S., et al., *Bio-based α,ω -Functionalized Hydrocarbons from Multi-step Reaction Sequences with Bio- and Metallo-catalysts Based on the Fatty Acid Decarboxylase OleTJE*. ChemCatChem, 2018. **10**: p. 1192-11201.
112. Choi D.S., et al., *Photoelectroenzymatic Oxyfunctionalization on Flavin-Hybridized Carbon Nanotube Electrode Platform*. ACS Catalysis, 2017. **7**: p. 1563-1567.
113. Zhang W., et al., *Selective activation of C-H bonds by cascading photochemistry with biocatalysis*. Angewandte Chemie International Edition, 2017. **129**: p. 15451-15455.
114. Zhang W., et al., *Selective aerobic oxidation reactions using a combination of photocatalytic water oxidation and enzymatic oxyfunctionalizations*. Nature Catalysis, 2018. **1**: p. 55-62.
115. Willot S.J.P., et al., *Expanding the Spectrum of Light-Driven Peroxygenase Reactions*. ACS Catalysis, 2019. **9**: p. 890-4.
116. Girhard M., *Light-driven biocatalysis with cytochrome P450 peroxygenases*. Biotechnology and Applied Biochemistry, 2013. **60**: p. 111-118.
117. Seel C.J., et al., *Atom-Economic Electron Donors for Photobiocatalytic Halogenations*. ChemCatChem, 2018. **10**: p. 3960-3963.
118. Lauder K., et al., *Photo-biocatalytic One-Pot Cascades for the Enantioselective Synthesis of 1,3-Mercaptoalkanol Volatile Sulfur Compounds*. Angewandte Chemie International Edition, 2018. **57**: p. 5803-5807.
119. Ding X., et al., *Concurrent Asymmetric Reactions Combining Photocatalysis and Enzyme Catalysis: Direct Enantioselective Synthesis of 2,2-Disubstituted Indol-3-ones from 2-Arylindoles*. Angewandte Chemie International Edition, 2019. **58**: p. 118-124.
120. Guo X., et al., *Enantioselective synthesis of amines by combining photoredox and enzymatic catalysis in a cyclic reaction network*. Chemical Science, 2018. **9**: p. 5052-5056.
121. Guo X., Wenger O.S., *Reductive Amination by Photoredox Catalysis and Polarity-Matched Hydrogen Atom Transfer*. Angewandte Chemie International Edition, 2018. **57**: p. 2469-2473.
122. Yang Q., et al., *Mild dynamic kinetic resolution of amines by coupled visible-light photoredox and enzyme catalysis*. Chemical Communications, 2018. **54**: p. 14065-14068.
123. Litman Z.C., et al., *Cooperative asymmetric reactions combining photocatalysis and enzymatic catalysis*. Nature, 2018. **560**: p. 355-359.
124. Zhang W., et al. *Combining Photo-Organic Redox- and Enzyme Catalysis Facilitates Asymmetric C-H Bond Functionalization*. European Journal of Organic Chemistry, 2019. **10**: p. 80-84.
125. Gacs J., et al., *A Photo-Enzymatic Cascade to Transform Racemic Alcohols into Enantiomerically Pure Amines*. Catalysts, 2019. **9**: p. 305.
126. Schmidt S., et al., *Towards environmentally acceptable synthesis of chiral α -hydroxy ketones via oxidase-lyase cascades*. Green Chemistry, 2017. **19**: p. 1226-1229.
127. Chitnis P.R., *Photosystem I: Function and physiology*. Annual Review of Plant Biology, 2001. **52**: p. 593-626.

128. Barber J., *Photosystem II: the water splitting enzyme of photosynthesis and the origin of oxygen in our atmosphere*. Quarterly Reviews of Biophysics, 2016. **49**: p. 20.
129. Sancar A., *Structure and Function of DNA Photolyase and Cryptochrome Blue-Light Photoreceptors*. Chemical Reviews, 2003. **103**: p. 2203-2238.
130. Sancar A., *Mechanisms of DNA Repair by Photolyase and Excision Nuclease (Nobel Lecture)*. Angewandte Chemie International Edition, 2016. **55**: p. 8502-8527.
131. Schoefs B., Franck F., *Protochlorophyllide reduction: Mechanisms and evolution*. Photochemistry & Photobiology, 2003. **78**: p. 543-557.
132. Sorigué D., et al., *An algal photoenzyme converts fatty acids to hydrocarbons*. Science, 2017. **357**: p. 903-907.
133. Sorigue D., et al. *Microalgae Synthesize Hydrocarbons from Long-Chain Fatty Acids via a Light-Dependent Pathway*. Plant Physiology, 2016. **171**: p. 2393-2405.
134. Huijbers M., Zhang W., Hollmann F., *Light-driven enzymatic decarboxylation of fatty acids*. Angewandte Chemie International Edition, 2018. **57**: p. 13648-13651.
135. Zhang W., et al., *Hydrocarbon synthesis via photoenzymatic decarboxylation of carboxylic acids*. Journal of the American Chemical Society, 2019. **141**: p. 3116–3120.
136. Wu Q., et al., *Light-Driven Kinetic Resolution of α -Functionalized Carboxylic Acids Enabled by Engineered Fatty Acid Photodecarboxylase*. Angewandte Chemie International Edition, 2019.
137. Biegasiewicz KF, et al., *Catalytic promiscuity enabled by photoredox catalysis in nicotinamide-dependent oxidoreductases*. Nature Chemistry, 2018. **10**: p. 770-775.
138. Emmanuel M.A., et al., *Accessing non-natural reactivity by irradiating nicotinamide-dependent enzymes with light*. Nature, 2016. **540**: p. 414-417.
139. Sandoval B.A., Meichan A.J., Hyster T.K., *Enantioselective Hydrogen Atom Transfer: Discovery of Catalytic Promiscuity in Flavin-Dependent 'Ene'-Reductases*. Journal of the American Chemical Society, 2017. **139**: p. 11313-11316.
140. Sandoval B.A., et al., *Photoenzymatic Catalysis Enables Radical-Mediated Ketone Reduction in Ene-Reductases*. Angewandte Chemie International Edition, 2019.

Chapter 3



Photoenzymatic epoxidation of styrenes

Morten M.C.H. van Schie, Caroline E. Paul, Isabel W.C.E. Arends, Frank Hollmann

Based on:

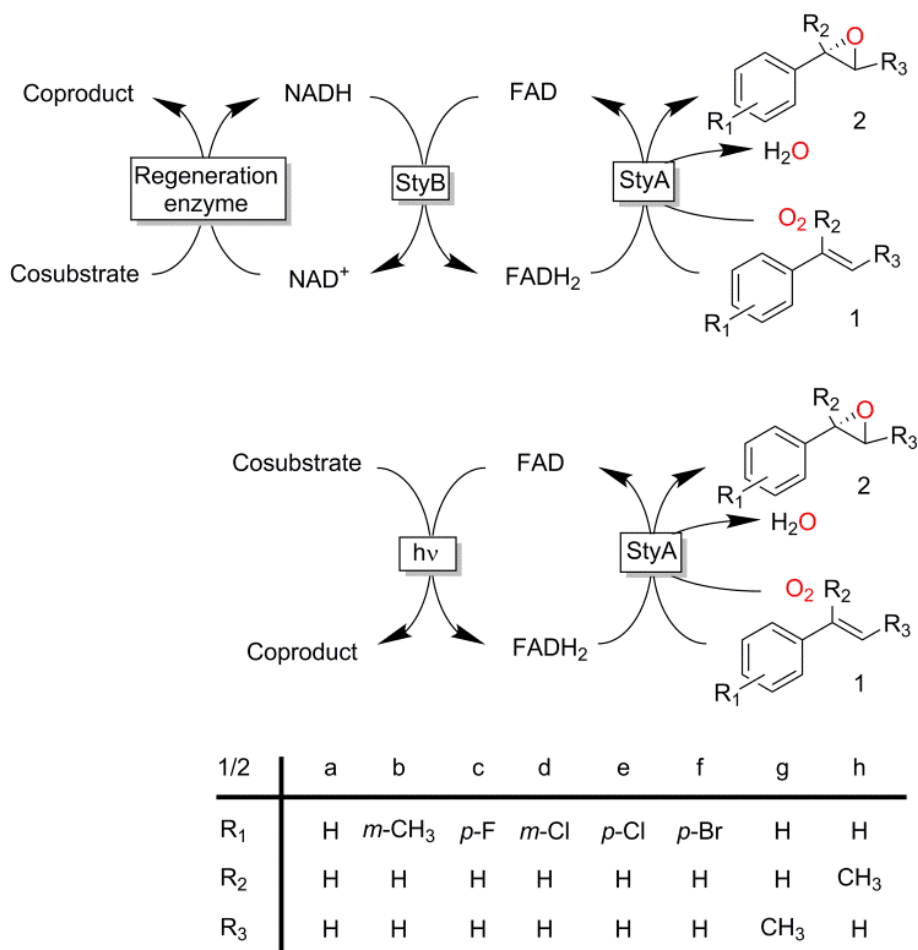
Van Schie, M.M.C.H., *et al.*, *Photoenzymatic epoxidation of styrenes*. Chemical Communications, 2019. **55**: p. 1790 - 1792

Summary

Two-component-diffusible-flavomonooxygenases are versatile biocatalysts for selective epoxidation-, hydroxylation- or halogenation reactions. Their complicated molecular architecture can be simplified using photochemical regeneration of the catalytically active, reduced FADH₂ prosthetic group. In this contribution we provide the proof-of-concept and characterization for the direct regeneration of the styrene monooxygenase from *Pseudomonas*.

Introduction

So-called two-component, diffusible flavin monooxygenases (2CDFMOs) are a diverse and preparatively highly interesting class of enzymes. For example, 2CDFMOs catalyse regioselective aromatic hydroxylations and halogenation reactions as well as stereoselective epoxidation reactions [1-4]. For this, 2CDFMOs rely on the reductive activation of molecular oxygen mediated by an enzyme-bound, reduced flavin cofactor (generally the reduced form of flavin adenine dinucleotide, FADH₂). FADH₂ itself is regenerated by a NAD(P)H-dependent reductase. There is an ongoing debate on the mechanism on how FADH₂ reaches the monooxygenase subunit. Some studies suggest a freely diffusible FADH₂ [5] while others found indications for a complex between the reductase- and monooxygenase subunits thereby channelling the reduced flavin and protecting it from spontaneous aerobic reoxidation [6-8]. The complicated molecular architecture of 2CDFMOs poses a challenge for their preparative application, which is mostly addressed by whole-cell systems [9-12]. More recently, also fusion proteins combining the reductase- and monooxygenase subunits in one polypeptide chain are moving into the research focus [13, 14]. Reactions utilising isolated enzymes require the entire cascade outlined in Scheme 1 [15-17]. Hence, it is no surprise that alternative, more direct and simple regeneration systems for the reduced flavin cofactor have been evaluated. Examples include, transition metal-catalysed reduction of FAD [18, 19], direct electrochemical regeneration [20, 21] or using chemical reductants [22].



Scheme 1. Comparison of the traditional regeneration system for StyA involving two additional enzymes (top) and the nicotinamide cofactor with the simplified, direct photochemical regeneration of FADH₂ (bottom).

All these methods, however, despite significantly simplifying the reaction scheme, exhibited drawbacks such as reliance on specialized equipment or dependency on costly and enzyme inactivating transition metal complexes. Instead, direct photochemical regeneration of reduced enzyme prosthetic groups is gaining increasing attention [23, 24]. We therefore set out to explore the possibility of direct, photocatalytic regeneration of FADH₂ to promote StyA-catalysed epoxidations of styrene and its derivatives (Scheme 1, bottom). Very recently, Kottke and coworkers reported the successful application of this approach to promote a 2CDFMO-driven halogenation reaction [25].

Results

The biocatalyst used in our study was styrene monooxygenase from *Pseudomonas* sp. VLB120 (StyA) [5, 26]. The enzyme was recombinantly expressed in *Escherichia coli* and purified in one step yielding approximately 0.11 g of technically pure StyA per gram of cell free extract. Crude cell free extracts (CFE) were used for the first experiments (figure 1). Even though the CFE contained significant catalase activity (figure 7), we routinely added catalase externally to circumvent any possible negative effect of stemming from the spontaneous aerobic reoxidation of FADH_2 [27]. Pleasingly, already in a first experiment under arbitrary reaction conditions, catalytic turnover and production of enantiopure *S*-styrene oxide was observed (figure 1). It is worth mentioning here that all negative control experiments (i.e. performing the reaction under identical conditions while leaving out one of the reaction components StyA, FAD, EDTA or light) did not yield detectable product formation (data not shown)

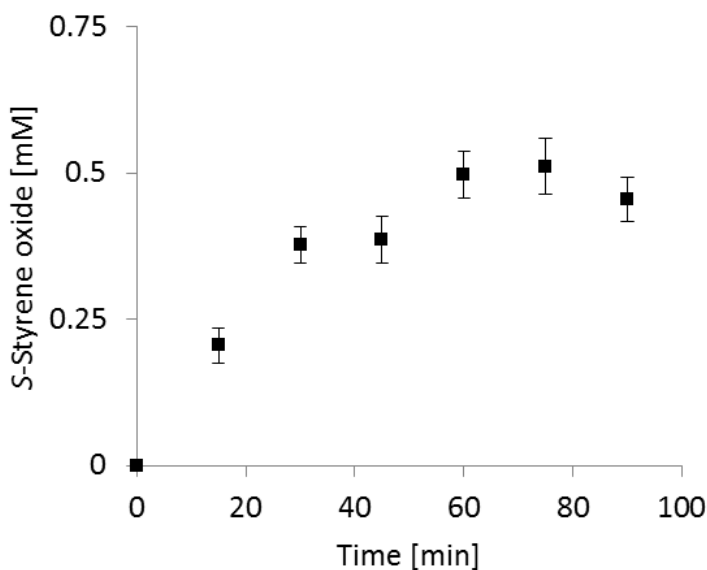
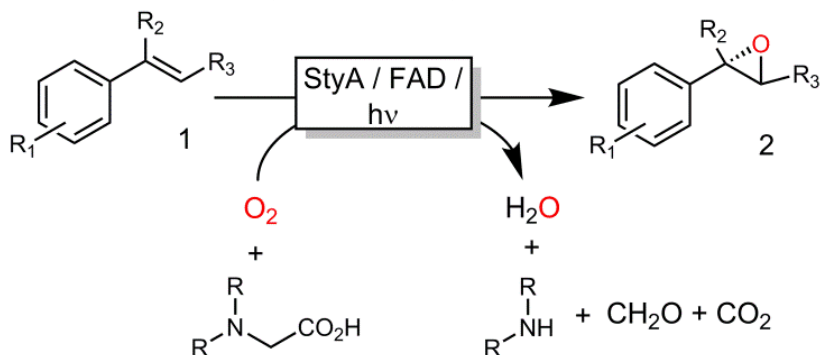


Figure 1: Time-course of the first photobiocatalytic epoxidation of styrene to *S*-styrene oxide. General conditions: $[\text{styrene}]_0 = 5 \text{ mM}$, $[\text{cell free extract}] = 1.7 \text{ g l}^{-1}$ containing $4 \text{ }\mu\text{M}$ StyA, $[\text{FAD}] = 200 \text{ }\mu\text{M}$, $[\text{EDTA}] = 20 \text{ mM}$, catalase = 600 U ml^{-1} , 100 mM KPi buffer pH 7.0, $30 \text{ }^\circ\text{C}$, stirring at 300 rpm , light intensity of 20% . Error bars show the standard deviation for three independent experiments.

Table 1. Product scope of the photo-enzymatic epoxidation system.



Product	[Product] [mM]	ee [%]
2a	0.60 ± 0.04	>99
2b	2.12 ± 0.11	98
2c	0.86 ± 0.13	>99
2d	3.10 ± 0.19	95
2e	1.06 ± 0.14	97
2f	0.65 ± 0.15	>99
2g	1.45 ± 0.09	>99
2h	0.40 ± 0.12	>99

Conditions: [substrate]₀ = 5 mM, [StyA] = 5.3 μ M, [FAD] = 200 μ M, [EDTA] = 20 mM, [catalase] = 600 U ml⁻¹, [DMSO] = 1.25% (v/v), 100 mM KPi buffer pH 7, 35 °C, stirring at 300 rpm, light intensity of 40% for 1 h. The standard deviations represent those for three independent experiments.

Encouraged by these results, the substrate scope of this photoenzymatic reaction system was investigated. As shown in table 1, both the relative reaction rates and the enantioselectivity of the photoenzymatic epoxidation reaction are comparable to results reported previously [11]. Indeed, excellent enantiomeric excess was achieved (95 to 99%).

Chapter 3

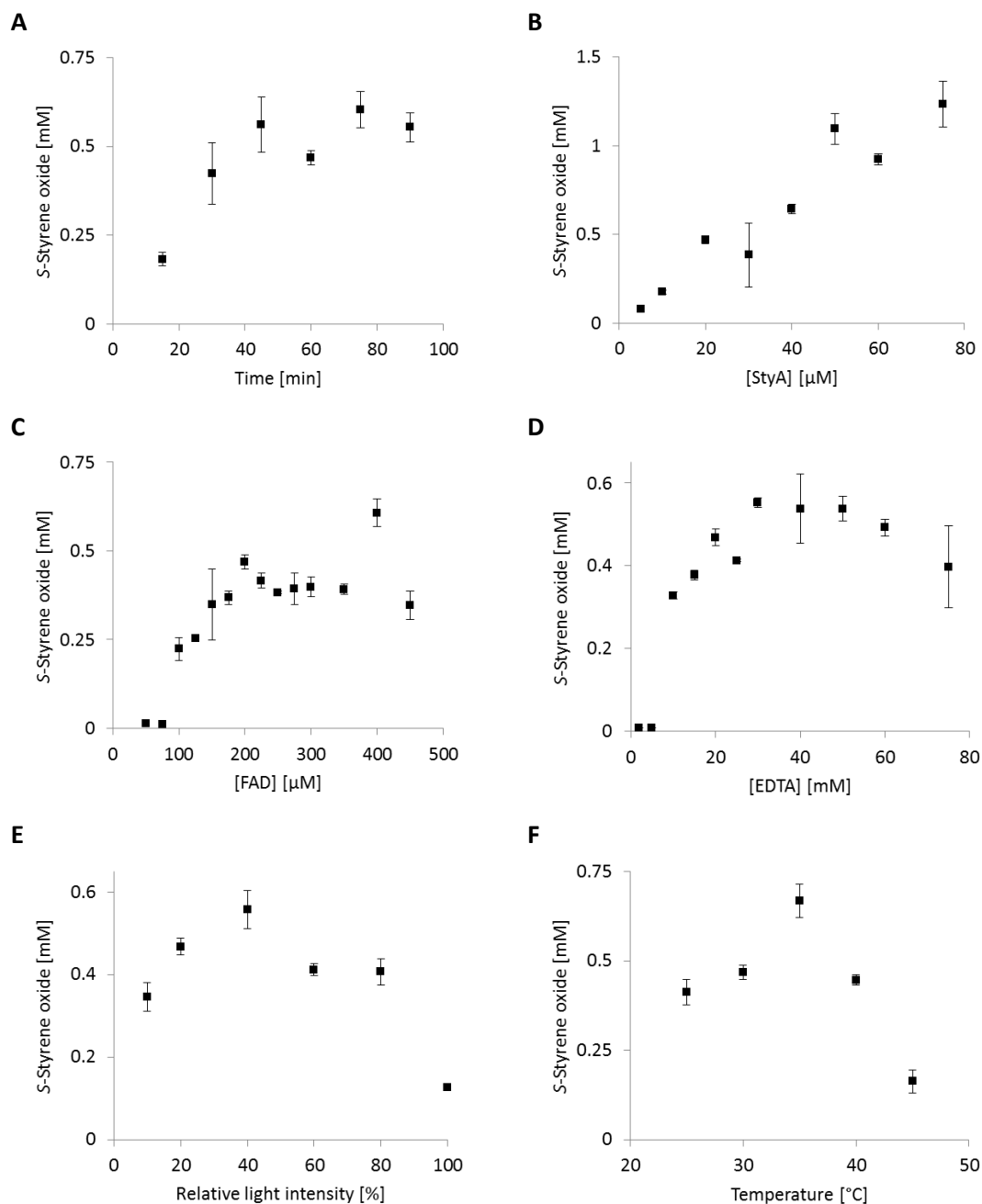


Figure 2. Influence of some reaction parameters on the rate of the photoenzymatic epoxidation of styrene. General conditions (unless indicated otherwise in the figure): [styrene]₀ = 5 mM, [StyA] = 20 μM, [FAD] = 200 μM, [EDTA] = 20 mM, catalase = 600 U ml⁻¹, [DMSO] = 1.25% (v/v), 100 mM KPi buffer (pH 7), 30 °C, stirring at 300 rpm, light intensity of 20% for 1 h. Error bars show the standard deviation for three independent experiments.

In order to further understand this system, we further characterised the influence of the single reaction components on the efficiency of the overall reaction using the technically pure StyA (figure 2). As compared to the cell free extract (figure 1) the technically pure enzyme had lost a considerable amount of its activity (figure 2A). The product formation rate correlated linearly with the biocatalyst concentration applied (figure 2B), indicating that the biocatalytic step was overall rate-limiting. Also increasing the concentration of the photocatalyst increased the overall product formation reaction (figure 2C) indicating that the concentration of the photoexcited FAD was ratelimiting as well. Below an FAD concentration of 100 μM no product formation was detectable, which may be attributed to the corresponding low concentration of FADH_2 and inefficient utilisation by StyA [28, 29]. Above approximately 200 μM FAD, no further acceleration of the reaction rate was observed. Possibly this can be attributed to the decreasing optical transparency of the reaction mixture at elevated FAD concentration resulting in a complete utilization of all photons offered to the reaction system. Alternatively, elevated FAD concentrations may also favour the (undesired) futile oxidation of FADH_2 to FAD and H_2O_2 as observed in previous experiments [27]. Similar observations have been made previously [19, 20, 30]. Variation of the concentration of the sacrificial electron donor (EDTA) had a similar effect (figure 2D). Additionally, the light intensity significantly influenced the overall reaction (figure 2E). To a certain extent, brighter reaction conditions favoured increased product formation. However, at very high light intensities also a dramatic reduction of the reaction rate was observed. We attribute this to an increased photobleaching of FAD leading to flavin degradation products [31], which are not accepted by StyA as prosthetic group. Finally, it is worth mentioning that an apparent optimal temperature of ca. 35 $^\circ\text{C}$ was observed (figure 2F). This is perfectly in line with the mesophilic character of the original host of StyA.

One shortcoming of the current photoenzymatic reaction setup, however, is the comparably poor robustness of the reactions (figure 2A). In general, after reaction times of ca. 1 hour, no further conversion could be detected. In order to shed light on the reason for this limitation, a range of control experiments was conducted (figure 3). The biocatalyst (StyA) itself was stable under the reaction conditions (figure 3, column 2). However, when illuminating the photocatalyst (FAD) for 30 minutes prior to the start of the reaction (figure 3, columns 3 and 4) significantly reduced styrene oxide accumulation was observed. This inactivation was almost complete illuminating FAD alone and was somewhat less pronounced in the presence of EDTA (serving as reducing agent for photoexcited FAD; the resulting reduced flavin being less photoactive). Clearly, the photoinstability of FAD represents the major limitation of the current reaction setup. This is also supported by the changes of the FAD spectrum upon illumination (figure 4) and is in line with the well-known photodegradation of FAD to lumichrome [32]. While the latter

still possesses the desired photochemical properties it is not accepted by StyA as a prosthetic group, thereby explaining the poor robustness of the current reaction setup.

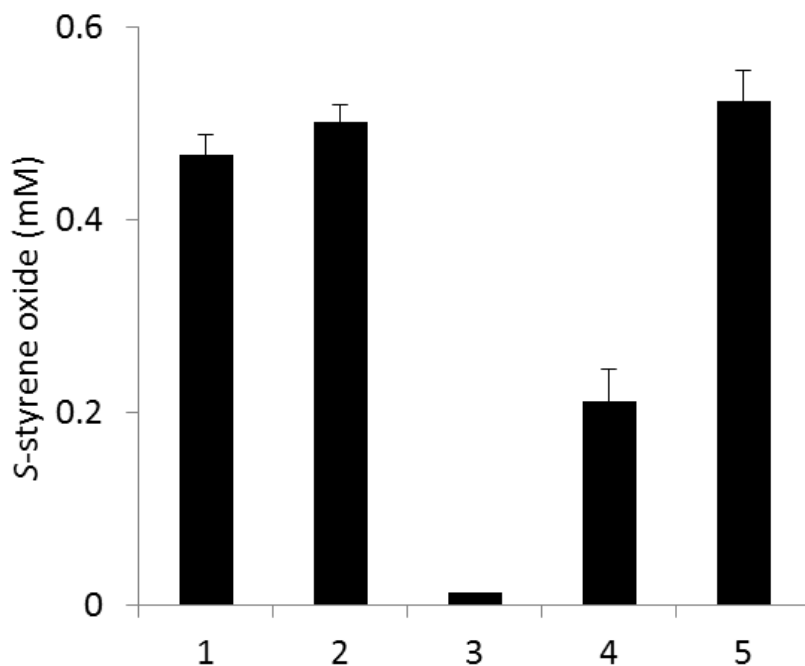


Figure 3. Control reactions to determine the robustness of the system. 1: Standard reaction. 2: StyA illuminated for 30 min before starting the reaction. 3: StyA and FAD illuminated for 30 min before starting the reaction. 4: StyA, FAD and EDTA illuminated for 30 min before starting the reaction. 5: Total reaction mixture incubated in the dark for 30 min before starting the reaction. General conditions: $[\text{styrene}]_0 = 5 \text{ mM}$, $[\text{StyA}] = 20 \text{ }\mu\text{M}$, $[\text{FAD}] = 200 \text{ }\mu\text{M}$, $[\text{EDTA}] = 20 \text{ mM}$, catalase = 600 U ml^{-1} , $100 \text{ mM KPi buffer (pH 7)}$, $30 \text{ }^\circ\text{C}$, stirring at 300 rpm , light intensity of 20% for 1 h . Error bars show the standard deviation for three independent experiments.

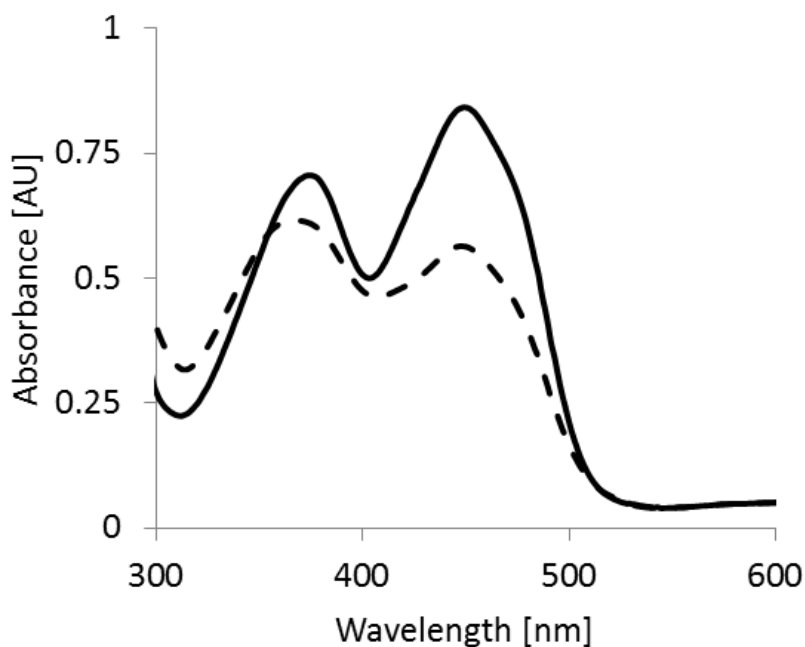


Figure 4. Absorption spectra of the FAD before (solid) and after (dashed) illumination under the reaction conditions. The spectra correspond to the degradation of the FAD as reported before [31].

Another factor decreasing the efficiency of the reaction is the uncoupling of the electrons at the reduced flavin to oxygen instead of the intended StyA. A phenomenon previously named the oxygen dilemma, as the O_2 is needed for the reaction, but also decreases the efficient use of the inserted electrons [27]. This process becomes even more pronounced upon illumination of the (oxidized) flavin as is shown in figure 5.

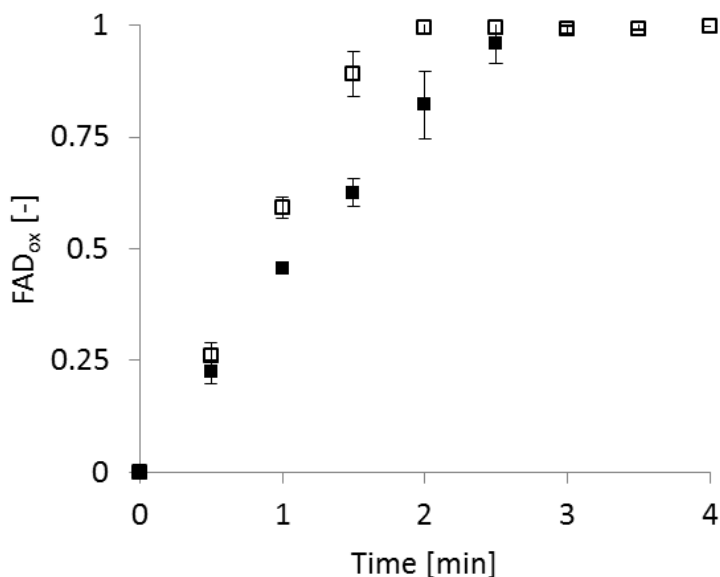


Figure 5: The reoxidation of FADH₂ in dark (solid) or upon illumination (open) over time in the absence of StyA and styrene. The FAD was previously reduced under anaerobic conditions with a stoichiometric amount of EDTA. Conditions: [FADH₂] = 100 μ M, 100 mM KPi buffer (pH 7), RT, stirring at 300 rpm, light intensity of 10%. Error bars show the error for two independent experiments.

Conclusion

Overall, in the present study, we have provided a proof-of-concept for the direct, photochemical regeneration of styrene monooxygenase for the generation of enantiomerically pure epoxides. The photoinstability of the photocatalyst/prosthetic group FAD was identified as the major limitation of the current setup. Even though at the present stage of development this system is not suitable for preparative application we are convinced that it's conceptual simplicity will convince others to further improve the system.

Material and methods

Chemicals

All chemicals were obtained from Sigma Aldrich in the highest purity available and used without further treatment. BNAH and the styrene oxides were synthesized

following published procedures [22, 33], with the exception of styrene oxide, 4-fluorostyrene oxide, 4-chlorostyrene and 4-bromostyrene oxide, which were commercially available.

Synthesis of BNAH

1-Benzyl-1,4-dihydronicotinamide (BNAH) was synthesized exactly as previously described [33]. Briefly, a reaction mixture containing benzyl bromide (1.1 equivalence) and nicotinamide in acetonitrile (1 M) was refluxed overnight. After cooling, diethyl ether was added, the resulting white precipitate was filtered and further washed with diethyl ether, obtaining 1-benzyl-3-carbamoylpyridinium bromide. The reduction was carried out in distilled water with Na_2CO_3 (3 equivalences) and $\text{Na}_2\text{S}_2\text{O}_4$ (5 equivalence) at room temperature over 3 hours. The yellow precipitate formed was filtered, recrystallized in methanol-water, filtered and washed with cooled distilled water, and dried over P_2O_5 in a vacuum desiccator. The ^1H NMR spectrum was recorded on a Bruker Avance III 400 spectrometer.

The synthesis of racemic epoxides was carried out as previously described [2]: the styrene derivative (2 mmol) was diluted in CH_2Cl_2 (10 mL) and mixed with distilled water (10 mL) containing NaHCO_3 (1 g); m-CPBA (2.2 mmol) was slowly added. The reaction mixture was stirred at room temperature for 3 h. The reaction was quenched with aqueous Na_2SO_3 (1.3 g in 10 mL) and left to stir for 20 min. The aqueous phase was extracted with CH_2Cl_2 (2 × 10 mL) and the combined organic phases were washed with NaHCO_3 (2 × 25 mL) and distilled water (25 mL). The organic phase was dried over anhydrous MgSO_4 , filtered and evaporated under reduced pressure to provide the product. The epoxide products were not further purified as NMR and GC/MS analyses were in agreement with literature [22]. Small peaks of impurities may appear on the GC chromatograms of the racemic epoxides.

Catalyst preparation

Styrene monooxygenase A (StyA) from *Pseudomonas* sp. strain VLB120 production was based on a previous protocol [5]. 5 ml of autoclaved LB media containing $50\ \mu\text{g}\ \text{ml}^{-1}$ kanamycin and $10\ \text{mg}\ \text{ml}^{-1}$ glucose (both filter sterilized) were inoculated with *E. coli* JM101, with the pSPZ10 plasmid containing StyA genes, from a glycerol stock and incubated overnight. According to the original protocol, overexpression was performed in 2 l flasks with 0.5 l of autoclaved M9* medium. The medium was supplemented with $5\ \text{g}\ \text{l}^{-1}$ glucose, $50\ \mu\text{g}\ \text{ml}^{-1}$ kanamycin, 0.1 % (v/v) 1000x US* trace element solution, 1 mM MgSO_4

Chapter 3

and 0.010 g l⁻¹ thiamine HCl, which were all filter sterilized. The compositions of M9* medium and US* trace elements are shown in table 2. The cells were grown at 30 °C while shaking at 250 rpm. StyA gene overexpression was induced by addition of 0.05% (v/v) dicyclopropyl ketone at an A₄₅₀ of 0.4 AU. After 16 h of further incubation, the cells were harvested by centrifugation (15 min at 11 300 x g) and resuspended in 20 mM Tris buffer pH 7.5 containing 1 mM DTT, 1 mM MgCl₂ and 10 % (v/v) glycerol. The solutions were stored at -80 °C until further use.

Table 2. Composition of the media and trace elements used for the fermentation.

M9* Minimal medium	US* Trace elements
18.0 g L ⁻¹ KH ₂ PO ₄	10 mM HCl
9.0 g L ⁻¹ K ₂ HPO ₄	1.50 g L ⁻¹ MnCl
0.5 g L ⁻¹ NaCl	1.05 g L ⁻¹ ZnSO ₄
1.0 g L ⁻¹ NH ₄ Cl	0.30 g L ⁻¹ H ₃ BO ₃
	0.25 g L ⁻¹ Na ₂ MoO ₄ – 2 H ₂ O
pH adjusted to 7.4	0.15 g L ⁻¹ CuCl – 2 H ₂ O
	0.84 g L ⁻¹ Na ₂ EDTA – 2 H ₂ O
	4.87 g L ⁻¹ FeSO ₄ – 7 H ₂ O
	4.12 g L ⁻¹ CaCl ₂ – 2 H ₂ O

0.1 mg ml⁻¹ of DNase was added to the resuspended cell pellet. The solution was then passed twice through a cooled French press (1.9 bar, using a multi-shot Constant Cell Disruption Systems) and centrifuged (20 min at 11 300 x g and 4 °C). The supernatant was collected and subsequently concentrated using Amicon Ultra centrifugal filter units (15 ml, 30 kDa MWCO) and was either frozen in liquid nitrogen in order to obtain the cell free extract sample, or further purified. A 5 ml HiTrap QFF column (GE Healthcare, UK) was used for the purification. StyA was eluted with a linear NaCl gradient (0 – 0.5 M, elution at 0.36 M) using a 20 mM Tris buffer at pH 7.5. Samples containing StyA were pooled, desalted, concentrated and frozen in liquid nitrogen. The protein concentrations of both the cell free extract as the purified StyA were determined using a Bradford assay. The purity of the extracts was checked via a protein gel (SDS 12% PAGE) (figure 6). 18% of the StyA activity remained. A purification table is shown in table 3. Monooxygenase activity was confirmed (not quantified) via GC by the conversion of styrene to styrene oxide by the protein sample using the direct reduction of FAD by a NADH mimic (BNAH) [33]. Reaction mixtures consisted of 1.7 mg mL⁻¹ of the cell free extract, 5 mM styrene, 100 µM FAD, 600

U ml⁻¹ of catalase and 10 mM BNAH (from a 1 M stock in DMSO) in a 100 mM KPi buffer at pH 7.0 at 30 °C. Frozen protein samples were stored at -80 °C.

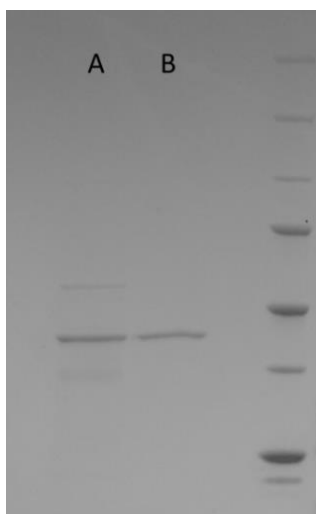


Figure 6. SDS PAGE of cell free extract containing StyA (lane A) and technically pure StyA (lane B).

Table 3. Purification table for the production of technically pure StyA

Purification step	Total protein content [mg]
Cell free extract	115
Cell free extract (>30 kDa)	81.1
Technically pure StyA	12.7

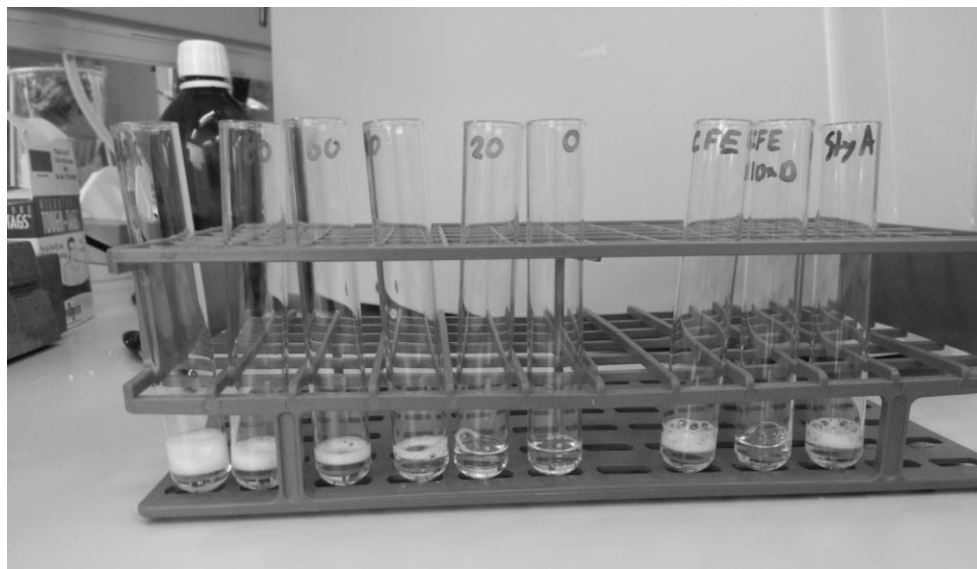


Figure 7. Catalase activity assay, performed as reported by Iwase *et al* [34]. Reaction mixtures all contained 10% H_2O_2 and 0.33 % Triton X-100 in 600 μl water. To those test tubes we further added 300 μL of 1000 to 0 U mL^{-1} catalase (first six test tubes), cell free extract (1.1 mg mL^{-1} and 0.11 mg mL^{-1}) or technically pure StyA ($55 \mu\text{M}$). Catalase would dismutate the hydrogen peroxide forming oxygen causing foam with the Triton X-100. These experiments show the presence of catalase already in the cell free extract and the technically pure StyA.

Reaction procedure

In general, reaction mixtures contained 5 mM substrate, 6.25% (v/v) DMSO, 20 μM StyA, 200 μM FAD, 20 mM EDTA and 600 U mL^{-1} catalase in a 100 mM KPi buffer at pH 7.0. 500 μl reactions solutions were incubated in 1.5 ml glass screw cap vials held upside down in a temperature controlled water bath. The mixture was stirred by a 6 mm Teflon magnetic bar at 300 rpm. The vials were illuminated through the bottom of the glass vials using a lightningcuretm LC8 - L9588 spot light source (Hamamatsu, Japan). In general, the intensity of the lamp was set to 20% or 40% (figure 8). A schematic representation of the setup is shown in figure 9. Samples were extracted by injecting 250 μl of ethyl acetate, containing 5 mM of dodecane, directly in the vial using a syringe. This method minimized the evaporation of the volatile styrenes. The organic phase was dried over MgSO_4 , mixed for several seconds, centrifuged and subsequently analysed by gas chromatography.

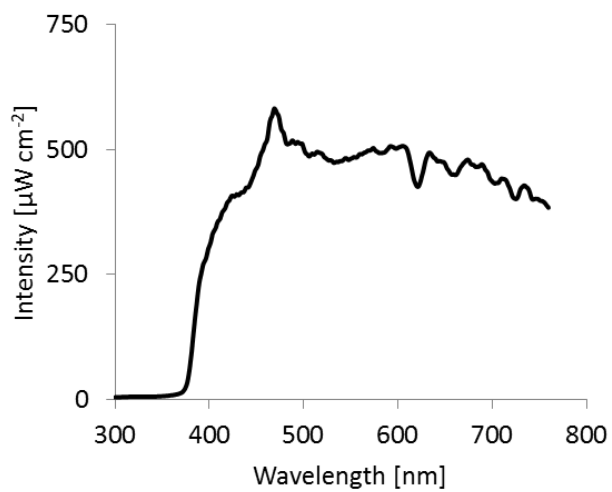


Figure 8. Spectrum of the light source at 10% intensity at a distance of 30 cm. The intensity was determined using a spectrophotometer, calibrated by a calibrated light source.

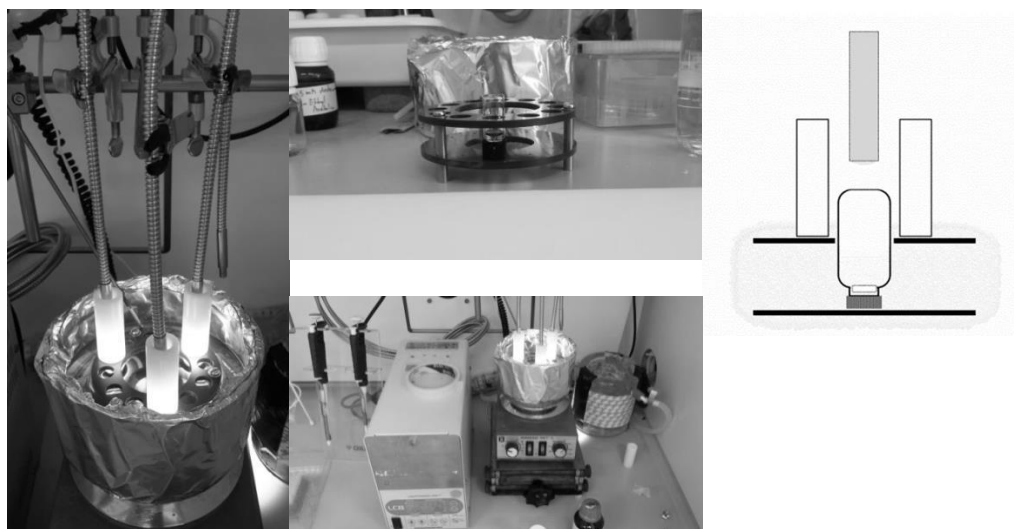


Figure 9. Representation of the photo-reactor setup.

Chapter 3

Gas chromatography

Measurements were performed on Shimadzu GC-2010 Plus gas chromatographs with an AOC-20i Auto injector with FID (Shimadzu, Japan), using helium as the carrier gas. The following columns were used:

Column A: Chirasil Dex CB: length: 25 m, inner diameter: 0.32 mm, film thickness: 0.25 μm

Column B: Hydrodex β -6TBDM, length: 50 m, inner diameter: 0.25 mm, film thickness: 0.15 μm

Column C: Lipodex E, length: 50 m, inner diameter: 0.25 mm, film thickness: 0.25 μm

The calibration curve of 4-chlorostyrene was used for the quantification of 3-chlorostyrene. The calibration curve of trans- β -methylstyrene was used for the quantification of 3-methylstyrene and α -methylstyrene. Representative gas chromatograms can be found in the supporting information.

References

1. Huijbers, M.M., et al., *Flavin dependent monooxygenases*. Archives of Biochemistry and Biophysics, 2014. **544**: p. 2-17.
2. Heine, T., et al., *Two-component FAD-dependent monooxygenases: current knowledge and biotechnological opportunities*. Biology-Basel, 2018. **7**(3): p. 42-Article No.: 42.
3. Ceccoli, R.D., D.A. Bianchi, and D.V. Rial, *Flavoprotein monooxygenases for oxidative biocatalysis: recombinant expression in microbial hosts and applications*. Frontiers in Microbiology, 2014. **5**.
4. Dijkman, W.P., et al., *Flavoprotein oxidases: classification and applications*. Applied Microbiology and Biotechnology, 2013. **97**(12): p. 5177-5188.
5. Otto, K., et al., *Biochemical characterization of StyAB from Pseudomonas sp strain VLB120 as a two-component flavin-diffusible monooxygenase*. Journal of Bacteriology, 2004. **186**(16): p. 5292-5302.
6. Kantz, A., et al., *Mechanism of flavin transfer and oxygen activation by the two-component flavoenzyme styrene monooxygenase*. Archives of Biochemistry and Biophysics, 2005. **442**(1): p. 102-116.
7. Kantz, A. and G.T. Gassner, *Nature of the reaction intermediates in the flavin adenine dinucleotide-dependent epoxidation mechanism of styrene monooxygenase*. Biochemistry, 2011. **50**(4): p. 523-532.
8. Morrison, E., et al., *Structure and mechanism of styrene monooxygenase reductase: New insight into the FAD-transfer reaction*. Biochemistry, 2013. **52**(35): p. 6063-6075.
9. Buehler, B., et al., *NADH availability limits asymmetric biocatalytic epoxidation in a growing recombinant Escherichia coli strain*. Applied and Environmental Microbiology, 2008. **74**(5): p. 1436-1446.
10. Park, J.-B., et al., *The efficiency of recombinant Escherichia coli as biocatalyst for stereospecific epoxidation*. Biotechnology and Bioengineering, 2006. **95**(3): p. 501-512.
11. Schmid, A., et al., *Integrated biocatalytic synthesis on gram scale: The highly enantio selective preparation of chiral oxiranes with styrene monooxygenase*. Advanced Synthesis & Catalysis, 2001. **343**(6-7): p. 732-737.
12. Toda, H., et al., *Microbial production of aliphatic (S)-epoxyalkanes by using Rhodococcus sp strain ST-10 styrene monooxygenase expressed in organic-solvent-tolerant Kocuria rhizophila DC2201*. Applied and Environmental Microbiology, 2015. **81**(6): p. 1919-1925.
13. Heine, T., et al., *Engineering styrene monooxygenase for biocatalysis: Reductase-epoxidase fusion proteins*. Applied Biochemistry and Biotechnology, 2017. **181**(4): p. 1590-1610.
14. Corrado, M.L., T. Knaus, and F.G. Mutti, *A chimeric styrene monooxygenase with increased efficiency in asymmetric biocatalytic epoxidation*. Chembiochem, 2018. **19**(7): p. 679-686.
15. Hofstetter, K., et al., *Coupling of biocatalytic asymmetric epoxidation with NADH regeneration in organic-aqueous emulsions*. Angewandte Chemie International Edition, 2004. **43**(16): p. 2163-6.
16. Toda, H., et al., *Expression and characterization of styrene monooxygenases of Rhodococcus sp. ST-5 and ST-10 for synthesizing enantiopure (S)-epoxides*. Applied Biochemistry and Biotechnology, 2012. **96**(2): p. 407-18.
17. Toda, H., R. Imae, and N. Itoh, *Efficient biocatalysis for the production of enantiopure (S)-epoxides using a styrene monooxygenase (SMO) and Leifsonia alcohol dehydrogenase (LSADH) system*. Tetrahedron-Asymmetry, 2012. **23**(22-23): p. 1542-1549.
18. Unversucht, S., et al., *FADH(2)-dependence of tryptophan 7-halogenase*. Advanced Synthesis & Catalysis, 2005. **347**(7-8): p. 1163-1167.

Chapter 3

19. Hollmann, F., et al., *Stereospecific biocatalytic epoxidation: The first example of direct regeneration of a FAD-dependent monooxygenase for catalysis*. Journal of the American Chemical Society, 2003. **125**(27): p. 8209-8217.
20. Ruinatscha, R., et al., *Productive asymmetric styrene epoxidation based on a next generation electroenzymatic methodology*. Advanced Synthesis & Catalysis, 2009. **351**(14-15): p. 2505-2515.
21. Hollmann, F., et al., *Direct electrochemical regeneration of monooxygenase subunits for biocatalytic asymmetric epoxidation*. Journal of the American Chemical Society, 2005. **127**(18): p. 6540-6541.
22. Paul, C.E., et al., *Nonenzymatic regeneration of styrene monooxygenase for catalysis*. Acs Catalysis, 2015. **5**(5): p. 2961-2965.
23. Zhang, W. and F. Hollmann, *Nonconventional regeneration of redox enzymes - a practical approach for organic synthesis?* Chemical Communications, 2018. **54**(53): p. 7281-7289.
24. Lee, S.H., et al., *Photobiocatalysis: Activating redox enzymes by direct or indirect transfer of photoinduced electrons*. Angewandte Chemie-International Edition, 2018. **57**(27): p. 7958-7985.
25. Schroeder, L., et al., *Photochemically driven biocatalysis of halogenases for the green production of chlorinated compounds*. Chemcatchem, 2018. **10**(15): p. 3336-3341.
26. Panke, S., et al., *Towards a biocatalyst for (S)-styrene oxide production: Characterization of the styrene degradation pathway of Pseudomonas sp. strain VLB120*. Applied and Environmental Microbiology, 1998. **64**(6): p. 2032-2043.
27. Holtmann, D. and F. Hollmann, *The oxygen dilemma: A severe challenge for the application of monooxygenases?* Chembiochem, 2016. **17**(15): p. 1391-1398.
28. Tischler, D., et al., *StyA1 and StyA2B from Rhodococcus opacus 1CP: a multifunctional styrene monooxygenase system*. Journal of Bacteriology, 2010. **192**(19): p. 5220-7.
29. Ukaegbu, U.E., et al., *Structure and ligand binding properties of the epoxidase component of styrene monooxygenase*. Biochemistry, 2010. **49**(8): p. 1678-1688.
30. Hollmann, F. and A. Schmid, *Electrochemical regeneration of oxidoreductases for cell-free biocatalytic redox reactions*. Biocatalysis and Biotransformation, 2004. **22**(2): p. 63-88.
31. Holzer, W., et al., *Photo-induced degradation of some flavins in aqueous solution*. Chemical Physics, 2005. **308**(1-2): p. 69-78.
32. Song, P.S. and D.E. Metzler, *Photochemical degradation of flavins. 4. Studies of anaerobic photolysis of riboflavin*. Photochemistry and Photobiology, 1967. **6**(10): p. 691-&.
33. Paul, C.E., et al., *Mimicking nature: synthetic nicotinamide cofactors for C=C bioreduction using enoate reductases*. Organic Letters, 2013. **15**(1): p. 180-183.
34. Iwase, T., et al., *A simple assay for measuring catalase activity: A visual approach*. Scientific Reports, 2013. **3**: p. 4.

Supporting figures

Styrene and styrene oxide

Method: Column A

Ramp [$^{\circ}\text{C min}^{-1}$]	Temperature [C]	Hold time [min]
-	100	12.5
20	225	1

Retention times

Compound	Retention time (min)
Styrene	3.4
DMSO	3.6
<i>R</i> -Styrene oxide	8.6
<i>S</i> -Styrene oxide	9.1
Phenylacetaldehyde	9.7
Dodecane	11.0

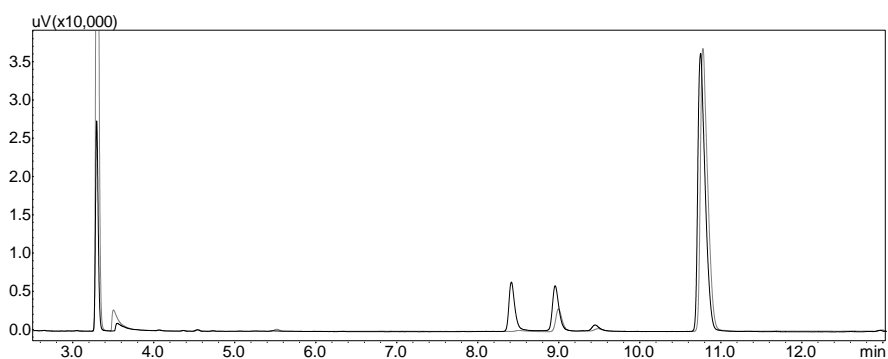


Figure S1: Gas chromatograms of styrene and racemic styrene oxide (black) and an example of a reaction sample (gray).

Chapter 3

3-Methylstyrene and 3-methylstyrene oxide

Method: Column C

Ramp [$^{\circ}\text{C min}^{-1}$]	Temperature [C]	Hold time [min]
-	100	24
20	220	1

Retention times

Compound	Retention time (min)
3-methyl Styrene	6.1
Dodecane	8.7
Synthesis by-product	16.0
S-3-methyl Styrene oxide	20.3
DMSO	21.6
R-3-methyl Styrene oxide	22.6

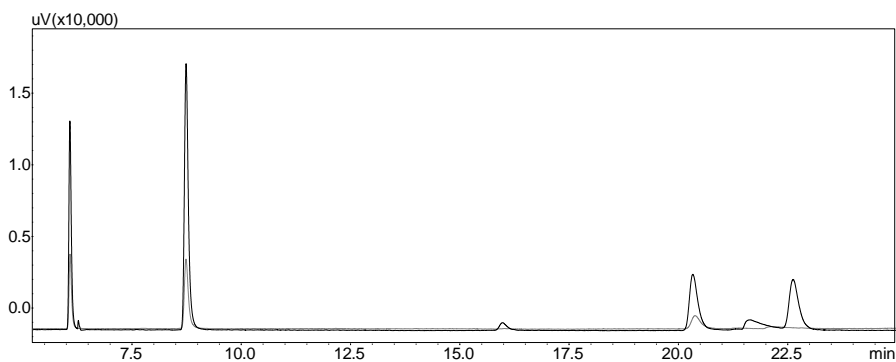


Figure S2: Gas chromatograms of 3-methylstyrene and racemic 3-methylstyrene oxide (black) and an example of a reaction sample (gray).

4-Fluorostyrene and 4-fluorostyrene oxide

Method: Column C

Ramp [$^{\circ}\text{C min}^{-1}$]	Temperature [C]	Hold time [min]
-	100	15
20	220	1

Retention times

Compound	Retention time (min)
4-Fluorostyrene	4.5
Isomerisation by-product	8.0
Dodecane	8.7
<i>S</i> -4-Fluorostyrene oxide	11.9
Product impurity	12.8
<i>R</i> -4-Fluorostyrene oxide	13.7
DMSO	17.5

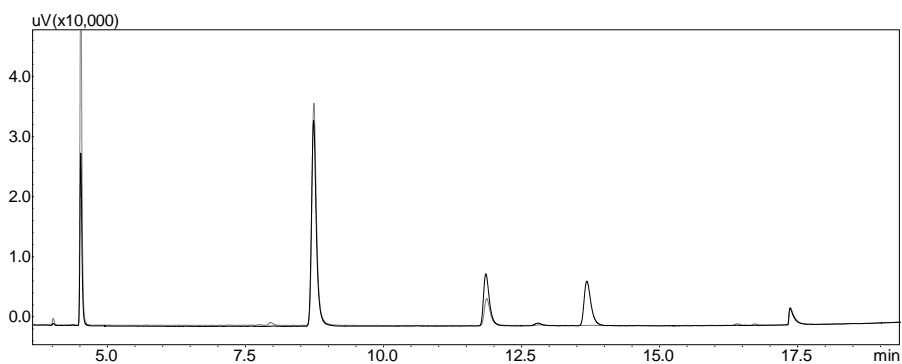


Figure S3: Gas chromatograms of 4-fluorostyrene and racemic 4-fluorostyrene oxide (black) and an example of a reaction sample (gray).

3-Chlorostyrene – 3-chlorostyrene oxide

Chapter 3

Method: Column C

Ramp [$^{\circ}\text{C min}^{-1}$]	Temperature [C]	Hold time [min]
-	120	23
20	220	1

Retention times

Compound	Retention time (min)
Dodecane	5.5
3-Chloro styrene	6.0
DMSO	9.0
Synthesis by-product	11.2
<i>S</i> -3-Chloro styrene oxide	16.7
<i>R</i> -3-Chloro styrene oxide	21.9
Dodecane	5.5

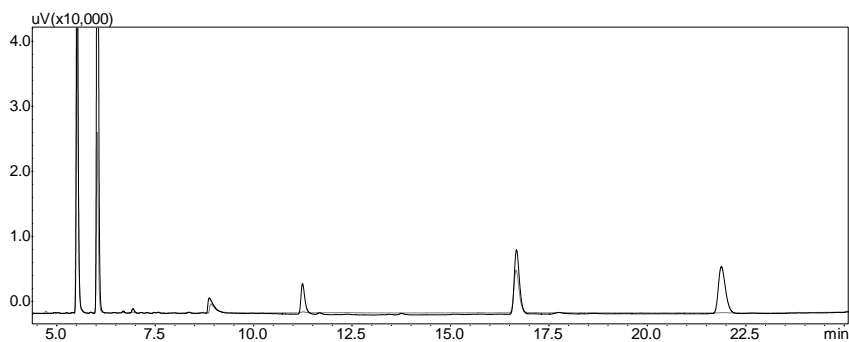


Figure S4: Gas chromatograms of 3-chlorostyrene and racemic 3-chlorostyrene oxide (black) and an example of a reaction sample (gray).

4-Chlorostyrene and 4-chlorostyrene oxide

Method: Column C

Ramp [$^{\circ}\text{C min}^{-1}$]	Temperature [C]	Hold time [min]
-	110	13
5	120	7
20	220	1

Retention times

Compound	Retention time (min)
Dodecane	6.8
4-Chloro styrene	7.5
DMSO	13.4
Isomerisation by-product	13.8
<i>S</i> -4-Chloro styrene oxide	20.2
<i>R</i> -4- Chloro styrene oxide	20.7

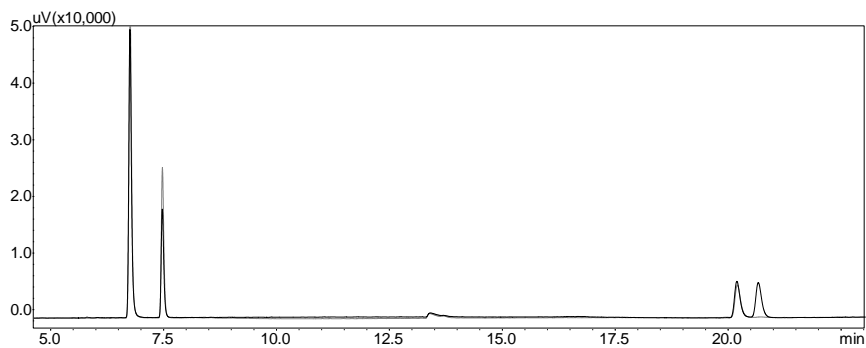


Figure S5: Gas chromatograms of 4-chlorostyrene and racemic 4-chlorostyrene oxide (black) and an example of a reaction sample (gray).

Chapter 3

4-Bromostyrene and 4-bromostyrene oxide

Method: Column B

Ramp [$^{\circ}\text{C min}^{-1}$]	Temperature [C]	Hold time [min]
-	100	4
15	175	2.2
10	205	2
25	250	2

Retention times

Compound	Retention time (min)
Dodecane	9.9
4-Bromo styrene	11.1
<i>R</i> -4-Bromo styrene oxide	14.2
<i>S</i> -4-Bromo styrene oxide	14.9

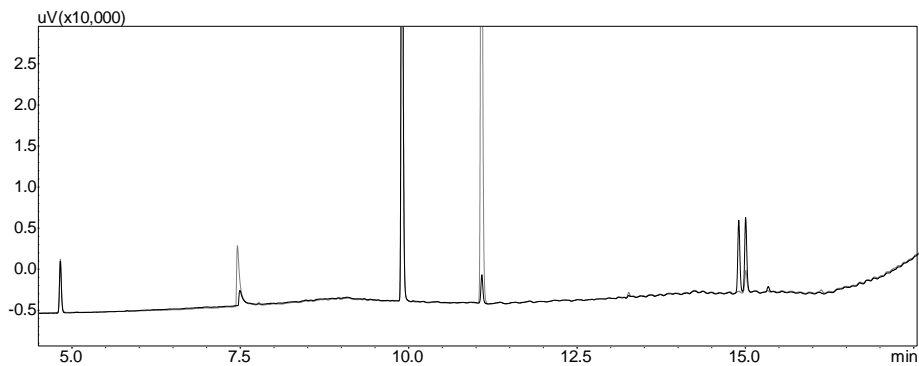


Figure S6: Gas chromatograms of 4-bromostyrene and racemic 4-bromostyrene oxide (black) and an example of a reaction sample (gray).

trans- β -Methylstyrene and *trans*- β -methylstyrene oxide

Method: Column C

Ramp [$^{\circ}\text{C min}^{-1}$]	Temperature [C]	Hold time [min]
-	100	15
20	220	1

Retention times

Compound	Retention time (min)
<i>Trans</i> - β -methyl styrene	6.8
Dodecane	8.5
Synthesis by-product	9.5
<i>S,S-Trans</i> - β -methyl styrene oxide	11.9
<i>R,R-Trans</i> - β -methyl styrene oxide	13.1

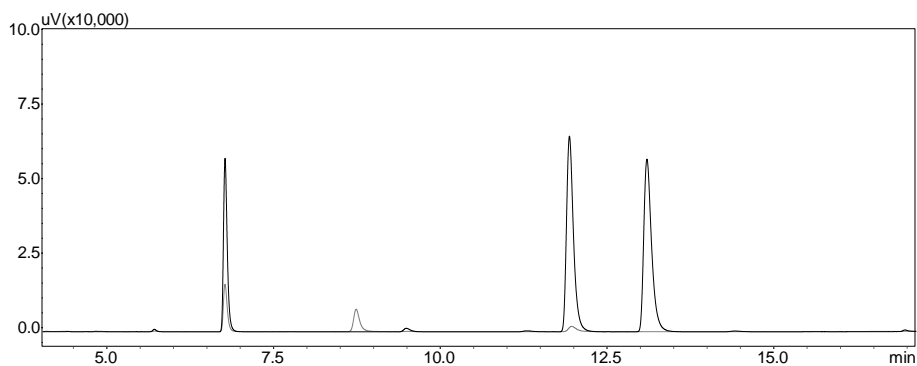


Figure S7: Gas chromatograms of *trans*- β -methylstyrene and racemic *trans*- β -methylstyrene oxide (black) and an example of a reaction sample (gray).

Chapter 3

α -Methylstyrene and α -methylstyrene oxide

Method: Column C

Ramp [$^{\circ}\text{C min}^{-1}$]	Temperature [C]	Hold time [min]
-	75	42
20	220	1

Retention times

Compound	Retention time (min)
α -methyl styrene	11.1
Dodecane	22.8
<i>S</i> - α -methyl styrene oxide	38.4
<i>R</i> - α -methyl styrene oxide	39.9

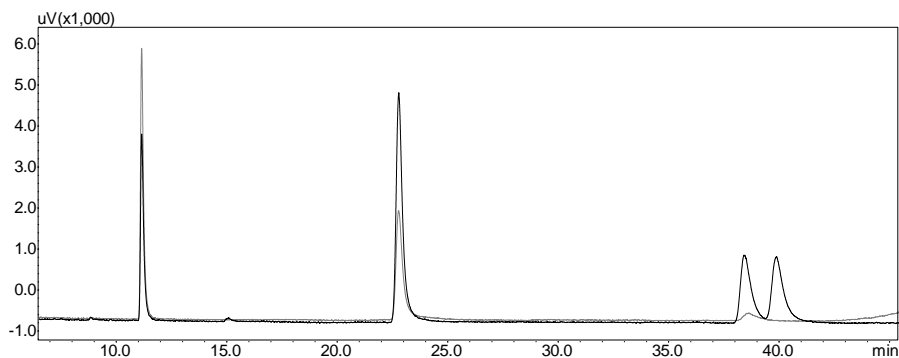


Figure S8: Gas chromatograms of α -methylstyrene and racemic α -methylstyrene oxide (black) and an example of a reaction sample (gray).

Chapter 4



Deazaflavins as photocatalyst for the direct reductive regeneration of flavoenzymes

Morten M.C.H. van Schie, Sabry H.H. Younes, Marine C.R. Rauch, Milja Pesic, Caroline E. Paul, Isabel W.C.E. Arends and Frank Hollmann

Based on:

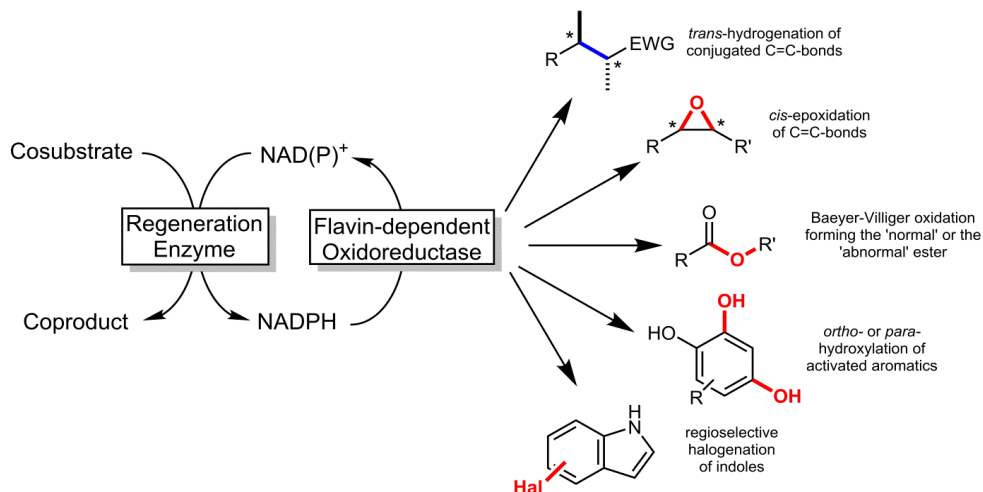
Van Schie, M.M.C.H., *et al.*, *Deazaflavins as photocatalyst for the direct reductive regeneration of flavoenzymes*. *Molecular Catalysis*, 2018. **452**: p. 277–283

Summary

Deazaflavins are potentially useful redox mediators for the direct, nicotinamide-independent regeneration of oxidoreductases. Especially the stability to molecular oxygen of their reduced forms have attracted significant interest for the regeneration of monooxygenases. In this contribution we further investigate the photochemical properties of deazaflavins and investigate the scope and limitations of deazaflavin-based photoenzymatic reaction systems.

Introduction

Oxidoreductases are amongst the most promising catalysts for preparative organic synthesis for selective reduction, oxidation and oxyfunctionalisation reactions. Amongst them, flavin-dependent oxidoreductases are of particular interest due to the versatility of the flavin-prosthetic group for selective reduction [1-5] and oxyfunctionalisation reactions (Scheme 1) [6-9]. For most of these reactions, the catalytic mechanism entails reductive activation of the enzyme-bound flavin cofactor. The reduced flavin cofactor then either reduces a substrate molecule (as in the case of ene reductases) or reacts with molecular oxygen forming a peroxoflavin capable of selective oxyfunctionalisation reactions such as epoxidation [10-16], Baeyer-Villiger oxidations [17-20], or aromatic hydroxylation reactions [13, 21-32].



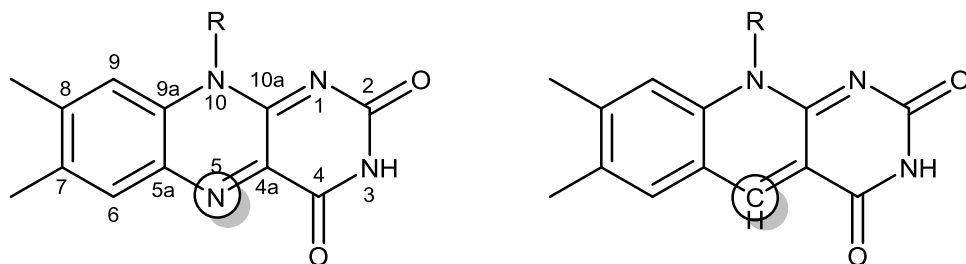
Scheme 1. Simplified scope of flavin-dependent oxidoreductases for selective reduction of C=C double bonds, epoxidations, Baeyer-Villiger oxidations, aromatic hydroxylations and halogenations. All reactions depend on the reduced nicotinamide cofactor, which for economic reasons has to be regenerated *in situ* using an (enzymatic) regeneration system.

As mentioned above, all these structurally and mechanistically diverse enzymes have a reductive activation of the enzyme-bound flavin in common. Generally, the reducing equivalents required for this reaction are obtained from the natural nicotinamide cofactors (NAD(P)H). For practical and economic reasons stoichiometric use of NAD(P)H is not feasible, which is why a myriad of different *in situ* regeneration approaches have been

developed in the past decades, allowing for the use of NAD(P)H in catalytic amounts only [33-35].

Despite the success of these methodologies, a more direct approach to regenerate the enzyme-bound flavin group could offer some advantages such as more simplified reaction schemes. For this, we and others have developed a range of chemical [36-42], electrochemical [43-45], and photochemical [46-51] approaches to target the flavin prosthetic group directly while circumventing the natural nicotinamide cofactor (together with the enzymatic regeneration system).

The mediators of choice for such NAD(P)H-independent regeneration systems are flavins themselves. However, while flavin-based regeneration systems perform well with O_2 -independent enzymes such as the OYEs, their performance with O_2 -dependent monooxygenases is rather poor; the major limitation being the poor O_2 -stability of reduced flavins. One possibility to circumvent this Oxygen Dilemma [52] was suggested by Reetz and coworkers [49], i.e. to utilise synthetic deazaflavins instead of the 'normal' ones (Scheme 2) to promote a P450-BM3-catalysed aerobic hydroxylation of lauric acid. Compared to using 'normal' flavins, significantly higher productivities were observed, which was attributed to the higher oxidative stability of reduced deazaflavins. These findings are in line with much earlier findings by Massey and coworkers who demonstrated that fully reduced deazaflavins, in contrast to their 'normal' analogues, exhibit a high stability against O_2 [53].



Scheme 2. Simplified representation of flavins (left) and their deazaflavin analogues (right). For reasons of clarity the 5' position wherein both differ are marked.

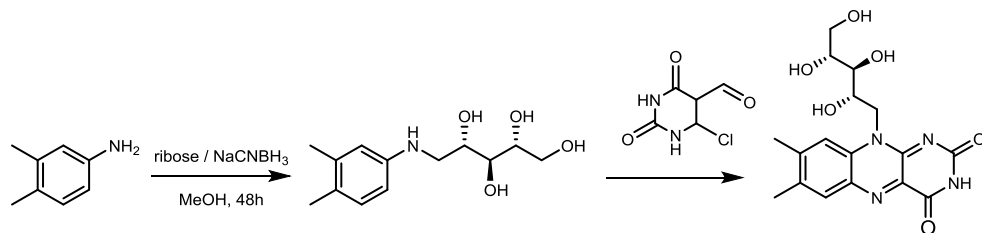
Already in the 1970s, deazaflavins have been subject of extensive research efforts. Especially Massey, Hemmerich and coworkers have worked out the reactivity of deazaflavins revealing that the deaza-semiquinone radical is significantly less stable

Chapter 4

compared to the 'normal' semiquinone [53-60]. This behaviour favours disproportionation and dimerization reactions leading to non-radical products exhibiting low(er) O_2 reactivity. Furthermore, reduction of deazaflavins by exclusive 1 e^- donors like dithionite proceeds relatively slow compared to natural flavins and *via* a covalent adduct intermediate. These findings motivated us to further evaluate the applicability of deazaflavins as photocatalysts/mediators to promote flavoenzyme catalysed reactions.

Results and discussion

5-deazariboflavin (dRf) was synthesized from 3,4-dimethylaniline in a two-step synthesis following a recently published procedure (Scheme 3) [61]. Overall, 457 mg of pure dRf (28% overall yield) were produced.



Scheme 3. Synthetic route for 5-deaza riboflavin (dRf).

Having dRf at hand, we investigated its photoreduction using either sodium ethylene diamine tetraacetate (EDTA, a single electron donor) or NADH (a hydride donor) (Figure 1). In addition to EDTA, 3-(N-morpholino)propanesulfonic acid (MOPS) and other amino alcohols such as Triethanolamine (TEOA) can serve as single electron donors (Figure 2). Alternatively, NADH can be replaced by the nicotinamide mimic benzyl dihydronicotinamide (BNAH). In all cases illumination was necessary to induce dRf reduction, with the exception of BNAH, where significant formation of H_2dRf was also observed in dark. One possible explanation for this reduction may be the more negative redox potential of BNAH compared to NADH (−0.36 V and −0.315 V SHE, respectively) [62, 63].

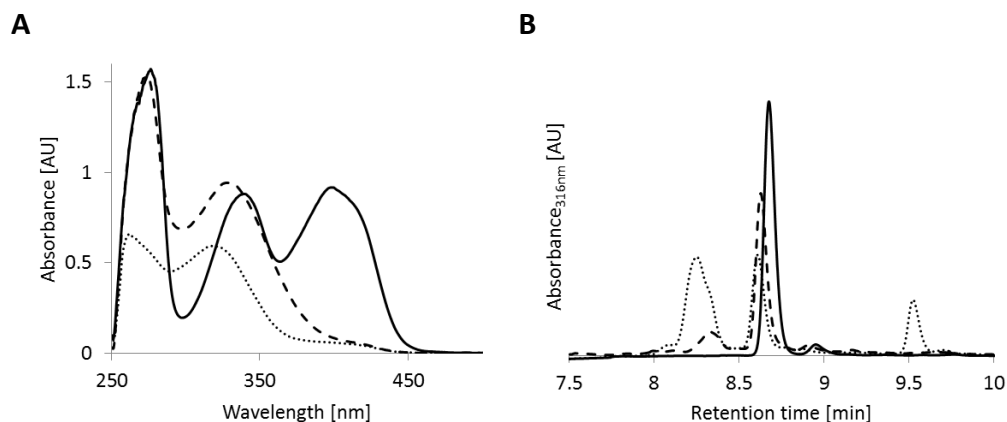


Figure 1. Photochemical reduction of deazariboflavin (dRf) using NADH or EDTA as sacrificial electron donor. A: UV/Vis spectra of the various dRf species observed during the photoreduction of dRf^{ox} (red) with EDTA (blue) and NADH (green). General conditions: 75 μ M dRf, 10 mM EDTA or 75 μ M NADH in a 100 mM KPi buffer pH 6.0, Blue LED light setup, max light intensity, anaerobic conditions, RT. B: HPLC chromatograms recorded of photochemical reductions of dRf (solid) using NADH (dashed) or EDTA (dots) as stoichiometric reductant.

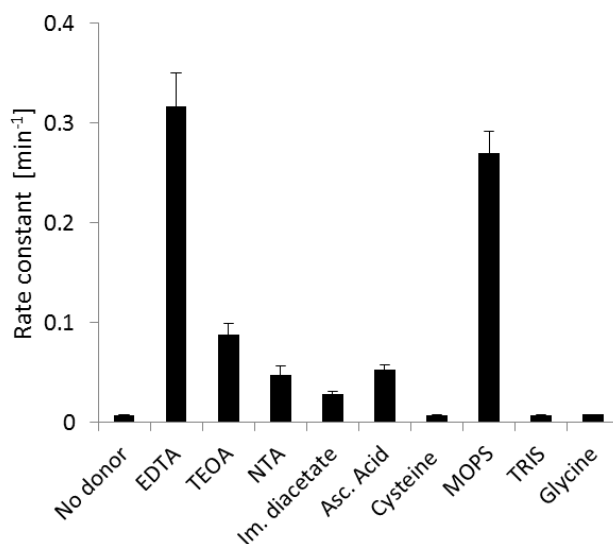


Figure 2. Influence of the electron donor on the dRf^{ox} photo-reduction rate (expressed as rate constant). General conditions: 100 μ M dRf, 10 mM electron donor in a 100 mM KPi buffer pH 6.0, Blue LED light setup, max light intensity, anaerobic conditions, RT. Abbreviations: EDTA: Ethylenediaminetetraacetic acid. TEOA: Triethanolamine. NTA: Nitrilotriacetic acid. MOPS: 3-(N-morpholino)propanesulfonic acid. TRIS: tris(hydroxymethyl)aminomethane.

The spectra of single electron donor- and hydride-donor reduced dRfs differed significantly in shape suggesting different reduction products. This assumption was corroborated by chromatographic separation of the reaction products (Figure 1B). While NADH-reduced dRf gave only one product (H_2dRf , as confirmed by its characteristic UV spectrum) [56], EDTA-reduction of dRf yielded H_2dRf and another product (most likely assigned to the dimeric, half-reduced semiquinone product) appearing simultaneously over time. These findings are in line with previous reports using EDTA or NaBH_4 as reductants [58, 64].

Next, we characterised the light-driven reduction of dRf^{ox} using EDTA as a sacrificial electron donor in some more detail. The photochemical reduction of dRf proceeded approximately 14 times slower than the reduction of ‘normal’ riboflavin. This is most likely attributed to the better overlap of the riboflavin absorption spectrum with the emission spectrum of the LED used in this study (Figure 8) [65]. The differences in the redox potentials of Rf (-0.146 V vs. SHE) and dRf (-0.237 V vs. SHE) [66] and quantum yield of the reaction may contribute as well [65]. Using the Nernst equation, the redox potential of dRf was estimated to be -0.332 V vs. SHE at pH 6.0 (see material and methods for the calculations).

The reduction rate of dRf was linearly dependent on the light intensity applied (Figure 3A) and unaffected by the dRf concentration itself (Figure 3B). Hence, we conclude that the *in situ* concentration of photoexcited dRf is overall rate limiting. Varying the concentration of the sacrificial electron donor (EDTA) revealed a saturation-type dependency of the dRf reduction rate on the EDTA concentration applied (Figure 3C). Above approximately 1.5–2 mM EDTA (pH 6), no further increase of the dRf reduction rate was observed. Finally, there was a sigmoidal pH-dependency of the dRf^{ox} reduction rate with a turning point at approximately pH 9 (Figure 3D). Furthermore, the substitution pattern of the N-atom in the sacrificial electron donor had an influence on the reduction rate (Figure 2). Overall, it appears that higher electron densities around the N-atom of the donors facilitate the electron transfer to dRf. These observations are in line with the oxidation mechanism suggested by Kramer and coworkers [67]. These authors suggested a methylene radical intermediate being formed after single electron transfer of the amino acid donor, followed by subsequent decarboxylation. The extend of hyperconjugative stabilisation of this intermediate radical should increase with the N-substitution pattern as well as with occurrence of a non-protonated N-substituent.

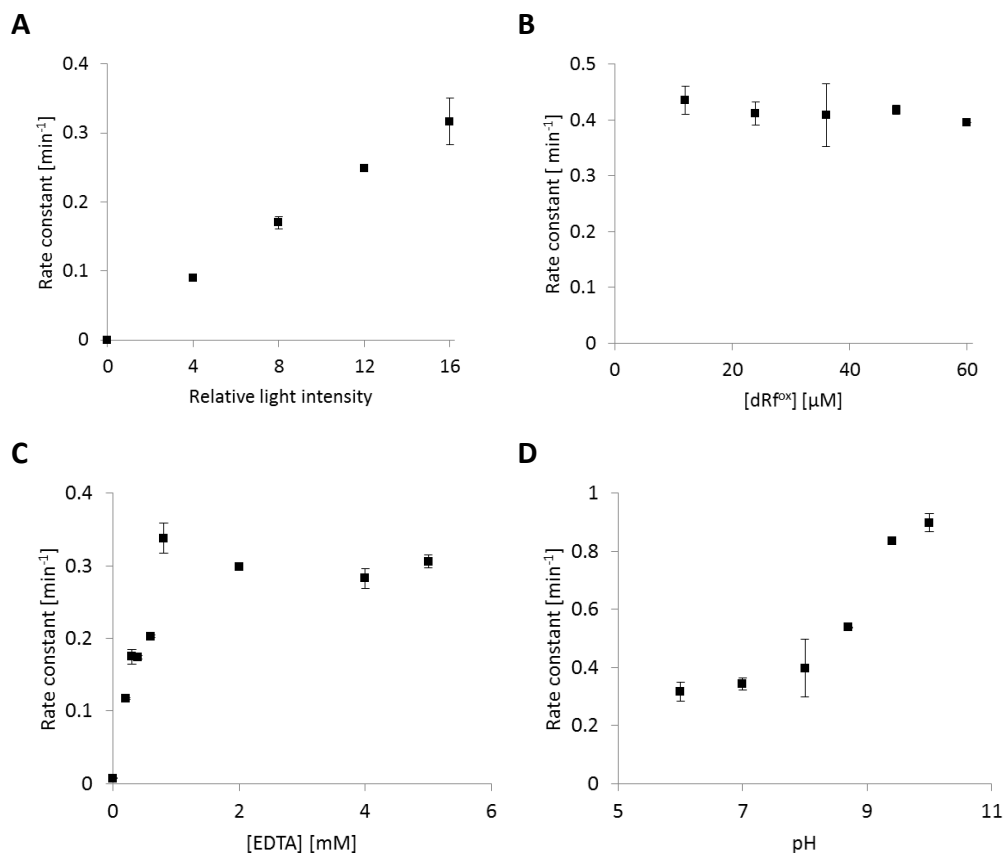


Figure 3. Dependency of the dRf reduction rate (expressed as turnover frequency of dRf, TF) on A: intensity of the blue LED light source, B: dRf^{ox} concentration, C: Concentration of the sacrificial electron donor and D: pH. General conditions: 60 μM dRf^{ox}, 10 mM EDTA in a 100 mM KPi buffer pH 6.0, blue LED light setup, max light intensity, anaerobic conditions, RT. $\text{TF} = (\text{initial dRf reduction rate } [\mu\text{M min}^{-1}]) \times (c(\text{dRf}) [\mu\text{M}])^{-1}$.

To further examine the applicability of photoreduced dRf^{red} to regenerate oxidoreductases, we used it to reduce the FMN-dependent old yellow enzyme homologue from *Bacillus subtilis* (YqjM) [36, 68, 69]. The different spectral properties of dRf^{ox} ($\lambda_{\text{max}} = 390 \text{ nm}$) and YqjM-bound FMN^{ox} ($\lambda_{\text{max}} = 455 \text{ nm}$) allow for the simultaneous determination and quantification of the electron transfer between photoregenerated dRf^{red} and YqjM-bound FMN^{ox} (Figure 4). In accordance to previous findings by Massey and Hemmerich [70] we found that photoregeneration of YqjM was possible. Using e.g. 1.5 eq of (prior reduced) dRf full reduction of YqjM was observed within 4 minutes. This reaction was observed under blue light illumination only. Incubation of YqjM with pre-reduced dRf in the dark or upon illumination with other wavelengths yielded no significant reduction of

the YqjM-bound FMN. Currently, we are lacking a satisfactory explanation for this observation. Possibly the interaction of $(\text{dRf})_2^{\text{red}}$ with the enzyme-bound FMN is sterically hindered and photoexcitation of the latter may accelerated the long-distance electron transfer.

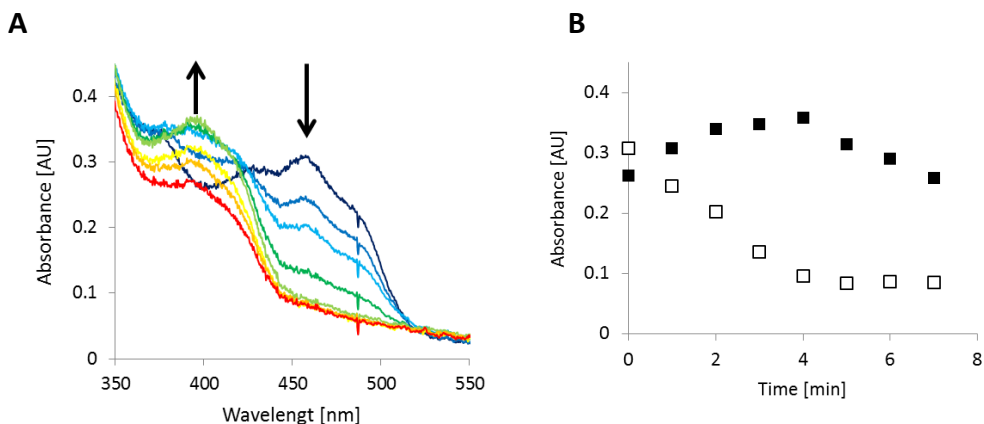


Figure 4. Time course of the $(\text{dRf})_2^{\text{red}}$ mediated reduction of YqjM. A: spectra recorded over time (1 min intervals) and B: time courses of the characteristic absorption maxima for YqjM-FMN^{ox} (390 nm, ■) and dRf^{ox} (455 nm, □). General conditions: A solution of 60 μM dRf^{ox} in 100 mM KPi buffer pH 6.0 containing 0.5 mM EDTA was illuminated (blue LED) until full reduction was achieved. This reaction mixture was then supplemented with the same volume of 40 μM YqjM (in the same buffer) and subsequently illuminated using a blue LED. Within that period the characteristic peak for dRf^{ox} (400 nm) partially recovered while it decreased again upon full reduction of YqjM. Most likely this can be attributed to the continuous photoreduction of dRf^{ox} in the reaction mixture by the excess of EDTA used to reduce it earlier.

To test if catalytic turnover of both, dRf and YqjM is feasible, we used the enantioselective reduction of 2-methyl cyclohexanone to (*R*)-2-methyl cyclohexanone as model reaction (Figure 5). In the absence of dRf no conversion of the starting material was observed indicating that direct photochemical reduction of YqjM-bound FMN by EDTA was not efficient. However, already in the presence of 5 μM dRf (equimolar to YqjM) a product formation rate of approximately 50 $\mu\text{M h}^{-1}$ was observed. Hence, a turnover frequency of approximately 10 h^{-1} was calculated for YqjM and dRf. This corresponds well to the YqjM-reduction rate observed before (Figure 4) indicating that the reduction of the biocatalyst was overall rate-limiting. The overall rate of the photoenzymatic reduction reaction increased steadily with increasing photocatalyst concentration (up to 200 μM , representing the solubility limit for dRf). With it, the catalytic efficiency of YqjM increased

to 40 h^{-1} . In all experiments (*R*)-2-methyl cyclohexanone was formed almost exclusively (Figure 10).

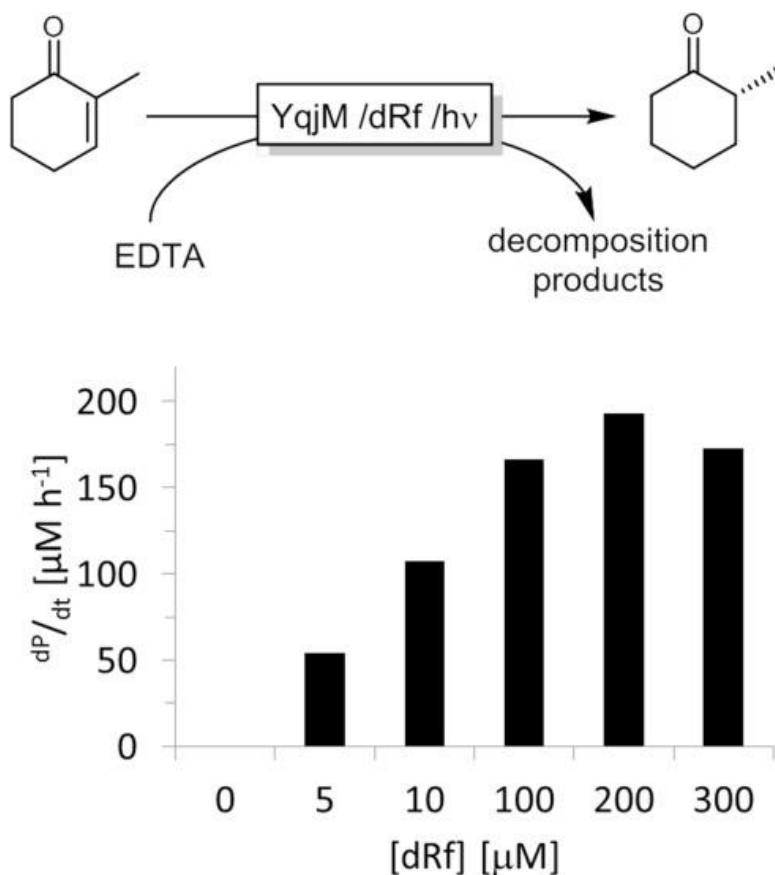


Figure 5. Photoenzymatic reduction of 2-methyl cyclohexenone. General conditions: 5 μM YqjM, 1 mM 2-methyl cyclohexenone, 10 mM EDTA in a 100 mM KPi buffer pH 6.0, blue LED light setup, blue LED at maximal light intensity, anaerobic conditions, RT. It should be mentioned, that the solubility limit of dRf was around 250 μM , therefore, the sample at 300 μM dRf was non-homogeneous, which possibly influenced the regeneration reaction.

While these numbers are comparable to recently reported photoenzymatic systems [46], the catalytic performance of YqjM falls back by orders of magnitude behind its potential (1.8 s^{-1} using NADPH as reductant) [36]. A plausible explanation for this is to assume an unfavourable interaction of the reduced dRf mediators with the enzyme-bound FMN

Chapter 4

resulting in poor electron transfer rates. Both, cofactor- and enzyme engineering may generate artificial binding sites and thereby accelerate the regeneration reaction [71, 72].

Finally, we re-visited the O₂-stability of reduced dRfs. As mentioned above, significant reduction of YqjM-bound FMN and product formation in the photoenzymatic system was observed only under strictly anaerobic conditions. We therefore investigated the influence of O₂ on the photochemical reduction of dRf (Figure 6). Independent from the sacrificial electron donor used (NADH or EDTA) reduction of dRf was observed under anaerobic conditions only while it was negligible in the presence of O₂. In the latter cases, H₂O₂ was detectable as well as NADH oxidation (in case of Figure 6A) suggesting dRf^{red} reoxidation occurring simultaneously.

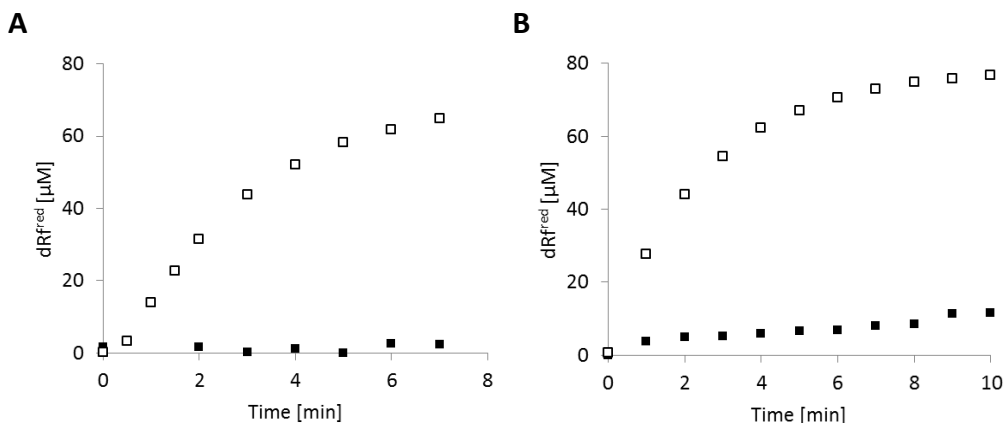


Figure 6. Photochemical reduction of deazariboflavin using NADH (A) or EDTA (B) as sacrificial electron donor under aerobic (■) and anaerobic (□) conditions. Conditions: 80 μM dRf, 10 mM EDTA or 1 mM NADH, 100 mM KPi buffer pH 6.0, blue LED light setup, max light intensity, RT.

Therefore, we determined the reoxidation rates of photochemically reduced dRf in the dark and under illumination (Table 1). Both, the dimeric (dRf)₂ as well as the fully reduced H₂dRf were rather stable against O₂ in the dark whereas they swiftly reoxidized in the presence of (blue) light. Similar observations had previously been made by Hemmerich and coworkers [58].

Table 1. Aerobic reoxidation rates observed for deazariboflavin reduced by EDTA or NADH. Conditions: 10 mM EDTA or 1 mM NADH, 100 mM KPi buffer pH 6.0, blue LED light setup, max light intensity, RT.

	Reoxidation rate [$\mu\text{M h}^{-1}$]	
	Dark	Light
(dRf) ₂	1.7	96
H ₂ dRf	0.78	30

The influence of light can be rationalised assuming that (trace amounts) of photoexcited, oxidised dRf synproportionate with H₂dRf or (dRf)₂ forming a reactive semiquinone radical reacting with O₂ via single electron transfer. This reaction should be autocatalytic, for which we have found indications in the reoxidation time-course.

Furthermore, EPR-measurements during BNAH-mediated reduction of dRf in the presence and absence of light support this assumption (Figure 7). As dRf also is a photosensitiser capable of generating singlet oxygen (¹O₂) [73], an involvement of ¹O₂ cannot be ruled out completely. ¹O₂ oxidations, however, generally do not involve radical species, which is in contrast to the observations of radicals mentioned above.

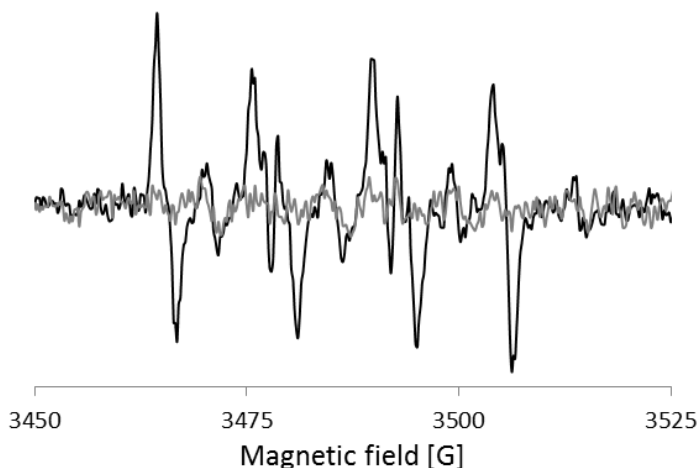
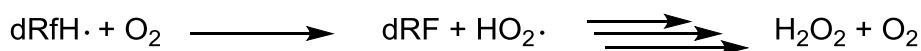


Figure 7. EPR spectra recorded using the spin trap technique during the aerobic reduction of dRf with BNAH under illumination (black) and in dark (gray). Conditions: 60 μM dRf, 1mM BNAH, 1% v/v DMSO, 100mM KPi pH 6.0, Kaiser Fibre Optic Lighting system 15 V, 150 W, on half intensity, aerobic conditions. Simulation of the EPR spectra showed the couplings of AN \approx 1.43 mT, AH β \approx 1.15 mT and AH γ \approx 0.12 mT, corresponding to the signal of superoxide. [74]

Conclusions

Direct reductive regeneration of flavoenzymes circumventing the expensive and unstable nicotinamide cofactors is an attractive alternative to established systems utilizing the nicotinamide cofactor together with an (enzymatic) regeneration system.

In case of O₂-dependent enzymes, the Oxygen Dilemma, however, severely impairs the utility of these approaches. While the high reactivity of 'normal flavins' with molecular oxygen is well-known [75], reduced deazaflavins are considered to be much more stable due to the spin-forbidden character of the reoxidation with triplet oxygen (³O₂) [52]. This motivated us to evaluate 5-deazariboflavin (dRf) as photocatalyst and mediator to regenerate flavin-dependent enzymes. Indeed, fully reduced H₂dRf is fairly stable in the presence of molecular oxygen. In the presence of oxidised dRf (especially if illuminated), however, radical species are formed via synproportionation, which react quickly with molecular oxygen (Scheme 4) [58].



Scheme 4. Aerobic reoxidation of reduced deazaflavin species. The reactive semiquinone radical (dRf[•]) reacts fast with O₂ eventually leading to H₂O₂ and O₂. dRf itself is formed either via the dimerization equilibrium of (dRf)₂ or through synproportionation of H₂dRf with (photoexcited) dRf. For reasons of simplicity, protonation equilibria have not been included in this scheme.

Indeed, neither accumulation of reduced dRf or catalytic turnover was observed under aerobic conditions. Therefore, we conclude that a simple one-pot reaction cascade entailing photochemical reduction of dRf and biocatalytic reaction is not feasible due to the uncoupling reaction described above.

Possibly, technical solutions such as compartmentalised reaction setups (anaerobic reduction of the flavin followed by aerobic biocatalytic reaction) as suggested by Schmid and coworkers [44] may be doable.

Acknowledgements

We thank the Netherlands Organisation for Scientific Research for financial support through a VICI grant (No. 724.014.003). Excellent technical support by M. Gorseling and support by prof. W.R. Hagen with the EPR measurements is gratefully acknowledged.

Material and methods

Chemicals

Chemicals were purchased from Sigma-Aldrich, Fluka, Acros or Alfa-Aesar with the highest purity available and used as received. The NADH mimic N-benzyl nicotinamide (BNAH) was synthesized following published procedures [39, 62].

Synthesis of 5-deazariboflavin

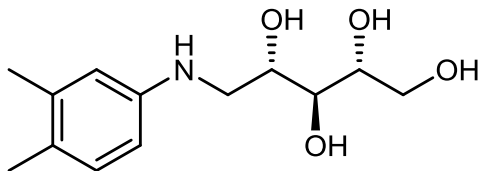
5-deazariboflavin (dRf) was synthesized following a literature method [61]. Reactions were carried out under inert atmosphere of dry argon. Reactions were followed and Rf values are obtained using thin layer chromatography (TLC) on silica gel-coated plates (Merck 60 F254) with the indicated solvent mixture. Flash chromatography was carried out using Acros silica gel (0.035–0.070 mm, and ca. 6 nm pore diameter). NMR spectra were recorded on a Varian 400 (400 MHz) spectrometer in CDCl₃. Chemical shifts are given in ppm with respect to tetramethylsilane. Coupling constants are reported as J-values in Hz.

Synthesis of 3,4-dimethyl-N-D-ribitylaniline (2):

3,4-Dimethylaniline **1** (3.14 g, 26 mmol) was dissolved in anhydrous methanol (150 ml), sodium cyanoborohydride (NaCNBH₃) (3.11 g, 2 equiv.), followed by addition of D-ribose (11.2 g, 74.3 mmol) under stirring. The reaction mixture was further stirred under reflux for 48 hrs. The solvent was removed under reduced pressure, the residue was re-dissolved in 1M HCl (50 ml), swirled until gas evolution ceased. The solution was carefully neutralised with an saturated solution of sodium bicarbonate, extracted with EtOAc (6 × 50 ml), washed with brine, dried with MgSO₄, and the solvent was removed under

Chapter 4

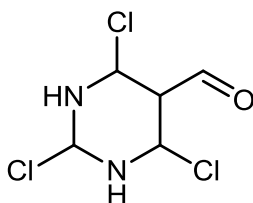
reduced pressure. Recrystallization of the solid product from absolute ethanol gave *N*-ribitylaniline as a white crystalline solid. (6.17 g, 97%)



^1H NMR (400 MHz, $\text{MeOH-}d_4$) δ 6.88 (d, $J = 8.1$ Hz, 1H, H-3), 6.55 (d, $J = 2.4$ Hz, 1H, H-6), 6.47 (dd, $J = 8.1, 2.5$ Hz, 1H, H-4), 3.91 (ddd, $J = 7.8, 6.2, 3.5$ Hz, 1H, H-13), 3.81 – 3.71 (m, 2H, H-12, 14''), 3.68 – 3.59 (m, 2H, H-11, 14'), 3.43 (dd, $J = 12.8, 3.5$ Hz, 1H, H-10''), 3.09 (dd, $J = 12.8, 7.9$ Hz, 1H, H-10'), 2.17 (s, 3H, H-8), 2.12 (s, 3H, H-9). ^{13}C NMR (100 MHz, $\text{MeOH-}d_4$) 148.1 (C-5), 137.9 (C-1), 131.1 (C-3), 126.7 (C-2), 116.7 (C-6), 112.5 (C-4), 74.9 (C-11), 74.4 (C-12), 72.1 (C-13), 64.6 (C-14), 48.1 (C-10), 20.1 (C-8), 18.8 (C-9)

Synthesis of 2,4,6- trichloropyrimidine-5-carbaldehyde (3):

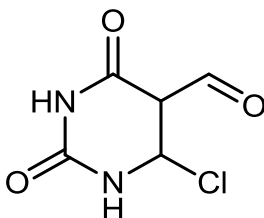
Anhydrous *N,N*-dimethyl formamide (DMF) (5 ml, 65 mmol) was added dropwise to the stirred solution of barbituric acid (8.45 g, 66 mmol) in phosphorus oxichloride (POCl_3) (40 ml, 429 mmol) at 0 °C for 1h. the reaction mixture was followed by reflux for 16 h. at 130 °C. The solvent was removed under reduced pressure, the thick residue was poured into ice-water and stirred to form a solid product, the crude product was collected by filtration and purified by flash chromatography with an eluent (Hexane:EtOAc, 9:1) to provide a white solid (9.7 g, 70 %).



^1H NMR (400 MHz, $\text{DMSO-}d_6$): δ 10.39 (s, 1H).

Synthesis of 6-chloropyrimidine-5-carbaldehyde (4):

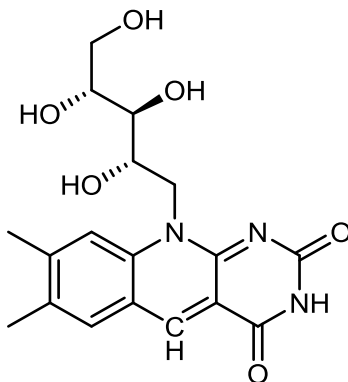
A mixture of 2,4,6-trichloropyrimidine-5-carbaldehyde **3** (1g, 4.73 mmol) and K_2CO_3 (0.650 g, 4.73 mmol) were added to 40 ml of ethanol:water mixture (2:1) and the solution was stirred for 4 hrs. at room temperature. The reaction mixture was neutralized with conc. acetic acid (4-5 drops) and the reaction was concentrated to 10 ml by rotary evaporation and kept at 4 °C for 2 days. The compound was isolated as white solid by filtration (0.760 g, 91%).



1H NMR (400 MHz, $DMSO-d_6$): δ 10.03 (s, 1H).

Synthesis of 5-deazariboflavin (5):

A mixture of 3,4-dimethyl-N-D-ribitylaniline **2** (1.02 g, 2.9 mmol) and 6-chloropyrimidine-5-carbaldehyde **4** (0.31 g, 1.8 mmol) were mixed in 10 ml of anhydrous N,N-dimethylformamide. The reaction mixture was stirred under reflux at 130 °C for 3 h and then the reaction mixture was cooled to room temperature. Diethyl ether 20 ml was added with stirring for 1 h and kept in freezer overnight. The compound was collected by filtration and recrystallized from water to form yellow solid powder (457 mg, 70%).



Chapter 4

^1H NMR (400 MHz, $\text{DMSO-}d_6$) δ 11.04 (s, 1H), 8.85 (s, 1H), 7.94 (s, 1H), 7.87 (s, 1H), 5.15 (d, J = 5.0 Hz, 1H), 4.99 (s, 1H), 4.90 (d, J = 4.6 Hz, 1H), 4.82 (d, J = 6.2 Hz, 1H), 4.66 (d, J = 14.1 Hz, 1H), 4.50 (t, J = 5.6 Hz, 1H), 4.23 (s, 1H), 3.69–3.59 (m, 3H), 3.47 (m, J = 6.1 Hz, 2H), 2.46 (s, 3H), 2.34 (s, 3H). ^{13}C NMR (100 MHz, $\text{DMSO-}d_6$) δ 162.6, 141.5, 131.0, 118.3, 74.1, 73.4, 70.0, 63.9, 40.6, 40.4, 40.2, 39.9, 39.7, 39.5, 39.3, 21.4, 19.1.

Production and purification of YqjM

The old yellow enzyme homologue from *Bacillus subtilis* (YqjM) was produced and purified using a protocol recently established in our group [36]. *Escherichia coli* BL21 (DE3) competent cells harboring pET28a plasmid containing the gene encoding for YqjM were used for the expression. 1 l of autoinduction ZYM-5052 medium [76] supplied with $50\text{ }\mu\text{g ml}^{-1}$ kanamycin was inoculated with 10 ml of overnight culture and incubated overnight in baffled shake flasks (37°C , 180 rpm).

For the purification of YqjM, cells were harvested by centrifugation ($10\,000\times g$, 15 min, 4°C), washed with potassium phosphate buffer (20 mM, pH 6.5) and centrifuged again at the same speed. Subsequently, the cell pellet was resuspended in the same buffer. Cell disruption was effected as described above. Cell debris was separated from the crude extract by centrifugation at $10\,000\times g$ for 30 min at 4°C . Supernatant was loaded to 5 ml Ni-NTA chromatography column (Thermo Fisher Scientific Inc) using NGCTM Chromatography system (Bio-Rad). After loading, various successive washing with 20 mM potassium phosphate 30 mM imidazole pH 6.5 were performed. The elution of YqjM was performed by using 20 mM potassium phosphate 250 mM imidazole pH 6.5. Fractions containing YqjM were collected and incubated with 5 mM FMN. After 30 min of incubation on ice, enzyme suspension was desalted twice using PD-10 Desalting Columns (GE Healthcare) in order to remove the excess of FMN and imidazole, and concentrated using Amicon[®] Ultra-15 Centrifugal Filter Device (cut-off 30K).

Experimental setup

Photo-reduction reactions were performed in 1 ml reaction mixtures in 1.5 ml glass vials. The reaction mixtures were illuminated from all sides from a distance of 10 cm by a LED light source. The intensity spectrum of the LED light source was determined by a calibrated spectrophotometer (Figure 8). Samples were stirred at 300 rpm using magnetic bars. Anaerobic experiments were performed in an anaerobic chamber (on average 98% N_2 , 2% H_2) with oxygen levels below ppm levels. UV-Vis spectra were recorded using an Avantes DH-2000 UV-vis-NIR light source and an Avispec 3648 spectrophotometer.

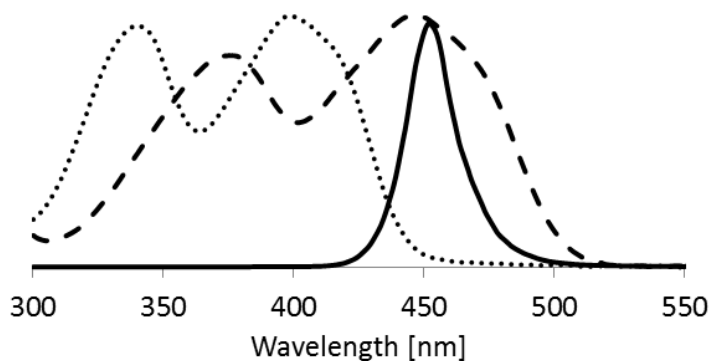
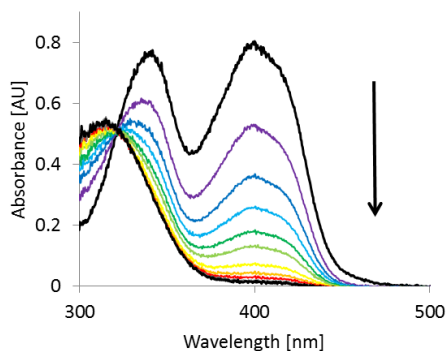


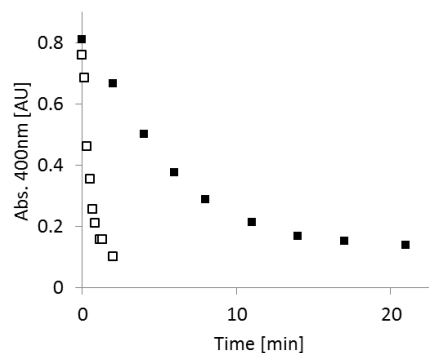
Figure 8. Absorption spectra of riboflavin (dashed) and 5-deazariboflavin (dots), compared to the emission spectrum of the blue LED light (solid), normalized.

In a typical experiment 100 μM dRf was reduced by 10 mM sacrificial single electron donor or 1 mM hydride donor in a 100 mM KPi buffer at pH 6.0. The absorbance at 400 nm ($\epsilon = 12\,500\text{ M}^{-1}\text{ cm}^{-1}$) was followed to determine the oxidation state of dRf over time (Figure 8). Due to interference of absorption when using either hydride donors, the oxidation state was determined by following the absorbance at 430 nm ($\epsilon = 5\,700\text{ M}^{-1}\text{ cm}^{-1}$). Stock solutions (0.2 mM in 100 mM phosphate buffer, pH 6.0) of the deazariboflavin were prepared freshly every day.

A



B



Chapter 4

Figure 9. Photochemical reduction of dRf^{ox}. A: UV-spectra recorded over time. B: Absorption at local maximum over time for dRf (■) and Rf (□). General conditions: 60 μ M of dRf^{ox} or Rf^{ox}, 10 mM EDTA, 100 mM KPi buffer pH 6.0, blue LED light setup, light intensity 8 out of 16, anaerobic conditions, RT.

Due to the FMN, YqjM has a typical absorbance spectrum with a peak extinction coefficient at 455 nm which decreases as the FMN in the active site is reduced. At 400 nm the extinction coefficient does not change significantly with the redox-state of the enzyme, which made it possible to determine the redox-state of the dRf and the YqjM simultaneously. For the reduction of YqjM, a dRf solution was first photo-reduced by five equivalents of EDTA. Thereafter, 20 μ M of YqjM was mixed with 100 μ M of the reduced dRf.

GC analyses

Photoenzymatic syntheses were performed using 5 μ M YqjM in the presence of 1 mM of 2-methyl cyclohexanone and 10 mM of EDTA in a 100 mM KPi buffer pH 6.0. The 2.5 ml reaction mixtures were extracted with 0.5 ml ethyl acetate and analysed on a CP-Chirasil-Dex CB GC column (50 m x 0.53 mm x 2 μ m)(GC method: 70 °C for 2 min. 2 °C min⁻¹ to 80 °C. 80 °C for 2 min. 2 °C min⁻¹ to 90 °C. 90 °C for 3 min. 25 °C min⁻¹ to 150 °C. 150 °C for 1 min. 25 °C min⁻¹ to 225 °C. 225 °C for 1 min). 5 mM of dodecane was used as internal standard. A representative GC graph is shown in figure 10.

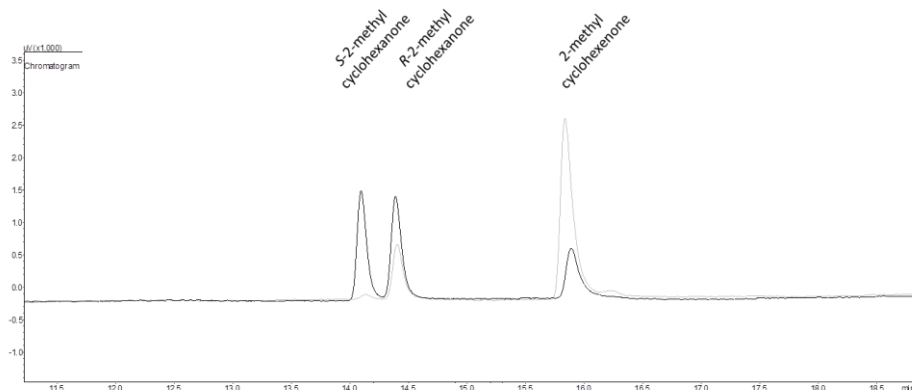


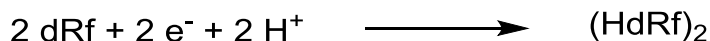
Figure 10. The GC chromatograms of a mixture of racemic 2-methyl cyclohexanone and 2-methyl cyclohexenone (black) and that of the enzymatic reaction upon illumination (grey).

Calculations

The Nernst equation was applied in order to estimate the redox potential of the reduction of deazariboflavin at a pH of 6.0.

$$E = E^0 - \frac{RT}{nF} \ln Q$$

Here, E^0 is the redox potential at pH 7.0 (0.273 V vs. SHE), R is the gas constant, T is the temperature in Kelvin, n is the amount of electrons involved in the reaction and F is the faraday constant. The following half reaction was assumed:



Scheme 5: Reductive half-reaction for the deazariboflavins.

With this, Q was defined as:

$$Q = \frac{[\text{dRf}]^2 * [\text{H}^+]^2}{[(\text{HdRf})_2]}$$

Compared to the conditions at pH 7, the proton concentration is increased 10-fold at pH 6. This implies that Q increases with a factor of 100. Assuming that the reaction takes place at room temperature, the redox potential at pH 6.0 can be determined.

$$E_{\text{pH } 6} = -0.273 - \frac{8.314 * 298.15}{2 * 96\,485} * \ln(100)$$

This gives a redox potential of -0.332 V vs SHE for the dimerization of deazariboflavin at pH 6.0.

References

1. Toogood, H.S. and N.S. Scrutton, *New developments in 'ene'-reductase catalysed biological hydrogenations*. Current Opinion in Chemical Biology, 2014. **19**: p. 107-115.
2. Toogood, H.S., J.M. Gardiner, and N.S. Scrutton, *Biocatalytic reductions and chemical versatility of the old yellow enzyme family of flavoprotein oxidoreductases*. ChemCatChem, 2010. **2**(8): p. 892-914.
3. Nestl, B.M., et al., *New generation of biocatalysts for organic synthesis*. Angewandte Chemie-International Edition, 2014. **53**(12): p. 3070-3095.
4. Stuermer, R., et al., *Asymmetric bioreduction of activated C=C bonds using enoate reductases from the old yellow enzyme family*. Current Opinion in Chemical Biology, 2007. **11**(2): p. 203-213.
5. Hollmann, F., I.W.C.E. Arends, and D. Holtmann, *Enzymatic reductions for the chemist*. Green Chemistry, 2011. **13**(9): p. 2285-2313.
6. Winter, R.T. and M.W. Fraaije, *Applications of flavoprotein oxidases in organic synthesis: Novel reactivities that go beyond amine and alcohol oxidations*. Current Organic Chemistry, 2012. **16**(21): p. 2542-2550.
7. de Gonzalo, G. and M.W. Fraaije, *Recent developments in flavin-based catalysis*. ChemCatChem, 2013. **5**(2): p. 403-415.
8. Hollmann, F., et al., *Enzyme-mediated oxidations for the chemist*. Green Chemistry, 2011. **13**: p. 226-265.
9. Huijbers, M.M., et al., *Flavin dependent monooxygenases*. Archives of Biochemistry and Biophysics, 2014. **544**: p. 2-17.
10. Schmid, A., et al., *Integrated biocatalytic synthesis on gram scale: The highly enantio selective preparation of chiral oxiranes with styrene monooxygenase*. Advanced Synthesis & Catalysis, 2001. **343**(6-7): p. 732-737.
11. Panke, S., et al., *Production of enantiopure styrene oxide by recombinant Escherichia coli synthesizing a two-component styrene monooxygenase*. Biotechnology and Bioengineering, 2000. **69**(1): p. 91-100.
12. Panke, S., et al., *Towards a biocatalyst for (S)-Styrene oxide production: Characterization of the styrene degradation pathway of Pseudomonas sp. strain VLB120 (vol 64, pg 2032, 1998)*. Applied and Environmental Microbiology, 1998. **64**(9): p. 3546-3546.
13. Montersino, S., et al., *Catalytic and structural features of flavoprotein hydroxylases and epoxidases*. Advanced Synthesis & Catalysis, 2011. **353**(13): p. 2301-2319.
14. Tischler, D., et al., *Identification of a novel self-sufficient styrene monooxygenase from Rhodococcus opacus 1CP*. Journal of Bacteriology, 2009. **191**(15): p. 4996-5009.
15. Toda, H., et al., *Microbial production of aliphatic (S)-epoxyalkanes by using Rhodococcus sp strain ST-10 styrene monooxygenase expressed in organic-solvent-tolerant Kocuria rhizophila DC2201*. Applied and Environmental Microbiology, 2015. **81**(6): p. 1919-1925.
16. Toda, H., R. Imae, and N. Itoh, *Bioproduction of chiral epoxyalkanes using styrene monooxygenase from Rhodococcus sp ST-10 (RhSMO)*. Advanced Synthesis & Catalysis, 2014. **356**(16): p. 3443-3450.
17. Oberleitner, N., et al., *From waste to value - direct utilization of limonene from orange peel in a biocatalytic cascade reaction towards chiral carvolactone*. Green Chemistry, 2017. **19**(2): p. 367-371.
18. Fink, M.J., F. Rudroff, and M.D. Mihovilovic, *Baeyer-Villiger monooxygenases in aroma compound synthesis*. Bioorganic & Medicinal Chemistry Letters, 2011. **21**(20): p. 6135-6138.

19. Rehdorf, J., et al., *Enzymatic synthesis of enantiomerically pure beta-amino ketones, beta-amino esters, and beta-amino alcohols with Baeyer-Villiger monooxygenases*. Chemistry-a European Journal, 2010. **16**(31): p. 9525-9535.
20. Rehdorf, J., M.D. Mihovilovic, and U.T. Bornscheuer, *Exploiting the regioselectivity of Baeyer-Villiger monooxygenases for the formation of beta-amino acids and beta-amino alcohols*. Angewandte Chemie-International Edition, 2010. **49**(26): p. 4506-4508.
21. Lutz, J., et al., *Bioorganometallic chemistry: biocatalytic oxidation reactions with biomimetic NAD(+)/NADH co-factors and Cp*Rh(bpy)H (+) for selective organic synthesis*. Journal of Organometallic Chemistry, 2004. **689**(25): p. 4783-4790.
22. Meyer, A., et al., *Changing the substrate reactivity of 2-hydroxybiphenyl 3-monooxygenase from Pseudomonas azelaica HBP1 by directed evolution*. Journal of Biological Chemistry, 2002. **277**(7): p. 5575-5582.
23. Lutz, J., et al., *Preparative application of 2-hydroxybiphenyl 3-monooxygenase with enzymatic cofactor regeneration in organic-aqueous reaction media*. Journal of Molecular Catalysis B-Enzymatic, 2002. **19**: p. 177-187.
24. Hollmann, F., A. Schmid, and E. Steckhan, *The first synthetic application of a monooxygenase employing indirect electrochemical NADH regeneration*. Angewandte Chemie-International Edition, 2001. **40**(1): p. 169-171.
25. Held, M., et al., *An integrated process for the production of toxic catechols from toxic phenols based on a designer biocatalyst*. Biotechnology and Bioengineering, 1999. **62**(6): p. 641-648.
26. Held, M., et al., *Preparative scale production of 3-substituted catechols using a novel monooxygenase from Pseudomonas azelaica HBP 1*. Journal of Molecular Catalysis B-Enzymatic, 1998. **5**(1-4): p. 87-93.
27. Suske, W.A., et al., *Purification and characterization of 2-hydroxybiphenyl 3-monooxygenase, a novel NADH-dependent, FAD-containing aromatic hydroxylase from Pseudomonas azelaica HBP1*. Journal of Biological Chemistry, 1997. **272**(39): p. 24257-24265.
28. Gygli, G. and W.J.H. van Berkel, *Oxizymes for biotechnology*. Current Biotechnology, 2015. **4**(2): p. 100-110.
29. Sucharitakul, J., et al., *The reaction kinetics of 3-hydroxybenzoate 6-hydroxylase from Rhodococcus jostii RHA1 provide an understanding of the para-hydroxylation enzyme catalytic cycle*. Journal of Biological Chemistry, 2013. **288**(49): p. 35210-35221.
30. Montersino, S., et al., *Crystal structure of 3-hydroxybenzoate 6-hydroxylase uncovers lipid-assisted flavoprotein strategy for regioselective aromatic hydroxylation*. Journal of Biological Chemistry, 2013. **288**(36): p. 26235-26245.
31. Kara, S., et al., *More efficient redox biocatalysis by utilising 1,4-butanediol as a 'smart cosubstrate'*. Green Chemistry, 2013. **15**(2): p. 330-335.
32. Montersino, S. and W.J. van Berkel, *Functional annotation and characterization of 3-hydroxybenzoate 6-hydroxylase from Rhodococcus jostii RHA1*. Biochimica et Biophysica Acta (BBA)-Protein Structure and Molecular Enzymology, 2012. **1824**(3): p. 433-42.
33. Kara, S., et al., *Recent trends and novel concepts in cofactor-dependent biotransformations*. Applied Microbiology and Biotechnology, 2014. **98**(4): p. 1517-1529.
34. Wichmann, R. and D. Vasic-Racki, *Cofactor regeneration at the lab scale*, in *Technology Transfer in Biotechnology: From Lab to Industry to Production*. 2005. p. 225-260.
35. Chenault, H.K. and G.M. Whitesides, *Regeneration of Nicotinamide Cofactors for Use in Organic-Synthesis*. Applied Biochemistry and Biotechnology, 1987. **14**(2): p. 147-197.
36. Pesic, M., E. Fernandez-Fueyo, and F. Hollmann, *Characterization of the old yellow enzyme homolog from Bacillus subtilis (YqjM)*. Chemistryselect, 2017. **2**(13): p. 3866-3871.

Chapter 4

37. Paul, C.E., I.W.C.E. Arends, and F. Hollmann, *Is Simpler Better? Synthetic Nicotinamide Cofactor Analogues for Redox Chemistry*. *Acs Catalysis*, 2014. **4**(3): p. 788-797.
38. Paul, C.E., et al., *Nonenzymatic regeneration of styrene monooxygenase for catalysis*. *ACS Catalysis*, 2015. **5**(5): p. 2961-2965.
39. Paul, C.E., et al., *Mimicking nature: synthetic nicotinamide cofactors for C=C bioreduction using enoate reductases*. *Organic Letters*, 2013. **15**(1): p. 180-183.
40. Unversucht, S., et al., *FADH(2)-dependence of tryptophan 7-halogenase*. *Advanced Synthesis & Catalysis*, 2005. **347**(7-8): p. 1163-1167.
41. Hollmann, F., et al., *Stereospecific biocatalytic epoxidation: The first example of direct regeneration of a FAD-dependent monooxygenase for catalysis*. *Journal of the American Chemical Society*, 2003. **125**(27): p. 8209-8217.
42. Winkler, C.K., et al., *NAD(P)H-independent asymmetric C=C bond reduction catalyzed by ene reductases by using artificial co-substrates as the hydrogen donor*. *Chemistry-a European Journal*, 2014. **20**(5): p. 1403-1409.
43. Ruinatscha, R., et al., *Productivity of selective electroenzymatic reduction and oxidation reactions: Theoretical and practical considerations*. *Advanced Synthesis & Catalysis*, 2006. **348**(15): p. 2015-2026.
44. Ruinatscha, R., et al., *Productive asymmetric styrene epoxidation based on a next generation electroenzymatic methodology*. *Advanced Synthesis & Catalysis*, 2009. **351**(14-15): p. 2505-2515.
45. Hollmann, F., et al., *Direct electrochemical regeneration of monooxygenase subunits for biocatalytic asymmetric epoxidation*. *Journal of the American Chemical Society*, 2005. **127**(18): p. 6540-6541.
46. Lee, S.H., et al., *Cofactor-free, direct photoactivation of enoate reductases for the asymmetric reduction of C=C bonds*. *Angewandte Chemie-International Edition*, 2017. **56**(30): p. 8681-8685.
47. Choi, D.S., et al., *Photoelectroenzymatic oxyfunctionalization on flavin-hybridized carbon nanotube electrode platform*. *ACS Catalysis*, 2017. **7**(3): p. 1563-1567.
48. Mifsud, M., et al., *Photobiocatalytic chemistry of oxidoreductases using water as the electron donor*. *Nature Communications*, 2014. **5**.
49. Zilly, F.E., et al., *Deazaflavins as mediators in light-driven cytochrome P450 catalyzed hydroxylations*. *Chemical Communications*, 2009(46): p. 7152-7154.
50. Grau, M.M., et al., *Photoenzymatic reduction of C=C double bonds*. *Advanced Synthesis & Catalysis*, 2009. **351**(18): p. 3279-3286.
51. Hollmann, F., et al., *A light-driven stereoselective biocatalytic oxidation*. *Angewandte Chemie-International Edition*, 2007. **46**(16): p. 2903-2906.
52. Holtmann, D. and F. Hollmann, *The Oxygen Dilemma: A Severe Challenge for the Application of Monooxygenases?* *Chembiochem*, 2016. **17**(15): p. 1391-1398.
53. Hemmerich, P., V. Massey, and H. Fenner, *Flavin and 5-Deazaflavin - Chemical Evaluation of Modified Flavoproteins with Respect to Mechanisms of Redox Biocatalysis*. *Febs Letters*, 1977. **84**(1): p. 5-21.
54. Heelis, P.F., et al., *One-electron reduction of 5 deazalumiflavin in aqueous-solution - a pulse radiolysis study*. *International Journal of Radiation Biology*, 1989. **55**(4): p. 557-562.
55. Tanaka, K., et al., *Preparation of chiral 5-deazaflavin derivatives and their asymmetric reduction of ethyl benzylformate*. *Tetrahedron Letters*, 1984. **25**(16): p. 1741-1742.
56. Bliese, M., et al., *Photo-Reduction of Deazaflavin - Spectroscopic Investigations*. *Australian Journal of Chemistry*, 1983. **36**(9): p. 1873-1883.
57. Goldberg, M., et al., *Structure and properties of 5-deazaflavin radicals as compared to natural flavosemiquinones*. *Biochimica Et Biophysica Acta*, 1981. **673**(4): p. 570-593.

58. Duchstein, H.J., et al., *(Photo)Chemistry of 5-Deazaflavin - Clue to the Mechanism of Flavin-Dependent (De)Hydrogenation*. European Journal of Biochemistry, 1979. **95**(1): p. 167-181.
59. Knappe, W.R., et al., *Photochemical formation of deazaflavin dimers*. Biochemistry, 1978. **17**(1): p. 16-7.
60. Blankenhorn, G., *Nicotinamide-dependent one-electron and 2-electron (flavin) oxydoreduction - thermodynamics, kinetics, and mechanism*. European Journal of Biochemistry, 1976. **67**(1): p. 67-80.
61. Hossain, M.S., et al., *Convenient synthesis of deazaflavin cofactor FO and its activity in F-420-dependent NADP reductase*. Organic & Biomolecular Chemistry, 2015. **13**(18): p. 5082-5085.
62. Knaus, T., et al., *Better than nature: Nicotinamide biomimetics that outperform natural coenzymes*. Journal of the American Chemical Society, 2016. **138**(3): p. 1033-1039.
63. Taylor, K.E. and J.B. Jones, *Nicotinamide coenzyme regeneration by dihydropyridine and pyridinium compounds*. Journal of the American Chemical Society, 1976. **98**(18): p. 5689-5694.
64. Spencer, R., J. Fisher, and C. Walsh, *Preparation, characterization, and chemical properties of flavin coenzyme analogs 5-deazariboflavin, 5-deazariboflavin 5'-phosphate, and 5-deazaflavin 5'-diphosphate, 5'-5'-adenosine ester*. Biochemistry, 1976. **15**(5): p. 1043-1053.
65. Salzmann, S., et al., *Photophysical properties of structurally and electronically modified flavin derivatives determined by spectroscopy and theoretical calculations*. Journal of Physical Chemistry A, 2009. **113**(33): p. 9365-9375.
66. Stankovich, M.T. and V. Massey, *Determination of Redox Potential of Deazariboflavin by Equilibration with Flavins*. Biochimica Et Biophysica Acta, 1976. **452**(2): p. 335-344.
67. Traber, R., H.E.A. Kramer, and P. Hemmerich, *Mechanism of light-induced reduction of biological redox centres by amino-acids - a flash-photolysis study of flavin photo-reduction by ethylenediaminetetraacetate and nitrilotriacetate*. Biochemistry, 1982. **21**(7): p. 1687-1693.
68. Kitzing, K., et al., *The 1.3 Å crystal structure of the flavoprotein YqjM reveals a novel class of Old Yellow Enzymes*. Journal of Biological Chemistry, 2005. **280**(30): p. 27904-27913.
69. Fitzpatrick, T.B., N. Amrhein, and P. Macheroux, *Characterization of YqjM, an old yellow enzyme homolog from Bacillus subtilis involved in the oxidative stress response*. Journal of Biological Chemistry, 2003. **278**(22): p. 19891-19897.
70. Massey, V. and P. Hemmerich, *Photoreduction of Flavoproteins and Other Biological Compounds Catalyzed by De-Aza-Flavins*. Biochemistry, 1978. **17**(1): p. 9-16.
71. Tosstorff, A., et al., *Mediated electron transfer with monooxygenases-Insight in interactions between reduced mediators and the co-substrate oxygen*. Journal of Molecular Catalysis B-Enzymatic, 2014. **108**: p. 51-58.
72. Stroehle, F.W., et al., *A computational protocol to predict suitable redox mediators for substitution of NAD(P)H in P450 monooxygenases*. Journal of Molecular Catalysis B-Enzymatic, 2013. **88**: p. 47-51.
73. Insinska-Rak, M., et al., *Spectroscopy and photophysics of flavin-related compounds: 5-deaza-riboflavin*. Journal of Molecular Structure, 2006. **783**(1-3): p. 184-190.
74. Clement, J.L., et al., *Assignment of the EPR spectrum of 5,5-dimethyl-1-pyrroline N-oxide (DMPO) superoxide spin adduct*. Journal of Organic Chemistry, 2005. **70**(4): p. 1198-1203.
75. Massey, V., *Activation of Molecular-Oxygen by Flavins and Flavoproteins*. Journal of Biological Chemistry, 1994. **269**(36): p. 22459-22462.
76. Studier, F.W., *Protein production by auto-induction in high-density shaking cultures*. Protein Expression and Purification, 2005. **41**(1): p. 207-234.

Chapter 5



Selective oxyfunctionalisation reactions driven by sulfite oxidase-catalysed *in situ* generation of H₂O₂

Morten M.C.H. van Schie, Alexander T. Kaczmarek, Florian Tieves,
Patricia Gomez de Santos, Caroline E. Paul, Isabel W.C.E. Arends, Miguel Alcalde,
Günter Schwarz, Frank Hollmann

Based on:

Van Schie, M.M.C.H., *et al.*, Selective oxyfunctionalisation reactions driven by sulfite oxidase-catalysed *in situ* generation of H₂O₂. Manuscript under review.

Summary

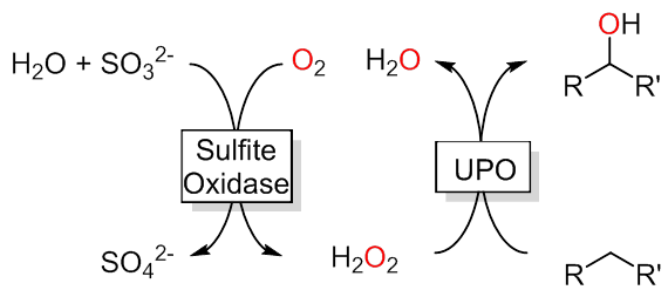
For this chapter we examined the feasibility of applying sulfite oxidases (SO) for the *in situ* generation of H₂O₂, in order to drive peroxygenases. SO are able to oxidize sulfite to sulfate and subsequently reduce oxygen. One key element in this scheme is the reactivity of the sulfite itself, as it can participate in a direct futile reaction with H₂O₂, as well in epoxide ring opening reactions. These side reactions can be minimized by using calcium sulfite, a poorly soluble salt, as the substrate. Conveniently, CaSO₃ is a product in industrial processes where flue gasses are desulfurized with lime stone. This waste can thus be used to drive interesting biocatalytic reactions.

Introduction

Peroxygenases (E.C. 1.11.2.1, UPO for unspecific peroxygenases) are powerful catalysts for the selective oxyfunctionalisation of (inert) C-H and C=C-groups [1, 2]. Especially their high catalytic activity, robustness and simplicity of application make them potentially useful catalysts for organic oxyfunctionalisation chemistry.

As heme-enzymes, UPOs suffer from a pronounced instability towards hydrogen peroxide, the stoichiometric oxidant in UPO-reactions [3]. This issue is met by *in situ* generation of H_2O_2 at rates, which maximize productive UPO-turnover while minimizing the undesired oxidative inactivation of the enzymes [4]. Today, a broad range of *in situ* H_2O_2 generation systems are available raising the question about the environmental impact of such systems, especially with large-scale applications in mind. In this respect, we drew our attention to sulfite as stoichiometric reductant, as sulfite is a by-product from flue gas treatment and thus produced at large amounts.

To use sulfite as stoichiometric reductant for the *in situ* generation of H_2O_2 , we envisioned the application of sulfite oxidases (SO), which are ubiquitously found in all kingdoms of life. SO play a central role in the sulfur metabolism of living cells [5]. As the name implies, SO oxidizes sulfite to sulfate using a unique pterin-based molybdenum cofactor (MoCo) in the active site [6]. In vertebrates, SO localizes into the intermembrane space of mitochondria and consists of three distinguishable domains, the N-terminal heme domain, incorporating a cytochrome b5-type heme cofactor, followed by the MoCo-binding domain, and the C-terminal dimerization domain. Upon oxidation of sulfite, the molybdenum in the active site is reduced from Mo^{VI} to Mo^{IV} and the two electrons are subsequently transferred via an intra-molecular electron transfer from the MoCo to the heme domain and finally to cytochrome c [7]. Alternatively, sulfite-derived electrons can be transferred to nitrite, forming the radical nitric oxide [8, 9]. In contrast, in plants, SO consists only of the MoCo and dimerization domain and localizes in peroxisomes [10, 11]. Here, the redox balance is closed *via* the reaction with molecular oxygen, forming superoxide, which rapidly dismutates to H_2O_2 . When the heme domain in the mammalian SO is deleted, similar behaviour of H_2O_2 formation is observed [12]. It is therefore that we envisioned the application this H_2O_2 generation system in the application of peroxygenase reactions (Scheme 1).



Scheme 1: The cascade of sulfite oxidase and peroxygenases.

To test our hypothesis, we chose the evolved, recombinant peroxygenase from *Agrocyste aegerita* (rAaeUPO) as model enzyme for the (*R*)-selective hydroxylation of ethyl benzene to (*R*)-1-phenyl ethanol. Various SO enzymes from different sources (all recombinantly expressed in *Escherichia coli*) were tested; one plant SO (from *Arabidopsis thaliana*) and two mammalian SO (either in their natural configuration containing the heme moiety (Full) or a shortened, devoid of heme (MoCo))(figure 1).

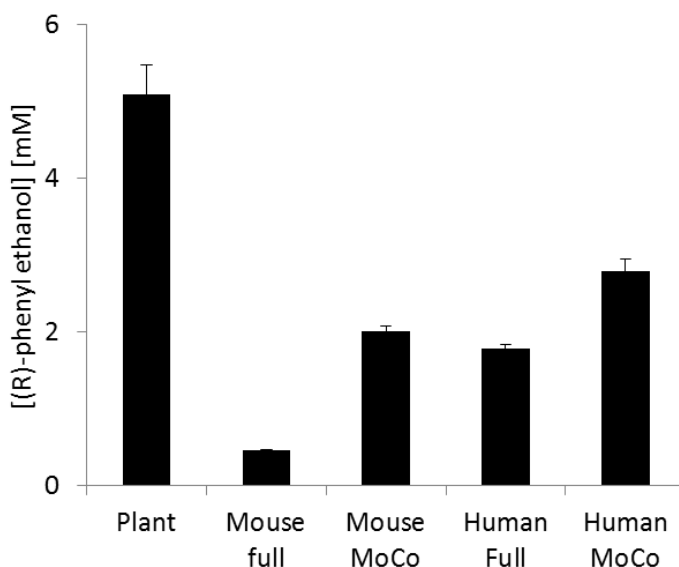


Figure 1. Comparison of different sulfite oxidases to drive the rAaeUPO-catalysed hydroxylation of ethyl benzene. General conditions: [SO] = 100 nM, [rAaeUPO] = 500 nM, [Na₂SO₃]₀ = 10 mM, [ethyl benzene]₀ = 100 mM in a 50 mM Bis-Tris buffer at pH 7.0. 250 µl reactions were performed in duplicates in a thermos shaker at 30 °C and 500 rpm for 24 hours.

Pleasingly, all SO enabled *rAaeUPO*-catalysed hydroxylation of ethyl benzene. The heme-depleted SO gave higher activities (i.e. overall product concentrations) than the heme-containing ones, which is most likely due to the faster direct aerobic reoxidation at the Mo^{IV} centers. For all further experiments we focussed on the plant SO (PSO). To get further insights into the parameters influencing the performance of the SO-*rAaeUPO*-oxygenfunctionalisation system we systematically varied some reaction parameters such as pH and sulfite concentration (figure 2).

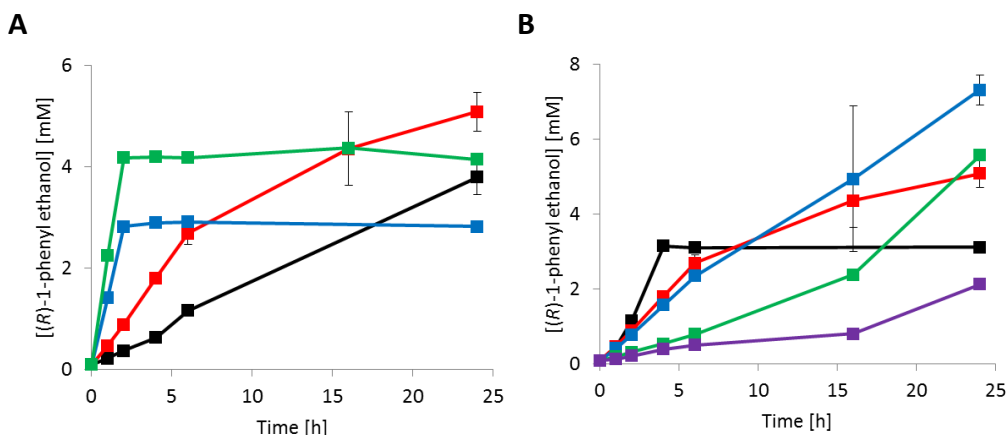


Figure 2. Influence of the reaction pH (A) and sulfite concentration (B) on the plant-SO – *rAaeUPO* cascade performance. General conditions: $[\text{PSO}] = 100 \text{ nM}$, $[\text{rAaeUPO}] = 500 \text{ nM}$, $[\text{Na}_2\text{SO}_3]_0 = 10 \text{ mM}$, $[\text{ethyl benzene}]_0 = 100 \text{ mM}$ in a 50 mM Bis-Tris buffer at pH 7.0. 250 μL reactions were performed in duplicates in a thermos shaker at 30 $^\circ\text{C}$ and 500 rpm. A: performance at pH 6.5 (black), pH 7.0 (red), pH 7.5 (blue) or pH 8.0 (green). B: Sodium sulfite concentration of 5 mM (black), 10 mM (blue), 20 mM (red), 50 mM (green) and 100 mM (purple).

The reaction functioned optimally at neutral pH values, which appears to be a compromise between the preferred conditions for SO (basic) and the peroxygenase (slightly acidic).

Increased sulfite concentrations corresponded to an increased reaction stability, but also a decreased reaction rate. Furthermore, sub-stoichiometric product formation was observed in respect to sulfite added. These effects are most likely explained by the spontaneous reaction between sulfite and H_2O_2 yielding sulfate and H_2O [11, 13]. As the reaction between H_2O_2 and SO_3^{2-} is linearly dependent on the in situ concentration of both reagents, we thought to limit the concentration of SO_3^{2-} in the reaction mixture by using CaSO_3 as the sulfite source. CaSO_3 is poorly water soluble, only up to 0.15 mM, and will

therefore form a second solid phase in the reaction acting as a sulfite reservoir. Advantageously, CaSO_3 is also the primary product from flue gas desulfurisation with lime stone [14, 15]. Very pleasingly, this strategy indeed enhanced the product accumulation significantly (figure 3).

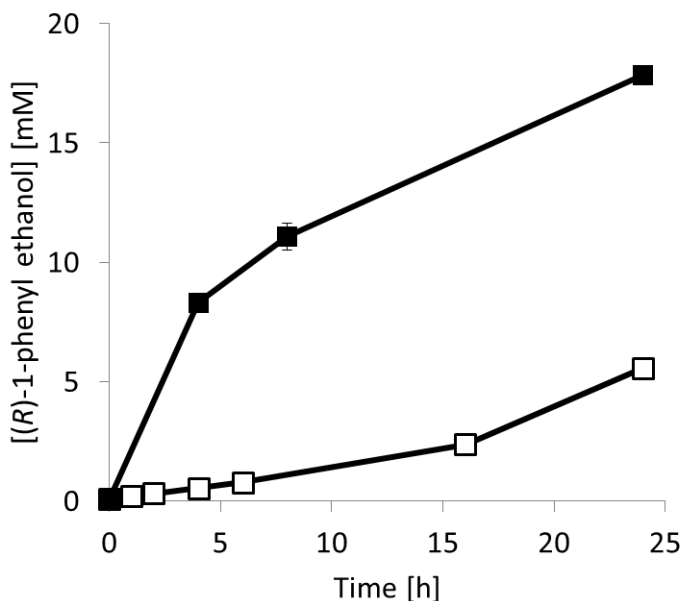
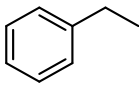
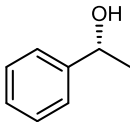
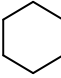
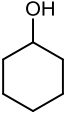
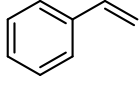
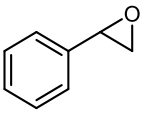
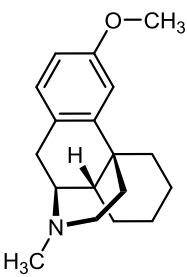
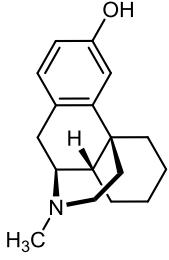
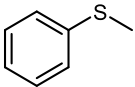
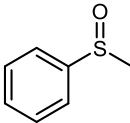
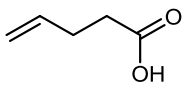
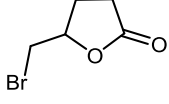


Figure 3: Comparison of Na_2SO_3 (red) and CaSO_3 (blue) on the PSO – *rAaeUPO* cascade. General conditions: $[\text{PSO}] = 100 \text{ nM}$, $[\text{rAaeUPO}] = 500 \text{ nM}$, $[\text{SO}_3^{2-}]_0 = 50 \text{ mM}$, $[\text{ethyl benzene}]_0 = 100 \text{ mM}$ in a 50 mM Bis-Tris buffer at pH 7.0. 250 μl reactions were performed in duplicates at 30 °C and 500 rpm. Reactions with Na_2SO_3 were performed in a thermos shaker, while the samples with CaSO_3 were mixed by a magnetic stirrer in a water bath.

Encouraged by these results we also explored the scope of the proposed sulfite-driven oxidation reaction (table 1). The requirement of the slurry to be homogeneously dispersed in solution did, in some occasions, induce significant standards deviations.

Chapter 5

Table 1: Substrate scope for the reaction of PSO coupled to various peroxygenases. General conditions: [SO] = 200 nM, [peroxygense] = 500 nM, [CaSO₃]₀ = 100 mM, [substrate]₀ = 50 mM in a 50 mM Bis-Tris buffer. 500 μ l reactions were performed in triplicates at 30 °C with magnetic stirrers mixing at 500 rpm. For dextromethorphan, the substrate concentration was 10 mM. For thioanisole, 100 U ml⁻¹ of CFO from *Caldariomyces fumago* was added as the peroxygenase. a: TTN: mol product mol⁻¹_{cat.} b: *vide infra*. c: the low enantiomeric excess (ee) for styrene has been reported before.

Substrate	Product	Catalyst	TTN ^a SO / (Peroxygenase)	Conversion [mM]	ee [%]
		<i>rAaeUPO</i>	77 000 / (30 800)	15.4 (\pm 1.8)	98.2
		<i>rAaeUPO</i>	83 500 / (33 400)	16.7 (\pm 4.6)	-
		<i>rAaeUPO</i>	70 000 / (28 000)	14.0 ^b (\pm 0.41)	5.8 ^c
		<i>rAaeUPO</i> (Solo)	26 350 / (10 540)	5.72 (\pm 0.52)	-
		<i>CfuCPO</i>	67 000 / (n.d.)	13.4 (\pm 0.16)	98.4
		<i>CivCPO</i>	-	0.0	-

As shown in table 1, a range of classical peroxygenase reactions could be promoted by the proposed SO-H₂O₂ generation system ranging from the (stereospecific) hydroxylation of sp³-C-H-bonds *via* oxidative demethylation [16] and epoxidation [17] to sulfoxidation [18] reactions. We also evaluated SO for the chemoenzymatic halogenation reaction based on hypohalites generated *in situ* from halides using the vanadium-dependent haloperoxidase from *Curvularia inaequalis* [19]; albeit without success. We ascribe this observation to the deactivation of SO by the bleach formed by VCPO, as observed for other oxidases and showed in a control reaction where 10 μM NaClO nearly fully inhibited the SO [20]. Sulfite itself did not seem to affect the activity of VCPO.

Finally, we also investigated yet another application of sulfite except just as sacrificial electron donor for the *in situ* H₂O₂ generation reaction. Namely, using sulfite as nucleophile to further convert epoxides into corresponding hydroxyl sulfonate (Scheme 2). As for the futile reaction of sulfite with peroxide, this ring opening reaction is reported to follow first order kinetics [21, 22]. Therefore, the epoxide is primarily observed if CaSO₃ is the sulfite source. For Na₂SO₃, only the sulfonated product, 1-phenyl-2-hydroxyethanesulfonate with the other regioisomer as a side-product (16%), is obtained as previously described in literature [22].

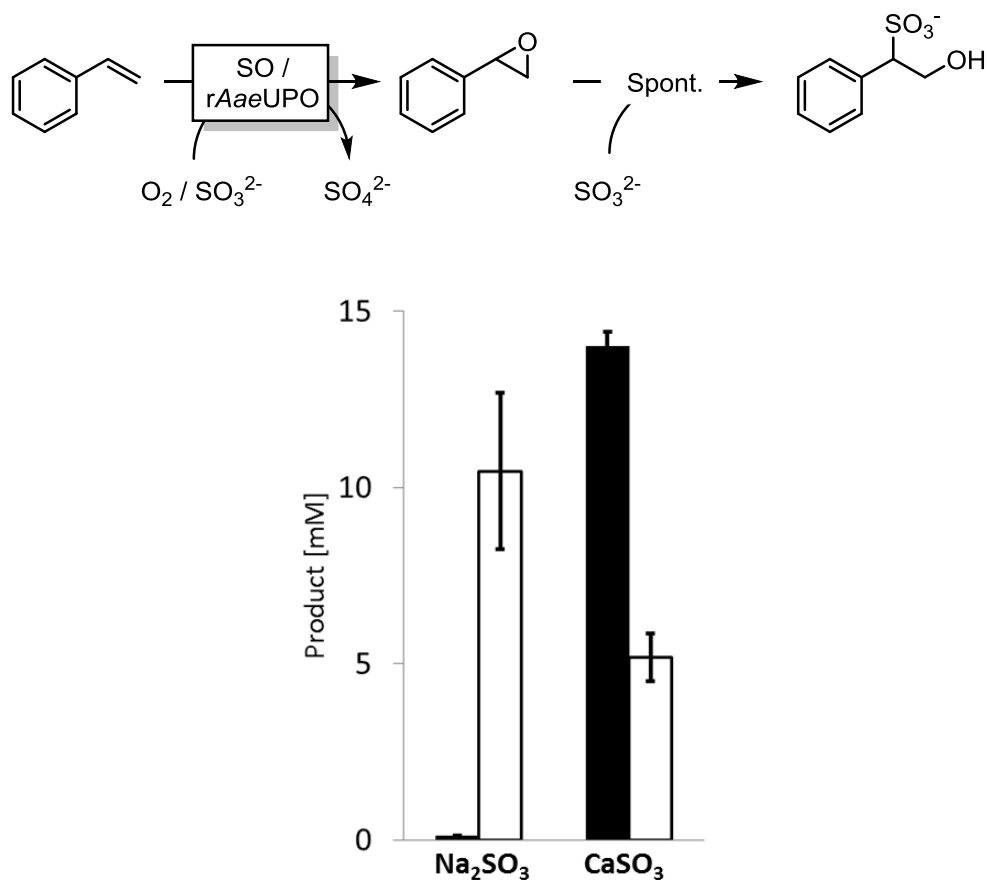


Figure 4: Chemoenzymatic transformation of styrene into styrene oxide (full) or 1-phenyl-2-hydroxyethanesulfonate (open), depending on the sulfite salt used. General conditions: $[\text{SO}] = 200 \text{ nM}$, $[\text{peroxygenase}] = 500 \text{ nM}$, $[\text{SO}_3^{2-}]_0 = 100 \text{ mM}$, $[\text{styrene}]_0 = 50 \text{ mM}$ in a 50 mM Bis-Tris buffer. $500 \mu\text{l}$ reactions were performed in triplicates at 30°C with magnetic stirrers mixing at 500 rpm .

Conclusion

Overall, we provide the proof of principle of using sulfite oxidases coupled to various peroxygenases, thereby enabling oxyfunctionalisation reactions at the expense of a waste product. The total turnover numbers for the oxidase and peroxygenases are not as high yet as previously reported for, for instance, formate oxidase [23]. However, in contrast to FOx, SO variants can be found in all organisms which is why other promising catalysts can easily be obtained via enzyme database mining [24]. In terms of applications,

the possibility of sulfite to further participate in chemo-enzymatic cascades opens up new ways of conveniently product various hydroxyl-sulfonates.

Material and methods

Chemicals

Dextrormethorphan and dextrorphan were purchased from Santa Cruz Biotechnology Europe (Germany). CaSO_3 was purchased from ABCR (Switzerland). All other chemicals were purchased from Sigma-Aldrich in the highest purity available and used without further purifications.

Enzymes

Two mutants of *rAaeUPO* were used for this study: The PaDal (an expression-engineered version of the wild-type enzyme) and SoLo (engineered for the hydroxylation of aromatic substrates). Both mutants were produced in *Pichia pastoris* as described previously.

Vanadium dependent haloperoxidase from *Curvularia inaequalis* (CIVCPO) was produced in *E. coli* as described previously.

Chloroperoxidase from *Caldariomyces fumago* was bought from Fluka.

SO variants were recombinantly expressed within the *E.coli* strain TP1004 [25] and purified as previously described [8]. Full-length HSO (aa 80-545), MSO (aa 81-546) were expressed with an N-terminal 6xHis-tag. Plant SO (aa 1-393) was expressed with a C-terminal 6xHis-tag. Heme-truncated HSO Mo (aa 167-545) and MSO Mo (168-546) were expressed with a N-terminal 6xHis-tag followed by PreScission Cleavage Site (LEVLFQ/GP). Expression was performed in 2 L cultures LB-medium supplemented with 1 mM sodium molybdate. Expression was induced at an $\text{OD}_{600\text{nm}}$ of 0.6 by adding 250 μM IPTG and took place for 72 h at 18°C. His-tagged SO variants were purified via Nickel-NTA affinity chromatography and/or with PreScission Protease (GE Healthcare) on-column cleavage, as previously described [8]. Purified proteins were buffer-exchanged into 20 mM Tris/Ac pH 8.0, 50 mM NaCl, using PD10 buffer exchange columns (GE Healthcare).

Chapter 5

Reaction conditions

Reactions for the characterization of the SO - rAaeUPO cascade were performed in Bis-Tris (pH 6.0 to 7.0) or Tris (pH 7.5 to 8.0) buffers (50 mM, 0.250 ml) using the plant SO. Generally, the reactions were performed in the Bis-Tris buffer at pH 7.0 and contained ethyl benzene (100 mM), rAaeUPO (500 nM), SO (100 nM) and sodium sulfite (10 mM). For the time courses, single experiments were performed in duplicate, in glass 1.5 ml vials in a thermos shaker mixing at 500 rpm at 30 °C. To evaluate the effect of the sulfite salt, either 50 mM Na₂SO₃, from a 1 M stock, or 6 mg CaSO₃ salt was added as the substrate.

At designated time points, the reactions were stopped by extraction of the samples with an equal volume of ethyl acetate. The organic phase contained 5 mM of either octanol, acetophenone or dodecane as an internal standard. After extraction and centrifugation, the organic phase was dried with magnesium sulfate and subsequently analyzed *via* gas chromatography.

Gas Chromatography

Sample analyses were performed on Shimadzu GC-2010 Plus gas chromatographs with an AOC-20i Auto injector with FID (Shimadzu, Japan), using nitrogen or helium as the carrier gas. The following columns and methods were used:

Column A: CP wax 52 CB	Length: 25 m. ID: 0.25 mm. Film thickness: 1.20 µm. Carrier gas: Nitrogen. Split.
Column B: CP sil 5 CB	Length: 50 m. ID: 0.53 mm. Film thickness: 1.00 µm. Carrier gas: Nitrogen. No split.
Column C: CP Chirasil Dex CB	Length: 25 m. ID: 0.32 mm. Film thickness: 0.25 µm. Carrier gas: Helium. Split.
Column D: Lipodex E	Length: 50 m. ID: 0.25 mm. Film thickness: 0.25 µm. Carrier gas: Helium. Split.
Column E: CP sil 5 CB	Length: 25 m. ID: 0.25 mm. Film thickness: 1.20 µm. Carrier gas: Nitrogen. Split.

Ethyl benzene

Measured on column A. Octanol as internal standard. Split of 30. Linear velocity of 27.4 cm s⁻¹.

Ramp [°C min ⁻¹]	Temperature [°C]	Hold time [min]
-	150	2.2
25	210	3.8
30	250	1.0

Retention times

Compound	Retention time (min)
Ethyl benzene	2.9
Octanol	5.2
Acetophenone	6.7
Phenyl ethanol	8.0

Ethyl benzene (Enantiomers)

Measured on column C. Octanol as internal standard. Split of 75. Linear velocity of 29.5 cm s⁻¹.

Ramp [°C min ⁻¹]	Temperature [°C]	Hold time [min]
-	120	2.6
15	135	3.3
25	225	1.0

Retention times

Compound	Retention time (min)
Ethyl benzene	2.5
Acetophenone	4.3
Octanol	4.6
<i>R</i> -Phenyl ethanol	6.1
<i>S</i> -Phenyl ethanol	6.3

Chapter 5

Cyclohexane

Measured on column A. Octanol as internal standard. Split of 50. Linear velocity of 29.3 cm s^{-1} .

Ramp [$^{\circ}\text{C min}^{-1}$]	Temperature [$^{\circ}\text{C}$]	Hold time [min]
-	60	3.5
25	200	2.0
30	250	1.0

Retention times

Compound	Retention time (min)
Cyclohexane	2.5
Octanol	8.0
Cyclohexanone	9.3
Cyclohexanol	9.9

Dextormethorphan

Measured on column B: Dodecane as internal standard. Linear velocity of 20 ml min^{-1} .

Ramp [$^{\circ}\text{C min}^{-1}$]	Temperature [$^{\circ}\text{C}$]	Hold time [min]
-	120	1.0
20	270	4.0
20	325	1.0

Retention times

Compound	Retention time (min)
Dodecane	3.0
Dextormethorphan	8.6
Dextrorphan	9.0

Styrene

Measured on column C. Dodecane as internal standard. Split of 25. Linear velocity of 29.5 cm s⁻¹.

Ramp [°C min ⁻¹]	Temperature [°C]	Hold time [min]
-	100	11.0
25	225	1.0

Retention times

Compound	Retention time (min)
Styrene	3.1
<i>S</i> -Styrene	5.6
<i>R</i> -Styrene	8.0
Phenyl acetaldehyde	8.4
Dodecane	9.8

Thioanisole

Measured on column D. Dodecane as internal standard. Split of 100. Linear velocity of 37.4 cm s⁻¹.

Ramp [°C min ⁻¹]	Temperature [°C]	Hold time [min]
-	120	6.0
20	200	4.0
25	225	1.0

Retention times

Compound	Retention time (min)
Dodecane	5.0
Thioanisole	6.0
<i>R</i> -Methyl phenyl sulfoxide	12.6
<i>S</i> -Methyl phenyl sulfoxide	13.2

4-pentenoic acid

Chapter 5

Measured on column E. Acetophenone as internal standard. Split of 10. Linear velocity of 26.4 cm s^{-1} .

Ramp [$^{\circ}\text{C min}^{-1}$]	Temperature [$^{\circ}\text{C}$]	Hold time [min]
-	70	1.0
30	140	1.0
30	195	2.0
30	225	2.0
30	345	1.0

Retention times

Compound	Retention time (min)
4-Pentenoic acid	5.1
Acetophenone	7.6
Bromolactone	9.8

Determination of hydroxyl-sulfonate compound concentrations by NMR

The concentrations of the sulfonated compounds were determined *via* ^1H NMR using maleic acid as an internal standard. After the reaction was stopped, 5 mM of maleic acid was added to the solution and the reaction mixture was left under vacuum to dry, removing the water content, styrene and styrene oxide. The remaining solid was redissolved in D_2O and analysed on a Agilent 400 spectrometer. The product concentrations were calculated by determining the peak areas of the aromatic region (five proton equivalents) and those related to the internal standard (two proton equivalents). Authentic standards were prepared by incubation of 50 mM styrene oxide (which forms a second phase) with 100 mM of NaSO_3 in double distilled water at room temperature for at least three hours [22]. Chemical shifts are given in ppm with respect to tetramethylsilane. Coupling constants are reported as *J*-values in Hz (s: singlet; d: doublet; t: triplet; q: quartet; m: multiplet; br: broad). Due to a mixture of product isomers, multiplets were observed for the non-aromatic protons.

^1H NMR (400 MHz, CDCl_3) δ 7.42-7.24 (m, 5H), 6.02 (s, 2H, maleic acid), 4.25-4.20 (m, 1H), 4.15-4.01 (m, 2H).

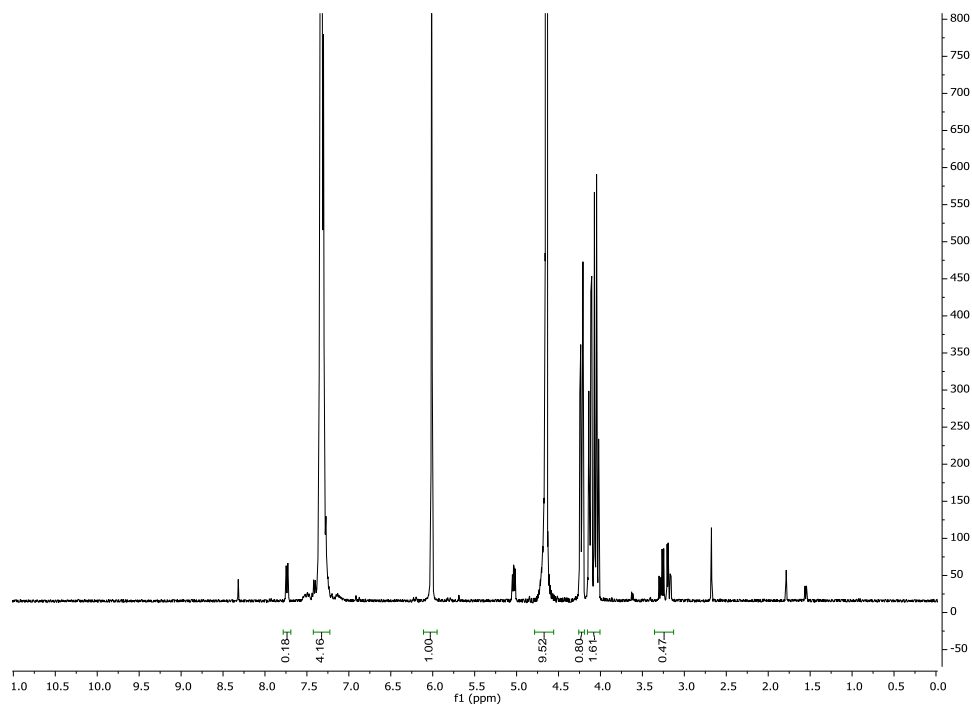


Figure 5. Example of a ^1H NMR spectrum of the reaction product with the maleic acid (at 6.02 ppm) as an internal standard.

References

1. Wang, Y.H., et al., *Peroxygenases en route to becoming dream catalysts. What are the opportunities and challenges?* Current Opinion in Chemical Biology, 2017. **37**: p. 1-9.
2. Bormann, S., et al., *Specific oxyfunctionalisations catalysed by peroxygenases: opportunities, challenges and solutions.* Catalysis Science & Technology, 2015. **5**(4): p. 2038-2052.
3. Valderrama, B., M. Ayala, and R. Vazquez-Duhalt, *Suicide inactivation of peroxidases and the challenge of engineering more robust enzymes.* Chemistry & Biology, 2002. **9**(5): p. 555-565.
4. Burek, B.O., et al., *Hydrogen peroxide driven biocatalysis.* Green Chemistry, 2019.
5. Kappler, U. and J.H. Enemark, *Sulfite-oxidizing enzymes.* JBIC Journal of Biological Inorganic Chemistry, 2015. **20**(2): p. 253-264.
6. Schwarz, G., *Molybdenum cofactor and human disease.* Current Opinion in Chemical Biology, 2016. **31**: p. 179-87.
7. Brody, M.S. and R. Hille, *The kinetic behavior of chicken liver sulfite oxidase.* Biochemistry, 1999. **38**(20): p. 6668-6677.
8. Kaczmarek, A.T., et al., *Reciprocal regulation of sulfite oxidation and nitrite reduction by mitochondrial sulfite oxidase.* Nitric Oxide, 2019. **89**: p. 22-31.
9. Bender, D., et al., *Mechanism of nitrite-dependent NO synthesis by human sulfite oxidase.* Biochemical Journal, 2019: p. BCJ20190143.
10. Schrader, N., et al., *The crystal structure of plant sulfite oxidase provides insights into sulfite oxidation in plants and animals.* Structure, 2003. **11**(10): p. 1251-1263.
11. Hänsch, R., et al., *Plant sulfite oxidase as novel producer of H₂O₂ combination of enzyme catalysis with a subsequent non-enzymatic reaction step.* Journal of Biological Chemistry, 2006. **281**(10): p. 6884-6888.
12. Belaidi, A.A., et al., *Oxygen reactivity of mammalian sulfite oxidase provides a concept for the treatment of sulfite oxidase deficiency.* Biochemical Journal, 2015. **469**(2): p. 211-221.
13. Hoffmann, M.R. and J.O. Edwards, *Kinetics of the oxidation of sulfite by hydrogen peroxide in acidic solution.* The Journal of Physical Chemistry, 1975. **79**(20): p. 2096-2098.
14. Manahan, S., *Environmental chemistry.* 2017: CRC press.
15. Srivastava, R.K. and W. Jozewicz, *Flue gas desulfurization: the state of the art.* Journal of the Air & Waste Management Association, 2001. **51**(12): p. 1676-1688.
16. de Santos, P.G., et al., *Benchmarking of laboratory evolved unspecific peroxygenases for the synthesis of human drug metabolites.* Tetrahedron, 2019. **75**(13): p. 1827-1831.
17. Rauch, M.C., et al., *Peroxygenase-catalysed epoxidation of styrene derivatives in neat reaction media.* ChemCatChem, 2019.
18. Allenmark, S.G. and M.A. Andersson, *Chloroperoxidase-induced asymmetric sulfoxidation of some conformationally restricted sulfides.* Chirality, 1998. **10**(3): p. 246-252.
19. Dong, J.J., et al., *Halofunctionalization of alkenes by vanadium chloroperoxidase from *Curvularia inaequalis*.* Chemical Communications, 2017. **53**(46): p. 6207-6210.
20. But, A., et al., *Enzymatic halogenation and oxidation using an alcohol oxidase-vanadium chloroperoxidase cascade.* Molecular Catalysis, 2017. **443**: p. 92-100.
21. Schenck, R.T.E. and S. Kaizerman, *The reaction of bisulfite with epoxy compounds.* Journal of the American Chemical Society, 1953. **75**(7): p. 1636-1641.
22. Swan, J.D., *Determination of Epoxides with Sodium Sulfite.* Analytical Chemistry, 1954. **26**(5): p. 878-880.
23. Tieves, F., et al., *Formate oxidase (FOx) from *Aspergillus oryzae*: One catalyst enables diverse H₂O₂-dependent biocatalytic oxidation reactions.* Angewandte Chemie International Edition, 2019. **58**(23): p. 7873-7877.

24. Steinkellner, G., et al., *Identification of promiscuous ene-reductase activity by mining structural databases using active site constellations*. Nature Communications, 2014. **5**: p. 4150.
25. Palmer, T., et al., *Involvement of the narJ and mob gene products in distinct steps in the biosynthesis of the molybdoenzyme nitrate reductase in Escherichia coli*. Molecular Microbiology, 1996. **20**(4): p. 875-884.

Chapter 6



H₂O₂ Production at low over-potentials for biocatalytic halogenation reactions

Sebastian Bormann, Morten M.C.H. van Schie, Tiago Pedroso de Almeida, Wuyuan Zhang, Roland Ulber, Frank Hollmann, Dirk Holtmann

Based on:

Bormann, S.⁺, Van Schie, M.M.C.H.⁺, *et al.*, *H₂O₂ Production at low over-potentials for biocatalytic halogenation reactions*. *ChemSusChem*, **12**.

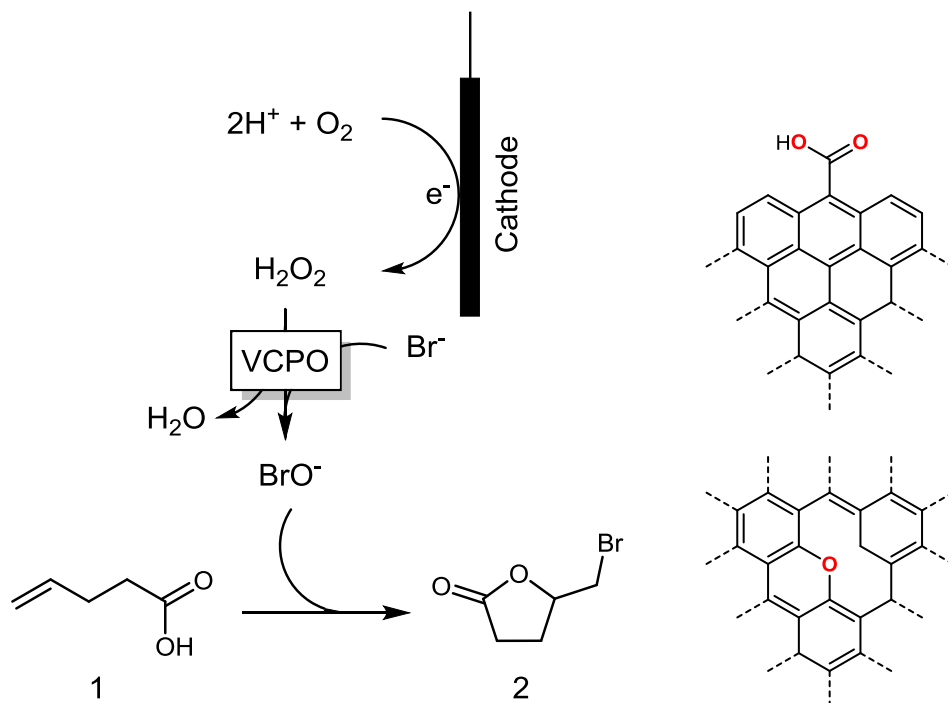
⁺ equally contributed

Summary

The electrochemical reduction of oxygen can be used as an in situ generation method for hydrogen peroxide in order to drive peroxidases. From an atom efficiency point of view, this is an ideal method, as no cosubstrates or coproducts are involved. However, an over-potential on the system is needed for the reduction of oxygen, resulting in an increase in power needed. Here we report a method to coat the cathode in the system with oxidized nanotubes, thereby greatly reducing the over-potential needed to perform this reaction. We then couple this set-up to a chloroperoxidase-catalysed reaction to show a proof of principle and calculate the amount of power saved.

Introduction

Vanadium dependent chloroperoxidase is able to efficiently produce hypohalides at the expense of hydrogen peroxide and a halide [1-3]. These reactive compounds are then able to participate in various halogenation reactions [4-6]. For reasons of reaction stability, prevention of bleach dismutation and enzyme activity, it is preferable to keep the concentration of the peroxide minimal in the reaction solution. One attractive way to achieve this would be *via in situ* generation of the H_2O_2 using electrochemistry [7, 8]. Electrochemical generation of H_2O_2 bears several advantages over other presented methods [9, 10], as no additional chemicals are needed and no hazardous residues are left. Instead, electricity is used, which is readily available and can be generated cleanly. Several papers on driving chloroperoxidases using electrochemistry to generate H_2O_2 have therefore already been reported, showing excellent performances [11-13]. One reoccurring issue in these processes, however, is the requirement of an over-potential at the cathodic reaction to reduce oxygen. The electrodes can be doped with catalysts to decrease this over-potential, but these catalysts are generally made from alloys containing noble metals like platinum or gold [14-16]. Recently, the group of Cui reported the application of oxidized carbon nanotubes (o-CNT) doped graphite, solely containing earth abundant compounds, to significantly improve selectivity and decrease the potential for H_2O_2 production [17]. The increased performance was ascribed to the presence of several oxygen functional groups, in specific -COOH at the edges and -C-O-C- within the structure, abundantly present in the graphite framework. We therefore contemplated when we could use these oxidized nanotube doped catalysts in order to improve the electroenzymatic generation of hypohalides using peroxidases in order to perform chemical reactions (Scheme 1).



Scheme 1: Left: Schematic overview of the biocatalytic generation of hypobromite by VCPO, reacting with 4-pentenoic acid (**1**) to form the 5-(Bromomethyl)dihydrofuran-2(3H)-one (**2**). The hydrogen peroxide needed for the enzymatic reaction is generated electrochemically. Right: The proposed oxygen functional groups in the graphite structure responsible for increased catalytic activity.

Results

Several electrodes, graphite paper (Sigracet® GDL 38 BC) doped with different amounts of the oxidized carbon nanotubes (o-CNT), were prepared to evaluate their efficiency in producing H_2O_2 at low potentials. An overview of the prepared electrodes is shown in table 1.

Chapter 6

Table 1: Overview of the prepared electrodes of oxidized carbonnanotubes on Sigracet® GDL38 BC graphite paper.

Electrode #	[o-CNT] [$\mu\text{g cm}^{-2}$]	Nafion [w/v %]
1	0	1.0
2	100	1.0
3	200	1.0
4	500	1.0
5	1000	1.0

All experiments were performed in a two component electrochemical chamber, which contained a 100 ml buffered reaction solution with bromide. The treated graphite paper sheets were used as gas diffusion electrodes. In a first set of experiments the performance of the electrodes was tested by performing linear sweep experiments. Here the cell current was measured as a function of the applied potential between the working and the counter electrode. The results are shown in figure 1.

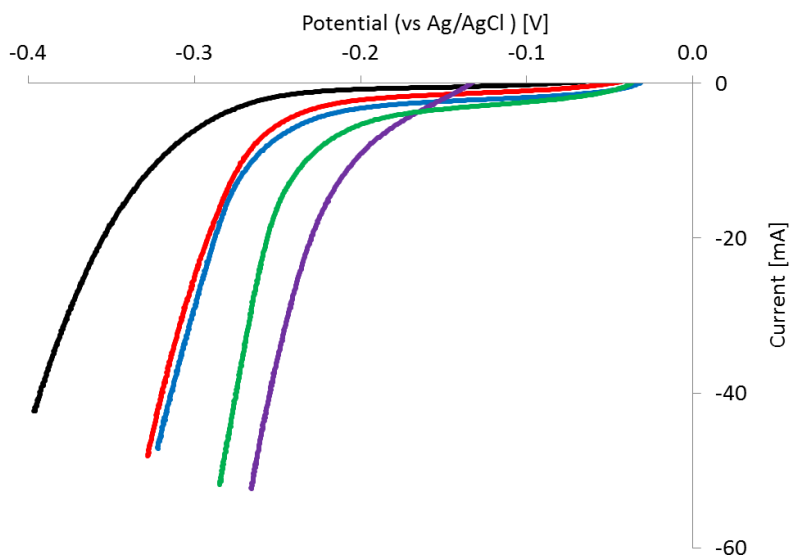


Figure 1. Cyclic voltammetry of electrodes loaded with increasing amounts of oxidized carbon nanotubes. The Voltage is internal resistance corrected. Scan rate of 5 mV s^{-1} . Electrode 1 (black), electrode 2 (red), electrode 3 (blue), electrode 4 (green) and electrode 5 (purple).

As expected, a higher o-CNT loading resulted in a lowered potential needed to reach higher currents. To test whether this also related to higher H_2O_2 production, we also determined the H_2O_2 formation at different potentials for the electrodes 1, 2 and 5, loaded with 0, 100 and 1000 $\mu\text{g cm}^{-2}$ o-CNT respectively. As shown in figure 2, the doped catalysts showed higher formation rates for H_2O_2 independent of the potential applied. At -250 mV, electrode 5 already facilitated the formation of 2 mM of peroxide per hour, while the undoped control electrode showed very little peroxide generation. At increased potentials, the doped cathodes further outperformed the control, proving the beneficial effect of the o-CNT on the cathodic reaction. Due to a limitation in terminal voltage, higher potentials than -350 mV could not be applied for electrode 5, but the linear relation between potential and H_2O_2 evolution show the limits of the system were not yet reached. Another important parameter for the performance of the catalyst is the efficiency in electron use. In other words, the amount of peroxide formed per electron couple supplemented by the cathode. Cui et al reported a higher peroxide formation efficiency at neutral to basic conditions [17]. However, under the slightly acidic conditions used here, similar efficiencies were observed for all electrodes, as shown in figure 3. Interestingly, the efficiency did generally seem to increase at higher potentials in the cases of the doped cathodes.

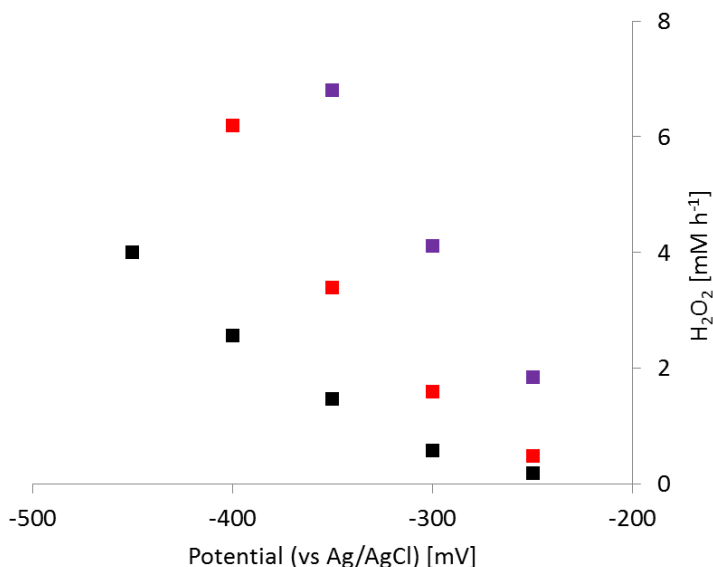


Figure 2. H_2O_2 generation rates for the prepared cathodes at varied potentials. Electrode 1 (black), electrode 2 (red) and electrode 5 (purple).

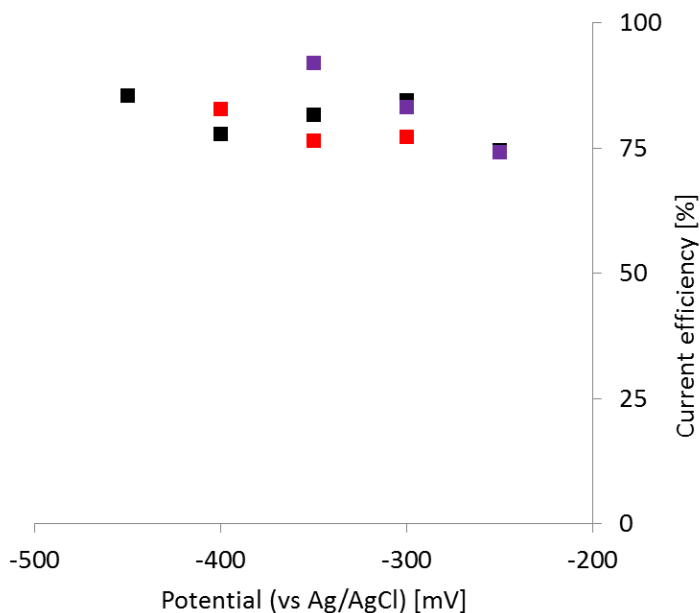


Figure 3. Current efficiency of the prepared cathodes at varied potentials in respect to H_2O_2 formation. Efficiencies were calculated by dividing the formation of by the electrons inserted in the reaction, as calculated from the current determined. Electrode 1 (black), electrode 2 (red) and electrode 5 (purple).

In a final set of experiments, we coupled the electrochemical peroxide evolution to the bleach production by a vanadium containing chloroperoxidase from *Curvularia inaequalis* (CVCPO). As the model reaction we chose the formation of hypobromide, from H_2O_2 and bromine, which would in turn attack 4-pentenoic acid (**1**) to form 5-(Bromomethyl)dihydrofuran-2(3H)-one (**2**) (scheme 1). To evaluate the reaction, we compared the electrode doped with $1000 \mu\text{g cm}^{-2}$ o-CNT to the electrode without the catalyst at -250 mV and -350 mV. As is shown in figure 4 and figure 5, the treated electrode significantly outperforms the untreated one. Unfortunately, in all cases, the bromolactone formation rate was only roughly half the H_2O_2 the evolution rate as observed in figure 2. Most likely, the formed bleach can directly react with the hydrogen peroxide, which would result in the formation of singlet oxygen, bromine and water. This futile reaction would be responsible for the loss of two equivalents of product. If this side reaction can be negated, the efficiency of the system will double. Furthermore, the

accumulation of a sideproduct (up to 10%) was observed, which we determined to be the 5-(hydroxymethyl)dihydrofuran-2(3H)-one.

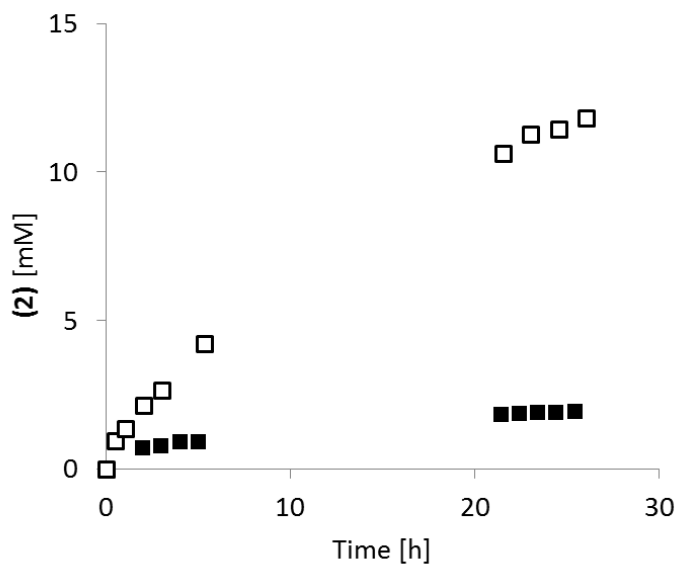


Figure 4: The electrochemical generation of H_2O_2 at -250 mV, resulting in the formation of **(2)** *via* the bleach made by *CVCPO*. The graphite paper electrodes were doped with (open) or without (closed) the o-CNT ($1000 \mu\text{g cm}^{-1}$). General conditions: $[\text{CVCPO}] = 25 \text{ nM}$, $[\text{4-pentenoic acid}]_0 = 50 \text{ mM}$, $[\text{KBr}]_0 = 100 \text{ mM}$, in a 100 mM citrate buffer pH 5.0 at room temperature. The 100 ml solutions were mixed by a magnetic stirring bar.

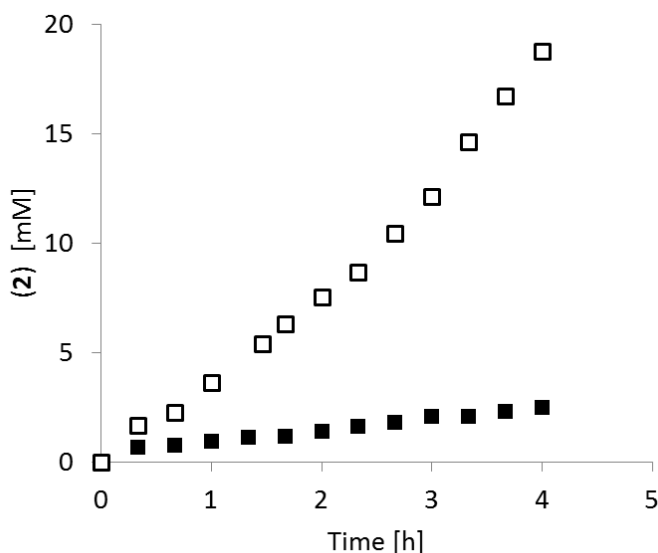


Figure 5: The electrochemical generation of H_2O_2 at -350 mV, resulting in the formation of (2) via the bleach made by CVCPO. The graphite paper electrodes were doped with (open) or without (closed) o-CNT ($1000 \mu\text{g cm}^{-2}$). General conditions: $[\text{CVCPO}] = 100$ nM, $[\text{4-pentenoic acid}]_0 = 50$ mM, $[\text{KBr}]_0 = 100$ mM, in a 100 mM citrate buffer pH 5.0 at room temperature. The 100 ml solutions were mixed by a magnetic stirring bar.

As is shown in figure 4 and figure 5, the catalyst doped electrode at -250 mV perform roughly as well as the untreated one at -350 mV. This allows us to compare these two conditions and to calculate the amount of energy saved for the same reaction at similar space time yields. Here we assumed the decreased CVCPO concentration at -250 mV not to limit the reaction, as turnovers up to 69 s^{-1} are reported for the enzyme under similar conditions. The results are summarized in table 2.

Table 2. Comparison of the two electrodes at similar VCPO reaction rates. Reaction rates were determined from figure 4 and 5 while the current applied was taken from figure 1. The carbon dioxide emission per mole of product was calculated from the reaction volume of 100 ml and a CO_2 emission of 404 g kWh^{-1} [18].

o-CNT loading [$\mu\text{g cm}^{-2}$]	Potential [mV]	Reaction rate [mM h^{-1}]	Current [mA]	Power [mW]	CO_2 emission [kg mole^{-1}]
0	-350	0.55	-18	6.3	167
500	-250	0.73	-16	4.0	80
Difference	-100	0.18	-2	-2.3	87

As shown in table 2, doping the cathode with the o-CNT already resulted in only half the energy consumption, and thus CO₂ emission, per amount of product generated. If the side reaction between bleach and peroxide can be circumvented, the efficiency would even further decrease to only a quarter of the undoped cathode. Though the conditions taken for these calculations account for low space time yields, the efficiency of H₂O₂ production compared to current remained similar for the electrodes (figure 3). The treated cathodes will thus in all cases significantly decrease the power needed to drive these reactions. Naturally, this environmentally benign method can also be translated to systems coupled to other chloroperoxidases [19] or peroxygenases [20].

Material and methods

All chemicals were purchased for Sigma Aldrich at the highest purity available. The oxidized carbon nanotubes (o-CNT) were a gift from the group of Yi Cui.

Synthesis of 5-(Bromomethyl)dihydrofuran-2(3H)-one (2):

The synthesis of the bromolactone as an authentic standard was performed at room temperature for 24 h while stirring. A 100 mM citrate buffer (pH 5, final volume of 50 ml) contained 160 mM of KBr, 10 mmol 4-pentenoic acid, 100 nM CVCPO and 100 mM of H₂O₂. At the end of the reaction, the mixture was extracted by dichloromethane (3x, 100 ml) and dried over anhydrous Na₂SO₄. The combined organic layers were reduced *in vacuo*. The bromolactone compound was isolated by using flash column chromatography on (silica gel, EtOAc:Hexane, 1:2) and analyzed by ¹H NMR to give 1.4 g, 80% isolated yield.

Enzyme preparation

100 mL pre-cultures of LB medium containing 50 µg ml⁻¹ of ampicillin were inoculated with *E. coli* TOP10 pBADgIIIB VCPO and incubated overnight at 37°C and 180 rpm. Overexpression was carried out in 5 l flasks with 1 l of TB medium supplemented with 50 µg ml⁻¹ of ampicillin and grown at 37°C and 180 rpm. At an OD₆₀₀ of 0.9 A.U., 0.02 % of L-arabinose was added. After induction, cultures were incubated for additional 24 h at 25°C and 180 rpm.

The bacterial pellets obtained after centrifugation were re-suspended in 50 mM Tris/H₂SO₄ buffer (pH 8.1). 0.1 mM PMSF (100 mM stock in isopropanol) was added to the

Chapter 6

re-suspended cells, which were ruptured by sonication on ice (output 4, cycle 40%). The samples were then centrifuged (10 000 rpm for 20 minutes) and the supernatant was incubated at 70 °C for 1.5 h. After centrifugation (10 000 rpm for 10 minutes), the absence of catalase activity was determined by adding the enzyme to a solution of 0.1% Triton and 3% H₂O₂ in a KPi puffer (50 mM pH 7.0).

The clarified protein solution was further purified with a Q Sepharose FF column. After washing the column with 2 volumes of 50 mM Tris/H₂SO₄, pH 8.1 and 2 volumes of 0.1 M NaCl in 50 mM Tris/H₂SO₄, pH 8.1, the enzyme was loaded at 7.5 ml min⁻¹ and thereafter eluted with 0.6 M NaCl in 50 mM Tris/H₂SO₄, pH 8.1. Fractions containing C₁VCPO (determined by the MCD activity assay) were pooled, concentrated (Amicon 10 kDa cut-off membrane) and desalted using HiTrap desalting or PD10 columns (GE Healthcare) and 50 mM Tris/H₂SO₄, pH 8.1 containing 100 μM ortho-vanadate.

C₁VCPO activity was quantified via the monochlorodimedone (MCD) assay. The enzyme solution was added to a reaction mixture containing MCD (50 μM), KBr (5 mM) and ortho-vanadate (100 μM) in a 100 mM citrate buffer at pH 5.0. After addition of H₂O₂ (5 mM), the enzyme activity could be determined by following the decrease of absorbance at 290 nm.

Electrode preparation

A solution of oxidized carbon nanotubes (o-CNTs) and was suspended in ethanol containing 1 % w/v Nafion 117 (Sigma-Aldrich, Germany) and sonicated for 60 min. This suspension was evenly pipetted onto 5 cm x 5 cm sheets of Sigracet® GDL 38 BC (a gift from SGL CARBON GmbH, Germany). For the reference electrode, o-CNTs were omitted. For the electrodes 2, 3 and 4, the o-CNT were dispersed in ethanol at 2 mg ml⁻¹. For the electrodes 5 and 6, the concentration of the stock was 5 mg ml⁻¹.

(Bio)-electrochemical setup

Experiments were carried out in a 2-Half-Cell Chamber [21] divided by a proton exchange membrane (Nafion 117, Sigma Aldrich, St. Louis, USA). The anode consisted of a platinum sheet of 2 by 4 cm, contacted by a glass coated platinum wire. The anode chamber was filled with 100 ml of a 100 mM Na-Citrate buffer of pH 5. The cathode was prepared as described above and used as a gas diffusion electrode (GDE) by mounting it to the circular opening at the side of the H-cell (2.5 cm diameter). A Ni-mesh was added to

the air side of the GDE to ensure proper contact. The cathode chamber was filled with 100 ml 100 mM Na-Citrate buffer at pH 5 containing 100 mM KBr. An Ag/AgCl electrode in a Luggin capillary filled with 0.5 M Na₂SO₄ was used as a reference electrode. The tip of the Luggin capillary was placed at a distance of about 4 mm from the cathode. All experiments were carried out using a GAMRY Reference 600 potentiostat/galvanostat. Prior to all experiments, the internal resistance was determined by impedance spectroscopy (about 17 Ω) using the manufacturer provided program "Get Ru". Linear sweep/cyclovoltametric measurements were carried out without iR-correction and were iR-corrected after the experiments. Chronoamperometric experiments were carried out using positive feedback iR compensation by applying 90% of the internal resistance that had been determined prior to starting the experiments.

Bioelectrochemical experiments were carried out in the same setup. For these experiments, 50 mM 4-pentenoic acid, and 25 nM or 100 nM CVCPO, for experiments carried out at -250 mV and -350 mV, respectively, were added to the cathode chamber containing 100 ml of 100 mM Na-Citrate buffer pH 5 containing 100 mM KBr. Experiments were started by applying a constant voltage using positive feedback iR compensation as described above.

Electrochemical H₂O₂ measurement

Hydrogen peroxide concentrations were determined electrochemically using a Select 2700 Biochemistry Analyzer (Yellow Springs Instruments, OH, USA) equipped with blank membranes. The calibration solution consisted of 30 mg l⁻¹ H₂O₂ in a 20 mM Na-citrate buffer. Sample size taken was 25 μ l while the measurement time was 30 seconds. A typical calibration sample yielded in a 10 nA signal with a baseline current below 2 nA.

Gas chromatography

Aqueous samples (500 μ l) were acidified by addition of 50 μ l 6 M HCl and extracted with 500 μ l ethyl acetate containing 10 mM acetophenone (AP) as internal standard. Concentrations of 4-pentenoic acid and the bromolactone were determined by gas chromatography equipped with a flame ionization detection (FID) (GC-17A, Shimadzu, Japan). The compounds were separated on a DB-WAXetr column (30 m x 0.25 mm x 0.25 μ m) (Agilent, CA, USA) with a split of 20, a linear velocity of 31.5 cm s⁻¹ using the following heating method:

Chapter 6

Ramp [$^{\circ}\text{C min}^{-1}$]	Temperature [C]	Hold time [min]
-	130	0
7	190	0
15	230	3

Retention times

Compound	Retention time (min)
Acetophenone	4.0
4 pentenoic acid	5.1
Bromolactone	10.4

References

1. Messerschmidt, A. and R. Wever, *X-ray structure of a vanadium-containing enzyme: chloroperoxidase from the fungus Curvularia inaequalis*. Proceedings of the National Academy of Sciences, 1996. **93**(1): p. 392-396.
2. van Schijndel, J.W., E.G. Vollenbroek, and R. Wever, *The chloroperoxidase from the fungus Curvularia inaequalis; a novel vanadium enzyme*. Biochimica et Biophysica Acta (BBA)-Protein Structure and Molecular Enzymology, 1993. **1161**(2-3): p. 249-256.
3. Wever, R. and P. Barnett, *Vanadium chloroperoxidases: The missing link in the formation of chlorinated compounds and chloroform in the terrestrial environment?* Chemistry-an Asian Journal, 2017. **12**(16): p. 1997-2007.
4. Dong, J.J., et al., *Halofunctionalization of alkenes by vanadium chloroperoxidase from Curvularia inaequalis*. Chemical Communications, 2017. **53**(46): p. 6207-6210.
5. Fernández-Fueyo, E., et al., *Chemoenzymatic halogenation of phenols by using the haloperoxidase from Curvularia inaequalis*. ChemCatChem, 2015. **7**(24): p. 4035-4038.
6. Fernández-Fueyo, E., et al., *A biocatalytic aza-Achmatowicz reaction*. ACS Catalysis, 2016. **6**(9): p. 5904-5907.
7. Drogui, P., et al., *Hydrogen peroxide production by water electrolysis: application to disinfection*. Journal of applied electrochemistry, 2001. **31**(8): p. 877-882.
8. Yamanaka, I. and T. Murayama, *Neutral H₂O₂ synthesis by electrolysis of water and O₂*. Angewandte Chemie International Edition, 2008. **47**(10): p. 1900-1902.
9. Pereira, P.C., I. Arends, and R.A. Sheldon, *Optimizing the chloroperoxidase-glucose oxidase system: The effect of glucose oxidase on activity and enantioselectivity*. Process Biochemistry, 2015. **50**(5): p. 746-751.
10. Zhang, W., et al., *Selective activation of C-H bonds in a cascade process combining photochemistry and biocatalysis*. Angewandte Chemie International Edition, 2017. **56**(48): p. 15451-15455.
11. Getrey, L., et al., *Enzymatic halogenation of the phenolic monoterpenes thymol and carvacrol with chloroperoxidase*. Green Chemistry, 2014. **16**(3): p. 1104-1108.
12. Holtmann, D., et al., *Electroenzymatic process to overcome enzyme instabilities*. Catalysis Communications, 2014. **51**: p. 82-85.
13. Krieg, T., et al., *Gas diffusion electrode as novel reaction system for an electro-enzymatic process with chloroperoxidase*. Green Chemistry, 2011. **13**(10): p. 2686-2689.
14. Choi, C.H., et al., *Hydrogen peroxide synthesis via enhanced two-electron oxygen reduction pathway on carbon-coated Pt surface*. The Journal of Physical Chemistry C, 2014. **118**(51): p. 30063-30070.
15. Choi, C.H., et al., *Tuning selectivity of electrochemical reactions by atomically dispersed platinum catalyst*. Nature Communications, 2016. **7**: p. 10922.
16. Jirkovský, J.S., et al., *Single atom hot-spots at Au-Pd nanoalloys for electrocatalytic H₂O₂ production*. Journal of the American Chemical Society, 2011. **133**(48): p. 19432-19441.
17. Lu, Z., et al., *High-efficiency oxygen reduction to hydrogen peroxide catalysed by oxidized carbon materials*. Nature Catalysis, 2018. **1**(2): p. 156.
18. Tieves, F., et al., *Energising the E-factor: The E⁺-factor*. Tetrahedron, 2019. **75**(10): p. 1311-1314.
19. Seelbach, K., et al., *Improvement of the total turnover number and space-time yield for chloroperoxidase catalyzed oxidation*. Biotechnology and Bioengineering, 1997. **55**(2): p. 283-288.
20. Wang, Y.H., et al., *Peroxygenases en route to becoming dream catalysts. What are the opportunities and challenges?* Current Opinion in Chemical Biology, 2017. **37**: p. 1-9.

Chapter 6

21. Stöckl, M., et al., *Extracellular polymeric substances from Geobacter sulfurreducens biofilms in microbial fuel cells*. ACS applied materials & interfaces, 2019. **11**(9): p. 8961-8968.

Chapter 7



Cascading g-C₃N₄ and peroxygenases for selective oxyfunctionalization reactions

Morten M.C.H. van Schie, Wuyuan Zhang, Florian Tieves, Da Som Choi, Chan Beum Park, Bastien O. Burek, Jonathan Bloh, Isabel W.C.E. Arends, Caroline E. Paul, Miguel Alcalde, Frank Hollmann

Based on:

Van Schie, M.M.C.H., et al., *Cascading g-C₃N₄ and peroxygenases for selective oxyfunctionalization reactions*. ACS Catalysis, 2019. **9**(8): p. 7409-7417.

Summary

Peroxygenases are very interesting catalysts for specific oxyfunctionalization chemistry. Their poor robustness against the stoichiometric oxidant (H₂O₂) can be addressed via in situ generation of H₂O₂. Here we report that simple graphitic carbon nitride (g-C₃N₄) is a promising photocatalyst to drive peroxygenase-catalyzed hydroxylation reactions. The system has been characterized outlining its scope but also its current limitations. In particular, spatial separation of the photocatalyst from the enzyme is shown as solution to circumvent the undesired inactivation of the biocatalyst. Overall, very promising turnover numbers of the biocatalyst of more than 60.000 have been achieved.

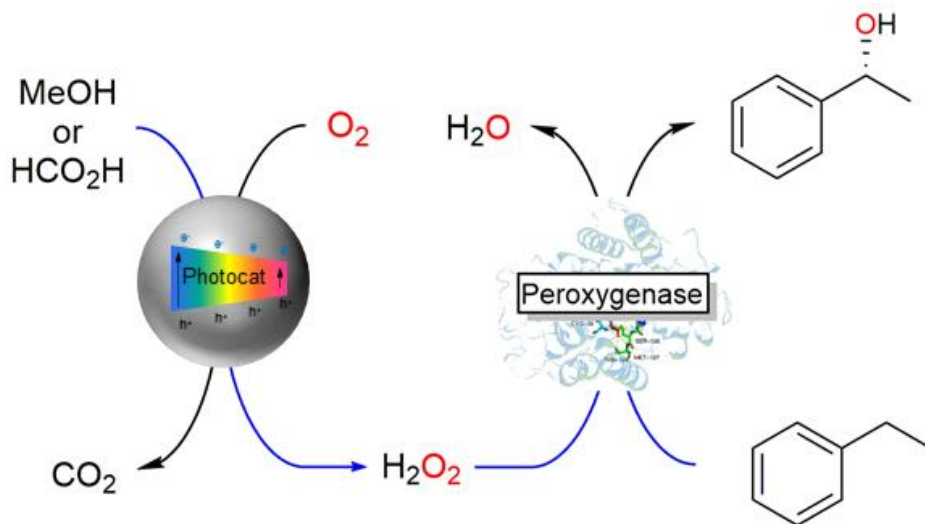
Introduction

Selective oxyfunctionalization of non-activated sp^3 carbon-hydrogen bonds is a challenge in organic synthesis. Catalysts exhibiting both high oxidation potential and high selectivity are rarely found [1]. In this respect, so-called unspecific peroxygenases (UPOs), next to the established P450 monooxygenases and some other non-heme-monooxygenases [2], have attracted considerable interest [3-5].

One attractive feature of UPOs is that they rely on simple H_2O_2 as oxidant instead of complicated electron transport chains [6]. This is in contrast to P450 monooxygenases which require NADH as the electron source and a complex electron transfer chain to deliver the electrons to the enzyme active site. H_2O_2 , however, is also a potent inhibitor of peroxygenases as already small excesses oxidatively inactivate the prosthetic heme group [7]. Generating H_2O_2 *in situ* through catalytic reduction of O_2 is the most common approach to alleviate the inactivation issue. In essence, these systems provide H_2O_2 at rates that enable efficient peroxygenase activity while minimizing the H_2O_2 -related inactivation. These methods comprise a range of chemical [8-13], electrochemical [14-19], enzymatic [20-23] and photocatalytic [24-32] approaches.

The latter is particularly interesting as it, in principle, enables using light energy to access simple sacrificial electron donors to drive the reduction of O_2 to H_2O_2 . To make light energy available for this reaction, a photosensitizer (or photocatalyst) is necessary. Both, homogeneously dissolved molecular and semiconductor-based solid material photocatalysts have been evaluated. While the first often suffer from issues of photobleaching and inactivation, the latter excel by their high robustness and reusability. So far, mainly TiO_2 -based semiconductor photocatalysts have been evaluated to promote peroxygenase-catalyzed oxyfunctionalization reactions.

Therefore, we set out to investigate a broader set of (in)organic photocatalyst systems [33] to promote peroxygenase-catalyzed reactions (scheme 1).



Scheme 1. Photoenzymatic hydroxylation of ethyl benzene combining heterogeneous photocatalysts for the reductive activation of O₂ to H₂O₂ with a peroxygenase-catalyzed oxyfunctionalization reaction.

Results

We chose the selective hydroxylation of ethyl benzene to (*R*)-1-phenyl ethanol catalyzed by the peroxygenase from *Agrocybe aegerita* (rAaeUPO) as the model reaction [34-37].

In a first set of experiments, we evaluated several reported and/or commercially available heterogeneous photocatalysts (figure 1) with respect to their ability to form H₂O₂; particularly, we investigated their performance in the envisioned photoenzymatic cascade transforming ethyl benzene to (*R*)-1-phenyl ethanol. It is worth mentioning that in the absence of the photocatalysts or light, no product formation was observed. In the absence of rAaeUPO, upon prolonged reaction times, traces of racemic product and the overoxidation product were observed in some cases.

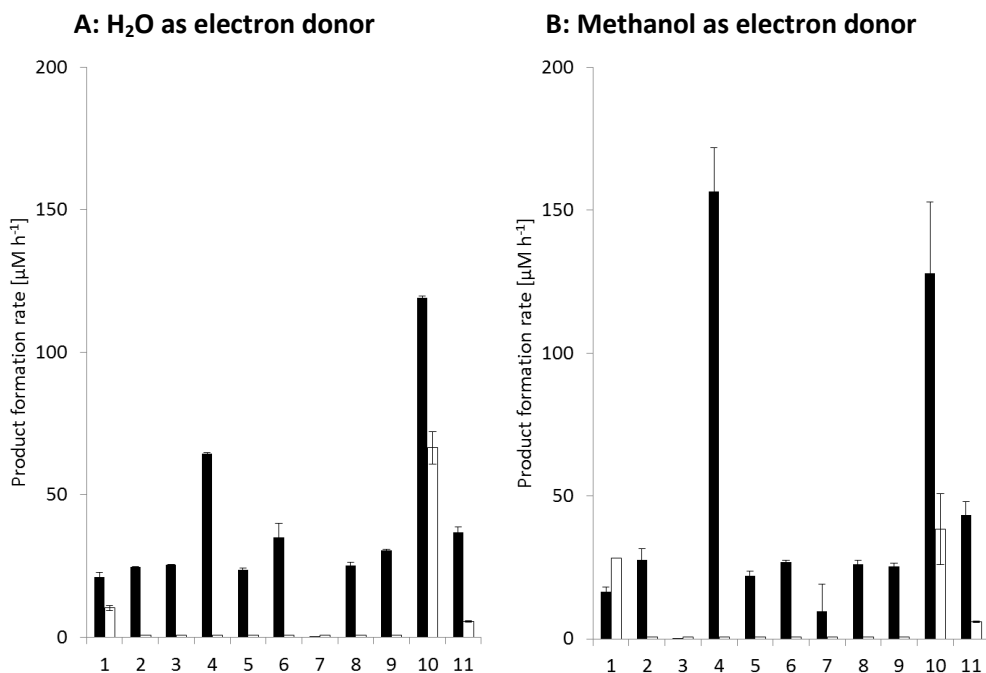
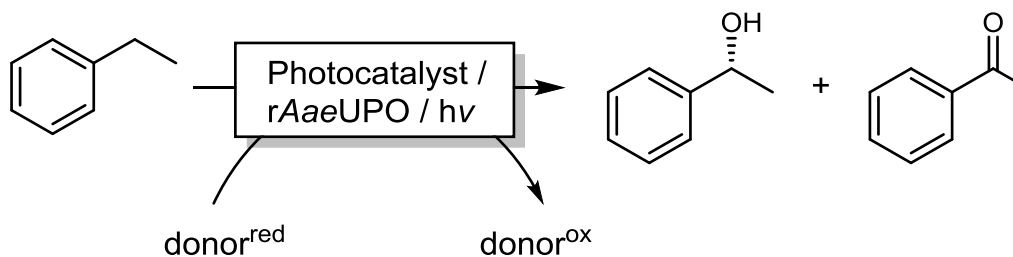


Figure 1. Performance of several heterogeneous photocatalysts to promote *rAaeUPO*-catalyzed oxyfunctionalization, forming phenyl ethanol (black) and the over-oxidation product acetophenone (white), in absence (left) or presence (right) of methanol. Conditions: 5 mg ml⁻¹ heterogeneous catalyst, 50 mM ethyl benzene, 0 or 250 mM methanol and 100 nM *rAaeUPO* in a 100 mM phosphate buffer at pH 7, 30 °C and stirring at 300 rpm. Illumination by a Osram 200W light bulb for 30 minutes. Reactions were performed in independent duplicates. **1:** Au-BiVO₄ [38]; **2:** Co₃O₄ (quantum dots) [39]; **3:** Co₄(H₂O)₂(W₉O₃₄)₂ [40]; **4:** Pt-TiO₂ (Rutile) [41]; **5:** MnO (on Faujasite) [42]; **6:** Co-TiO₂ [43]; **7:** MnO (nanowires) [44]; **8:** Ir@SiO₂; **9:** Fe₂O₃ [45, 46]; **10:** g-C₃N₄; **11:** ZnO (nanoclusters) [47].

Almost all heterogeneous photocatalysts tested enabled the desired reaction both in the presence and absence of an extra electron donor (methanol). However, reaction rates tended to be significantly lower in experiments where methanol was absent. In the first case, it may be assumed that water oxidation was the primary source for reducing equivalents [48]. In some cases, significant amounts of acetophenone were found along with the desired (*R*)-1-phenyl ethanol. We attribute this to the oxidation of the desired product by the photocatalysts [49]. Platinum loaded titanium oxide (Pt-TiO₂) and graphitic carbon nitride (g-C₃N₄) stood out in terms of product formation rate. For reasons of ease of preparation, we further focussed on g-C₃N₄ as photocatalyst. Furthermore, g-C₃N₄ has previously been reported to be highly selectively for H₂O₂ over other (partially reduced) reactive oxygen species [50].

Figure 2 shows the overall product formation of g-C₃N₄ using either water (blue), methanol (red), or formate (green) as sacrificial electron donor to promote the photoenzymatic hydroxylation of ethyl benzene. Assumptions made to obtain the bar-graphs can be found in the experimental section.

Chapter 7

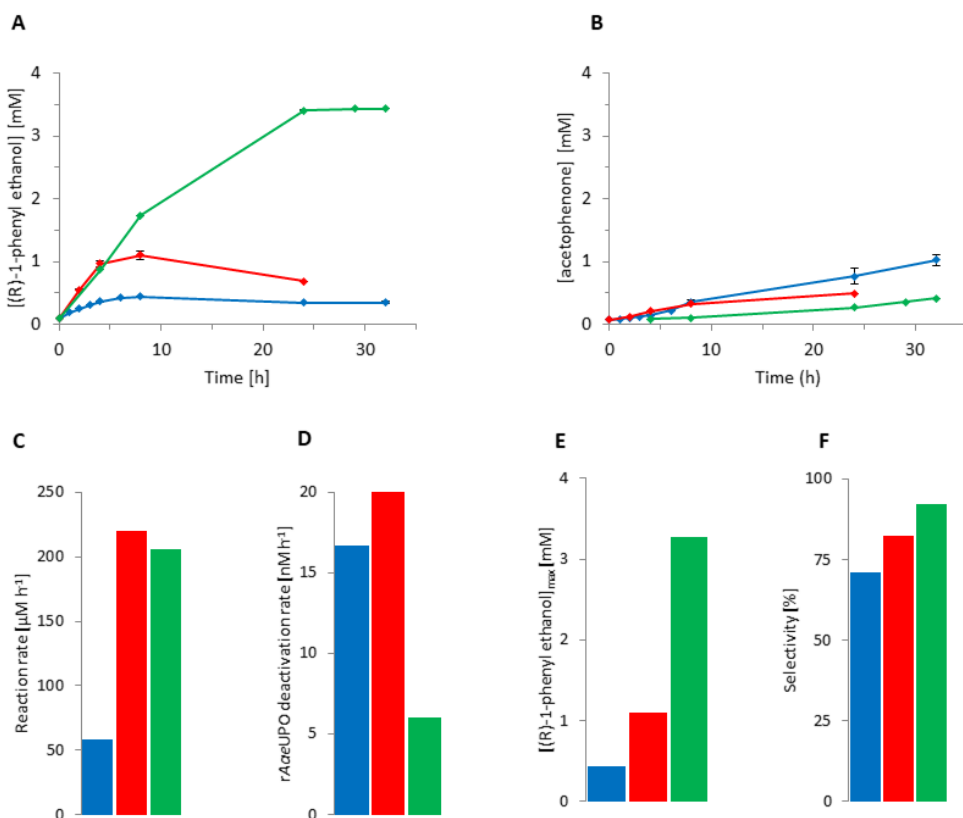


Figure 2. $\text{g-C}_3\text{N}_4$ as photocatalyst to promote *rAaeUPO*-catalyzed hydroxylation of ethyl benzene in the absence of external electron donors (blue), or 250 mM methanol (red) or 250 mM formate (green). A: time course of (R)-1-phenyl ethanol formation and B: time course of acetophenone formation. From these time courses, parameters such as reaction rate (C), *rAaeUPO* inactivation rate (D), maximal product concentration (E) and selectivity (F) were calculated. General conditions: $[\text{rAaeUPO}] = 100 \text{ nM}$, $[\text{ethyl benzene}] = 50 \text{ mM}$, $[\text{g-C}_3\text{N}_4] = 5 \text{ mg mL}^{-1}$, KPi buffer pH 7.0 (100 mM), 30°C , magnetic stirring at 600 rpm, Illumination by a Osram 200W light bulb. Reactions were performed in independent duplicates.

From a conceptual and an environmental point-of-view, water oxidation would have been the most desirable source of reducing equivalents. However, this system fell back in terms of catalytic rate and selectivity towards the phenyl ethanol compared with the use of methanol or formate as sacrificial electron donor. Similar observation have been made before for TiO_2 [51]. Thermodynamically, water oxidation is far more demanding than the oxidation of methanol or formate. As the redox potentials of the band gaps of $\text{g-C}_3\text{N}_4$ are unfavourable to perform water oxidation [52], other molecules are more likely to

participate at the oxidation reaction of the catalyst. Both the substrate as the enzymatic product can be oxidized by g-C₃N₄. This was evident from the increased overoxidation of (*R*)-phenyl ethanol to acetophenone and the lower optical purity of phenyl ethanol. In the absence of both enzyme and substrate the illumination of the g-C₃N₄ gave negligible H₂O₂ formation rates (<1.0 μM h⁻¹), which increased to 2.0 (± 0.02) μM min⁻¹ upon addition of formate. Another interesting effect of formate was that the robustness of the overall reaction was significantly higher than when using methanol or no sacrificial electron donor. We attribute this to the hydroxyl radical scavenging activity of formate (*vide infra*). Methanol oxidation proceeds via methoxy radicals, which again may be assumed to have a detrimental influence on the stability of the biocatalyst [25].

Overall, formate proved to be a suitable sacrificial electron donor for the reaction. We therefore systematically investigated the factors influencing the activity, selectivity and robustness of the formate-driven photoenzymatic reaction system.

Increasing the concentration of formate had a positive effect on the reaction rate, selectivity and robustness of the overall system (figure 3). Hence, we concluded that the photocatalytic oxidation of formate is the overall rate-limiting step in the reaction scheme. Increasing the amount of sacrificial electron donor in the case of methanol led to increased reaction rates, but had no effect on the robustness of the system or the accumulation of the acetophenone (figure 4).

Chapter 7

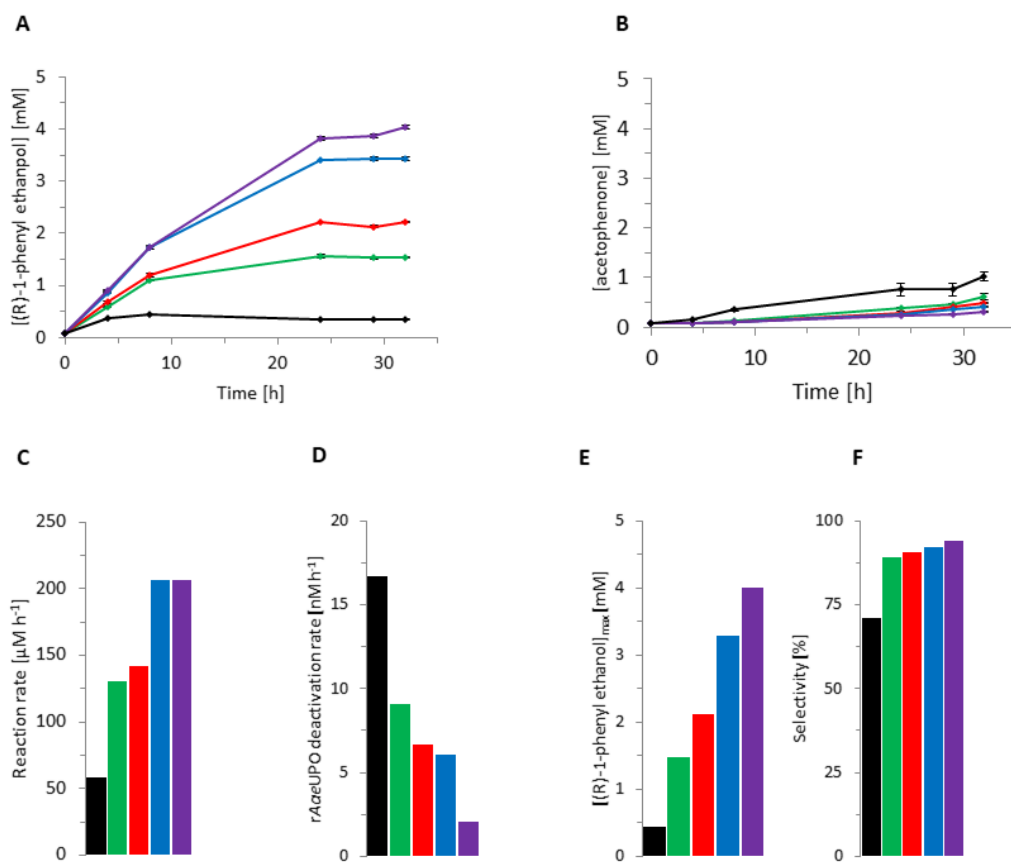


Figure 3. Influence of the formate concentration on the performance of the photoenzymatic hydroxylation of ethyl benzene. A: time course of (R)-1-phenyl ethanol formation and B: time course of acetophenone formation. From these time courses, parameters such as reaction rate (C), rAaeUPO inactivation rate (D), maximal product concentration (E) and selectivity (F) were calculated. $[\text{HCO}_2^-] = 0 \text{ mM}$ (black), 50 mM (green), 100 mM (red), 250 mM (blue) or 500 mM (purple). General conditions: $[\text{rAaeUPO}] = 100 \text{ nM}$, $[\text{ethyl benzene}] = 50 \text{ mM}$, $[\text{g-C}_3\text{N}_4] = 5 \text{ mg mL}^{-1}$, KPi buffer pH 7.0 (100 mM), 30 °C, magnetic stirring at 600 rpm, illumination by a Osram 200W light bulb. Reactions were performed in independent duplicates.

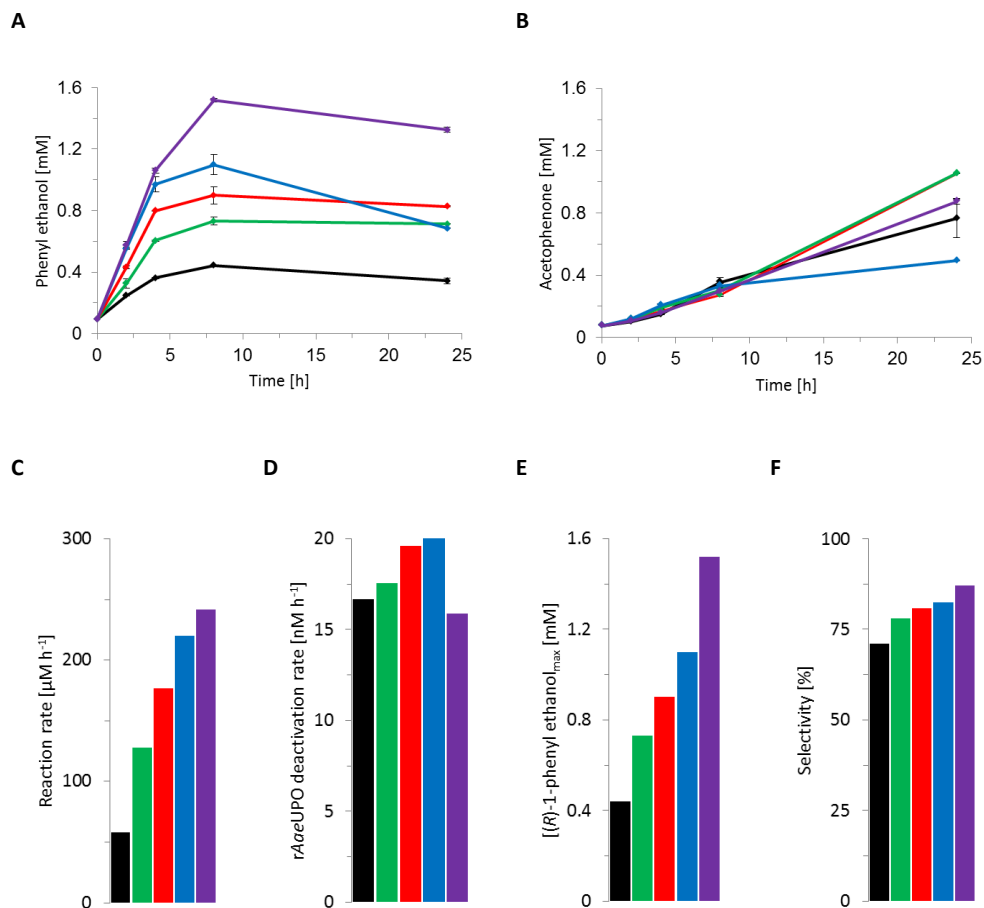


Figure 4. Influence of the methanol concentration on the performance of the photoenzymatic hydroxylation of ethyl benzene. A: time course of (R)-1-phenyl ethanol formation and B: time course of acetophenone formation. From these time courses, parameters such as reaction rate (C), r_{AaeUPO} inactivation rate (D), maximal product concentration (E) and selectivity (F) were calculated. [MeOH] = 0 mM (black), 50 mM (green), 100 mM (red), 250 mM (blue) or 500 mM (purple). General conditions: [r_{AaeUPO}] = 100 nM, [ethyl benzene] = 50 mM, [$\text{g-C}_3\text{N}_4$] = 5 mg ml⁻¹, KPi buffer pH 7.0 (100 mM), 30 °C, magnetic stirring at 600 rpm, Illumination by a Osram 200W light bulb. Reactions were performed in independent duplicates.

The concentration of the biocatalyst had a significant influence on the robustness of the overall reaction but hardly influenced the initial product formation rate (figure 5). In other words, the biocatalyst was slowly deactivated over time, while only a fraction of the enzyme present in solution was sufficient to take up the H₂O₂ generated. This supports the assumption that the photocatalytic H₂O₂ formation was rate-limiting and that undesired

Chapter 7

rAaeUPO-inactivation by the photocatalyst represented the major undesired side reaction. Consequently, the most efficient way of using the biocatalyst would be to feed it over time (*vide infra*).

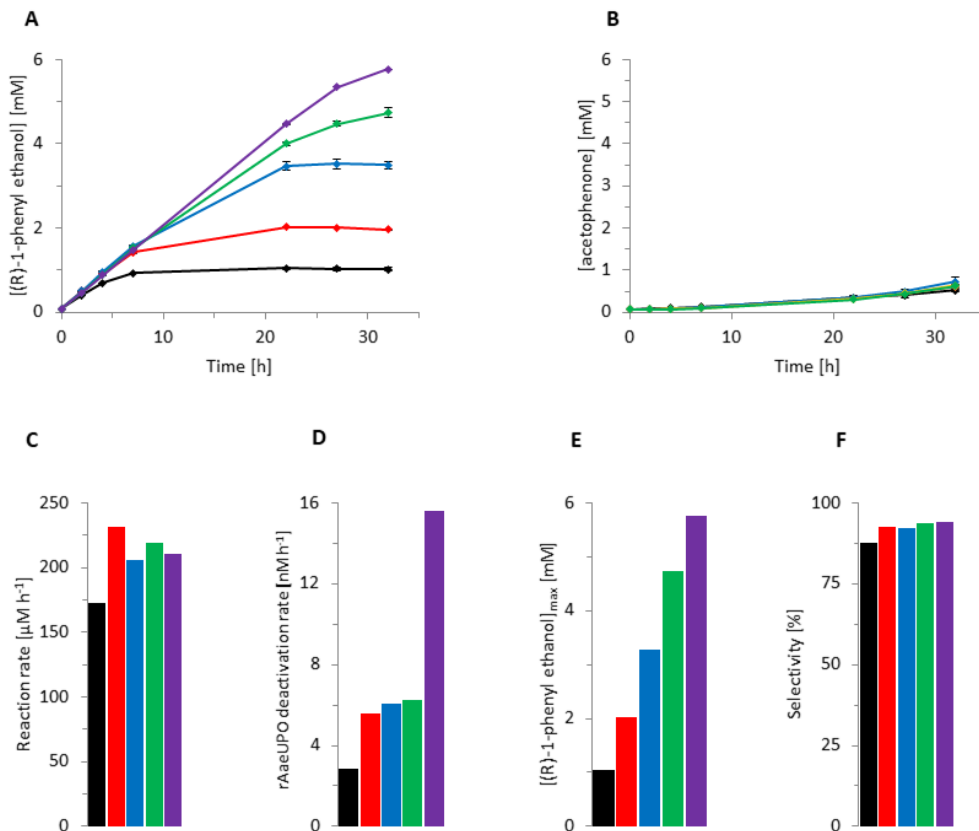


Figure 5. Influence of the *rAaeUPO* concentration on the performance of the photoenzymatic hydroxylation of ethyl benzene. A: time course of (*R*)-1-phenyl ethanol formation and B: time course of acetophenone formation. From these time courses, parameters such as reaction rate (C), *rAaeUPO* inactivation rate (D), maximal product concentration (E) and selectivity (F) were calculated. [*rAaeUPO*] = 20 nM (black), 50 nM (red), 100 nM (blue), 200 nM (green) or 500 nM (purple). General conditions: [NaHCO_2] = 250 mM, [ethyl benzene] = 50 mM, [$\text{g-C}_3\text{N}_4$] = 5 mg ml^{-1} , KPi buffer pH 7.0 (100 mM), 30 °C, magnetic stirring at 600 rpm, Illumination by a Osram 200W light bulb. Reactions were performed in independent duplicates.

Next, we systematically varied the concentration of the photocatalyst (figure 6). Very much to our surprise, the anticipated positive correlation between $\text{g-C}_3\text{N}_4$ concentration and H_2O_2 formation rate was less pronounced than expected. Moreover, *rAaeUPO*

inactivation even decreased at higher g-C₃N₄ concentrations. Currently, we are lacking a plausible explanation; possibly, self-shading of the heterogeneous g-C₃N₄ reduced its H₂O₂ generation activity; already at catalyst loadings of 1 mg ml⁻¹ reaction mixtures were very turbid. Further experiments will be necessary to fully understand the effect of the photocatalyst concentration. Possibly, the rates for the experiments with 2.5 mg ml⁻¹ of g-C₃N₄ were out-layers, as in these experiments the biocatalyst was also deactivated at a higher rate than expected.

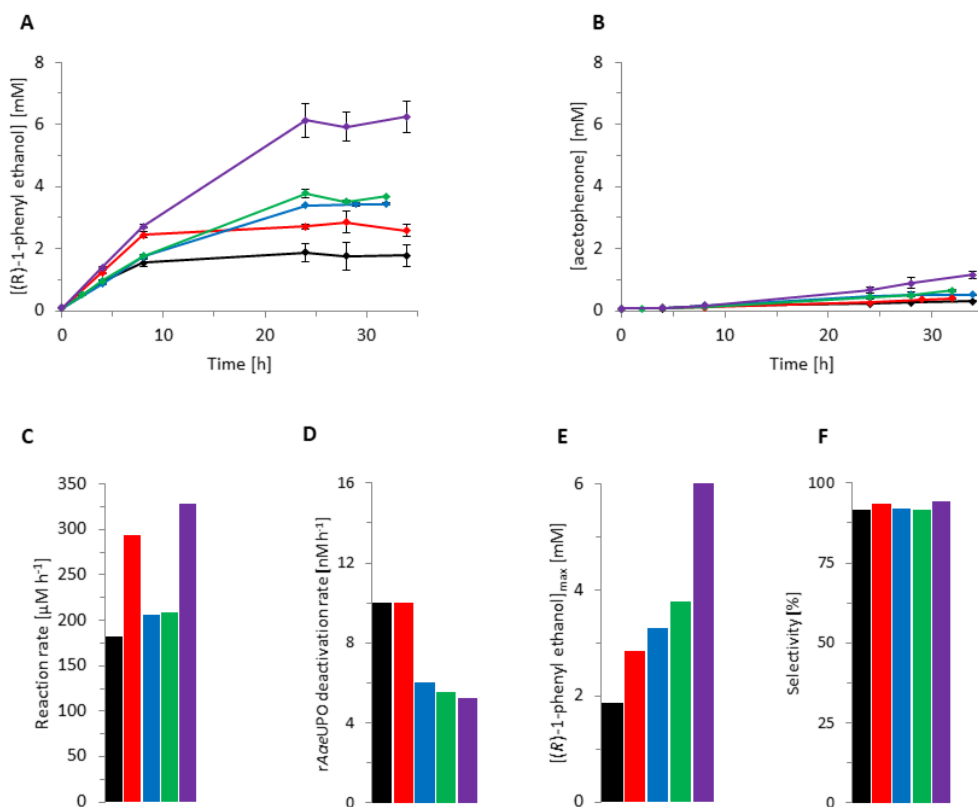


Figure 6. Influence of the g-C₃N₄ concentration on the performance of the photoenzymatic hydroxylation of ethyl benzene. A: time course of (R)-1-phenyl ethanol formation and B: time course of acetophenone formation. From these time courses, parameters such as reaction rate (C), *rAaeUPO* inactivation rate (D), maximal product concentration (E) and selectivity (F) were calculated. [g-C₃N₄] = 1 mg ml⁻¹ (black), 2.5 mg ml⁻¹ (red), 5 mg ml⁻¹ (blue), 10 mg ml⁻¹ (green) or 15 mg ml⁻¹ (purple). General conditions: [NaHCO₂] = 250 mM, [ethyl benzene] = 50 mM, [rAaeUPO] = 100 nM, KPi buffer pH 7.0 (100 mM), 30 °C, magnetic stirring at 600 rpm, Illumination by a Osram 200W light bulb. Reactions were performed in independent duplicates.

Chapter 7

The overall rate of the reaction was highest at neutral to slightly alkaline pH values (Figure 7). Currently, we are lacking a plausible explanation for this observation as the H_2O_2 generation rate of $g\text{-C}_3\text{N}_4$ was reported to be largely pH-independent [53] whereas the highest activity of *rAaeUPO* may be expected in slightly acidic media [37]. Similar trends in H_2O_2 generation rates were observed before for TiO_2 [54].

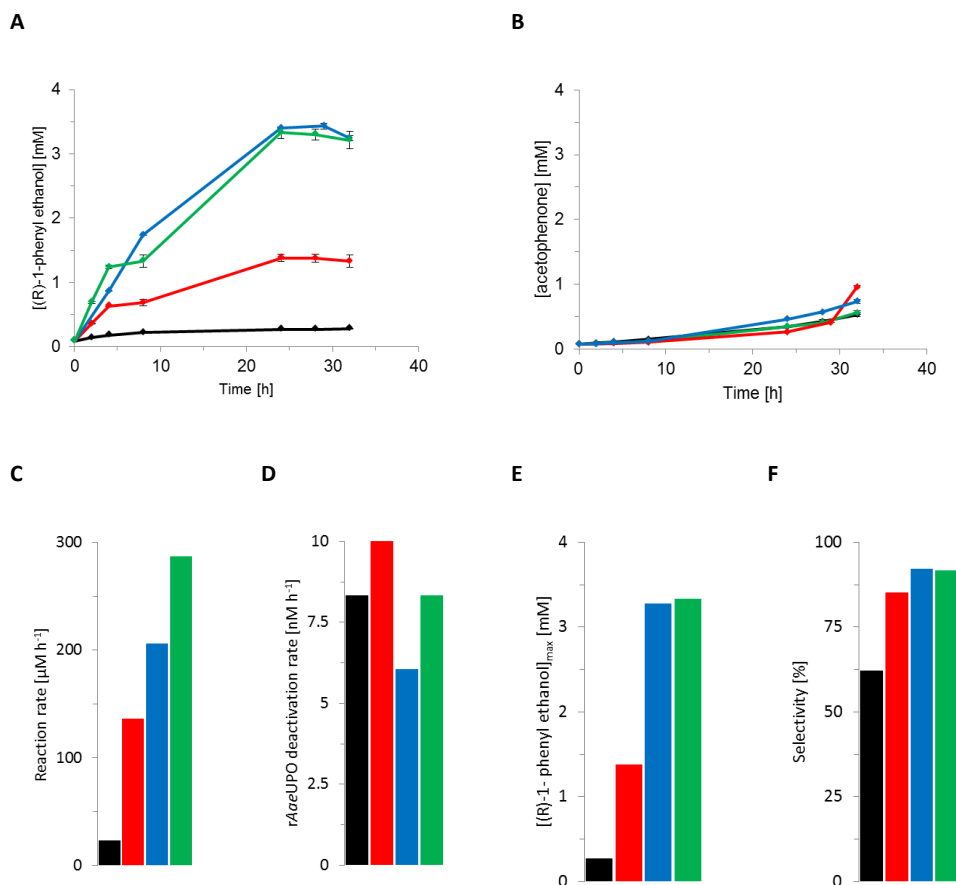


Figure 7. Influence of the reaction pH on the performance of the photoenzymatic hydroxylation of ethyl benzene. A: time course of (R)-1-phenyl ethanol formation and B: time course of acetophenone formation. From these time courses, parameters such as reaction rate (C), *rAaeUPO* inactivation rate (D), maximal product concentration (E) and selectivity (F) were calculated. pH 5.0 (black), pH 6.0 (red), pH 7.0 (blue) or pH 8.0 (green). General conditions: $[\text{NaHCO}_2] = 250 \text{ mM}$, $[\text{ethyl benzene}] = 50 \text{ mM}$, $[\text{rAaeUPO}] = 100 \text{ nM}$, KPi buffer pH 7.0 (100 mM), 30 °C, magnetic stirring at 600 rpm, Illumination by a Osram 200W light bulb. Reactions were performed in independent duplicates. Data points at 8 hours for pH 6.0 and pH 8.0 are most likely outliers caused by insufficient extraction.

Also the morphology of the $g\text{-C}_3\text{N}_4$ catalyst had a significant influence especially on the overall reaction rate as well as the $rAaeUPO$ inactivation rate. The form of $g\text{-C}_3\text{N}_4$ used so far are the so-called $g\text{-C}_3\text{N}_4$ sheets, obtained from calcinating urea [55]. Further, more intense, thermal treatment process leads to so-called amorphous $g\text{-C}_3\text{N}_4$, exhibiting a higher surface area [56]. A preparation with lower specific surface area (bulk $g\text{-C}_3\text{N}_4$) can be obtained by starting the synthesis from melamine instead of urea (figure 14) [55]. In line with our previous observations that the photocatalytic H_2O_2 generation is overall rate-limiting, we also observed a correlation between surface area and overall reaction rate (figure 8). The same, however was also true for the inactivation rate of $rAaeUPO$, which increased with increasing surface area.

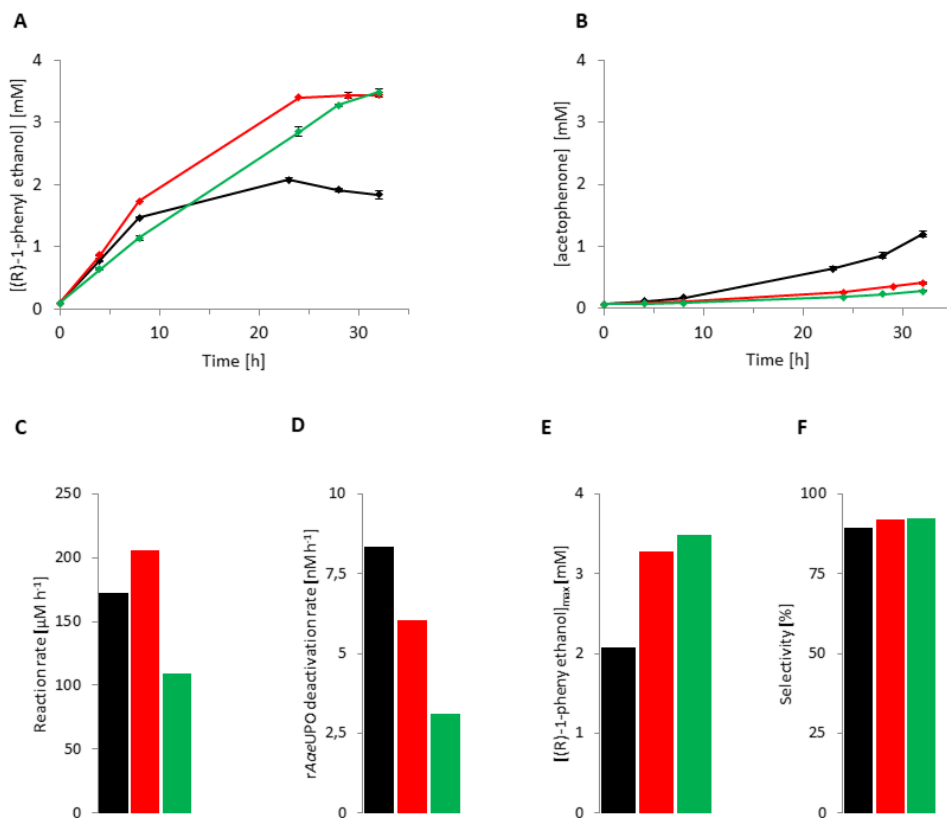


Figure 8. Influence of $g\text{-C}_3\text{N}_4$ morphology on the photoenzymatic hydroxylation of ethyl benzene. A: time course of (R) -1-phenyl ethanol formation and B: time course of acetophenone formation. From these time courses, parameters such as reaction rate (C), $rAaeUPO$ inactivation rate (D), maximal product concentration (E) and selectivity (F) were calculated. Amorphous $g\text{-C}_3\text{N}_4$ (black), $g\text{-C}_3\text{N}_4$ sheets (red) or $g\text{-C}_3\text{N}_4$ bulk (green). Reaction conditions: $[\text{NaHCO}_2] = 250 \text{ mM}$, $[\text{ethyl benzene}] = 50 \text{ mM}$, $[g\text{-C}_3\text{N}_4] = 5 \text{ mg ml}^{-1}$, $[rAaeUPO] = 100 \text{ nM}$, KPi buffer pH 7.0 (100 mM), 30°C , magnetic stirring at 600 rpm, Illumination by a Osram 200W light bulb. Reactions were performed in independent duplicates.

To determine the scalability of the suggested system, we decided to perform a semi-preparative scale experiment, where the enzyme was added over time. Due to issues with the volatility of ethyl benzene, the substrate was also added over time to sustain the substrate pool in the reaction. After 80 hours, 16.9 mM of enantiopure phenyl ethanol (ee of 97.8%) was produced (figure 9). Extraction and subsequent concentration under reduced pressure at room temperature yielded 42.2 mg of the product containing 16 % acetophenone. The phenomenon limiting this setup at the moment is the relative low reaction rate. Higher conversions could thus be achieved by designing $g\text{-C}_3\text{N}_4$ providing higher H_2O_2 generation rates.

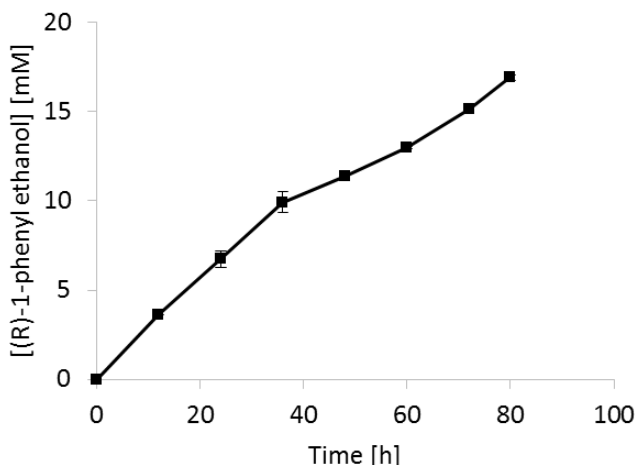


Figure 9. The $g\text{-C}_3\text{N}_4$ – $rAaeUPO$ cascade on a 24 ml scale over 12 samples. Conditions: $[\text{NaHCO}_2] = 250$ mM, $[rAaeUPO] = 100$ nM, $[\text{ethyl benzene}] = 50$ mM, $[g\text{-C}_3\text{N}_4] = 5$ mg ml^{-1} , KPi buffer pH 7.0 (100 mM), 30 °C, magnetic stirring at 600 rpm. Illumination by a Osram 200W light bulb. 100 nM of $rAaeUPO$ was added every 12 hours. 50 mM of ethylbenzene was added after 36 hours to compensate for evaporation.

The major bottleneck of the current system is its relative poor robustness; generally within 24h accumulation of (R) -1-phenyl ethanol ceased, which we attribute to the inactivation of the biocatalyst. As mentioned above, hydroxyl radicals may be assumed to be the primary products of $g\text{-C}_3\text{N}_4$ -catalyzed water photo-oxidations. Indeed, using the spin trap method [57] we could confirm the occurrence of hydroxyl radicals (figure 10). The short life time of $\cdot\text{OH}$ in aqueous media [58] suggests their predominant occurrence at the photocatalyst surface. We therefore also investigated whether $g\text{-C}_3\text{N}_4$ showed a tendency to absorb the

biocatalyst. Indeed we found that *rAaeUPO* and other proteins absorbed significantly to the polar surface of $g\text{-C}_3\text{N}_4$ (figure 10) [59]. Here they are exposed to locally high concentrations of hydroxyl radicals, which sufficiently explains the rather poor robustness of the photoenzymatic reactions so far. Direct enzyme deactivation by oxidation on the $g\text{-C}_3\text{N}_4$ might also contribute. Incubation of *rAaeUPO* with $g\text{-C}_3\text{N}_4$ in dark did not show any deactivation of the enzyme (figure 11).

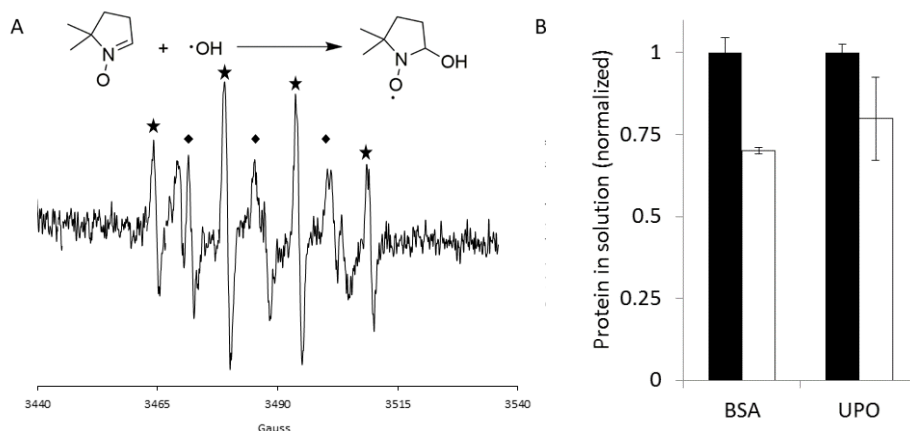


Figure 10. Investigating the molecular reasons for the decreased *rAaeUPO*-stability under process conditions. A: Detection of hydroxyl radicals formed by irradiated $g\text{-C}_3\text{N}_4$ using the spin-trap method. Signals marked with an asterisk (★) are assigned to the oxidation product of DMPO, 5,5-dimethyl-2-oxopyrrolidine-1-oxyl (DMPOX). Signals marked with triangles (▲) belong to the spin adduct DMPO-OH; B: Protein in solution before (black) or after (white) incubation with $g\text{-C}_3\text{N}_4$ in dark, for bovine serum albumin (BSA) or *rAaeUPO*.

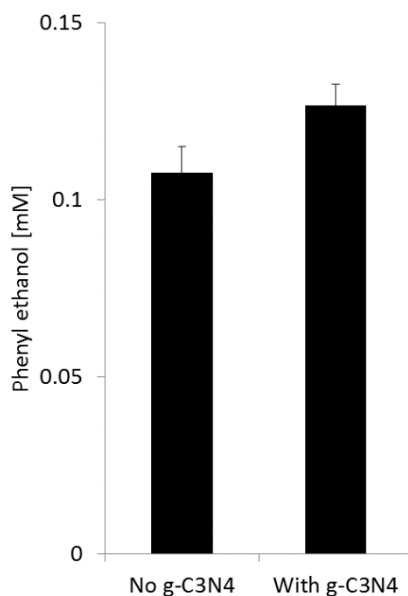


Figure 11. The effect of g-C₃N₄ on rAaeUPO in absence of the light source. 10 nM rAaeUPO in KPi buffer (100 mM, pH 7.0) was incubated in presence or absence of 5 mg ml⁻¹ of g-C₃N₄ for 13 hours at 30 °C. Thereafter, 50 mM ethyl benzene and 1 mM were added to all samples and the reaction was run of 30 minutes. Reaction solutions were extracted with ethylacetate and subsequently analysed on GC. Experiments were performed in triplicates.

We hypothesized that spatial separation of rAaeUPO from the photocatalyst may enhance the stability of the enzyme under reaction conditions. Therefore, we tested this hypothesis by placing rAaeUPO into a dialysis bag thereby preventing its direct contact with the photocatalyst (figure 12). Here, the UPO and g-C₃N₄ would be contained, while both ethyl benzene as H₂O₂ could pass the membrane.

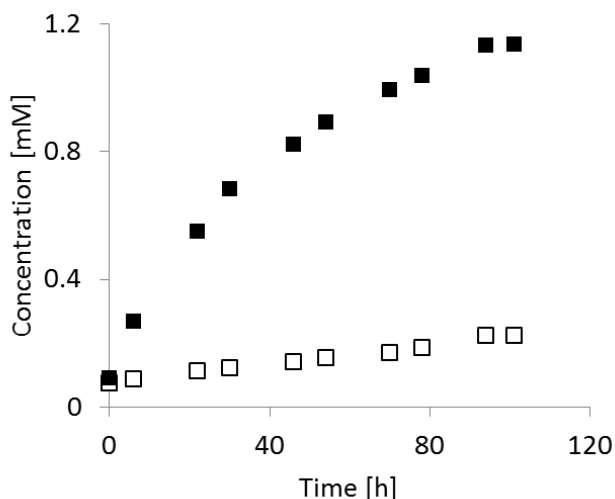


Figure 12. Time course of the photoenzymatic hydroxylation of ethyl benzene to (*R*)-1-phenyl ethanol (black) and overoxidation to acetophenone (white) using the dialysis bag approach. Conditions: 10 ml reaction solution equally divided inside and outside the dialysis bag (20 kDa cutoff). Inside the bag: $[\text{NaHCO}_2] = 250 \text{ mM}$, $[\text{ethyl benzene}] = 50 \text{ mM}$, $[\text{rAaeUPO}] = 100 \text{ nM}$, KPi buffer pH 7.0 (100 mM). Outside the bag: $[\text{NaHCO}_2] = 250 \text{ mM}$, $[\text{ethyl benzene}] = 50 \text{ mM}$, $[\text{g-C}_3\text{N}_4] = 5 \text{ mg ml}^{-1}$, KPi buffer pH 7.0 (100 mM). The reaction was performed once at room temperature while stirring at 600 rpm. The reaction solution was illuminated by a lightningcure spot light (Hamamatsu) at 50% intensity with an UV filter.

To our delight, physically separating the biocatalyst from the photocatalyst had the desired effect of stable product accumulation for more than four days. Compared to the previous experiments, this corresponds to an improvement by more than 4 times. However, this improvement came at the expense of a significantly decreased reaction rate, which is most likely to be attributed to diffusion limitations for the substrates over the dialysis membrane (figure 13).

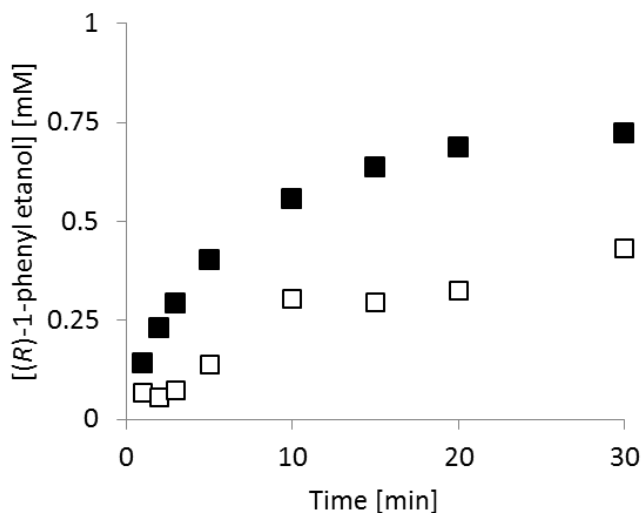


Figure 13. *rAaeUPO* catalyzed hydroxylation of ethyl benzene to phenyl ethanol upon addition of 1 mM of H_2O_2 , with the enzyme either in a dialysis bag (white) or free in solution (black). The reaction mixtures were equally divided inside as outside the bag. Conditions for the physically separated reaction: Inside the bag: [ethyl benzene] = 50 mM, [*rAaeUPO*] = 100 nM, KPi buffer pH 7.0 (100 mM). Outside the bag: [H_2O_2] = 2 mM, [ethyl benzene] = 50 mM, KPi buffer pH 7.0 (100 mM). Conditions for the free enzyme reaction: [ethyl benzene] = 50 mM, [H_2O_2] = 1 mM, [*rAaeUPO*] = 50 nM, KPi buffer pH 7.0 (100 mM). The single reactions were performed at room temperature while magnetically stirring at 600 rpm.

Conclusion

Overall, in this contribution we have expanded the scope of photoenzymatic oxyfunctionalization reactions to a broader range of heterogeneous photocatalysts. $\text{g-C}_3\text{N}_4$ appeared to be a good alternative to the established TiO_2 -based photocatalysts. In the end, total turnover numbers of over 60.000 were reached for the UPO. The major limitations identified in this study were (1) the relatively low specific H_2O_2 -generation rate of the photocatalysts and (2) the undesired inactivation of the biocatalysts at the photocatalyst surface. The first limitation can be addressed by further optimizing the catalyst and light intensity. The catalyst can be improved by chemically modifying the $\text{g-C}_3\text{N}_4$ e.g. by doping with donor- or acceptor type dopants may be successful [60]. Some preliminary results using KOH- or Co_2O_3 -modified $\text{g-C}_3\text{N}_4$ indeed demonstrated that doping can significantly influence the H_2O_2 -generation activity [61, 62]. Further systematic studies will validate this approach.

The second limitation, i.e. the oxidative inactivation of the biocatalyst by surface-borne reactive oxygen species can be alleviated by physical separation. To circumvent the massive diffusion limitations observed in this double-heterogeneous reaction system, a linear plug-flow reactor concept may prove beneficial.

Experimental section

Enzyme preparation

The recombinant unspecific peroxygenase from *Agrocybe aegerita* (rAaeUPO), evolved for functional expression in *Pichia pastoris*, was produced and purified as described previously [36]. The culture broth containing rAaeUPO excreted by the *P. pastoris* was centrifuged at 8000 rpm for 2 hours at 4 °C. The supernatant was filtered through a 20 µm filter and stored at -80 °C until further purification.

The supernatant was concentrated (Amicon 10 kDa cut-off) and dialysed against a 100 mM NaPi buffer, pH 7.0. rAaeUPO was one-step purified using a NGC Chromatography system (Bio-Rad) with a Q Sepharose FF 30-ml cartridge at a flow rate of 5 ml min⁻¹. After 90 ml, the retained protein was eluted with a 0-50 % NaCl gradient in 450 ml, followed by 50-100 % gradient in 50 ml and 100 % NaCl in 75 ml. Fractions containing peroxygenase activity, as determined by the oxidation of 2,2'-azino-bis (3-ethylbenzothiazoline-6-sulphonic acid) (ABTS) with H₂O₂, were pooled, concentrated and dialysed against a 100 mM NaPi buffer (pH 7.0).

The UV/Vis spectrum of purified rAaeUPO showed a Reinheitszahl (Rz: A420/A280) value of 1.6 and was essentially pure as judged by SDS-PAGE. The activity of rAaeUPO was determined to be 652 ± 5 U mg⁻¹ (pH 5.0 in NaPi buffer) after purification. One unit of the enzyme activity was defined as the amount of the enzyme catalysing the oxidation of 1 µmol of ABTS per minute at the expense of H₂O₂.

Photocatalyst

g-C₃N₄ was synthesized either from urea or melamine as starting compound by heating it up in a furnace to 550 °C (heat ramp: 5 °C min⁻¹). In a typical procedure from 10 g urea approximately 0.5 g g-C₃N₄ sheets were obtained whereas from 10 g melamine approximately 2 g of g-C₃N₄ bulk were obtained. Amorphous g-C₃N₄ was synthesized by further calcination of g-C₃N₄ sheets to 620 °C under an inert argon atmosphere [63].

Chapter 7

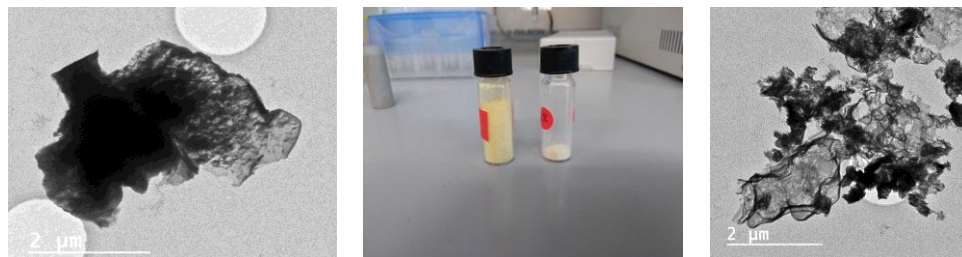


Figure 14: TEM images and physical appearance of g-CN bulk (left) and g-CN sheets (right).

All other photocatalysts were either commercially available or prepared following literature procedures.

GC analysis

Gas chromatography measurements were performed on a GC-214 (Shimadzu) with FID and an AOC-20i auto-injector.

Achiral measurements were performed with a CP-WAX 52 CB column from Agilent (25 m x 0.25 mm x 1.2 μm) at a split ratio of 30 using the following method:

Rate [$^{\circ}\text{C min}^{-1}$]	Temperature [$^{\circ}\text{C}$]	Hold time [min]
-	150	2.2
25	210	3.8
30	250	1.0

Chiral measurements were performed with a CP-Chirasil-Dex CB from Agilent (25 m x 0.32 mm x 0.25 μm) at a split ratio of 100 using the following method:

Rate [$^{\circ}\text{C min}^{-1}$]	Temperature [$^{\circ}\text{C}$]	Hold time [min]
-	120	2.6
15	135	3.3
25	225	1.0

Reaction setup.

Unless stated differently, reactions were performed in 4 ml glass vials. 2 ml reaction mixtures were stirred at 600 rpm using a small stirring magnet (6 mm). The vials were placed around an incandescent white light bulb (Osram, 205W Halolux Ceram) at a distance of approximately 1 cm (figure 15). The water bath was continuously cooled at 30 °C. Reaction mixtures generally contained 5 mg ml⁻¹ g-C₃N₄, 100 nM rAaeUPO and 50 mM ethylbenzene in a 100 mM KPi buffer at pH 7.0. Sacrificial electron donors were added to a concentration of 250 mM. Before use, the g-C₃N₄ was dispersed via sonication in 1 ml of the phosphate buffer. Samples were taken using a syringe and needle, keeping the reactors closed and preventing evaporation of the ethylbenzene. 200 µl of the reaction mixture was taken and extracted with an aliquot of ethyl acetate containing 5 mM octanol as internal standard. The mixtures were intensively mixed for 10 s, centrifuged for 2 min and the organic phase was dried over magnesium sulphate and subsequently analysed via achiral CG chromatography (CP-WAX 52 CB). Optical purities were determined using chiral GC (CP-Chirasil-Dex CB).

A

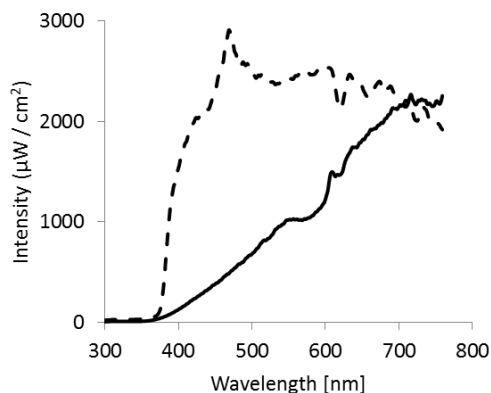


B



Figure 15. Reaction setups used for the photo-chemical reactions. Left: the temperature controlled reaction setup with the incandescent white light bulb. Reaction vials were put in the holder around the light source. Right: reaction setup with the Hamamatsu spotlight at room temperature. Reactions were performed in a closed off, cut off 50 ml falcon tube in order to minimize evaporation.

A



B

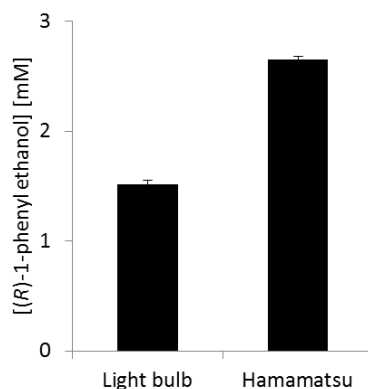


Figure 16. Left: Emission spectra of the white light bulb (solid) and the Hamamatsu (dashed) at 50%. Spectra were determined with a calibrated spectrophotometer and measured at a distance of 30 cm (for the light bulb) or 45 cm (for the Hamamatsu) with an integration time of 1.05 seconds. Holding the light sources closer to the detector would saturate the signal. Right: $g\text{-C}_3\text{N}_4$ and $rAaeUPO$ catalysed hydroxylation of ethyl benzene to phenyl ethanol using the two light setups. Conditions: $[rAaeUPO] = 100 \text{ nM}$, $[\text{ethyl benzene}] = 50 \text{ mM}$, $[g\text{-C}_3\text{N}_4] = 5 \text{ mg ml}^{-1}$, KPi buffer pH 7.0 (100 mM), magnetic stirring at 600 rpm for five hours. Reactions with the Osram white light bulb were performed at 30 °C. Reaction with the Hamamatsu light setup were performed at room temperature. Reactions were performed in duplicates.

Scale-up reaction

A 24 ml reaction, divided over 2 ml samples, was illuminated 80 hours for increased product titres. The reaction was performed at 30 °C in a KPi buffer (100 mM, pH 7.0) containing ethyl benzene (50 mM), $g\text{-C}_3\text{N}_4$ (5 mg ml^{-1}), *rAaeUPO* (100 nM) and sodium formate (250 mM). 100 nM of *rAaeUPO* was added to the reaction every 12 hours and the ethyl benzene was replenished by adding 50 mM extra substrate after 36 hours. At the end of the reaction, the compound was extracted with ethyl acetate, dried with MgSO_4 and purified under reduced pressure at room temperature, also evaporating remaining substrate. The purity of the product was determined by ^1H NMR, while optical purity was determined using chiral GC (CP-Chirasil-Dex CB). NMR spectra were recorded on an Agilent 400 spectrometer in CDCl_3 . Chemical shifts are given in ppm with respect to tetramethylsilane. Coupling constants are reported as J-values in Hz (s: singlet. d: doublet. t: triplet. q: quartet. m: multiplet. br: broad)

^1H NMR (400 MHz, CDCl_3) δ 7.40-7.26 (m, 5H), 4.91 (q, J = 6.5 Hz, 1H), 1.82 (br s, 1H, -OH), 1.51 (d, J = 6.4 Hz, 3H)

^{13}C NMR (100 MHz, CDCl_3) δ 128.5, 127.5, 125.4, 70.4, 25.10.

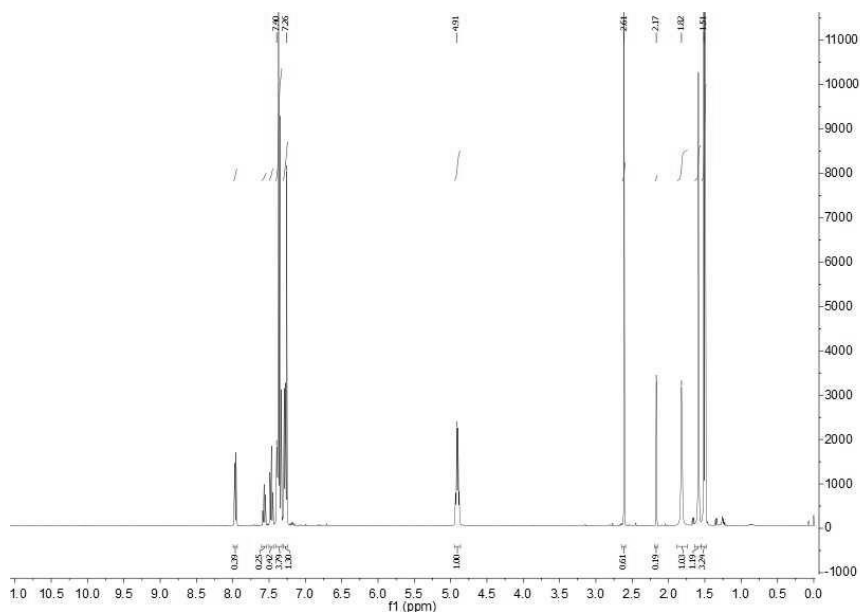


Figure 17. ^1H NMR spectrum of the reaction product.

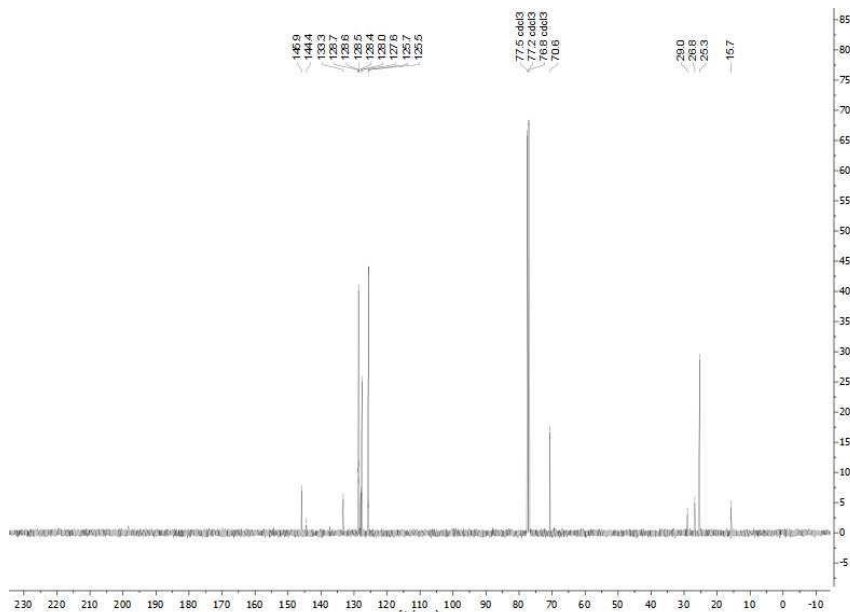


Figure 18. ^{13}C NMR spectrum of the reaction product.

Data manipulation

As the reaction rate, the initial formation rate of phenyl ethanol was taken, considering at least three data points. To estimate the enzyme deactivation rate, the following formula were used:

$$UPO \text{ deactivation rate} = \frac{[UPO]_0}{\text{Reaction time}}$$

With:

$$\text{Reaction time} = \frac{[\text{Max phenyl ethanol}]}{\text{reaction rate}}$$

The reaction selectivity was calculated by dividing the maximum amount of phenyl ethanol reached by the total amount of product formed in that same point in time.

$$\text{Selectivity} = \frac{[\text{Max phenyl ethanol}]}{[\text{Max phenyl ethanol}] + [\text{Acetophenone}]_t}$$

References

1. Roduner, E., et al., *Selective catalytic oxidation of C-H bonds with molecular oxygen*. ChemCatChem, 2013. **5**(1): p. 82-112.
2. Dong, J.J., et al., *Biocatalytic oxidation reactions: A chemist's perspective*. Angewandte Chemie-International Edition, 2018. **57**(30): p. 9238-9261.
3. Wang, Y.H., et al., *Peroxygenases en route to becoming dream catalysts. What are the opportunities and challenges?* Current Opinion in Chemical Biology, 2017. **37**: p. 1-9.
4. Martinez, A.T., et al., *Oxidoreductases on their way to industrial biotransformations*. Biotechnology Advances, 2017. **35**(6): p. 815-831.
5. Hofrichter, M. and R. Ullrich, *Oxidations catalyzed by fungal peroxygenases*. Current Opinion in Chemical Biology, 2014. **19**: p. 116-125.
6. Holtmann, D. and F. Hollmann, *The oxygen dilemma: A severe challenge for the application of monooxygenases?* ChemBioChem, 2016. **17**(15): p. 1391-1398.
7. Valderrama, B., M. Ayala, and R. Vazquez-Duhalt, *Suicide inactivation of peroxidases and the challenge of engineering more robust enzymes*. Chemistry & Biology, 2002. **9**(5): p. 555-565.
8. Hollmann, F. and A. Schmid, *Towards [Cp* Rh (bpy)(H₂O)]²⁺-promoted P450 catalysis: Direct regeneration of CytC*. Journal of Inorganic Biochemistry, 2009. **103**(3): p. 313-315.
9. Paul, C.E., et al., *In situ formation of H₂O₂ for P450 peroxygenases*. Bioorganic & Medicinal Chemistry, 2014. **22**(20): p. 5692-5696.
10. Karmee, S.K., et al., *Chemo-enzymatic cascade oxidation in supercritical carbon dioxide/water biphasic media*. Green Chemistry, 2009. **11**(7): p. 1052-1055.
11. Ranganathan, S. and V. Sieber, *Recent advances in the direct synthesis of hydrogen peroxide using chemical catalysis—A review*. Catalysts, 2018. **8**(9): p. 379.
12. Ranganathan, S., S. Zeithofer, and V. Sieber, *Development of a lipase-mediated epoxidation process for monoterpenes in choline chloride-based deep eutectic solvents*. Green Chemistry, 2017. **19**(11): p. 2576-2586.
13. Ranganathan, S. and V. Sieber, *Development of semi-continuous chemo-enzymatic terpene epoxidation: combination of anthraquinone autooxidation and the lipase-mediated epoxidation process*. Reaction Chemistry & Engineering, 2017. **2**(6): p. 885-895.
14. Kohlmann, C. and S. Lütz, *Electroenzymatic synthesis of chiral sulfoxides*. Engineering in Life Sciences, 2006. **6**(2): p. 170-174.
15. Lütz, S., E. Steckhan, and A. Liese, *First asymmetric electroenzymatic oxidation catalyzed by a peroxidase*. Electrochemistry Communications, 2004. **6**(6): p. 583-587.
16. Horst, A.E.W., et al., *Electro-enzymatic hydroxylation of ethylbenzene by the evolved unspecific peroxygenase of *Agrocybe aegerita**. Journal of Molecular Catalysis B: Enzymatic, 2016. **133**: p. S137-S142.
17. Holtmann, D., et al., *Electroenzymatic process to overcome enzyme instabilities*. Catalysis Communications, 2014. **51**: p. 82-85.
18. Getrey, L., et al., *Enzymatic halogenation of the phenolic monoterpenes thymol and carvacrol with chloroperoxidase*. Green Chemistry, 2014. **16**(3): p. 1104-1108.

19. Krieg, T., et al., *Gas diffusion electrode as novel reaction system for an electro-enzymatic process with chloroperoxidase*. Green Chemistry, 2011. **13**(10): p. 2686-2689.
20. Pereira, P.C., I. Arends, and R.A. Sheldon, *Optimizing the chloroperoxidase-glucose oxidase system: The effect of glucose oxidase on activity and enantioselectivity*. Process Biochemistry, 2015. **50**(5): p. 746-751.
21. Pesic, M., et al., *Multienzymatic in situ hydrogen peroxide generation cascade for peroxxygenase-catalysed oxyfunctionalisation reactions*. Zeitschrift Fur Naturforschung Section C-a Journal of Biosciences, 2019. **74**(3-4): p. 100-103.
22. Ma, Y., et al., *Natural deep eutectic solvents as multifunctional media for the valorisation of agricultural wastes*. ChemSusChem, 2019.
23. Ni, Y., et al., *Peroxygenase-catalyzed oxyfunctionalization reactions promoted by the complete oxidation of methanol*. Angewandte Chemie International Edition, 2016. **55**(2): p. 798-801.
24. Willot, S.J.P., et al., *Expanding the spectrum of light-driven peroxxygenase reactions*. ACS Catalysis, 2019. **9**(2): p. 890-894.
25. Zhang, W., et al., *Selective activation of C-H bonds in a cascade process combining photochemistry and biocatalysis*. Angewandte Chemie International Edition, 2017. **56**(48): p. 15451-15455.
26. Zachos, I., et al., *Photobiocatalytic decarboxylation for olefin synthesis*. Chemical Communications, 2015. **51**(10): p. 1918-1921.
27. Churakova, E., I.W.C.E. Arends, and F. Hollmann, *Increasing the productivity of peroxidase-catalyzed oxyfunctionalization: A case study on the potential of two-liquid-phase systems*. ChemCatChem, 2013. **5**(2): p. 565-568.
28. Churakova, E., et al., *Specific photobiocatalytic oxyfunctionalization reactions*. Angewandte Chemie International Edition, 2011. **50**(45): p. 10716-10719.
29. Zhang, W.Y., et al., *Selective aerobic oxidation reactions using a combination of photocatalytic water oxidation and enzymatic oxyfunctionalizations*. Nature Catalysis, 2018. **1**(1): p. 55-62.
30. Perez, D.I., et al., *Visible light-driven and chloroperoxidase-catalyzed oxygenation reactions*. Chemical Communications, 2009(44): p. 6848-6850.
31. Girhard, M., et al., *Light-driven biocatalysis with cytochrome P 450 peroxxygenases*. Biotechnology and Applied Biochemistry, 2013. **60**(1): p. 111-118.
32. Seel, C.J., et al., *Atom-economic electron donors for photobiocatalytic halogenations*. ChemCatChem, 2018. **10**(18): p. 3960-3963.
33. Goldstein, S., et al., *Photolysis of aqueous H₂O₂: quantum yield and applications for polychromatic UV actinometry in photoreactors*. Environmental Science & Technology, 2007. **41**(21): p. 7486-7490.
34. Ullrich, R. and M. Hofrichter, *The haloperoxidase of the agaric fungus Agrocybe aegerita hydroxylates toluene and naphthalene*. FEBS Letters, 2005. **579**(27): p. 6247-6250.
35. Ullrich, R., et al., *Novel haloperoxidase from the agaric basidiomycete Agrocybe aegerita oxidizes aryl alcohols and aldehydes*. Applied and Environmental Microbiology, 2004. **70**(8): p. 4575-4581.

36. Molina-Espeja, P., et al., *Tandem-yeast expression system for engineering and producing unspecific peroxygenase*. Enzyme and Microbial Technology, 2015. **73**: p. 29-33.
37. Molina-Espeja, P., et al., *Directed evolution of unspecific peroxygenase from *Agrocybe aegerita**. Applied and Environmental Microbiology, 2014. **80**(11): p. 3496-3507.
38. Hirakawa, H., et al., *Au nanoparticles supported on BiVO₄: effective inorganic photocatalysts for H₂O₂ production from water and O₂ under visible light*. ACS Catalysis, 2016. **6**(8): p. 4976-4982.
39. Shi, N., et al., *Facile synthesis of monodisperse Co₃O₄ quantum dots with efficient oxygen evolution activity*. Chemical Communications, 2015. **51**(7): p. 1338-1340.
40. Yin, Q., et al., *A fast soluble carbon-free molecular water oxidation catalyst based on abundant metals*. Science, 2010. **328**(5976): p. 342-345.
41. Priebe, J.B., et al., *Solar hydrogen production by plasmonic Au–TiO₂ catalysts: impact of synthesis protocol and TiO₂ phase on charge transfer efficiency and H₂ evolution rates*. ACS Catalysis, 2015. **5**(4): p. 2137-2148.
42. Najafpour, M.M. and B. Pashaei, *Nanoscale manganese oxide within Faujasite zeolite as an efficient and biomimetic water oxidizing catalyst*. Dalton Transactions, 2012. **41**(34): p. 10156-10160.
43. Maeda, K., et al., *Cobalt oxide nanoclusters on rutile titania as bifunctional units for water oxidation catalysis and visible light absorption: understanding the structure–activity relationship*. ACS applied materials & interfaces, 2017. **9**(7): p. 6114-6122.
44. Boppana, V.B.R. and F. Jiao, *Nanostructured MnO₂: an efficient and robust water oxidation catalyst*. Chemical Communications, 2011. **47**(31): p. 8973-8975.
45. Idris, A., et al., *Photocatalytic magnetic separable beads for chromium (VI) reduction*. Water Research, 2010. **44**(6): p. 1683-1688.
46. Idris, A., et al., *Kinetic and regeneration studies of photocatalytic magnetic separable beads for chromium (VI) reduction under sunlight*. Journal of Hazardous Materials, 2011. **186**(1): p. 629-635.
47. Hamid, S.B.A., S.J. Teh, and C.W. Lai, *Photocatalytic water oxidation on ZnO: a review*. Catalysts, 2017. **7**(3): p. 93.
48. Kim, H.W., et al., *Efficient hydrogen peroxide generation using reduced graphene oxide-based oxygen reduction electrocatalysts*. Nature Catalysis, 2018. **1**(4): p. 282.
49. Zhang, W., et al., *Visible-light-driven photooxidation of alcohols using surface-doped graphitic carbon nitride*. Green Chemistry, 2017. **19**(9): p. 2096-2100.
50. Shiraishi, Y., et al., *Highly selective production of hydrogen peroxide on graphitic carbon nitride (g-C₃N₄) photocatalyst activated by visible light*. Acs Catalysis, 2014. **4**(3): p. 774-780.
51. Burek, B.O., et al., *Kinetic effects and oxidation pathways of sacrificial electron donors on the example of the photocatalytic reduction of molecular oxygen to hydrogen peroxide over illuminated titanium dioxide*. Catalysis Today, 2018.
52. Zhu, B., et al., *First-principle calculation study of tri-s-triazine-based g-C₃N₄: a review*. Applied Catalysis B: Environmental, 2018. **224**: p. 983-999.

53. Li, S., et al., *Effective photocatalytic H₂O₂ production under visible light irradiation at g-C₃N₄ modulated by carbon vacancies*. Applied Catalysis B: Environmental, 2016. **190**: p. 26-35.
54. Burek, B.O., D.W. Bahnemann, and J.Z. Bloh, *Modeling and optimization of the photocatalytic reduction of molecular oxygen to hydrogen peroxide over titanium dioxide*. ACS Catalysis, 2018. **9**(1): p. 25-37.
55. Zheng, Y., Z. Zhang, and C. Li, *A comparison of graphitic carbon nitrides synthesized from different precursors through pyrolysis*. Journal of Photochemistry and Photobiology A: Chemistry, 2017. **332**: p. 32-44.
56. Kang, Y., et al., *An amorphous carbon nitride photocatalyst with greatly extended visible-light-responsive range for photocatalytic hydrogen generation*. Advanced Materials, 2015. **27**(31): p. 4572-4577.
57. Dvoranová, D., Z. Barbieriková, and V. Brezová, *Radical intermediates in photoinduced reactions on TiO₂ (an EPR spin trapping study)*. Molecules, 2014. **19**(11): p. 17279-17304.
58. Buxton, G.V., et al., *Critical review of rate constants for reactions of hydrated electrons, hydrogen atoms and hydroxyl radicals (\cdot OH/ \cdot O $^-$ in aqueous solution*. Journal of Physical and Chemical Reference Data, 1988. **17**(2): p. 513-886.
59. Hu, R., et al., *Application of graphitic carbon nitride for the removal of Pb (II) and aniline from aqueous solutions*. Chemical Engineering Journal, 2015. **260**: p. 469-477.
60. Moon, G.-h., et al., *Eco-friendly photochemical production of H₂O₂ through O₂ reduction over carbon nitride frameworks incorporated with multiple heteroelements*. ACS Catalysis, 2017. **7**(4): p. 2886-2895.
61. Hu, S., et al., *Band gap-tunable potassium doped graphitic carbon nitride with enhanced mineralization ability*. Dalton Transactions, 2015. **44**(3): p. 1084-1092.
62. Zhang, H., et al., *Monodisperse Co₃O₄ quantum dots on porous carbon nitride nanosheets for enhanced visible-light-driven water oxidation*. Applied Catalysis B: Environmental, 2018. **223**: p. 2-9.
63. Son, E.J., et al., *Amorphous carbon nitride as a robust photocatalyst for biocatalytic solar-to-chemical conversion*. ACS Sustainable Chemistry & Engineering, 2018. **7**(2): p. 2545-2552.

Chapter 8



Biocatalytic synthesis of Green Note *trans*-2-hexenal using aryl alcohol oxidase from *Pleurotus eryngii*: overcoming solubility limitations

Morten M.C.H. van Schie, Tiago P. de Almeida, Gabriele Laudadio, Florian Tieves, Elena Fernández-Fueyo, Anping Ma, Sabry H.H. Younes, Antonio Riul Jr., Timothy Noël, Isabel W.C.E. Arends and Frank Hollmann

Based on:

Van Schie, M.M.C.H., *et al.*, *Biocatalytic synthesis of the Green Note trans-2-hexenal in a continuous-flow microreactor*. Beilstein Journal of Organic Chemistry, 2018. **14**: p. 697–703

and

De Almeida, T.P., *et al.*, *Efficient aerobic oxidation of trans-2-hexen-1-ol using the aryl alcohol oxidase from Pleurotus eryngii*, Advanced Synthesis and Catalysis, 2019. **361**(11): p. 2668-2672

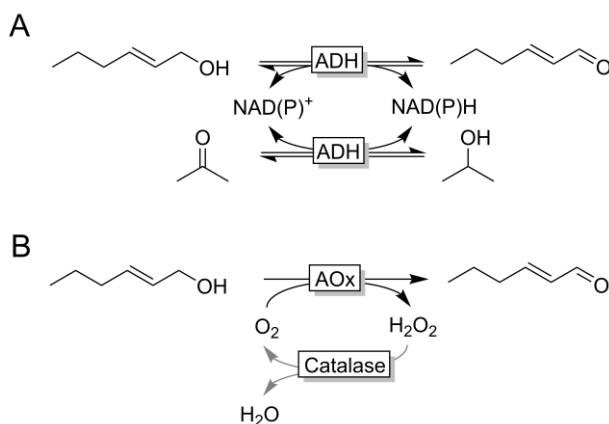
Summary

The biocatalytic preparation of *trans*-2-hexenal from *trans*-2-hexenol using a novel aryl alcohol oxidase from *Pleurotus eryngii* (PeAAOx) is reported. Alcohol oxidases bear several advantages over the more conventional alcohol dehydrogenases for these kind of reactions, mostly because no cofactor regeneration system is needed. Instead, oxygen is used directly by this enzyme to close the reaction redox balance. However, both substrates, oxygen and *trans*-2-hexenol, are poorly soluble in aqueous solutions. We overcame both these limitations individually using flow chemistry and two liquid phases systems respectively. This way, we reached turnover frequencies and turnover numbers for the enzyme up to 38 s⁻¹ and 2.2 million, respectively.

Introduction

The selective oxidation of functionalised alcohols to the corresponding aldehydes still poses challenges in synthetic organic chemistry [1-3]. Issues with functional group tolerance, overoxidation and other undesired side reactions are still observed frequently [4]. Traditional chemical routes are sometimes plagued by a rather high energy demands and dependence on environmentally questionable oxidants [5]. When it comes to selectivity, enzymes are generally amongst the first catalysts to be mentioned [6-8]. Nevertheless, only a few synthetic oxidation reactions rely on biocatalysis, and preference usually is given to the well-established homogeneous and heterogeneous catalysts. Partially, this is due to the (perceived) high costs of enzyme production. Furthermore, product titres reported for biocatalytic oxidations still tend to be in the lower millimolar range (few g l⁻¹) and thus are unattractive from a preparative point-of-view. To address these issues, we chose the oxidation of *trans*-2-hexenol to the corresponding aldehyde as model reaction. The corresponding aldehyde is widely used in the flavour and fragrance industry as fresh flavour ingredient (Green Note) [9].

For clean conversion of primary alcohols to aldehydes principally two biocatalytic approaches are available (Scheme 1) [10-13]. Alcohol dehydrogenases catalyse the reversible oxidation of alcohols in a Meerwein–Ponndorf–Verley-type of reaction (Scheme 1A). The poor thermodynamic driving force of this reaction, however, necessitates significant molar surpluses of the stoichiometric oxidant (such as acetone). This not only negatively influences the environmental impact of the reaction [14] but also complicates downstream processing. Furthermore, the nicotinamide cofactor (even if used in catalytic amounts only) causes additional costs.

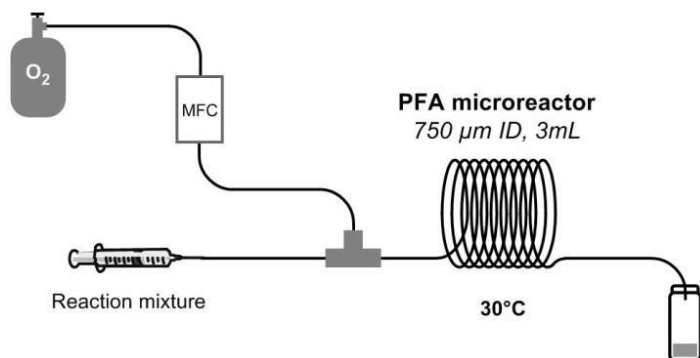


Scheme 1: Enzymatic reaction schemes for the selective oxidation of *trans*-2-hexenol. A: Alcohol dehydrogenase (ADH)-catalysed oxidation producing stoichiometric amounts of NAD(P)H, which needs to be recycled in situ; the overall reaction is reversible requiring surpluses of the cosubstrate (e.g., acetone) to shift the overall equilibrium to the side of *trans*-2-hexenal. B: Envisioned aerobic oxidation using alcohol oxidases (AOx). H₂O₂ is formed as byproduct and dismutated by catalase into H₂O and O₂.

Therefore, we concentrated on alcohol oxidase-catalysed reaction schemes (Scheme 1B). Oxidases utilise O₂ as terminal electron acceptor for the oxidation reaction yielding H₂O₂ as sole byproduct. The latter can be disproportionated easily by using catalase (Scheme 1B). Furthermore, O₂ reduction adds sufficient thermodynamic driving force to the reaction to make it essentially irreversible.

Despite these advantages, the AAOx catalysed reaction suffers from issues in solubility, as both the O₂ (0.25 mM) and the *trans*-2-hexenol (130 mM) are sparingly soluble in the buffer, hindering large scale applications. Dissolved O₂ is rapidly consumed in the course of an oxidation reaction and diffusion of O₂ into the reaction medium can easily become overall rate limiting. The O₂ diffusion rate into the reaction medium directly correlates with the interfacial area between aqueous medium and the gas phase. Large interfacial surface areas can be achieved via heterogeneous intake, by bubbling, stirring, etc. Soluble enzymes, however, are often rather unstable under these conditions, possibly owing to the mechanical stress leading to irreversible inactivation of the biocatalyst [15, 16]. The limited solubility of the substrate restricts the total possible production formation in a monophasic system. This can be overcome with the additions of cosolvents, like DMSO, which can influence both enzyme stability and further complicate downstream processing. For this chapter, we attempted to overcome both these challenges individually.

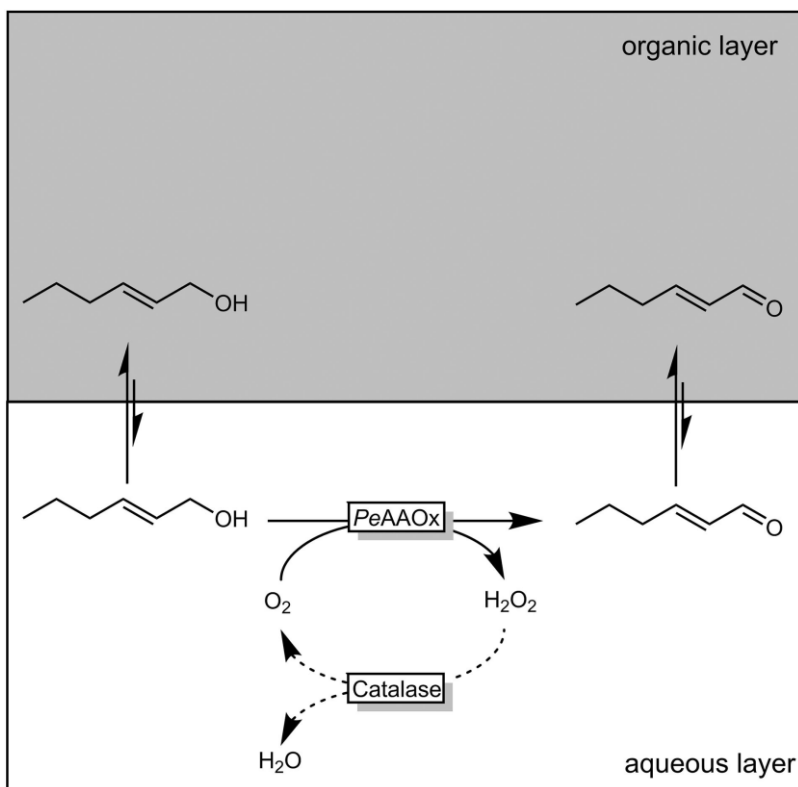
Though other methods of bubble-free aeration have been described in the literature [17-21], we chose to perform the reactions in a continuous-flow microreactor to increase oxygen availability. Continuous-flow microreactor technology has emerged as a safe and scalable way to approach oxidation reactions (scheme 2) [22, 23]. Due to its small dimensions, hazardous reactions can be easily controlled, owing to the large surface-to-volume ratio which can minimise hot-spot formation and allows for control over mixing and heating phenomena [24, 25]. Furthermore, a well-defined gas-liquid regime can be easily maintained [26, 27]. High mass-transfer coefficients are generally the consequence of small vortices induced by the segmented flow regime. This flow pattern guarantees an enhanced contact between the two phases and provides a uniform gas concentration in the liquid segment. For these reasons several biocatalytic processes have already been reported in flow reactors [28], mostly advocating easier process intensification in combination with enzyme immobilization [29-32]. Also the higher oxygen transfer rates in flow reactions compared to batch reactions have been emphasised by several groups. Here, reactor designs ranging from simple flow reactors, tube-in-tube reactors [33], agitated tube reactors [34, 35] and continuous agitated cell reactors [36] have been reported.



Scheme 2. Schematic view of the reaction setup. The oxygen gas flow was controlled by a mass flow controller (MFC). The reaction mixture flow was controlled by a syringe pump. The sample was collected on ice or directly in ethyl acetate at the end of the reactor.

To overcome substrate solubility limitations, we evaluated the so-called two-liquid-phase-system approach (2LPS, Scheme 3). Here, a hydrophobic organic phase serves both, as

substrate reservoir and product sink enabling overall high reagent loadings and reduction of both substrate and product inhibition. Furthermore, the separation of the two phases further facilitates downstream process and biocatalyst recycling. The advantages of 2LPS has been demonstrated previously for various reactions [14, 37-49].



Scheme 3. Biocatalytic oxidation of *trans*-2-hexenol. To achieve overall high reagent loadings, a hydrophobic organic phase is added to the aqueous reaction buffer. PeAAOx: aryl alcohol oxidase from *Pleurotus eryngii*. In order to alleviate the potentially harmful effect of H₂O₂, catalase is added to the reaction.

Results and Discussion

For this study we focussed on the recombinant aryl alcohol oxidase from *Pleurotus eryngii* (PeAAOx) as the biocatalyst [36, 50-52]. Its availability as recombinant enzyme, enabling future at-scale production and protein engineering, and its promising activity on allylic alcohols make PeAAOx a promising starting point. Commercially available

alcohol oxidases from *Pichia pastoris* and *Candida boidinii* showed no significant activity for the substrate under the same conditions.

As *trans*-2-hexenol had not been reported as substrate for *PeAAOx*, we first evaluated its operational window for *PeAAOx* in terms of optimal pH and temperature and kinetic behaviour (figure 1). Regarding the optimal pH, *PeAAOx* is active in a broad pH range, displaying the highest activity between pH 5 and 8 (figure 1A). Based on these results, pH 7 was selected for further experiments due to its compatibility with the activity of catalase (required for the dismutation of H_2O_2). *PeAAOx* exhibits the maximum activity at 30 °C with a turnover frequency of 25 s^{-1} . Above this temperature the activity dropped dramatically, with a 25 fold decrease at 40 °C ($\text{TF} < 1 \text{ s}^{-1}$, figure 1B). The decrease of the activity at elevated temperatures is most likely attributed to thermal denaturation of the biocatalyst. We therefore conducted all further experiments at 20 °C as a compromise between high activity and stability. Initial rate measurements revealed a Michaelis–Menten dependency of the enzyme activity (figure 1C). Apparent k_{cat} and K_{M} values of approximately 22 s^{-1} and 1 mM were estimated, respectively. These values are in the same order of magnitude as those for benzyl alcohol substrates reported previously [50]. The slightly decreasing enzyme activity at elevated substrate concentrations may be an indication for a slight substrate inhibition. Performing these initial rate measurements in the presence of varying product concentrations showed product inhibition (figure 1D).

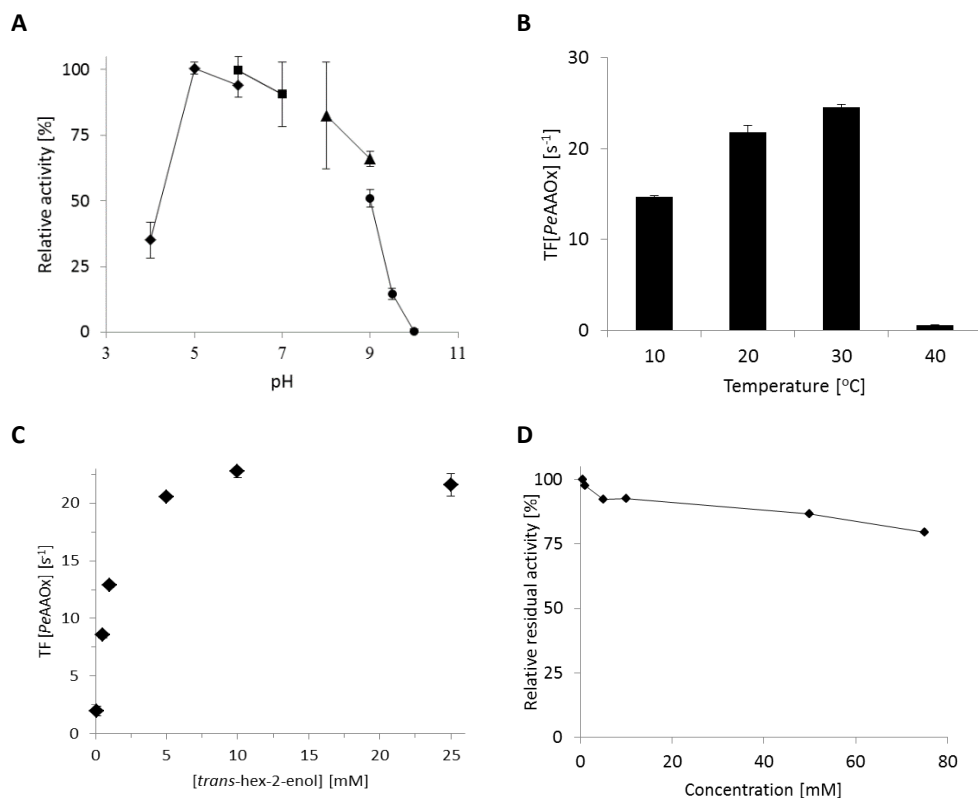


Figure 1. Characterization of the Aryl Alcohol Oxidase from *Pleurotus eryngii* (PeAAOx) The activity was determined by coupling the H_2O_2 formed during the alcohol oxidation to an ABTS assay with horseradish peroxidase (HRP). A: Influence of the pH on the enzyme activity for different buffers, citrate (diamonds), phosphate (squares), tris (triangles) and capso (squares). B: Influence of the reaction temperature on the enzyme activity. Reactions were performed at 10, 20, 30 or 40 °C in potassium phosphate buffer (50 mM, pH 7.0) containing 0.05 μM PeAAOx, 720 $U\ ml^{-1}$ catalase and 50 mM *trans*-2-hexenol. C: Kinetic behaviour of the PeAAOx at different substrate concentrations. D: Inhibitory effect of the product on the residual activity of the enzyme. General conditions (unless indicated otherwise): [*trans*-2-hexenol] = 3 mM, [ATBS] = 2mM, [PeAAOx] = 5 nM, [HRP] = 5 $U\ ml^{-1}$ in a 50 mM KPi buffer (pH 7) at 30 °C.

Next, we focussed on improving the oxygen transfer rate by performing the PeAAOx-catalysed oxidation of *trans*-2-hexenol in a slug-flow reactor setup. In a first set of experiments we systematically varied the residence time of the reaction mixture in the flow reactor (and thereby the reaction time, figure 2).

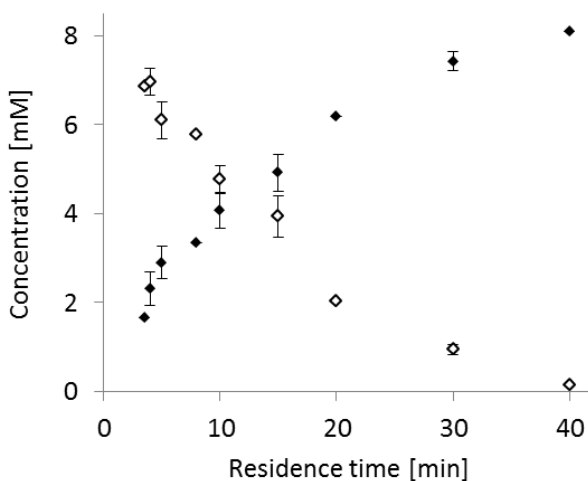


Figure 2: The influence of the residence time on the conversion of *trans*-2-hexenol (white) to *trans*-2-hexenal (black) in a flow reactor (3 ml volume). Conditions: [*trans*-2-hexenol]₀ = 10 mM, [PeAAOx] = 0.25 μ M, [catalase] = 600 U ml⁻¹ in a 50 mM KPi buffer (pH 7.0) at 30 °C.

Full conversion of the starting material into the desired *trans*-2-hexenal was observed at residence (reaction) times of approximately 40 min corresponding to a turnover number (TN) for the biocatalysts of 32 400 and an average turnover frequency (TF) of 13.5 s⁻¹. Even more interestingly, at higher flow rates apparent TF of up to 38 s⁻¹ (RT = 5 min) were observed. This value exceeds the previously determined k_{cat} (PeAAOx) (Figure 1C) significantly. We attribute this observation to an increased oxygen-transfer rate at high flow rates. In the case of the 5 minutes residence time this corresponds to an O₂-transfer rate of roughly 0.25 mM min⁻¹. Similarly high values could be obtained previously only under mechanically demanding reaction conditions or using surfactant-stabilised emulsions [15]. Varying the ratio of gas to liquid had no significant effect on the overall rate of the reaction (table 1).

Table 1. Effect of variation of the gas-to-liquid ratio on the rate of the *PeAAOx*-catalysed aerobic oxidation of *trans*-hex-2-enol. Conditions: 3 ml flow reactor, 50 mM KPi buffer (pH 7, 30 °C), [*trans*-2-hexenol]₀ = 10 mM, [*PeAAOx*] = 0.25 μM, [catalase] = 600 U ml⁻¹.

Ratio (liquid : gas)	Liquid flow [ml min ⁻¹]	Gas flow [ml min ⁻¹]	Residence time [min]	[Product] [mM]
1 : 1	0.20	0.20	15	5.48 (± 0.01)
1 : 3	0.10	0.30	15	5.18 (± 0.32)
1 : 5	0.067	0.333	16	4.99 (± 0.49)

Within the experimental error, the conversion in all experiments was identical indicating that even at a comparably low volumetric ratio of 1:1 the O₂ availability was already sufficient not to be overall rate-limiting. Under batch reaction conditions, similar progression curves were only attainable under mechanically very demanding conditions (i.e., very vigorous stirring and bubbling of O₂ directly into the reaction mixture) (figure 3). These conditions also caused a significant evaporation of the substrate at higher substrate concentration which was much less the case in the flow-reaction setup.

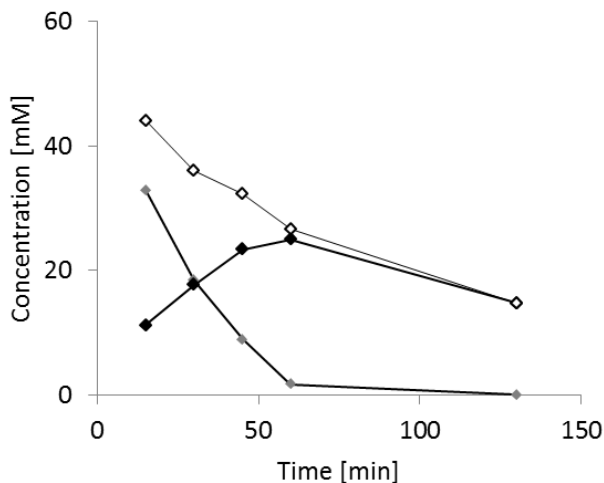


Figure 3. The conversion of *trans*-2-hexenol (grey) into *trans*-2-hexenal (black) by *PeAAOx*. The mass balance (white) decreases due to evaporation of compound at higher substrate loading and bubbling with oxygen. General conditions: [*trans*-2-hexenol] = 50 mM, [*PeAAOx*] = 0.5 μM, [catalase] = 720 U ml⁻¹ in a 50 mM KPi buffer (pH 7.0) at 30 °C on a 5 ml scale.

From an economical point-of-view the catalyst performance in terms of turnover number (TN) is of utmost importance as it directly correlates with the cost-contribution of the catalyst to the production costs [53-55]. Therefore we evaluated the TN attainable for *PeAAOx* in the flow setup (Figure 4). For this lower *PeAAOx* concentrations as well as significantly increased residence times were applied. The increased residence times were achieved by decreasing the flow rates and using a longer flow reactor (6 mL volume instead of 3 mL).

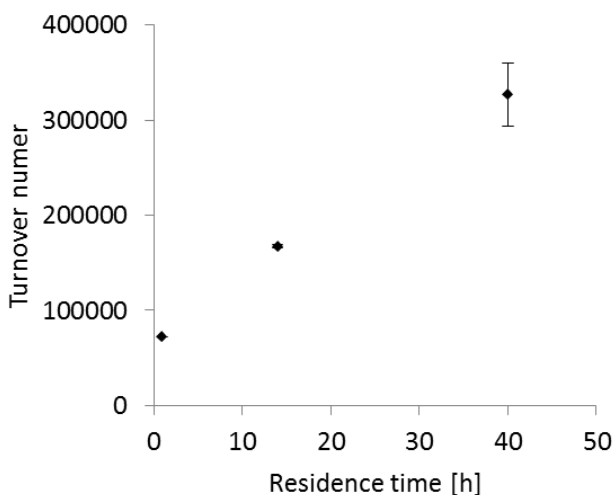


Figure 4: Increasing the *PeAAOx* turnover numbers (TN) in flow by increasing the residence time. Conditions: 6 ml flow reactor, $[trans\text{-}2\text{-hexenol}]_0 = 40 \text{ mM}$, $[PeAAOx] = 0.02 \text{ }\mu\text{M}$, $[catalase] = 600 \text{ U ml}^{-1}$ in a 50 mM KPi buffer (pH 7.0) at 30 °C. The TN value was calculated based on the GC yield of every run. The TN was obtained by dividing the product concentration (as determined chromatographically) by the biocatalyst concentration.

Pleasingly, already in these first experiments a TN for the enzyme of more than 300 000 was observed at long residence times. This also underlines the robustness of the enzyme under the flow conditions. Compared with Figure 2, somewhat lower TFs for *PeAAOx* were observed, which again can be attributed to a lower O_2 -transfer rate at lower flow rates. The quasi-linear relationship shown in figure 4 also suggests that even higher TN may be attainable – however at the expense of longer reaction times. Encouraged by these results, we also tried a semi-preparative scale reaction using 5 g l^{-1} (50 mM) substrate loading in a total of 50 mL with $0.75 \text{ }\mu\text{M}$ *PeAAOx*. As a result, 90% conversion was achieved after 18 hours of total reaction time (roughly 80 minutes of residence time in the 6 mL reactor). The product was purified by chromatography resulting in 200 mg of pure

trans-2-hexenal (determined by NMR) in 81% isolated yield, thereby demonstrating the preparative potential of the proposed reaction setup. To increase these numbers, significantly longer reactors and more powerful mass flow controllers will be needed.

In order to improve substrate availability with the 2LPS, we first needed to determine the stability of *PeAAOx* in the presence of various organic solvents. Hydrophobic solvents such as isooctane or dodecane were tolerated well by the enzyme and initial rates up to 13 turnovers per second were achieved (figure 5A). Using toluene gave no catalytic conversion at all. Possibly, π -stacking interactions of the aromatic ring with the flavin prosthetic group resulted in a strong competitive inhibition of *PeAAOx* [50]. Quite surprisingly, even ethyl acetate was tolerated by *PeAAOx* as organic phase even though reactions ceased rather quickly due to acidification of the aqueous layer caused by auto-hydrolysis. We chose dodecane as organic phase. Figure 5B shows a representative time course of a reaction in the biphasic reaction system.

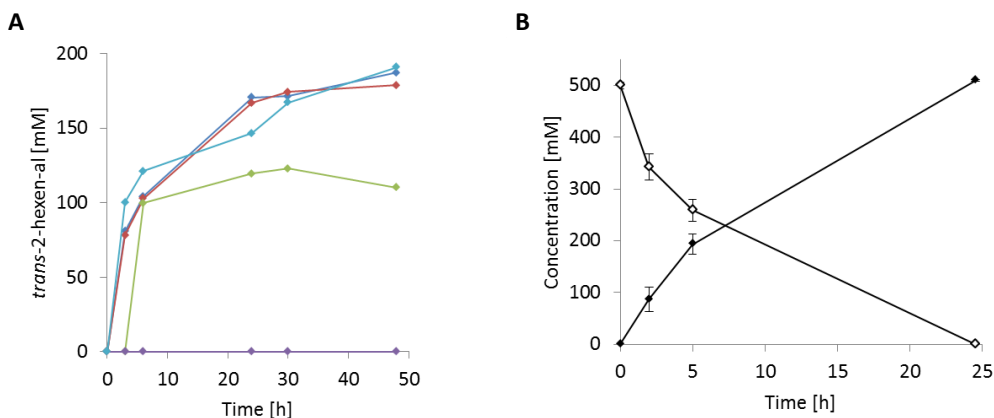


Figure 5. *PeAAOx* in two liquid phase systems (2PLS). A: Influence of the organic solvent on the *PeAAOx* activity. The solvents were added to the liquid phase in a 1 to 1 phase ratio, dodecane (blue), isooctane (red), ethyl acetate (green), toluene (purple) or the substrate, *trans*-2-hexenol, itself (sky-blue). Conditions: [*trans*-2-hexenol]₀ = 1 M, [*PeAAOx*] = 0.2 μ M, [catalase] = 720 U ml⁻¹ in a 50 mM KPi buffer (pH 7.0) at 20 °C mixing at 1000 rpm. B: *PeAAOx*-catalysed oxidation of *trans*-2-hexenol (white) to *trans*-2-hexenal (black) using a biphasic (2LPS) reaction system. Conditions: aqueous phase: 0.5 ml of 50 mM KPi (pH 7), [*PeAAOx*] = 0.75 μ M, [Catalase] = 720 U ml⁻¹; organic phase: 0.5 ml of dodecane, [*trans*-2-hexenol]₀ = 500 mM. Reaction were performed at 20 °C mixing at 1000 rpm.

Pleasingly, full conversion of the starting material into the desired product (49 g l⁻¹ organic phase) was observed within 24 hours. The nominal catalytic performance of *PeAAOx* in the

biphasic system (TF of 14.3 s^{-1} within the first 5 hours) was significantly lower compared to the microfluidic system (TF of 38 s^{-1} , Figure 2), which most likely is attributed to phase transfer limitations of the *trans*-2-hexenol and the oxygen [15]. Nevertheless, *PeAAOx* performed more than 650 000 catalytic turnovers corresponding to a catalyst loading of less than 0.0002 mol-% or almost 900 gram product per gram *PeAAOx*, respectively. The values for catalase are 0.00002 mol-% and 8166 gram product per gram enzyme, respectively. Another advantage of the 2LPS approach lies with the facile downstream processing as simple phase separation is sufficient to separate the dodecane-product mixture (in case of full conversion as shown in Figure 1) from the aqueous reaction buffer. Chromatographic and/or distillative separation of the solvent (dodecane, bp = $214\text{ }^{\circ}\text{C}$) from the product (*trans*-2-hexenal, bp = $145\text{ }^{\circ}\text{C}$) is straightforward. Encouraged by these results, we aimed at maximising the catalytic usage of the biocatalyst (maximising the turnover number). We decided to avoid any additional organic solvent and use *trans*-2-hexenol itself as the organic phase (Figure 5A). In a first set of experiments, we realised that after approximately 48 hours the rate of the oxidation reaction decreased to some extent. Therefore, at intervals, fresh *PeAAOx* and catalase were added (in total 6 times throughout the entire experiment) to the aqueous layer summing up to 300 nM and 600 nM of *PeAAOx* and catalase, respectively. This procedure allowed for at least 14 days of stable accumulation of more than 2.6 M of the desired product in the *trans*-2-hexen-1-ol layer. Overall, a superb turnover number of more than 2.2 Million was calculated for *PeAAOx*. Admittedly, 14 day of reaction time is not practical on the lab-scale or even industrial scale. The conversion of 31% of the starting material in case of the neat experiment (Figure 6A) is not satisfactory as it necessitates further chromatographic separation of the product from the starting material. Nevertheless, this experiment demonstrates the catalytic potential of *PeAAOx* for the synthesis of *trans*-2-hexenal and possibly further aldehyde products such as benzaldehydes [36]. According to the cost estimation by Tufvesson and Woodley [55] these turnover numbers correspond to a cost contribution of *PeAAOx* of less than $0.1\text{ }\text{€ mol}^{-1}$ of product (Figure 6B, assuming large-scale fermentation of the enzyme).

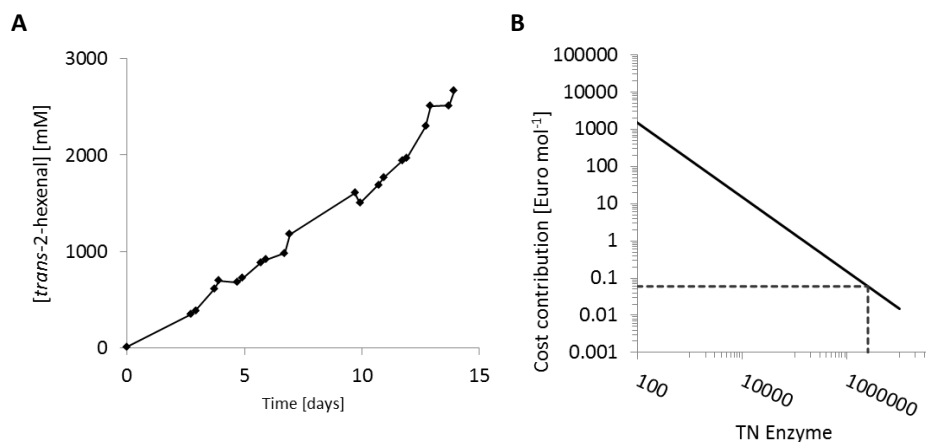


Figure 6. A: Time course of a long-term oxidation experiment utilising the 2LPS approach. Conditions: aqueous phase: 2.5 ml of 50 mM KPi (pH 7), [PeAAOx] = 0.3 mM (final) and [catalase] = 0.6 mM (final) (added at intervals of 2 days), organic phase: 7.5 ml of [*trans*-2-hexenol] = 8.4 M (neat). Reaction were performed at 20 °C mixing at 1000 rpm. B: Estimation of the cost contribution of PeAAOx to the final product.

Conclusion

Alcohol oxidase-catalysed oxidation of alcohols to aldehydes bears a significant potential for preparative biocatalysis. The reaction is independent from expensive and instable nicotinamide cofactors (and the corresponding co-substrates/co-products as well as possible regeneration enzymes) and produces only water as byproduct. However, to make these enzyme catalysed reactions truly interesting for industry, challenges in availability of both oxygen and substrate need to be overcome. Flow chemistry is a promising technique to provide the aqueous reaction mixture with O₂ needed for the oxidation. It enables high O₂ transfer rates while avoiding enzyme robustness issues frequently observed with ‘traditional’ aeration methods. The use of a two liquid phase system on the other hand will greatly improve the availability of the, only slightly water-soluble, substrate. Since mass transfer rates between organic and aqueous phases are also promoted in micro flow reactors [23], a combination of these two approaches would even further improve the performance of the PeAAOx. This would also enable high O₂ transfer rates while avoiding enzyme robustness issues frequently observed with ‘traditional’ aeration methods. In this case, longer tube reactors would be required, in turn resulting in higher pressures, as the reactor used in this research can only facilitate relatively short reaction times. Many other factors will play a role *en route* to economic feasibility of such a process but these numbers again underline the potential of this enzyme for preparative application. Overall, this contribution demonstrates that oxidase-catalysed alcohol oxidation reactions not only represent a selective approach for the production of

Chapter 8

aldehydes under non-problematic reaction conditions but also represent an economic promising methodology.

Material and methods

General

Turnover numbers (TN) and turnover frequencies (TF) reported in this manuscript were calculated based on Equation 1 and Equation 2.

$$\text{TN} [-] = \frac{c(\text{product})}{c(\text{PeAAOx})} \quad (1)$$

$$\text{TF} [\text{s}^{-1}] = \frac{\text{TN}}{\text{reaction time}} \quad (2)$$

Chemicals

2,2'-Azino-bis(3-ethylbenzothiazoline-6-sulfonic acid) diammonium salt (ABTS), *trans*-2-hexenal, dodecane, isooctane, toluene, magnesium sulphate and ethyl acetate were purchased from Sigma Aldrich and were used without further purification. *Trans*-2-hexenol was distilled before use. Columns or column material used during enzyme purification were purchased from GE healthcare. NMR spectra were recorded on a Varian 400 (400 MHz) spectrometer, with CDCl₃ as the solvent. Chemical shifts are given in ppm with respect to tetramethylsilane. Coupling constants are reported as J-values in Hz.

Production of PeAAOx

For the production, activation and purification of PeAAOx, a slightly modified literature protocol was used [36]. Pre-cultures of LB media containing 100 µg ml⁻¹ of ampicillin were inoculated with *E. coli* W3110 containing pFLAG1-AAO and incubated overnight at 37 °C and 180 rpm. Overexpression was carried out in 5 l flasks with 1 l of TB medium supplemented with 100 µg ml⁻¹ of ampicillin. The medium was inoculated with the pre-culture to an OD of 0.05 and grown at 37 °C and 180 rpm. At an OD₆₀₀ of 0.8, 1 mM isopropyl β-D-thiogalactopyranoside (IPTG) was added and the cultures were incubated for additional 4 h at 37 °C and 180 rpm. The bacterial pellets, obtained after

harvesting the cells, were re-suspended in a total volume of 40 ml 50 mM Tris/HCl buffer, pH 8.0, containing 10 mM EDTA and 5 mM dithiothreitol (DTT).

Refolding

The re-suspended cells were disrupted by incubation with 2 mg ml⁻¹ lysozyme for 1 h at 4 °C. Afterwards, 0.1 mg ml⁻¹ DNase, 1 mM MgCl₂ and 0.1 mM PMSF were added followed by sonication. The insoluble fraction was collected by centrifugation (30 min at 15 000 rpm and 4 °C), re-suspended and washed three times with 20 ml 20 mM Tris/HCl buffer, pH 8.0, containing 10 mM EDTA and 5 mM DTT using a potter homogenizing device. The pellets obtained after centrifugation (15 min at 15 000 rpm and 4 °C) were solubilized in a total volume of 30 ml 20 mM Tris/HCl buffer, pH 8.0, containing 2 mM EDTA, 50 mM DTT and 8 M urea. After incubation on ice for 30 min, the solution was cleared by centrifugation (15 min at 15 000 rpm and 4 °C). The obtained supernatant was used as stock solution for the in vitro refolding. The *PeAAOx* was solubilized using 150 µg ml⁻¹ protein in 20 mM Tris/HCl buffer, pH 9.0, containing 2.5 mM GSSG, 1 mM DTT, 0.02 mM FAD, 34% glycerol and 0.6 M urea at 4 °C for 80 h. After the incubation for *PeAAOx* activation/ refolding, the refolding mixture was concentrated to 100 mL and the buffer exchanged against 10 mM sodium phosphate buffer, pH 5.5 by diafiltration (DV 20) and subsequently concentrated using an Amicon Ultra 15 ml centrifugal filter (MWCO 10 kDa). After centrifugation (overnight at 15,000 rpm and 4 °C), the soluble fraction was further purified using anionexchange chromatography.

Purification

The concentrated *PeAAOx* solution was purified using a 58 mL Q Sepharose column (GE Healthcare). *PeAAOx* was eluted with a linear NaCl gradient (0–0.6 M over 6 CV) using 10 mM sodium phosphate buffer, pH 5.5. Fractions containing *PeAAOx* were pooled, concentrated and desalted using HiTrap desalting columns (GE Healthcare) and 10 mM sodium phosphate buffer, pH 5.5. The *PeAAOx* concentration was calculated based on the absorbance using the molar extinction coefficient of ϵ_{463} 11 050 M⁻¹ cm⁻¹.

Chapter 8

Reaction optimisation

The activity of *PeAAOx* was determined by UV–vis spectroscopy, using an Agilent Cary 60 UV–vis spectrophotometer, following the oxidation of ABTS ($\epsilon_{405} = 36\,800\text{ M}^{-1}\text{ cm}^{-1}$) by horseradish peroxidase (HRP) at the expense of hydrogen peroxide. In general, $0.044\text{ }\mu\text{M}$ *PeAAOx* was used to convert 3 mM of *trans*-2-hexenol. The hydrogen peroxide formed in this reaction was subsequently used to convert 2 mM of ABTS to $\text{ABTS}^{\cdot+}$ by an excess of POD (500 U ml^{-1}).

The activity of *PeAAOx* at different pH was measured via ABTS-assay in the presents of 5 U ml^{-1} horseradish peroxidase and 5 nM *PeAAOx* as described before following an incubation of 30 min at 20°C in the corresponding buffer. Citric acid buffer (50 mM , pH 4, 5 or 6), potassium phosphate buffer (50 mM , pH 6 or 7), Tris/HCl buffer (50 mM , pH 7 or 8) or CAPSO buffer (50 mM , pH 9 or 10) were tested. Additionally, product inhibition was investigated via the ABTS-assay as described before following an incubate of *PeAAOx* in the presence of different concentrations of *trans*-2-hexenal ($0.5, 1, 5, 10, 50, 75\text{ mM}$) for 30 min at 20°C .

To test the temperature dependence of the reaction, experiments were performed in phosphate buffer (50 mM , pH 7) at $10, 20, 30$ or 40°C using a thermoshaker device (1000 rpm). Oxygen was supplied to the headspace of the reaction by an oxygen filled balloon. The reaction mixture (1 ml) contained $0.05\text{ }\mu\text{M}$ *PeAAOx*, 720 U ml^{-1} catalase and 50 mM *trans*-2-hexenol.

Flow reactor experiments

PFA microreactor coils ($750\text{ }\mu\text{m}$ ID) with a volume of 3 and 6 mL were constructed. The reaction mixture was introduced *via* a syringe pump (Fusion 200, Chemyx), while the pure oxygen flow was controlled by a mass flow controller (ELFLOW, Bronkhorst), resulting in a segmented flow (figure 7). Residence times were taken as the time between the solution entering and exiting the coil and were varied by altering the flow, keeping the ratio of oxygen to liquid at three to one. Samples were collected on ice and, as soon as enough volume was collected, extracted with ethyl acetate and analysed by GC.

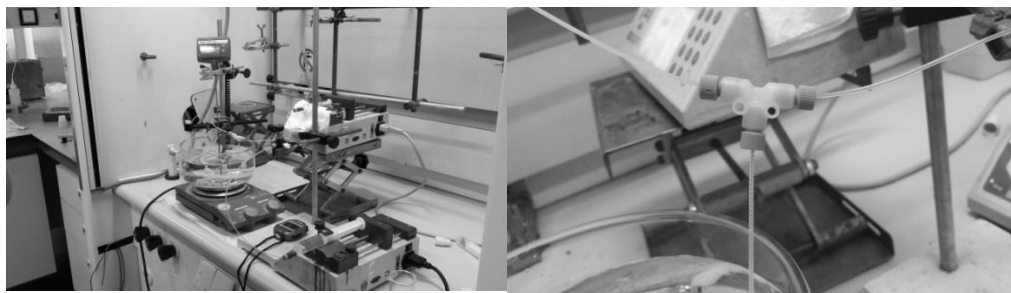


Figure 7: Pictures of the total reaction setup (left) and a close-up on the segmented flow.

Biphasic reaction system

All reactions were performed with phosphate buffer (50 mM, pH 7) at 20 °C using a thermoshaker device (1000 rpm). Oxygen was supplied to the headspace of the reaction by an oxygen filled balloon. The biphasic reaction systems (1 ml) were composed of an organic solvent layer and an aqueous layer in a 1:1 phase ratio. The organic layer solvent (dodecane, isooctane, ethyl acetate or toluene) was supplemented with 1 M *trans*-2-hexenol. In addition, *trans*-2-hexenol was used as organic layer. The aqueous phase contained 0.2 μM PeAAOx and 720 U ml⁻¹ catalase.

Scale-up and long-term experiment in the biphasic reaction system

In a scale-up experiment (10 ml), dodecane containing 500 mM *trans*-2-hexenol and potassium phosphate buffer (50 mM, pH 7.0) containing 0.75 μM PeAAOx and 720 U ml⁻¹ catalase were used in a 1:1 phase ratio. Long-term experiments were performed in glass flasks under magnetic stirring (100 rpm). In a total volume of 10 ml, a phase ratio of 1:4 using pure *trans*-2-hexenol as organic layer and phosphate buffer (50 mM, pH 7) containing 0.05 μM PeAAOx and 720 U ml⁻¹ as aqueous layer was applied. Every two days, 0.05 μM PeAAOx and 720 U ml⁻¹ was added to the solution in the total amount of 0.30 μM of PeAAOx.

GC analysis

The collected reaction mixtures were extracted into an equal volume of ethyl acetate, dried with magnesium sulphate and analysed on a CP-wax 52 CB GC column (50 m \times 0.53 mm \times 2 μm) (GC method: 60 °C for 3 min; 30 °C min⁻¹ to 105 °C; 105 °C for 7 min;

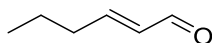
Chapter 8

30 °C min⁻¹ to 250 °C; 250 °C for 1 minute). 5 mM of dodecane was used as internal standard.

Work-up semi-preparative scale flow set up

The reaction mixture was directly collected in deuterated chloroform at the end of the flow reactor followed by recording the NMR spectrum in order to evaluate the conversion. The organic mixture was diluted and introduced into a separation funnel and washed with brine. The aqueous phase was washed once with DCM. The collected organic phase was dried over MgSO₄, filtered and concentrated under reduced pressure. Purification of the isolated mixture was performed by flash chromatography on silica (pure DCM). The final product was obtained as colourless oil (200 mg).

trans-Hex-2-enal



TLC (DCM) R_f 0.9; ¹H NMR (400 MHz, CDCl₃) δ 9.44 (d, *J* = 7.7 Hz, 1H), 6.78 (dt, *J* = 15.6, 6.8 Hz, 1H), 6.05 (ddq, *J* = 15.5, 7.8, 1.3 Hz, 1H), 2.33–2.18 (m, 2H), 1.48 (h, *J* = 7.4 Hz, 2H), 0.90 (t, *J* = 7.4 Hz, 3H); ¹³C NMR (100 MHz, CDCl₃) δ 194.3, 158.9, 133.3, 34.8, 21.3, 13.8.

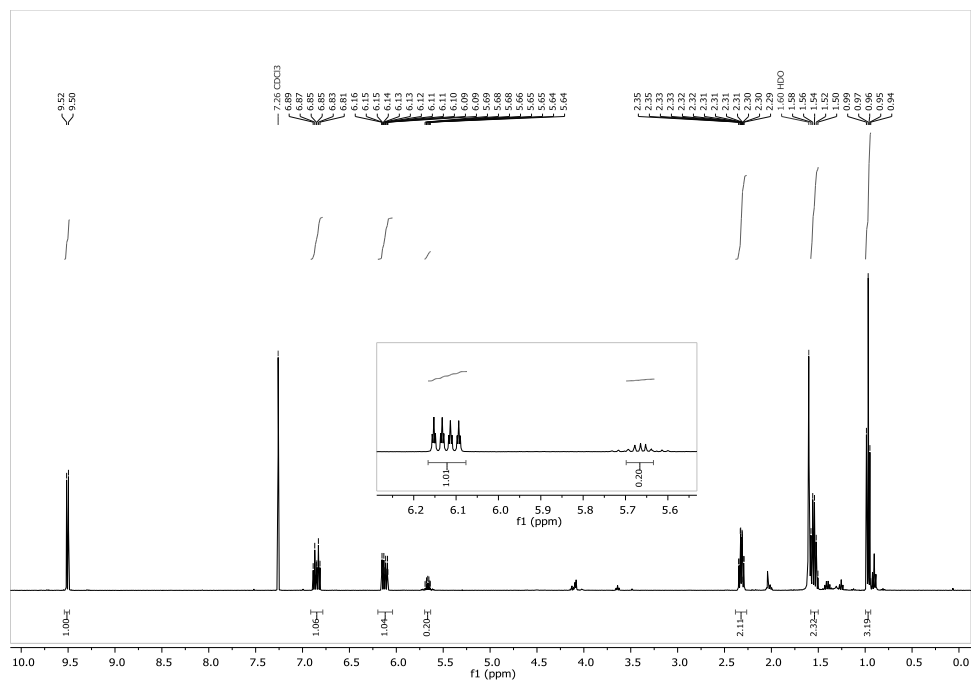


Figure 8: ¹H NMR of the isolated oxidized product.

References

1. Sheldon, R.A. and I.W.C.E. Arends, *Organocatalytic oxidations mediated by nitroxyl radicals*. Advanced Synthesis & Catalysis, 2004. **346**(9-10): p. 1051-1071.
2. Sheldon, R.A., et al., *Green, catalytic oxidations of alcohols*. Accounts of Chemical Research, 2002. **35**(9): p. 774-781.
3. ten Brink, G.J., I. Arends, and R.A. Sheldon, *Green, catalytic oxidation of alcohols in water*. Science, 2000. **287**(5458): p. 1636-1639.
4. Alshammari, H., et al., *Control of the selectivity in multi-functional group molecules using supported gold-palladium nanoparticles*. Green Chemistry, 2013. **15**(5): p. 1244-1254.
5. Procter, G., 2.9 - *oxidation adjacent to oxygen of alcohols by other methods*, in *Comprehensive Organic Synthesis*, B.M. Trost and I. Fleming, Editors. 1991, Pergamon: Oxford. p. 305-327.
6. Liu, J., S. Wu, and Z. Li, *Recent advances in enzymatic oxidation of alcohols*. Current Opinion in Chemical Biology, 2018. **43**: p. 77-86.
7. Kroutil, W., et al., *Biocatalytic oxidation of primary and secondary alcohols*. Advanced Synthesis & Catalysis, 2004. **346**(2-3): p. 125-142.
8. Dong, J.J., et al., *Biocatalytic oxidation reactions: A chemist's perspective*. Angewandte Chemie-International Edition, 2018. **57**(30): p. 9238-9261.
9. Fahlbusch, K.-G., et al., *Flavors and fragrances*. Ullmann's encyclopedia of industrial chemistry, 2003.
10. Turner, N.J., *Enantioselective oxidation of C-O and C-N bonds using oxidases*. Chemical Reviews, 2011. **111**(7): p. 4073-4087.
11. Hollmann, F., et al., *Enzyme-mediated oxidations for the chemist*. Green Chemistry, 2011. **13**: p. 226-265.
12. Kroutil, W., et al., *Recent advances in the biocatalytic reduction of ketones and oxidation of sec-alcohols*. Current Opinion in Chemical Biology, 2004. **8**(2): p. 120-126.
13. Pickl, M., et al., *The substrate tolerance of alcohol oxidases*. Applied Microbiology and Biotechnology, 2015. **99**(16): p. 6617-6642.
14. Ni, Y., D. Holtmann, and F. Hollmann, *How green is biocatalysis? To calculate is to know*. ChemCatChem, 2014. **6**(4): p. 930-943.
15. Churakova, E., I.W. Arends, and F. Hollmann, *Increasing the Productivity of Peroxidase-Catalyzed Oxyfunctionalization: A Case Study on the Potential of Two-Liquid-Phase Systems*. ChemCatChem, 2013. **5**(2): p. 565-568.
16. Bommarius, A.S. and A. Karau, *Deactivation of formate dehydrogenase (FDH) in solution and at gas-liquid interfaces*. Biotechnology Progress, 2005. **21**(6): p. 1663-1672.
17. Van Hecke, W., et al., *Bubble-free oxygenation of a bi-enzymatic system: effect on biocatalyst stability*. Biotechnology and Bioengineering, 2009. **102**(1): p. 122-131.
18. Van Hecke, W., et al., *Kinetic modeling of a bi-enzymatic system for efficient conversion of lactose to lactobionic acid*. Biotechnology and Bioengineering, 2009. **102**(5): p. 1475-1482.

19. Illner, S., et al., *A falling-film microreactor for enzymatic oxidation of glucose*. ChemCatChem, 2014. **6**(6): p. 1748-1754.
20. Kaufhold, D., et al., *Generation of Dean vortices and enhancement of oxygen transfer rates in membrane contactors for different hollow fiber geometries*. Journal of Membrane Science, 2012. **423**: p. 342-347.
21. Bolivar, J.M., et al., *Process intensification for O₂-dependent enzymatic transformations in continuous single-phase pressurized flow*. Biotechnology and Bioengineering, 2019. **116**(3): p. 503-514.
22. Gemoets, H.P.L., et al., *Liquid phase oxidation chemistry in continuous-flow microreactors*. Chemical Society Reviews, 2016. **45**(1): p. 83-117.
23. Plutschack, M.B., et al., *The hitchhiker's guide to flow chemistry(II)*. Chemical Reviews, 2017. **117**(18): p. 11796-11893.
24. Kockmann, N., et al., *Safety assessment in development and operation of modular continuous-flow processes*. Reaction Chemistry & Engineering, 2017. **2**(3): p. 258-280.
25. Gutmann, B., D. Cantillo, and C.O. Kappe, *Continuous-flow technology: A tool for the safe manufacturing of active pharmaceutical ingredients*. Angewandte Chemie-International Edition, 2015. **54**(23): p. 6688-6728.
26. Noel, T., Y. Su, and V. Hessel, *Beyond organometallic flow chemistry: The principles behind the use of continuous-flow reactors for synthesis*, in *Organometallic Flow Chemistry*, T. Noel, Editor. 2016. p. 1-41.
27. Mallia, C.J. and I.R. Baxendale, *The use of gases in flow synthesis*. Organic Process Research & Development, 2016. **20**(2): p. 327-360.
28. Tamborini, L., et al., *Flow bioreactors as complementary tools for biocatalytic process intensification*. Trends in Biotechnology, 2018. **36**(1): p. 73-88.
29. Peris, E., et al., *Tuneable 3D printed bioreactors for transaminations under continuous-flow*. Green Chemistry, 2017. **19**(22): p. 5345-5349.
30. Bolivar, J.M., J. Wiesbauer, and B. Nidetzky, *Biotransformations in microstructured reactors: more than flowing with the stream?* Trends in Biotechnology, 2011. **29**(7): p. 333-342.
31. Zor, C., et al., *H₂-Driven biocatalytic hydrogenation in continuous flow using enzyme-modified carbon nanotube columns*. Chemical Communications, 2017. **53**(71): p. 9839-9841.
32. Tang, X., R.K. Allemann, and T. Wirth, *Optimising terpene synthesis with flow biocatalysis*. European Journal of Organic Chemistry, 2017(2): p. 414-418.
33. Tomaszewski, B., et al., *Regioselective biocatalytic aromatic hydroxylation in a gas-liquid multiphase tube-in-tube reactor*. ChemCatChem, 2014. **6**(9): p. 2567-2576.
34. Jones, E., et al., *Biocatalytic oxidase: Batch to continuous*. Chemical Engineering Research & Design, 2012. **90**(6): p. 726-731.
35. Gasparini, G., et al., *Scaling up biocatalysis reactions in flow reactors*. Organic Process Research & Development, 2012. **16**(5): p. 1013-1016.
36. Ruiz-Dueñas, F.J., et al., *In vitro activation, purification, and characterization of Escherichia coli expressed aryl-alcohol oxidase, a unique H₂O₂-producing enzyme*. Protein expression and purification, 2006. **45**(1): p. 191-199.

37. Bühler, B., et al., *Use of the two-liquid phase concept to exploit kinetically controlled multistep biocatalysis*. Biotechnology and bioengineering, 2003. **81**(6): p. 683-694.
38. Schmid, A., et al., *Preparative regio-and chemoselective functionalization of hydrocarbons catalyzed by cell free preparations of 2-hydroxybiphenyl 3-monooxygenase*. Journal of Molecular Catalysis B: Enzymatic, 2001. **11**(4-6): p. 455-462.
39. Schmid, A., et al., *Integrated biocatalytic synthesis on gram scale: The highly enantio selective preparation of chiral oxiranes with styrene monooxygenase*. Advanced Synthesis & Catalysis, 2001. **343**(6-7): p. 732-737.
40. Wu, X., et al., *Enantioselective synthesis of ethyl (S)-2-hydroxy-4-phenylbutyrate by recombinant diketoreductase*. Tetrahedron: Asymmetry, 2009. **20**(21): p. 2504-2509.
41. Gandolfi, R., N. Ferrara, and F. Molinari, *An easy and efficient method for the production of carboxylic acids and aldehydes by microbial oxidation of primary alcohols*. Tetrahedron Letters, 2001. **42**(3): p. 513-514.
42. Molinari, F., et al., *Biotransformations in two-liquid-phase systems: production of phenylacetaldehyde by oxidation of 2-phenylethanol with acetic acid bacteria*. Enzyme and Microbial Technology, 1999. **25**(8-9): p. 729-735.
43. Churakova, E., et al., *Hydrophobic formic acid esters for cofactor regeneration in aqueous/organic two-liquid phase systems*. Topics in Catalysis, 2014. **57**(5): p. 385-391.
44. Ni, Y., et al., *A biocatalytic hydrogenation of carboxylic acids*. Chemical Communications, 2012. **48**(99): p. 12056-12058.
45. Karande, R., et al., *Biocatalytic conversion of cycloalkanes to lactones using an in-vivo cascade in Pseudomonas taiwanensis VLB120*. Biotechnology and bioengineering, 2018. **115**(2): p. 312-320.
46. Bornadel, A., et al., *Enhancing the productivity of the bi-enzymatic convergent cascade for ϵ -caprolactone synthesis through design of experiments and a biphasic system*. Tetrahedron, 2016. **72**(46): p. 7222-7228.
47. Kara, S., et al., *Access to lactone building blocks via horse liver alcohol dehydrogenase-catalyzed oxidative lactonization*. ACS Catalysis, 2013. **3**(11): p. 2436-2439.
48. Pennec, A., et al., *One-pot conversion of cycloalkanes to lactones*. ChemCatChem, 2015. **7**(2): p. 236-239.
49. Pennec, A., et al., *Revisiting cytochrome P450-mediated oxyfunctionalization of linear and cyclic alkanes*. Advanced Synthesis & Catalysis, 2015. **357**(1): p. 118-130.
50. Ferreira, P., et al., *Spectral and catalytic properties of aryl-alcohol oxidase, a fungal flavoenzyme acting on polyunsaturated alcohols*. Biochemical Journal, 2005. **389**: p. 731-738.
51. Guillen, F., A.T. Martinez, and M.J. Martinez, *Substrate-specificity and properties of the aryl-alcohol oxidase from the ligninolytic fungus Pleurotus eryngii*. European Journal of Biochemistry, 1992. **209**(2): p. 603-611.

52. Guillén, F., A.T. Martinez, and M.J. Martínez, *Production of hydrogen peroxide by aryl-alcohol oxidase from the ligninolytic fungus Pleurotus eryngii*. Applied Microbiology and Biotechnology, 1990. **32**(4): p. 465-469.
53. Bormann, S., et al., *Specific oxyfunctionalisations catalysed by peroxygenases: opportunities, challenges and solutions*. Catalysis Science & Technology, 2015. **5**(4): p. 2038-2052.
54. Pedersen, A.T., et al., *Process requirements of galactose oxidase catalyzed oxidation of alcohols*. Organic Process Research & Development, 2015. **19**(11): p. 1580-1589.
55. Tufvesson, P.r., et al., *Guidelines and cost analysis for catalyst production in biocatalytic processes*. Organic Process Research & Development, 2010. **15**(1): p. 266-274.

Chapter 9



Discussion

Discussion

As the recent Noble prize in chemistry shows [1], biocatalysis steadily increases its mark on how we perform chemical catalysis. The ability of enzymes to catalyse reactions with high selectivity, atom efficiency and under mild conditions makes them the perfect solution to our pressing issue of making our chemical industry “greener” [2]. Where we used to rely on cell extracts and, later, isolated proteins to perform these reactions, we now poses the computational tools to mine and engineer these catalysts for and increasing amount of examples [3]. Whether we have access to certain biocatalytic reactions thus becomes less of an issue. A challenge that remains is how to perform these reactions, especially if electron transfers are involved.

In this thesis, we explored an array of different possibilities to apply oxidoreductases for catalysis. The main goal was to avoid the classical scheme of nicotinamide adenine dinucleotide cofactors (NAD(P)H) and the corresponding enzymatic regeneration systems. These innovative regeneration methods will possibly open up the way to application of these oxidoreductases at a large industrial scale. The methods presented can be divided into photochemical, biocatalytic and electrochemical regeneration systems, as shown in table 1.

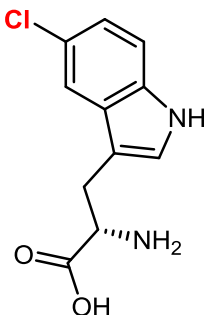
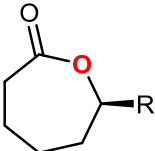
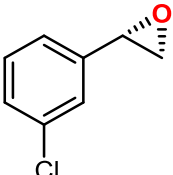
Table 1: Overview of the chapters in this thesis, organised by the method used.

Photochemistry	Biocatalysis	Electrochemistry
Chapter 3 Chapter 4 Chapter 7	Chapter 5 Chapter 8	Chapter 6

The first approach is that of photo-biocatalysis, the combined fields of photocatalysis and biocatalysis. As elaborated in **chapter 2**, the field of photo-biocatalysis is still in its infancy and far removed from application, but significant steps have been made in the past few years. To contribute to this field, a photo-regeneration system for reduced flavin adenine dinucleotide (FADH₂) was designed in **chapter 3** to drive the diffusible flavin dependent styrene monooxygenase (StyA). By direct photochemical regeneration of the reduced coenzyme we were able to eliminate the elaborate regeneration system normally needed for this class of enzymes [4, 5], thereby greatly simplifying its reaction scheme. The proof of concept for this highly simplified reaction scheme was developed and up to 3.10 mM of

a styrene oxide derivative was obtained. Though these product concentrations are much higher than shown in previous examples with halogenases [6] and Baeyer-Villiger monooxygenases [7, 8] in comparable systems (table 2), they are still two orders of magnitudes lower than in cases where StyA was used in whole cell systems [9, 10]. This system is therefore unlikely to become relevant for industrial applications [11].

Table 2: Several examples of photo-regenerations of oxygen-dependent enzymes. The introduced heteroatom is shown in bold. In all cases, EDTA was used as the electron donor. The maximum achieved conversion and total turnover numbers for the biocatalyst are shown. PyrH: Tryptophan 5-halogenase. PAMO: Phenyl acetone monooxygenase; StyA: Styrene monooxygenase A.

Enzyme	Product	Concentration [mM]	TON	Source
PyrH		0.29	8.3	[6]
PAMO		0.98	98	[8]
StyA		3.10	585	Chapter 3

For the photo-regeneration of FADH_2 , two main limitations were identified, both stemming from the chemistry of flavins:

- (1) The photo-instability of the FAD
- (2) The oxygen dilemma [12]

The photodegradation of flavins by visible light is a phenomenon known for decades [13-16]. Upon illumination, flavins degrade to a mixture of different lumiflavin derivatives which, though still photo-active, are not accepted by these monooxygenases. Possible solutions to the side-chain alteration of FAD would be to engineer a StyA able to accept these modified variants. Previous work has shown the feasibility of changing the chemistry of monooxygenases [17-19]. Alternatively, photo-bleaching could be minimized by keeping the flavin predominantly in the reduced state, as FADH₂ is less prone to degradation (also shown in **chapter 3**). This could, for instance, be achieved by controlling the oxygen supply [20].

The second challenge, as outlined in **chapter 2**, is the paradox of oxygen and is known to occur for most reductive oxygenase reactions [12, 21]; molecular oxygen is needed as a substrate in the reaction, but simultaneously is the main cause of electron loss in the system. As this paradox is paramount for oxygendependent oxidoreductase, concentrated our efforts on solving this challenge. We applied the following three tactics:

- (1) Block the oxygen dilemma
- (2) Exploit the oxygen dilemma
- (3) Turning around the oxygen dilemma

Block the oxygen dilemma

To block the oxygen dilemma, we intended to extend the work of the Reetz group using deazaflavins as the mediator [22]. This was elaborated in **chapter 4**. We found that deazaflavins could indeed function as catalytic photoactive mediators in anaerobic systems with ene-reductases and that the reduced species were indeed more stable against oxygen [23-28]. However, these analogues were not necessarily more resilient to oxygen-uncoupling upon illumination. This was attributed to the formation of radical species through disproportionation and subsequent reactions with oxygen, which results in the formation of hydrogen peroxide [28]. The deazaflavins are therefore not a viable

solution for the oxygen dilemma. A question that arises, is how the Reetz group was able to use this mediator for their CYP450 catalysed reactions. A theory could be the following:

It should be noted that, next to the deazaflavin, a catalytic amount of NADP^+ was added to their reactions, supposedly for stabilizing the enzyme structure. In the supporting information of the paper [22], the author states that the NADP^+ was not reduced by the deazaflavin, which indeed only happens under anaerobic conditions [**chapter 3**]. However, under partially anaerobic conditions, possibly caused by the depletion of oxygen by the reaction with deazaflavin, some NADPH might have been formed, directly driving the CYP450 reaction. As regular flavins are not able to directly reduce NADPH, their negative controls did indeed give no conversion.

Concluding, to block the oxygen dilemma, the pursuit for the ideal mediator is still ongoing. The mediator should be one that is photoexcitable and exclusively transfers hydrides, also upon excitation. One should wonder, though, if such a mediator even exists. In absence of light, deazaflavins are oxygen insensitive as their redox-chemistry is restricted to hydride transfers. However, this chemistry changes upon illumination, as the formation of radicals become possible. These traits are also observed for the related nicotinamide cofactors. This can be used to one's advantage, for instance as done by the group of Hyster [29, 30]. In relation to solve the oxygen dilemma however, one should rather focus on other options.

Exploit the oxygen dilemma

The second approach to deal with the oxygen dilemma was to reverse the uncoupling of the electrons *via* hydrogen peroxide. In other words, we focussed enzymes that can accept H_2O_2 to form the active oxidizing species in the active site: peroxygenases [31-34].

The use of H_2O_2 as a substrate is not straightforward, as addition of stoichiometric amounts of the peroxide to the solution can trigger several unwanted side-reactions like enzyme inactivation [31, 35]. To solve these challenges [36], we explored three different methodologies for the *in situ* generation of H_2O_2 : a biocatalytic method in **chapter 5**, an electrochemical method in **chapter 6** and a photochemical method using semiconductors in **chapter 7**.

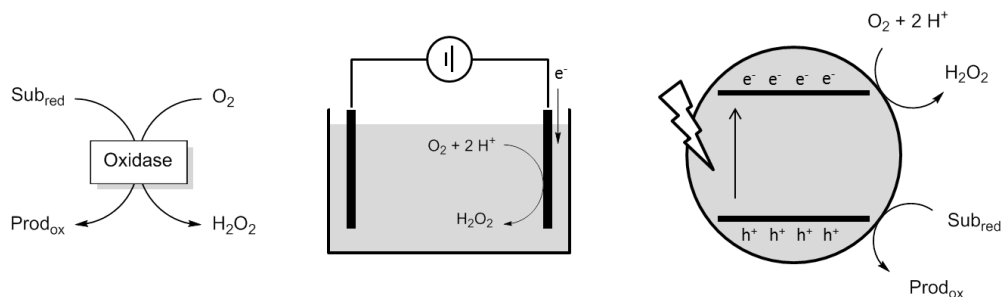


Figure 2: Schematic overview of the three methods used for the *in situ* generation of H_2O_2 . From left to right: the biocatalytic, the electrochemical and the photochemical method.

The applicability of sulphite oxidase (SO) to produce H_2O_2 was investigated in **chapter 5**. SO uses a small electron donor (MW sulphite = 80 g mol^{-1}) to generate the reductive equivalents for rAaeUPO catalysed reactions [37, 38]. As shown in table 3, the system still falls behind in turnover numbers and frequencies as compared to, for instance, FOx [39-41]. This can be *i.a.* attributed to the varying pH profiles between SO and most peroxygenases. However, the use of the sulphite as a nucleophile in follow-up reactions did open up some interesting cascades [42]. In a similar fashion, future work could focus on oxidases able to oxidize other inorganic salts, like nitrite oxidoreductase. Finally, in contrast to FOx, SO is abundant in all kingdoms in life and a better performing variant should therefore be easily attainable.

Table 3: Overview of several biocatalytic H_2O_2 generation methods reported in literature. TON: Total turnover number. GOx: Glucose oxidase. FDH: Formate dehydrogenase. YqjM: Ene-reductase for *Bacillus subtilis*. FOx: Formate oxidase. SO: Sulphite oxidase.

Regeneration enzyme	Co-substrate (MW [g mol^{-1}])	Regeneration enzyme (TON)	Peroxygenase (TON)	Source
GOx	Glucose (180)	1163	43 100	[31, 43-45]
FDH / YqjM	HCO_2H (40)	FDH: 39 000 YqjM: 3 600	390 000	[46]
FOx	HCO_2H (40)	318 000	31 800	[47]
SO	SO_3^{2-} (80)	17 000	34 000	Chapter 5

Considering atom efficiency and sustainability, the ideal source of electrons would be the electrons themselves in the form of electricity [48-51]. Especially as electricity itself can be generated in environmentally benign manners. One major shortcoming in this scheme is the relative high overpotential needed to achieve significant O₂ reduction rate at the cathode, which results in unnecessary power expenses. Inspired by a recent contribution by Cui's group [52], we demonstrated that cathodes doped with oxidized carbon nanotubes are able to produce H₂O₂ at much lower overpotentials in **chapter 6**. Already in the proof of principle study, several hundreds of milligrams of product were obtained, thereby showing an opening to a practical application [53]. It should be noted that, instead of the rAaeUPO used in **chapter 5** and **chapter 7**, a significantly more stable vanadium-containing chloroperoxidase (VCPO) was used in this study [54]. Nevertheless, as the conditions used for these experiments were not remarkably harsh, similar results can be expected when coupling this reaction to other peroxygenases. Though the electrochemical approach appears to be the best on paper, unique challenges can be foreseen when one attempts to scale up these reactions as the electrode surface will limit the reaction rates.

Photochemical generation of H₂O₂ occurs *via* a photo-excitabile compound able to take electrons from a sacrificial donor and to pass them on to oxygen [47, 55, 56]. Incidentally, this was the unwanted phenomenon in **chapter 3** and **chapter 4**. For heterogeneous photo-catalysts, not many examples are reported besides titanium dioxide (TiO₂) based systems, which is why we aimed at expanding this field [57-59]. In **chapter 7**, we found graphitic carbon nitride (g-C₃N₄) to be a very promising catalyst in a cascade with the unspecific peroxygenase from *Agrocyste aegerita* (rAaeUPO). Upon illumination with visible light, conversions in the same order of magnitude were obtained as compared to gold-doped titanium dioxide (Au-TiO₂). An important advantage of the g-C₃N₄ over Au-TiO₂ is the absence of noble metals in this catalyst [60, 61]. A comparison of several photochemical H₂O₂ generation methods in combination with biocatalysts are shown in table 4.

Chapter9

Table 4: overview of literature on the photo-generation of H₂O₂ for biocatalytic purposes. FMN: Flavin mononucleotide. MB: Methylene blue. PS: Phenosafranin. FDH: Formate dehydrogenase. Au-TiO₂: Gold doped titanium dioxide. g-C₃N₄: graphitic carbon nitride. EDTA: Ethylenediaminetetraacetic acid. MES: 2-(N-morpholino)ethanesulfonic acid. *rAaeUPO*: Unspecific peroxygenase from *Agrocybe aegerita*. *AmVHPO*: Vanadium-dependent haloperoxidase from *Acaryochloris marina* MBIC 11017.

Photo-catalyst	Electron donor	Enzyme	Max product concentration [mM]	Enzyme TON	Source
Homogeneous					
FMN	EDTA	<i>rAaeUPO</i>	7.2	18 080	[56]
FMN / MB / PS (+ FDH)	Formate	<i>rAaeUPO</i>	10	100 000	[47]
FMN	MES	<i>AmVHPO</i>	6.9	4 300	[58]
Heterogeneous					
Au-TiO ₂	Formate	<i>rAaeUPO</i>	12.6	84 000	[59]
Au-TiO ₂	Water	<i>rAaeUPO</i>	2.9	38 800	[57]
Au-TiO ₂	Water	<i>AmVHPO</i>	5.5	3 400	[58]
g-C ₃ N ₄	Formate	<i>rAaeUPO</i>	6.1	61 300	Chapter 7

The process limiting this system appeared to be the stability of the biocatalyst, which we found to originate from the formation of radicals at the g-C₃N₄ surface. As shown before in **chapter 3** and **chapter 4**, the challenge in combining photocatalysis and biocatalysis appeared to be the lack of chemoselectivity of the photocatalyst. In **chapter 3** several uncoupling and degeneration reactions occurred at the FAD, in **chapter 4** uncoupling and dimerization occurred for the mediator and with g-C₃N₄ in **chapter 7**, over-oxidation and enzyme oxidation were observed. Reaction separation was presented in **chapter 7** as a solution to this challenge. By keeping the biocatalytic and photocatalytic reactions

physically separated, reactive oxygen species would be dismutated before they caused damage to the enzyme. We therefore believe that, next to reaction design, reactor design will play a vital role in the progression of photo-biocatalysis.

For photo-biocatalytic reaction systems, one has the choice between two types of photocatalysts: either homogeneous mediators ([47], **chapter 3**) or heterogeneous semiconductors ([62], **chapter 7**). In general, homogeneous mediators can accept photons of longer wavelengths while still able to provide relatively high rates. On the downside, continuous photo-bleaching of the catalyst requires a constant replacement of these relatively complex compounds to the reaction. Contrarily, heterogeneous photocatalysts are generally cheap and easy to make and are easily separated from the reaction mixture. Moreover, semiconductor poisoning appears to occur at much lower rates than photodegradation is for mediators, though the reaction rates reported are also much lower (table 5). Also, high energy photons are needed to bridge the relatively high band gap of the semiconductors, which in turn are more likely to participate in side reactions. Finally, so far, the focus of heterogeneous catalysts has mainly been on generating H_2O_2 , while photo-mediators have also been shown to reduce other coenzymes [63, 64]. Altogether, the photocatalyst of choice will depend on the product of interest. In general, the cost contribution of semiconductors will be lower and thus be more suitable for bulk products whereas mediators are more suitable for specialized products.

Chapter9

Table 5: Comparison of cost and performance of homogeneous and heterogeneous photocatalysts in biocatalytic processes. FAD: Flavin adenine dinucleotide. dRf: deazariboflavin. FMN: Flavin mononucleotide. g-C₃N₄: graphitic carbon nitride. TiO₂: titanium dioxide. [a]: As found on Sigma Aldrich. [b]: Not commercially available. [c]: The light spectrum was only partially overlapping with the absorption spectrum, hence the low rate and long catalyst lifetime. [d]: Considering the synthesis methods in **chapter 7**. [e] from where absorption starts, depending on the morphology.

Photo-Catalyst (product)	Catalyst cost [€ g ⁻¹]	Catalyst concentration [g L ⁻¹]	λ max [nm]	Reaction rate [mM min ⁻¹]	Catalyst lifetime [h]	Source
Homogeneous						
FAD (FADH ₂)	380 [a]	0.16	450	3.10	1.0	Chapter 3
dRf (NADH)	- [b]	0.026	400	0.62 [c]	10	[64]
FMN (NAD ⁺)	2.50 [a]	0.001	450	8.0	3	[63]
FMN (H ₂ O ₂)	2.50 [a]	0.024	450	15.0	30	[65]
Heterogeneous						
g-C ₃ N ₄ (H ₂ O ₂)	0.56 [d]	5.0	300 [e]	0.33	> 100	Chapter 7
TiO ₂ (H ₂ O ₂)	0.27 [a]	2.0	< 300	2.6	-	[66]

Turn around the oxygen dilemma

The final method to deal with the oxygen dilemma was to turn around the oxygen dilemma. In other words, we focused on enzymes that actually use the elimination of H₂O₂ from the C4a-peroxide flavin intermediate as their mechanisms: the oxidases [67, 68]. In this case H₂O₂ is actually a by-product of the reaction, which can be dismutated by catalase. From a mechanistic point of view, these enzymes are significantly more applicable than their dehydrogenase counterparts. In **chapter 8**, we showed the industrial

potential of such a system as we produced over a molar of an industrially relevant product using aryl alcohol oxidases (AAOx).

In these reactions, not the enzyme but the reactor properties became the limiting factor of the reaction. This limitation shows itself in phase transfer limitations, which we managed to tackle via reactor design. The limitation of oxygen availability [69] was countered by performing the reaction in a segmented flow reactor. The availability of the substrate was improved by performing the reaction in a two liquid phase system. This way, we were able to increase the total turnover number of the enzyme to 2.2 million, paving the way for a role in larger segments than the fine chemical industry [53]. A combination of these two methods can be envisioned to even further improve the system. This would imply a three-phase system (gas – aqueous – organic) in a flow setup, as the Taylor flow should also maximize mixing between the aqueous and organic phase [70]. To further improve the relevance of oxidases for industry, new variants are needed to enlarge the substrate scope. Also, the enzyme production procedure needs to be simplified [71], since the refolding from inclusion bodies as done in **chapter 8**, will make the catalyst too expensive for application [53]. At the moment, both groups of Urlacher and Alcalde focus on the production of these catalysts in yeast, to circumvent the formation of inclusion bodies [71].

Conclusion

As stated before, the different oxidoreductase regeneration techniques shown in this thesis can generally be divided in one of three categories: biocatalytic, electrochemical and photochemical. Of these three methods, the biocatalytic regeneration of the active site is the most abundantly applied technique, both in academia as in industry. The dominance of this method, as compared to the other two, can be explained in several ways. The first one is simply the preference of those working with enzymes as catalysts; scientists in the field of biocatalysis will look for biocatalytic solutions to their challenges. Furthermore, as most enzymes generally require similar mesotrophic reaction conditions, combining them in cascades will require less reaction and reactor engineering, reducing the gap to application. For these reasons, the highest amounts of product and enzyme turnovers are reported for these systems (table 3 vs. table 4). On the other hand, from a scientific point of view, this field is quite saturated. For both the regeneration of NADH as generation of H_2O_2 , the “ideal” cosubstrate, formate, with the coproduct CO_2 leaving the reaction, is made available by formate dehydrogenase (FDH) and formate oxidase (FOx) respectively. New contributions, as in **chapter 5**, can still be developed, but the basic principles will stay the same.

Electrochemistry for oxidoreductase regeneration can be considered as less established, though **chapter 6** shows great promise for the combination of these fields, especially in combination with peroxygenases. In literature, the focus mainly lies on electrode and reactor design. Electrode design is needed to make the reaction more selective and to decrease required overpotentials. On the other hand, reactor design is of vital importance in electrochemistry, as the electrode surface area becomes decisive when scaling up [20, 72]. To retain a relative high surface area is important to increase productivity and decrease hot-spot formation. Segmented flow reactors, as used in **chapter 8**, might be able to play an important role in this process, as it will tackle both challenges of electrode surface area and oxygen supply, if required [73]. If these challenges are met, electrochemistry will most probably turn out to be the most promising method in the work with oxidoreductases, mostly because no sacrificial electron donors are needed.

As elaborated in **chapter 2**, photochemistry is still the least developed of the three methods. Consequently, some significant challenges emerge when designing these reactions, even on small scales. These challenges mainly originate from the lack of chemo-selectivity of light as a reactant. Though ideally solely the photo-catalyst should be excited, photons can also interact with the substrate, product, biocatalyst and other mediators in the reactions, initiating side reactions. This effect becomes more prominent as photons of higher energy are required or if a substrate contains aromatic groups. Furthermore, even if the mediator is excited selectively, chemo-selectivity can remain poor as these catalyst can perform side reactions, both intra- (**chapter 3**) as extra- (**chapter 7**) molecular.

In an attempt to scale up these reactions, challenges will emerge related to light penetration. With the increase of the reactor volume scaling up the photo reactor dimensions is required while increase in the reaction rate requires an increase in photocatalyst concentration [66]. Both challenges could be solved by increasing the reactor surface area. As with electrochemistry, flow reactors could play an important role in this process, even if heterogeneous catalysts are used [70, 74]. Furthermore, photocatalysts with better chemo-selectivity and increased photo-stability are needed. Though significant effort is made to design new catalysts, the collection of remaining issues will always make photo-biocatalysis lack behind the other alternatives.

At the moment, biocatalysis in industry is dominated by hydrolases and isomerases. The growing possibilities to further optimize these catalysts via protein engineering will hopefully ensure that, in the near future, enzymes will play a major role in our chemical industry [3]. Redox reactions catalysed by oxidoreductases are still a source of untapped

potential for this purpose [11, 75]. One reason for the slow adaptation of this class of enzymes are the relatively complicated reaction sequences needed for electron transfer. However, this is also what makes this field so exciting from an academic point of view; there are no singular solutions to all these challenges. In this thesis, we have shown several approaches to simplify reaction schemes to make the existing systems more applicable. Furthermore, we have shown that we can still look out for new biocatalysts for new reactions, even if the enzymes themselves are already known for decades. Finally, we showed reaching turnover numbers in the millions is possible for biocatalysts if one steps away from the conventional aqueous batch reactions. All together, we hope to have offered several tools to smoothen the way of these very promising catalysts to an application for our chemical industry and thus our daily lives.

References

1. Arnold, F.H., G.P. Smith, and G.P. Winter, *Directed evolution—bringing the power of evolution to the laboratory: 2018 Nobel Prize in Chemistry*. Current Science, 2018. **115**(9): p. 1627.
2. Sheldon, R.A. and J.M. Woodley, *Role of biocatalysis in sustainable chemistry*. Chemical Reviews, 2018. **118**(2): p. 801-838.
3. Bornscheuer, U., et al., *Engineering the third wave of biocatalysis*. Nature, 2012. **485**(7397): p. 185.
4. Heine, T., et al., *Two-component FAD-dependent monooxygenases: current knowledge and biotechnological opportunities*. Biology-Basel, 2018. **7**(3): p. 42-Article No.: 42.
5. Otto, K., et al., *Biochemical characterization of StyAB from Pseudomonas sp strain VLB120 as a two-component flavin-diffusible monooxygenase*. Journal of Bacteriology, 2004. **186**(16): p. 5292-5302.
6. Schroeder, L., et al., *Photochemically driven biocatalysis of halogenases for the green production of chlorinated compounds*. ChemCatChem, 2018. **10**(15): p. 3336-3341.
7. Hollmann, F., et al., *A light-driven stereoselective biocatalytic oxidation*. Angew Chem Int Ed Engl, 2007. **46**(16): p. 2903-6.
8. Taglieber, A., et al., *Light-driven biocatalytic oxidation and reduction reactions: scope and limitations*. ChemBioChem, 2008. **9**(4): p. 565-572.
9. Toda, H., R. Imae, and N. Itoh, *Efficient biocatalysis for the production of enantiopure (S)-epoxides using a styrene monooxygenase (SMO) and Leifsonia alcohol dehydrogenase (LSADH) system*. Tetrahedron: Asymmetry, 2012. **23**(22-23): p. 1542-1549.
10. Schmid, A., et al., *Integrated biocatalytic synthesis on gram scale: The highly enantio selective preparation of chiral oxiranes with styrene monooxygenase*. Advanced Synthesis & Catalysis, 2001. **343**(6-7): p. 732-737.
11. Huisman, G.W. and S.J. Collier, *On the development of new biocatalytic processes for practical pharmaceutical synthesis*. Current Opinion in Chemical Biology, 2013. **17**(2): p. 284-292.
12. Holtmann, D. and F. Hollmann, *The oxygen dilemma: A severe challenge for the application of monooxygenases?* ChemBioChem, 2016. **17**(15): p. 1391-1398.
13. Holzer, W., et al., *Photo-induced degradation of some flavins in aqueous solution*. Chemical Physics, 2005. **308**(1-2): p. 69-78.
14. Song, P.S. and D.E. Metzler, *Photochemical degradation of flavins. 4. Studies of anaerobic photolysis of riboflavin*. Photochemistry and Photobiology, 1967. **6**(10): p. 691-&.
15. Moore, W.M., et al., *Photochemistry of riboflavin. I. The hydrogen transfer process in the anaerobic photobleaching of flavins*. Journal of the American Chemical Society, 1963. **85**(21): p. 3367-3372.
16. Sheraz, M.A., et al., *Photo, thermal and chemical degradation of riboflavin*. Beilstein Journal of Organic Chemistry, 2014. **10**: p. 1999-2012.
17. Brondani, P.B., et al., *Finding the switch: Turning a Baeyer–Villiger monooxygenase into a NADPH oxidase*. Journal of the American Chemical Society, 2014. **136**(49): p. 16966-16969.
18. Leferink, N.G.H., et al., *Identification of a gatekeeper residue that prevents dehydrogenases from acting as oxidases*. Journal of Biological Chemistry, 2009. **284**(7): p. 4392-4397.
19. Huijbers, M.M.E., et al., *Proline dehydrogenase from Thermus thermophilus does not discriminate between FAD and FMN as cofactor*. Scientific Reports, 2017. **7**: p. 13.
20. Ruinatscha, R., et al., *Productivity of selective electroenzymatic reduction and oxidation reactions: Theoretical and practical considerations*. Advanced Synthesis & Catalysis, 2006. **348**(15): p. 2015-2026.

21. Holtmann, D., et al., *The taming of oxygen: biocatalytic oxyfunctionalisations*. Chemical Communications, 2014. **50**(87): p. 13180-13200.
22. Zilly, F.E., et al., *Deazaflavins as mediators in light-driven cytochrome P450 catalyzed hydroxylations*. Chemical Communications, 2009(46): p. 7152-7154.
23. Hemmerich, P., V. Massey, and H. Fenner, *Flavin and 5-deazaflavin - chemical evaluation of modified flavoproteins with respect to mechanisms of redox biocatalysis*. FEBS Letters, 1977. **84**(1): p. 5-21.
24. Heelis, P.F., et al., *One-electron reduction of 5 deazalumiflavin in aqueous-solution - a pulse radiolysis study*. International Journal of Radiation Biology, 1989. **55**(4): p. 557-562.
25. Bliese, M., et al., *Photo-reduction of deazaflavin - spectroscopic investigations*. Australian Journal of Chemistry, 1983. **36**(9): p. 1873-1883.
26. Goldberg, M., et al., *Structure and properties of 5-deazaflavin radicals as compared to natural flavosemiquinones*. Biochimica Et Biophysica Acta, 1981. **673**(4): p. 570-593.
27. Knappe, W.R., et al., *Photochemical formation of deazaflavin dimers*. Biochemistry, 1978. **17**(1): p. 16-7.
28. Duchstein, H.J., et al., *(Photo)chemistry of 5-deazaflavin - clue to the mechanism of flavin dependent (de)hydrogenation*. European Journal of Biochemistry, 1979. **95**(1): p. 167-181.
29. Biegasiewicz, K.F., et al., *Catalytic promiscuity enabled by photoredox catalysis in nicotinamide-dependent oxidoreductases*. Nature Chemistry, 2018. **10**(7): p. 770-775.
30. Emmanuel, M.A., et al., *Accessing non-natural reactivity by irradiating nicotinamide-dependent enzymes with light*. Nature, 2016. **540**: p. 414.
31. van Rantwijk, F. and R.A. Sheldon, *Selective oxygen transfer catalysed by heme peroxidases: synthetic and mechanistic aspects*. Current Opinion in Biotechnology, 2000. **11**(6): p. 554-564.
32. Hofrichter, M. and R. Ullrich, *Oxidations catalyzed by fungal peroxygenases*. Current Opinion in Chemical Biology, 2014. **19**: p. 116-125.
33. Wever, R. and P. Barnett, *Vanadium chloroperoxidases: The missing link in the formation of chlorinated compounds and chloroform in the terrestrial environment?* Chemistry-an Asian Journal, 2017. **12**(16): p. 1997-2007.
34. Wang, Y.H., et al., *Peroxygenases en route to becoming dream catalysts. What are the opportunities and challenges?* Current Opinion in Chemical Biology, 2017. **37**: p. 1-9.
35. Valderrama, B., M. Ayala, and R. Vazquez-Duhalt, *Suicide inactivation of peroxidases and the challenge of engineering more robust enzymes*. Chemistry & Biology, 2002. **9**(5): p. 555-565.
36. Burek, B.O., et al., *Hydrogen peroxide driven biocatalysis*. Green Chemistry, 2019.
37. Schrader, N., et al., *The crystal structure of plant sulfite oxidase provides insights into sulfite oxidation in plants and animals*. Structure, 2003. **11**(10): p. 1251-1263.
38. Belaidi, A.A., et al., *Oxygen reactivity of mammalian sulfite oxidase provides a concept for the treatment of sulfite oxidase deficiency*. Biochemical Journal, 2015. **469**(2): p. 211-221.
39. Doubayashi, D., et al., *Formate oxidase, an enzyme of the glucose-methanol-choline oxidoreductase family, has a His-Arg pair and 8-formyl-FAD at the catalytic site*. Bioscience, Biotechnology and Biochemistry, 2011. **75**(9): p. 1662-1667.
40. Robbins, J.M., A.S. Bommarius, and G. Gadda, *Mechanistic studies of formate oxidase from Aspergillus oryzae: A novel member of the glucose-Methanol-choline oxidoreductase enzyme superfamily that oxidizes carbon acids*. Archives of Biochemistry and Biophysics, 2018. **643**: p. 24-31.
41. Tieves, F., et al., *Formate oxidase (FOx) from Aspergillus oryzae: One catalyst enables diverse H₂O₂-dependent biocatalytic oxidation reactions*. Angewandte Chemie International Edition, 2019. **58**(23): p. 7873-7877.

42. Schenck, R.T.E. and S. Kaizerman, *The reaction of bisulfite with epoxy compounds*. Journal of the American Chemical Society, 1953. **75**(7): p. 1636-1641.
43. Bankar, S.B., et al., *Glucose oxidase — An overview*. Biotechnology Advances, 2009. **27**(4): p. 489-501.
44. van de Velde, F., et al., *Improved operational stability of peroxidases by coimmobilization with glucose oxidase*. Biotechnology and Bioengineering, 2000. **69**(3): p. 286-291.
45. Pereira, P.C., I. Arends, and R.A. Sheldon, *Optimizing the chloroperoxidase-glucose oxidase system: The effect of glucose oxidase on activity and enantioselectivity*. Process Biochemistry, 2015. **50**(5): p. 746-751.
46. Pesic, M., et al., *Multienzymatic in situ hydrogen peroxide generation cascade for peroxygenase-catalysed oxyfunctionalisation reactions*. Zeitschrift Fur Naturforschung Section C-a Journal of Biosciences, 2019. **74**(3-4): p. 100-103.
47. Willot, S.J.P., et al., *Expanding the spectrum of light-driven peroxygenase reactions*. ACS Catalysis, 2019. **9**(2): p. 890-894.
48. Holtmann, D., et al., *Electroenzymatic process to overcome enzyme instabilities*. Catalysis Communications, 2014. **51**: p. 82-85.
49. Choi, D.S., et al., *Photoelectroenzymatic oxyfunctionalization on flavin-hybridized carbon nanotube electrode platform*. ACS Catalysis, 2017. **7**(3): p. 1563-1567.
50. Getrey, L., et al., *Enzymatic halogenation of the phenolic monoterpenes thymol and carvacrol with chloroperoxidase*. Green Chemistry, 2014. **16**(3): p. 1104-1108.
51. Horst, A.E.W., et al., *Electro-enzymatic hydroxylation of ethylbenzene by the evolved unspecific peroxygenase of *Agrocye aegerita**. Journal of Molecular Catalysis B: Enzymatic, 2016. **133**: p. S137-S142.
52. Lu, Z., et al., *High-efficiency oxygen reduction to hydrogen peroxide catalysed by oxidized carbon materials*. Nature Catalysis, 2018. **1**(2): p. 156.
53. Tufvesson, P., et al., *Guidelines and Cost Analysis for Catalyst Production in Biocatalytic Processes*. Organic Process Research & Development, 2011. **15**(1): p. 266-274.
54. Dong, J.J., et al., *Halofunctionalization of alkenes by vanadium chloroperoxidase from *Curvularia inaequalis**. Chemical Communications, 2017. **53**(46): p. 6207-6210.
55. Perez, D.I., et al., *Visible light-driven and chloroperoxidase-catalyzed oxygenation reactions*. Chemical Communications, 2009(44): p. 6848-6850.
56. Churakova, E., et al., *Specific photobiocatalytic oxyfunctionalization reactions*. Angewandte Chemie International Edition, 2011. **50**(45): p. 10716-10719.
57. Zhang, W., et al., *Selective aerobic oxidation reactions using a combination of photocatalytic water oxidation and enzymatic oxyfunctionalizations*. Nature Catalysis, 2018. **1**(1): p. 55-62.
58. Seel, C.J., et al., *Atom-economic electron donors for photobiocatalytic halogenations*. ChemCatChem, 2018. **10**(18): p. 3960-3963.
59. Zhang, W., et al., *Selective activation of C–H bonds in a cascade process combining photochemistry and biocatalysis*. Angewandte Chemie International Edition, 2017. **56**(48): p. 15451-15455.
60. Kumar, S., S. Karthikeyan, and A. Lee, *g-C3N4-based nanomaterials for visible light-driven photocatalysis*. Vol. 8. 2018. 74.
61. Shiraishi, Y., et al., *Highly selective production of hydrogen peroxide on graphitic carbon nitride (g-C3N4) photocatalyst activated by visible light*. ACS Catalysis, 2014. **4**(3): p. 774-780.
62. Zhang, W.Y., et al., *Selective aerobic oxidation reactions using a combination of photocatalytic water oxidation and enzymatic oxyfunctionalizations*. Nature Catalysis, 2018. **1**(1): p. 55-62.

63. Rauch, M., et al., *Photobiocatalytic alcohol oxidation using LED light sources*. Green Chemistry, 2017. **19**(2): p. 376-379.
64. Hofler, G.T., et al., *A Photoenzymatic NADH Regeneration System*. ChemBioChem, 2018. **19**(22): p. 2344-2347.
65. Churakova, E., I.W.C.E. Arends, and F. Hollmann, *Increasing the productivity of peroxidase-catalyzed oxyfunctionalization: A case study on the potential of two-liquid-phase systems*. ChemCatChem, 2013. **5**(2): p. 565-568.
66. Burek, B.O., et al., *Photoenzymatic hydroxylation of ethylbenzene catalyzed by unspecific peroxygenase: Origin of enzyme inactivation and the impact of light intensity and temperature*. ChemCatChem. **11**(13): p. 3093-3100.
67. Chaiyen, P., M.W. Fraaije, and A. Mattevi, *The enigmatic reaction of flavins with oxygen*. Trends in Biochemical Sciences, 2012. **37**(9): p. 373-380.
68. Joosten, V. and W.J.H. van Berkel, *Flavoenzymes*. Current Opinion in Chemical Biology, 2007. **11**(2): p. 195-202.
69. Woodley, J.M., *Reaction engineering for the industrial implementation of biocatalysis*. Topics in Catalysis, 2019.
70. Plutschack, M.B., et al., *The hitchhiker's guide to flow chemistry*. Chemical Reviews, 2017. **117**(18): p. 11796-11893.
71. Viña-Gonzalez, J., et al., *Functional expression of aryl-alcohol oxidase in Saccharomyces cerevisiae and Pichia pastoris by directed evolution*. Biotechnology and Bioengineering, 2018. **115**(7): p. 1666-1674.
72. Ruinatscha, R., et al., *Productive asymmetric styrene epoxidation based on a next generation electroenzymatic methodology*. Advanced Synthesis & Catalysis, 2009. **351**(14-15): p. 2505-2515.
73. Laudadio, G., et al., *An environmentally benign and selective electrochemical oxidation of sulfides and thiols in a continuous-flow microreactor*. Green Chemistry, 2017. **19**(17): p. 4061-4066.
74. Pieber, B., et al., *Continuous heterogeneous photocatalysis in serial micro-batch reactors*. Angewandte Chemie International Edition, 2018. **57**(31): p. 9976-9979.
75. Martinez, A.T., et al., *Oxidoreductases on their way to industrial biotransformations*. Biotechnology Advances, 2017. **35**(6): p. 815-831.

Curriculum Vitae



Morten Martinus Cornelis Harald van Schie was born on the 15th of June in 1990 in Veghel in the Netherlands. Though half Norwegian, he was mainly raised Dutch. He grew up in Veghel and went to high school “het Zwijsen College” following both tracks of Natuur en Gezondheid and Natuur en Techniek. At 18 years old he moved to the west of the Netherlands for his bachelors Life Science and Technology, a combinational study between the TU Delft and the university of Leiden. During this time, he was on the boards of the Beta Banenmarkt and the Plaatselijke Kamer van Verenigingen. When he finished his bachelors, he continued his master Life Science and Technology in Delft. During his masters, he focussed on the tracks of Cell Factory and Biocatalysis. For his master thesis, he joined the group of BOC under supervision of prof. dr. Hagen, dr. Hagedoorn and dr. Ebrahimi. For this project, he worked on the application of a new microfluidic calorimeter, This project resulted in the publication of a paper and a patent. After an internship at Chiral Vision in Leiden, under supervision of Rob Schoevaart, he decided to stay in academia. He returned to the group of BOC as a PhD candidate. Under supervision of dr. Holmann, Morten worked on regenerating oxidoreductases using light.

List of publications

Zhang, W., Fernandez-Fueyo, E., Ni, Y., **van Schie, M.M.C.H.**, Gacs, J., Renirie, R. Wever, R., Mutti, F.G., Rother, D., Alcalde, M. and Hollmann, F. *Selective aerobic oxidation reactions using a combination of photocatalytic water oxidation and enzymatic oxyfunctionalizations*. Nature Catalysis, 2018. **1**(1): p. 55-62.

van Schie, M.M.C.H., Ebrahimi, K.H., Hagen, W.R. and Hagedoorn, P.L. *Fast and accurate enzyme activity measurements using a chip-based microfluidic calorimeter*. Analytical Biochemistry, 2018. **544**: p. 57-63.

van Schie, M.M.C.H., de Almeida, T.P., Laudadio, G., Tieves, F., Fernández-Fueyo, E., Noël, T., Arends, I.W.C.E. and Hollmann, F. *Biocatalytic synthesis of the Green Note trans-2-hexenal in a continuous-flow microreactor*. Beilstein journal of organic chemistry, 2018. **14**(1): p. 697-703.

van Schie, M.M.C.H., Younes, S.H.H., Rauch, M.C.R., Pesic, M., Paul, C.E., Arends, I.W.C.E. and Hollmann, F. *Deazaflavins as photocatalysts for the direct reductive regeneration of flavoenzymes*. Molecular Catalysis, 2018. **452**: p. 277-283.

van Schie, M.M.C.H., Paul, C.E., Arends I.W.C.E., and Hollmann, F. *Photoenzymatic epoxidation of styrenes*. Chemical Communications, 2019. **55**(12): p. 1790-1792.

Zhang, W.⁺, Ma, M.⁺, Huijbers, M.E.⁺, Filonenko, G.A., Pidko, E.A., **van Schie, M.M.C.H.**, de Boer, S., Burek, B.O., Bloh, J.Z., van Berkel, W.J.H., Smith, W.A. and Hollmann, F. *Hydrocarbon synthesis via photoenzymatic decarboxylation of carboxylic acids*. Journal of the American Chemical Society, 2019. **141**(7): p. 3116-3120

de Almeida, T.P., **van Schie, M.M.C.H.**, Ma, A., Tieves, F., Younes, S.H.H., Fernández-Fueyo, E., Arends, I.W.C.E., Riul, A. and Hollmann F. *Efficient Aerobic Oxidation of trans-2-Hexen-1-ol using the Aryl Alcohol Oxidase from Pleurotus eryngii*. Advanced Synthesis & Catalysis, 2019. **361**(11): p. 2668-2672

Tieves, F.⁺, Willot, S.J.-P.⁺, **van Schie, M.M.C.H.**, Rauch, M.C.R., Younes, S.H.H., Zhang, W., Dong, J., Gomez de Santos, P., Robbins, J.M., Bommarius, B., Alcalde, M., Bommarius, A.S. and Hollmann, F. *Formate oxidase (FOX) from Aspergillus oryzae: One catalyst enables diverse H₂O₂-dependent biocatalytic oxidation reactions*. Angewandte Chemie International Edition, 2019. **58**(23): p. 7873-7877.

Burek, B.O., de Boer, S.R., Tieves, F., Zhang, W., **van Schie, M.M.C.H.**, Bormann, S., Alcalde, M., Holtmann, D., Hollmann, F., Bahnemann, D.W. and Bloh, J.Z. *Photoenzymatic hydroxylation of ethylbenzene catalyzed by unspecific peroxygenase: Origin of enzyme inactivation and the impact of light intensity and temperature*. ChemCatChem. **11**(13): p. 3093-3100

van Schie, M.M.C.H.*, Zhang, W., Tieves, F., Choi, D.S., Park, C.B., Burek, B.O., Bloh, J., Arends, I.W.C.E., Paul, C.E., Alcalde, M. and Hollmann, F.* *Cascading g-C₃N₄ and peroxygenases for selective oxyfunctionalization reactions*. ACS Catalysis, 2019. **9**(8): p. 7409-7417

Bormann, S.[†], **van Schie, M.M.C.H.[†]**, de Almeida, T.P., Zhang, W., Stöckl, M., Ulber, R. Hollmann, F. and Holtmann, D. *H₂O₂ production at low over-potentials for electro-enzymatic halogenation reactions*. ChemSusChem, 2019.

van Schie, M.M.C.H.*, Kaczmarek, A.T., Tieves, F., Gomez de Santos, P., Paul, C.E., Arends, I.W.C.E., Alcalde, M., Schwarz, G. and Hollmann, F. *Selective oxyfunctionalisation reactions driven by sulfite oxidase-catalysed in situ generation of H₂O₂*. Manuscript under review.

Hobisch, M., **van Schie, M.M.C.H.**, Kim, J., Røjkjær Andersen, K., Alcalde, M., Kourist, R., Park, C.B., Hollmann, F. and Kara, S. *Solvent-free photobiocatalytic hydroxylation of cyclohexane*. Manuscript under review.

Zhang, W., Liu, H., **van Schie, M.M.C.H.**, Hagedoorn, P.L., Alcalde, M. Denkova, A., Djanashvili, K. and Hollmann, F. *Radiolysis-induced water splitting to drive H₂O₂-dependent oxyfunctionalisation reactions*. Manuscript in preparation.

Patent

Ebrahimi, K.H., **van Schie, M.M.C.H.**, Hagedoorn, P.L. and Hagen, W.R. *Calibration of a chip-based microfluidic calorimeter*. 2018. WO2017179981A1

[†] Authors contributed equally

* Corresponding author

Acknowledgements

It is an odd feeling to finalize this thesis, as it represents the last four years of my life. Although my name is the only one on the cover of this thesis, it could not have realized this thesis without the help of all the people around me. These pages are therefore to acknowledge and thank those who stood beside me or worked with me when compiling this work.

The first person I have to thank greatly is Frank. Not only for hiring me and providing an endless flow of project ideas, but mainly for being a mentor these past few years. I feel privileged to have been able to work besides you in the attempt to make an impact on the world of biocatalysis. Many thanks for giving me my “academic freedom”. Though I know you dislike this term, I mean it in the most positive way as it means you had faith in my scientific capabilities. I feel like I greatly synchronized with your way of working and you provided me with a kick-start in science. I hope you can find your philosophy in this thesis.

Also, many thanks to Caroline. You already had a big mentorship role at the beginning of my PhD, when I was still new to the world of academics and chemistry. A role that became official when you became my copromotor. Thank you for always making time for me when I needed it the most. Time, either for scientific or personal advice or for meticulously checking all my writing. This thesis would be a linguistic embarrassment without your effort.

For me and my fellow PhD's, it was a luxury to have three promotor, all with different roles. Thank you Isabel for showing us how to put our work in a grander perspective. Normally, I would have been absorbed in my world of 500 μ L reactions and sub-millimolar conversions. You taught me how this work could contribute to our society. A personal example was the Avond van Wetenschap en Maatschappij, where we showed the Netherlands what biocatalysis has to offer.

Then, my main companions during this adventure: Marine, Seb and Georg. Together, we were on the frontier of driving enzyme catalysis with light. And, as we were one of the first to try out this relatively new field, a path full of stumbling blocks awaited us.

And stumbling we did. A lot.

Who would have guessed that enzymes “die” rather quickly when one tries to regenerate them with light? Nevertheless, I could not have wished for better partners than that I got with you. We all had to face the same challenges, though we approached them in different ways. This resulted in us always able to support each other. Although we spend “only” four years together, it seems much longer. We were always together, in our office and on our trips to conferences. And, as we were not yet tired of each other, we regularly planned holidays thereafter! Without you guys, these last few years would not have been the same. Thank you from the bottom of my heart.

We were lucky to always have the support from skillful scientists in the lab: the PostDocs. Many thanks to Yan Ni, Milja (also for pointing out this position), Elena, Sandy, Mieke, JiaJia and Andrada for having the patience, knowledge and devotion to always make time for my struggles, scientific or not. On top of that, it felt we always had a great atmosphere in our group. Furthermore, I personally got great help from Sabry, who has been there from the beginning till the end to help fill in the blanks I had in chemistry. I was also greatly supported by Flo. Not only *via* his production of massive amounts of enzyme, but also by his dedication to skill me in how to convey information and support me on a personal level. Finally, a big thanks to Wuyuan, and not only because it is convenient to publish together with someone who is getting nearly all his papers in journals of IF > 10. Mainly because you were able to show me how profitable it is to get out of my scientific comfort zone by keeping an eye on other fields of science for creative solutions. I am sure you will do great things back in China!

During my PhD, I also had the pleasure to get help from students. Therefore, many thanks to Haje, Timon, Andrea and Panos. It might not have been always that clear, but you probably taught me as much as I hoped I have taught you. I hope to have also shown you the fun sides of science. I greatly thank you for all for your enthusiasm.

As the world of biocatalysis is an internationally orientated one, I have met many great people from around the world who brought new insight's, knowledge and a lot of fun into our group. These scientists always made me look forward to the next yearly congress or trip, in order to meet again. Many thanks therefore to Sumanth, Gaurav, Laura, Andres, Carmen, Elia, Pati and Yann. Good luck to Alice, Robert and Markus for continuing the photo-biocatalysis work. Thanks to Xioamin for keeping me well fed during the last stages of my PhD. And finally, a special thanks to Tiago for our work and good times together. I was amazed by your ability to keep smiling and being positive, even in the most stressful moments.

I am also greatly in debt to those in a supporting role and who are constant and appreciated factors in our group. First of all I need to thank Mieke, our secretary. Without

your help and devotion this group would certainly wind up in total chaos. Furthermore, a big thanks to all our technicians. It is a true luxury to have such a devoted team supporting our work. Marc and Laura, not only were you pivotal in all the work needed to produce the enzymes, but you were always available to step in if any problem came our way. A big thanks to Maarten, whose move to Scotland was a great loss for our group. You taught me how to design creative reaction setups for unusual reactions. Luckily Lloyd has now picked up your empty place and fills it formidably. Also, thank you to Stephen, for juggling all the things that come with supporting NMR for two whole departments and for always providing the pictures after a group event. I also want to acknowledge Marcel, for crafting me new light-setups each time I would melt one down... Finally, a special thanks to Remco. Thank you for your eagerness to help with GC and other facets. Sitting next to you was never dull, though I did not always wanted to acknowledge this (might have something to do with differences in music taste and levels of football-knowledge).

And finally, a general thanks to the rest of the group, whom I did not manage to put in nice boxes as those mentioned above. As is often stated, I think we are lucky with the open and levelled atmosphere in our group and I think this greatly contributes to what BOC is capable of. First, a big thanks to Luuk, Hanna and Stefan. You were also there from the beginning to the end, and though we did not share any topics, we encountered the same things in life. It was always good to blow off steam during our day to day work. Many thanks to the other researchers in our group. Nati, for at least trying to respect my dislike for hugs. Fabio for help in puzzling reaction setups together and for artworks on our whiteboard. Furthermore, thanks to Caro, Jose, Albert, Eman, Tania, Durga, Julia, Kai, Rosario, Retna, Alexandra, Paula, and Jie for contributing to the great (scientific) atmosphere in our group. Thanks to all those who oversee us, for keeping the group running, Ulf, Kristina, Linda and Duncan. Finally, special thanks to Fred, Peter Leon and Kourosh for truly introducing me to the wondrous world of enzymes.

During my PhD, I had the pleasure of going on a few research trips outside of Delft. There I was always cordially received and adopted into the hosting groups. Therefore, many thanks to Adrie and Willem from Wageningen, although I did not manage to get the "Stefamox" to work as we wanted. It was also a great pleasure to work with Gabriele and Timothy from Eindhoven. I will probably never work on a more efficient project! Many thanks to the guys in Frankfurt: Sebastian, Basti, Jonathan and Dirk. The collaborations were always a great pleasure and so were our meetings, both in Germany as well as in The Netherlands. Furthermore, a big thanks for Alexander and Guenter for our work together. What started as sophisticated procrastination ended up as a whole project and even led to a chapter! Finally, thank you to Margit for inviting me to Graz. With AOR, you have the greatest nemesis of my PhD in hand, but I am sure you will be able to make it work!

Tot slot heeft niet alles de afgelopen vier jaar gedraaid om werk. Ik heb ook veel steun kunnen halen uit mijn vrienden om mij heen. Ten eerste ben ik veel dank verschuldigd aan de C's, de boys, de heren, voor alle steun en toeverlaat al deze jaren. Daarnaast is ook de Compagnie van Faust altijd een constante factor geweest. Furthermore, I could always blow of steam at my football club Wilhelmus.

Opgroeien in een familiebedrijf is de fundering geweest voor de rest van mijn leven. Frases als "Nie mauwen maar doorgaan" en "Samen staan we sterk" zijn gunstig genoeg ook zeer bruikbaar voor het werk aan een PhD. Mijn dank gaat dan ook uit naar mijn grootouders en alle ooms, tantes, neefjes en nichtjes. Tusen takk til alle i Norge. Jeg føler meg alltid hjartelig velkommen, Norge er for meg som mitt andere hjem. Ook Arnold, Mariëtte en Tim voelen inmiddels aan als echte familie. Daarnaast ben ik natuurlijk alles verschuldigd aan mijn ouders en mijn broertje, voor hun onvoorwaardelijke steun bij alles wat ik doe.

Tot slot, mijn grootste steunpilaar in alles wat ik denk en doe: Julie. Jij bent mijn grootste maatje en mijn soulmate, degene die mij het beste begrijpt en andersom. Dank voor alle jaren die al achter ons liggen en ik kijk uit naar de jaren en avonturen die wij nog samen mee gaan maken.

